TRANSPORTATION RESEARCH

RECORD

No. 1331

Soils, Geology, and Foundations

Integrity Testing of Foundations 1991

A peer-reviewed publication of the Transportation Research Board

TRANSPORTATION RESEARCH BOARD
NATIONAL RESEARCH COUNCIL
WASHINGTON, D.C. 1991

Transportation Research Record 1331
Price: $21.00

Subscriber Category
IIIA soils, geology, and foundations

TRB Publications Staff
Director of Publications: Nancy A. Ackerman
Senior Editor: Naomi C. Kassabian
Associate Editor: Alison G. Tobias
Assistant Editors: Luanne Crayton, Norman Solomon
Graphics Coordinator: Diane L. Snell
Production Coordinator: Karen W. McClain
Office Manager: Phyllis D. Barber
Production Assistant: Betty L. Hawkins

Printed in the United States of America

Library of Congress Cataloging-in-Publication Data
National Research Council. Transportation Research Board.

Integrity testing of foundations 1991.
p. cm.—(Transportation research record, ISSN 0361-1981; no. 1331)
ISBN 0-309-05168-1
1. Foundations—Testing. 2. Non-destructive testing. I. Series.
TE7.H5 no. 1331
[TA775]
388 s—dc20
[625.7'3] 92-8979
CIP

Sponsorship of Transportation Research Record 1331

GROUP 2—DESIGN AND CONSTRUCTION OF TRANSPORTATION FACILITIES
Chairman: Raymond A. Forsyth, Sacramento, California

Soil Mechanics Section
Chairman: Michael G. Katona, Tyndall AFB

Committee on Foundations of Bridges and Other Structures
Chairman: Richard S. Cheney, Federal Highway Administration
Secretary: Richard P. Long, University of Connecticut
Gregg Batchelder Adams, Roy H. Borden, Jean-Louis Briaud, Joseph A. Caliendo, Ronald G. Chassie, Murty S. Devata, Albert F. Dimillio, Victor Elias, Richard L. Engel, George G. Goble, Robert C. Houghton, Alan P. Kilian, John F. Ledbetter, Jr., Larry Lockett, James H. Long, Randolph W. Losch, Thomas Neff, Peter J. Nicholson, Gary M. Norris, Michael Wayne O'Neill, John L. Walkinshaw, Gdalyah Wiseman, James L. Withiam

G. P. Jayaprakash, Transportation Research Board staff

The organizational units, officers, and members are as of December 31, 1990.

Transportation Research Record 1331

Contents

Foreword

The design of foundations involves consideration of both the structural capacity of the foundation elements as well as the capacity of the earth to support the load transferred from the foundation. The 13 papers in this Record are primarily devoted to post-construction evaluation of the foundation element or the supporting capacity of the ground. The use of dynamic test methods for foundation evaluation will provide owners with a quick, inexpensive procedure to verify foundation performance.

Lepert et al. present a simple procedure called the WAK test to assess the stiffness of the soil under a spread footing foundation. They summarize the theoretical aspects of the method and detail several case histories in which the WAK test was used.

O'Neill identifies categories of defects in drilled shafts and suggests general methods that may be appropriate for understanding the defects. Emphasis is placed on avoiding defects during construction by proper inspection techniques.

Davis and Hertlein review the advancement of nondestructive test (NDT) methods for foundation elements. Examples of proper use of NDT methods are discussed, as is development of specifications for NDT testing.

A comparison has been made of Pulse Echo and Transient Response methods by Rausche et al. Advantages and weaknesses of these methods are discussed and related to data obtained from field tests.

Baker et al. discuss the results of a drilled shaft test program held at two sites with different soil conditions. The results of various NDT methods that were used at these sites are compared, and general conclusions are drawn on strengths or weaknesses of the methods.

Aggour applies a nondestructive test method to examine the soundness of timber piles. The paper includes the type of data collected, the information needed for data interpretation, equipment description, and factors that affect testing.

A case history is presented by Camp and Hussein that illustrates application of NDT methods to assess damage to in-place piling. Test results and costs are discussed.

Heritier et al. discuss potential error sources involved with dynamic testing. A comparison is made between the SIMBAT method developed for bored piles and the CASE method for driven piles.

Azam and Wang studied the procedures to compute strip footing bearing capacity for two layered soil systems. They discuss existing theories and propose a new equation. Information on critical depths for footing bearing computations is also presented.

Wong proposes the use of a procedure using equivalent subgrade modulus to predict pile lateral load behavior. The modulus is shown to be related to pile properties and undrained shear strength.

The effects of base resistance on lateral load behavior of short rigid piles is presented by Borden and Gabr. A subgrade reaction model is presented to include the base component. Effects of pier length to diameter ratio and amount of base deformation are discussed.

Brown and Bollman present an experimental procedure to account for ship impact loads on pile groups. Modification procedures for p-y curves based on pile group geometry are explained, and an example problem is solved.

Satter examines the behavior of model piles driven into fine grained soil by low-frequency vibrations. Threshold values for pile penetration and optimum amplitude levels are presented.

Dynamic Method to Assess the Stiffness of Soil Underlying Spread Foundations

P. LEPERT, J.-L. BRIAUD, AND J. MAXWELL

A simple and easily implemented experimental method, the WAK test (wave activated stiffness K test), was proposed by Briaud and Lepert (*1*) to estimate, on site, the stiffness of the soil underlying a rigid foundation. The theoretical background of the method is summarized, and the interpretation of the results is explained. Case histories are presented to illustrate the method, its performances, and its potential applications.

Many theoretical and experimental studies have been devoted in the last few years to spread foundations. Nevertheless, there is still a lack of quick nondestructive testing methods to check the design of such foundations. In situ static load tests can be performed, but they are expensive.

An easily implemented method, called the WAK test (wave activated stiffness K test) was proposed by Briaud and Lepert (*1*). It enables the measurement of some basic parameters of the foundation, mainly the elastic stiffness of the soil underlying the foundation, in the small strain range (10^{-4} to 5.10^{-3} percent) a useful parameter to predict the short-term behavior of the foundation under design loads. The method also enables an estimate of the actual mass of the foundation and the equivalent damping of the soil. This was rigorously proven on several scaled foundation models resting on a layer of sand (*1*,*2*).

Recently, other experiments were performed on full-scale foundations. The results of these experiments, which are reported here, confirm the reliability of the WAK test. Furthermore, these case histories illustrate several potential applications of the method.

METHOD

In the proposed method, the "soil + foundation" system is considered as a single degree of freedom (d.o.f.) system (Figure 1). The WAK test is aimed at identifying the equivalent dynamic parameters of this system: M, K, and C. The static parameters of the foundation, m and k, can then be derived. Finally, the shear modulus of the soil in the small strain range, G_o, can be estimated from the latter values.

Theoretical Background

The equilibrium equation of the single d.o.f. system of Figure 1 can be written as

$$Mx'' + Cx' + Kx = F_o e^{j\omega t} \quad (1)$$

where F_o is the amplitude of the applied harmonic force and ω is its frequency in radians per second. The steady state solution of this equation is as follows [see work by Brebbia et al. (*3*) for more details]:

$$x(t) = x_o \cdot e^{j(\omega t + \phi)} \quad (2)$$

with

$$x_o = F_o/[(K - M\omega^2)^2 + C^2\omega^2]^{1/2} \quad (3)$$

$$\tan(\phi) = C\omega/(K - M\omega^2) \quad (4)$$

The ratio x_o/F_o is a function of called the "displacement versus force transfer function" or "compliance" of the single d.o.f. system. The modulus of this transfer function is thus expressed as

$$|x_o/F_o| = 1/[(K - M\omega^2)^2 + C^2\omega^2]^{1/2} \quad (5)$$

whereas its phase is given by Equation 4. The "velocity versus force transfer function" or "mobility" of the same system can be derived by multiplying Equation 5 by ω and shifting the phase angle ϕ by a value of $\pi/2$. This function is shown in Figure 2. An important feature of the curve is a peak that appears on the modulus function at a frequency (ω_n) close to the natural resonance (ω_o) of the system:

$$\omega_n \sim \omega_o = (K/M)^{1/2} \quad (6)$$

Application to the "Foundation + Soil" System

Because the dynamic analysis is limited to the low frequency range (<100 Hz), the foundation can be considered a rigid block. Furthermore, the test induces only small strains in the soil, which may thus be regarded as an elastic medium radiating energy. Following work by Barkan (*4*), the "soil + foundation" system is assumed to behave as a single d.o.f. system.

The dynamic parameters of this system are related to the characteristics of the foundation and of the half-space through the following relationships:

$$M = \beta \cdot m \quad (7)$$

$$K = 2\pi^{1/2} G r_o c_s/(1 - \nu) \quad (8)$$

$$C = 2M\omega_o \xi \quad (9)$$

P. Lepert, Laboratoire Central des Ponts et Chaussées, B.P. No. 19, 44340, Bouguenais, France. J.-L. Briaud and J. Maxwell, Department of Civil Engineering, Texas A&M University, College Station, Tex. 77843-3136.

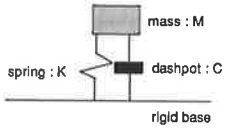

FIGURE 1 Single d.o.f. system.

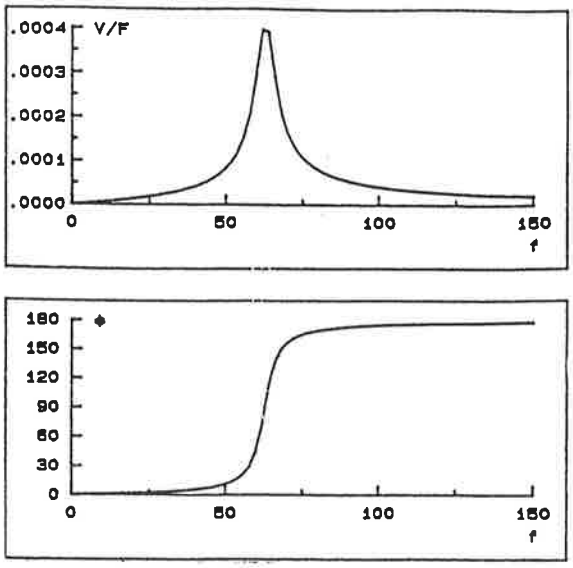

FIGURE 2 Typical transfer function of single d.o.f. system.

where

$$\omega_o = (K/M)^{1/2}, \tag{10}$$

m = mass of the foundation,
r_o = equivalent radius of foundation [i.e., $(S/\pi)^{1/2}$],
S = horizontal area of foundation,
c_s = a factor depending on shape of foundation [see Table 1 in work by Barkan (*4*)],
G = shear modulus of soil, and
ν = Poisson's ratio.

β and ξ are two factors that depend on the dimensionless mass factor b according to Figure 3. This mass factor is defined as

$$b = m/\gamma r_o^3 \tag{11}$$

where γ is the soil density. The following table presents auxiliary values for the shape factor c_s (*4*):

α	c_s
1.0	1.08
1.5	1.09
2.0	1.10
3.0	1.15
5.0	1.24
10.0	1.41

where α is the length-width ratio of the foundation.

Other authors, such as Bycroft (*5*) and Lysmer (*6*), confirmed that the "soil + foundation" system could be approximated by a single d.o.f. system. For instance, Lysmer and Richart (*7*) derived, for usual cases of circular foundations, the following relationships:

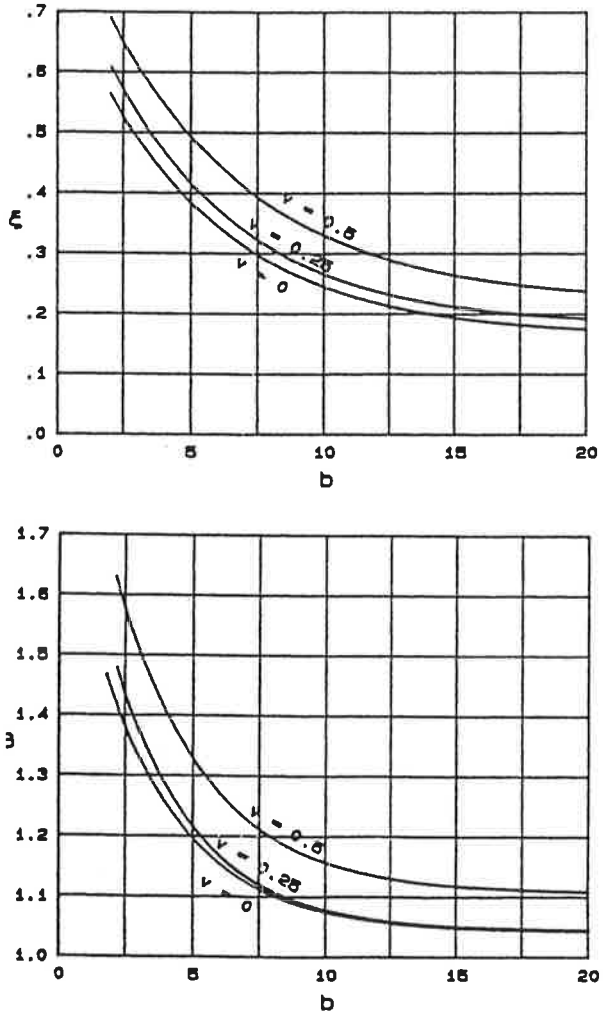

FIGURE 3 Auxiliary diagrams for determination of reduced damping coefficient ξ (top) and added mass coefficient β (bottom) (*3*).

$$M = m \tag{12}$$

$$K = 4\,Gr/(1 - \nu) \tag{13}$$

$$C = 3.4r\,(G\rho)^{1/2}/(1 - \nu) \tag{14}$$

Although this approach seems somewhat different from Barkan's, both lead to similar results in most engineering applications. The difference in K values is generally within a few percent. The approach from Barkan is usually retained because it seems more straightforward and yields results closer to those obtained experimentally.

Test Procedure

A small vertical impact is applied to the foundation along its gravity axis by means of a sledgehammer (see Figure 4). This

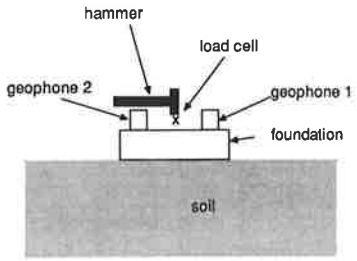

FIGURE 4 Experimental set-up and instrumentation.

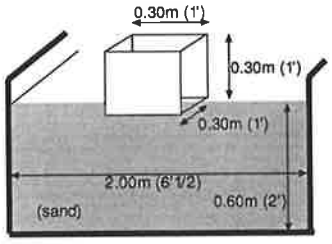

FIGURE 6 Model of concrete foundation used for first laboratory tests.

hammer is instrumented with a load cell which provides the force versus time signal $f(t)$. The vertical response of the foundation is measured by two geophones that are fixed, symmetrical with respect to the impact location, on the upper face of the foundation.

The vertical velocity of the center of gravity $v(t)$ of the foundation is derived by averaging the two velocity versus time signals:

$$v(t) = 0.5[v_1(t) + v_2(t)] \tag{15}$$

A Fast Fourier Transform analyzer is used to compute the transfer function $T(\omega)$ between the velocity $v(t)$ and the force $f(t)$.

Figure 5 shows the mobility measured on the "foundation + soil" system shown in Figure 6. This function is similar to the one in Figure 2. Equation 5 (multiplied by ω because velocity is used instead of displacement) is adjusted to the experimental curve in Figure 5. A set of dynamic parameters (M, K, and C) is derived from this adjustment. The shear modulus (G) can be calculated from these dynamic parameters through equations 7 to 11 and Figure 3.

LABORATORY INVESTIGATIONS

To validate the method, some laboratory investigations were first conducted on a scaled model—a cubic concrete mass resting on a layer of loose coarse sand (Figure 6). The mobility measured on this model is displayed in Figure 5 (solid line).

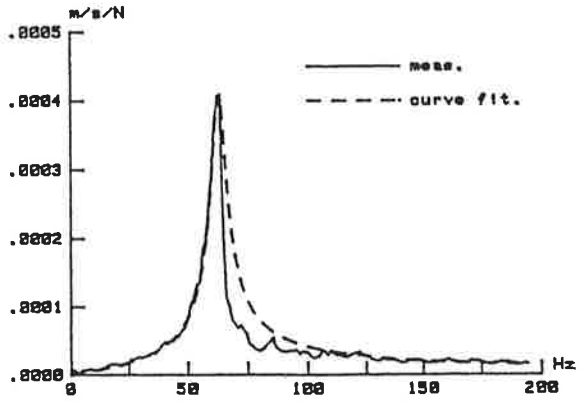

FIGURE 5 Mobility measured on the "foundation + soil" system shown in Figure 6.

The soil stiffness resulting from these tests using a curve fitting procedure and equations 7 to 11 compared quite well with the value estimated from static loading tests. The results from these investigations, and the related conclusions, were reported in detail by Briaud and Lepert (*1*).

Other tests were performed on steel scaled models resting on Fontainebleau sand. They demonstrated that the soil stiffness derived from the WAK test was representative of the mechanical characteristics of a significant thickness of soil under the foundation. For more details about these investigations and the related conclusions, see work by Lepert and Briaud (*2*).

CASE HISTORIES

Case 1: Site Correlation Between WAK and Static Loading Tests

Static load tests on small spread footings were conducted at the FHWA Research Center. The footings, ranging in size from 0.3 m × 0.3 m × 0.15 m (1 ft × 1 ft × 6 in.) to 0.6 m × 0.6 m × 0.2 m (2 ft × 2 ft × 7.5 in.), were set in a test pit 5.5 m × 7 m × 6.1 m (18 ft × 23 ft × 20 ft). The properties of the sandy soil are as follows: density, 1475 kg/m³ (92.4 lb/ft³); SPT, 4 to 7 blows/ft; CPT (cone b.), 2 MPa (20 tons/ft²); and friction resistance, 9.5 kPa (200 lb/ft²).

Before each static load test was performed, the WAK test was used in an attempt to predict the static stiffness of the soil-footing system. The test procedure consisted of four steps:

1. Place the footing on smoothed level sand and seat it by rotating back and forth about a gravity axis while pushing down.
2. Fix two geophones at the extremities of a diagonal of the footing (see section on test procedure).
3. Impact the footing at center; record and process the data (WAK test).
4. Load the footing to failure.

Step 3 was repeated about 10 times to obtain a significant set of dynamic results. Figure 7 (top) shows the soil-footing stiffness derived from 9 successive WAK tests on the 1.5-ft × 1.5-ft × 7.5-in. footing. Figure 7 (bottom) shows the average loading curve (average of four dial gauges: one at each corner of the footing) obtained on the same footing.

The stiffnesses shown, K33 and K50, were obtained from an intersection of the straight lines with the one-third and

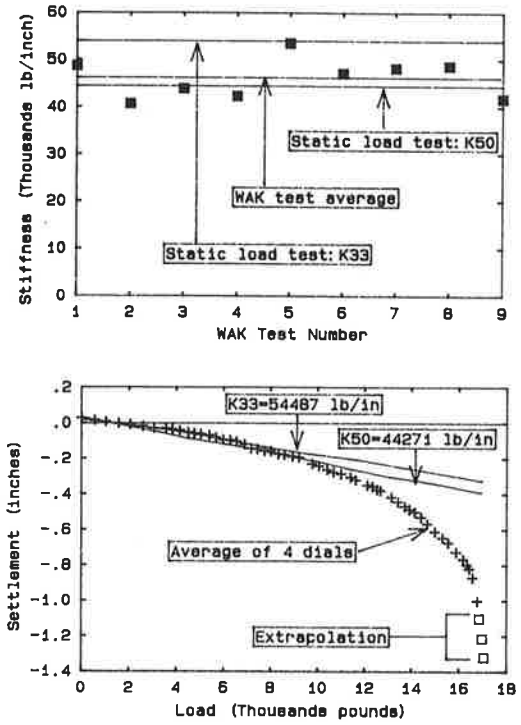

FIGURE 7 Soil-footing stiffness derived from nine successive WAK tests (*top*) and average loading curve obtained (*bottom*) on 1.5-ft × 1.5-ft × 7.5-in. footing.

one-half points of the curve, respectively. The points fall at one-third and one-half of the ultimate load, which was obtained through extrapolation. (Difficulties were encountered in obtaining measurements with settlements greater than 1 in.). This extrapolation is not results sensitive. The comparison indicates a good consistency between both tests.

Case 2: Application of WAK Test to Evaluation of Soil Strength after Dynamic Compaction

A landfill of rubbish, including everything from lumber to scrap metal, was covered with 22 in. of course gravel. Dynamic compaction was then used to improve the stiffness of the landfill in an attempt to allow building construction. The characteristics of the dynamic compaction mass are as follows: weight, 15 metric tons (16.5 tons); size, 1.5 × 1.5 × 0.9 m (5 × 5 × 3 ft); height of fall, 20 m (65.6 ft); and crater depth, 1 to 2 m (3 to 6 ft). A study was conducted to determine whether the WAK test would be a suitable means to monitor the progress of dynamic compaction. The test procedure involved nine steps:

1. Set the dynamic compaction mass on a new grid (the landfill was divided into grids for bookkeeping), and slack the crane's cable.
2. Place geophones at the opposite extremities of a diagonal of the mass.
3. Impact the mass with the test hammer, the mass of which is 5.4 kg (12 lb), and record data.
4. Remove the dynamic compaction mass.
5. Place a small concrete footing (1 ft × 1 ft × 6 in.) on the surface where the mass was set.
6. Fix the geophones at the extremities of a diagonal of the small footing.
7. Impact the footing with the test hammer, and record data.
8. Perform dynamic compaction.
9. Repeat steps 2 to 7, making sure that a good contact exists between the small footing and the bottom of the crater during steps 5 to 7.

Steps 5 to 7 were added to the intended procedure because of expected high noise-signal ratios when the compaction mass was struck directly. The data acquired from striking the small footing were used instead.

Figure 8 (top) shows that the measured soil stiffness is increasing with the number of drops of the dynamic compaction mass.

Thirty-one plate load tests were performed at the site with a 30-in.-diameter plate in accordance with ASTM D1194. The stiffness value (KPLATE) was determined from the beginning of the load settlement curve. Figure 8 (bottom) displays a comparison between these values and the corresponding ones derived from the WAK test (KWAK). The results match quite well.

Case 3: Application of WAK Test to Check Embedded Foundations

Even when an embedded foundation is correctly designed, its ability to support the design loads may be dangerously re-

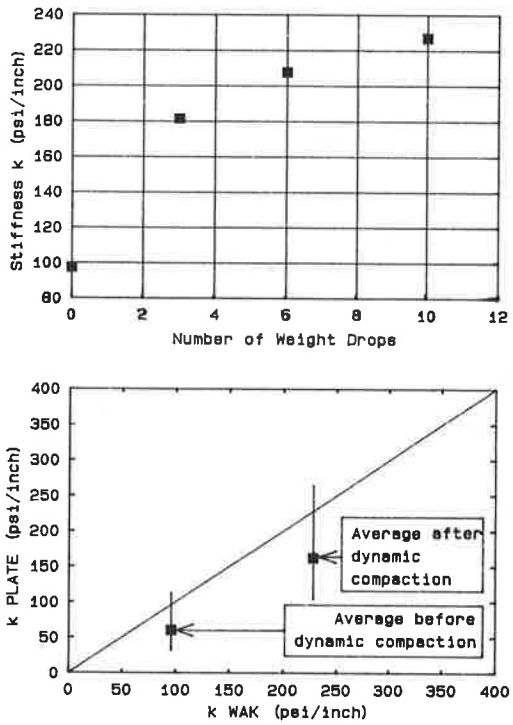

FIGURE 8 Soil stiffness versus number of drops (from WAK tests) (*top*) and stiffness values from plate tests versus WAK tests (*bottom*).

duced by errors made during construction. These may include an excavation that is too small, irrespective of the design dimensions, or an excavation that has not been properly cleared of excess rubble before casting. This observation especially applies to standardized foundations, such as foundations of pylons. Such faults are not detected through visual inspection. The WAK test could serve as a means to monitor the nonconformities to foundation design.

Investigations were conducted on the foundations of two identical concrete pylons. The first pylon was founded on a large (10 m^3) concrete block properly embedded in the soil, whereas the foundation of the second pylon was intentionally faulty: the excavation was too small (4 m^3) and uncleaned (Figure 9).

The WAK test was performed on both foundations and led to the following dynamic parameters: for the sound foundation,

$K_s = 1\ 10^9$ N/m
$M_s = 21\ 920$ kg

for the faulty foundation,

$K_f = 0.47\ 10^9$ N/m
$M_f = 9\ 370$ kg

The dynamic mass of the sound foundation (M_s) is approximately 2.3 times the mass of the faulty one (M_f), which is consistent with the known size of the excavations (10 and 4 m^3, respectively) and thus, with the actual mass of cast-in-place concrete. This difference in size can also be used to partly explain the difference between the dynamic stiffnesses (K_s and K_f) because this parameter is proportional to the size of the foundation (see Equation 8). The latter parameters were used to calculate the shear modulus of the soil (G_o) by using Equation 8. Although this equation takes into account the actual size of the foundation, the result of the calculation exhibits a significant gap between the value derived from the test performed on the sound foundation (G_o = 150 MPa) and the one derived from the test performed on the faulty foundation (G_o = 96 MPa). This difference can only be explained by the presence of disaggregated material between the concrete foundation and the surrounding soil (see Figure 9).

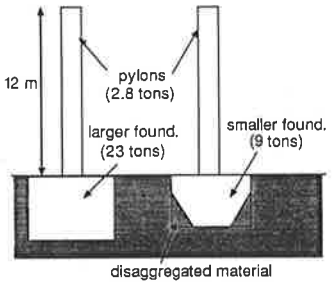

FIGURE 9 Sketch of two pylons with foundation.

Therefore, the WAK test appears as a discriminatory method to check standard foundations. Reliable information is given about the actual size of the foundations and the quality of their embedment in the surrounding soil.

CONCLUSIONS

A quick and inexpensive method was proposed by Briaud and Lepert (*2*) to measure the dynamic parameters of a spread foundation. Static characteristics (soil-foundation system stiffness, mass of the foundation) could be derived from these dynamic parameters. The first results, from laboratory tests, were encouraging.

The in situ experiments discussed here confirm these results. Furthermore, they show that the method can be useful in various contexts of geotechnical engineering: as a design control tool in the field for spread footings, a monitoring tool during dynamic compaction, and a construction control tool for embedded foundations.

ACKNOWLEDGMENTS

The authors would like to acknowledge Albert DiMillio, Carl Ealy, and Mike Adams, who conducted the static tests at the FHWA Research Center, and also contributed to the WAK tests discussed in the section on Case 1. The authors would also like to acknowledge Greg Gifford, of Union College, who performed the plate load tests reported in the section on Case 2 and contributed to the associated WAK tests.

REFERENCES

1. J.-L. Briaud and P. Lepert. The WAK Test To Find Spread Footing Stiffness. *Journal of Geotechnical Engineering,* ASCE, Vol. 116, No. 3, March 1990.
2. P. Lepert and J.-L. Briaud. *Dynamic Non Destructive Testing of Footing Stiffness.* European Conference on Structural Dynamics: Eurodyn '90, Bochum, West Germany, June 5–6, 1990.
3. C. A. Brebbia et al. *Vibrations of Engineering Structures,* Computational Mechanics Ltd, Southampton, United Kingdom, 1976.
4. D. D. Barkan. *Dynamics of Bases and Foundations.* McGraw-Hill Book Co., New York, N.Y., 1962, pp. 85–103.
5. G. N. Bycroft. Forced Vibration of a Rigid Circular Plate on a Semi-Infinite Elastic Space or an Elastic Stratum. *Philosophical Transaction,* Royal Society of London, Vol. 248, 1956, pp. 327–368.
6. J. Lysmer. *Vertical Motion of Rigid Footing.* Contract Report 3-115. U.S. Army Waterways Experiment Station, Vicksburg, Miss., 1965.
7. J. Lysmer and F. E. Richart. Dynamics Response of Footings to Vertical Loading. *Journal of the Soil Mechanics and Foundation Division,* ASCE, Vol. 92, No. SM1, 1966, pp. 65–91.

Construction Practices and Defects in Drilled Shafts

MICHAEL W. O'NEILL

Certain construction practices can lead to defects in drilled shafts. Defects can occur in the form of voids; degraded or debonded concrete; entrapped cuttings, slurry, or groundwater; and geometric errors. They are considered generically according to the place in the construction cycle at which the defect occurs: general defects, defects due to drilling, defects arising from casing management, defects arising from slurry management, and defects related to design. Examples are presented, and suggestions are made for post-construction integrity evaluation techniques that might be effective in locating a given defect and defining its extent. Methods are also suggested for avoiding defects, which often involve subtle factors. Because of modern construction techniques, experienced contractors, and knowledgeable inspectors, relatively few defective drilled shafts are currently constructed.

The wide variety of subsurface soil, rock, and groundwater conditions encountered throughout the United States has given rise to a number of general drilled shaft construction techniques, which often must be modified because of the individuality of subsurface conditions. In effect, each drilled shaft is a unique construction project, complicated by the fact that the drilling and concreting occur mostly out of sight of the drilled-shaft contractor and the inspector. On occasion, structural defects result from incorrect construction or design details, or evidence may exist that such defects may have occurred in the completed shaft that require the services of integrity testing specialists to investigate the nature, location, and extent of the defects. The objective of this paper is to describe how and where common defects can occur and to suggest general methods for investigating their presence. It should be clear that all of these defects can be prevented by contractors and inspectors who are conscious of the actions in the subsurface that occur during construction.

Several methods are in use in the United States for the evaluation of the location, nature, and extent of defects or potential defects in drilled shafts, including the following:

1. Excavation of the soil and visual inspection of the shaft (EVI) (for suspected defects near the ground surface);
2. Reflection of sonic waves, usually from a surface source back to a surface receiver, with various types of signal analysis and, with some systems, wave equation simulation of the signal to identify the defect [termed low-strain testing (LST)];
3. Driving the completed drilled shaft with redundant measurements of force and velocity at the shaft head and interpreting the defect through the use of stress wave theory [termed high-strain testing (HST)];
4. Backscatter gamma logging (GL), which gives information on concrete density within about 0.1 m of the nuclear probe;
5. Crosshole ultrasonic testing (UST), in which velocities of shear and compression waves are measured between two instruments in a shaft and from which concrete quality can be inferred;
6. Drilling and coring through the shaft (CD); and
7. Slow or rapid quasi-static load testing of the drilled shaft (QSLT).

Methods 1–3 and 6 can be used if the decision is made to investigate integrity after construction has been completed, although Method 2 should be performed with redundant measurements or special acoustic source hammers if it is to be used to distinguish defects within about 10 ft (3 m) of the top of the drilled shaft. Methods 4 and 5, which involve searching for anomalies, require that access tubes be placed in the shaft to be tested and must be planned before construction. Method 7 is appropriate only if systematic defects are suspected on a large number of shafts, although new methods of conducting quasi-static loading tests using slow-burning explosives may make load testing of individual shafts with nonsystematic defects economically feasible. Procedures not included in this list, including vibration of the shaft head and probing the exterior of the shaft, are occasionally used. Baker and Khan (*1*) describe many of these methods in detail and discuss other integrity-evaluation methods that have been used in the Chicago area. They also suggest that a single method may not always provide definitive results and recommend that multiple procedures be used wherever feasible.

TYPES OF CONSTRUCTION

Reese and O'Neill (*2*) describe three general techniques for constructing drilled shafts: (a) the dry method, in which a borehole is excavated and backfilled directly with concrete; (b) the casing method, in which a temporary casing lines the borehole to prevent caving of soil or intrusion of groundwater until the concrete can be placed, after which the casing is usually removed; and (c) the direct slurry displacement, or "wet," method, in which a drilling fluid is used to stabilize the borehole during excavation and the fluid is displaced directly by placing concrete under the fluid using a tremie or pump. A number of variations on the casing method are common: (a) drilling the borehole to completion and dropping a casing into place to prevent long-term sloughing of soil or rock into the borehole (when conditions permit); (b) drilling

Department of Civil and Environmental Engineering, University of Houston, Houston, Tex. 77204-4791.

the borehole under a fluid to bypass waterbearing or caving soil or rock layers, then sealing the casing into an impermeable material below the bypassed layer, followed by removal of the fluid from inside the casing; (c) driving the casing directly into a material of low permeability, usually through cohesionless soil with a vibratory driver, and excavating the material from within the casing; and (d) setting casings that are successively smaller in diameter in the borehole as required to develop seals in deeper and deeper strata (when excavating overburden over weathered rock or in boulder fields).

With each method of excavation and borehole retention, concrete must be placed in the borehole in such a way that it does not produce voids or seams of weakness. Furthermore, it must displace any extraneous cuttings, water, or drilling fluid in the excavation. These performance criteria require a fluid concrete with coarse aggregate as small as is feasible and slump generally in the range of 7 to 9 in. (175 to 225 mm). In addition, slump loss must be controlled such that if delays occur in placing the concrete, the concrete will retain at least marginally acceptable fluidity. The use of well-graded aggregate and high cement factors (6.5 to 7 sacks per yard) is advisable when water, even in small amounts, will be present in the borehole during concreting.

CATEGORIES OF DEFECTS

Common defects arising from incorrect application of the details of the construction procedures just described were first described by Reese and Wright (*3*). These and other defects described here can be placed in several categories for purposes of discussion. In this context, defects are defined as structural flaws that may or may not affect the serviceability of the foundation. Only a careful evaluation of the location and extent of defects relative to zones of high load transfer and high internal stresses can determine whether the defect requires repair. Repair methods are beyond the scope of this paper but are discussed by Baker and Khan (*1*), Reese and O'Neill (*2*), and others.

Categories of defects are as follows:

- Defects arising from general construction problems,
- Defects arising from drilling problems,
- Defects arising from casing management problems,
- Defects arising from slurry management problems, and
- Defects resulting from design deficiencies.

Although concreting is an important step in the construction cycle and is critical in the production of a competent drilled shaft, it is not categorized separately because concreting is involved directly or indirectly in all of the categories. The last class of defects is not, of course, caused by incorrect construction but by ignorance on the part of the designer of the limitations of construction procedures or by errors in the geotechnical characterization of subsurface materials. Examples of specific defects in each of these categories are given next.

Defects Arising from General Construction Problems

Defects or construction errors leading to defects are depicted here schematically. To assist in the understanding of the intent of the various schematics, a legend of symbols is provided in Figure 1. In Figure 2 are shown four common general defects: (a) placing concrete by free fall without directing the stream away from reinforcing steel or the sides of the excavation, (b) excavating a borehole for a drilled shaft near a shaft that has just been concreted, (c) placing concrete through water that has accumulated in the borehole, (d) drilling the shaft out of position, and (e) developing mudwaves in surface soil without protecting the newly concreted shaft, placing lateral loads on

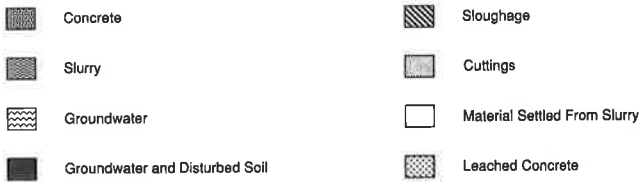

FIGURE 1 Key to symbols.

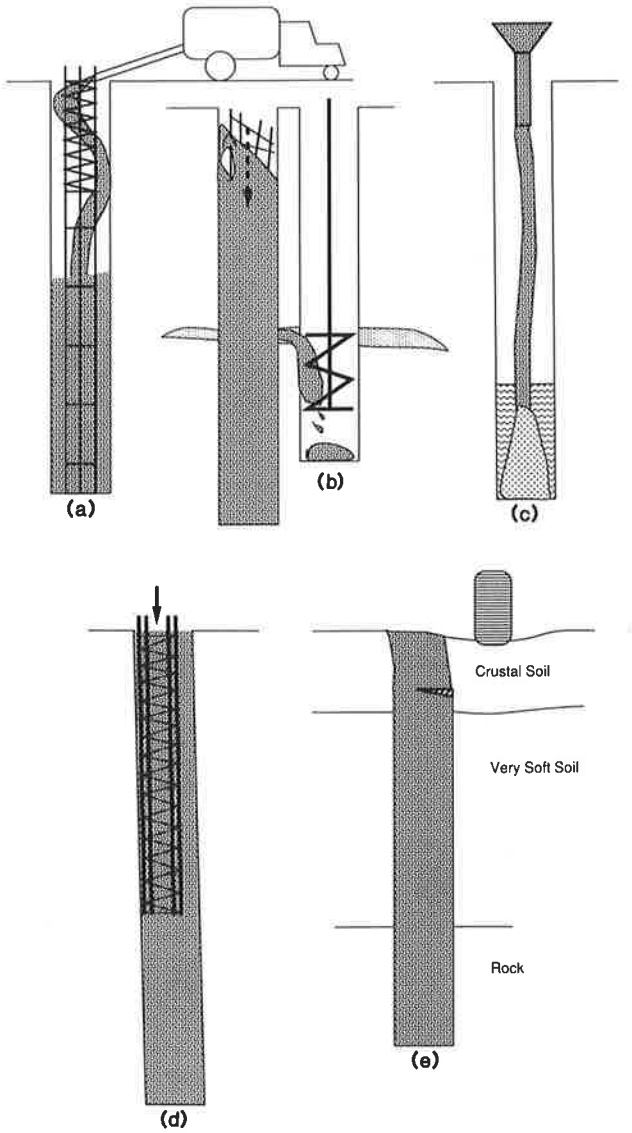

FIGURE 2 General construction problems.

the setting or green concrete at the shaft head, which causes cracks.

In Figure 2a the problem is not free fall. With small [0.75-in. (19 mm)], coarse aggregate, free fall of concrete through air to a direct impact in excess of 20 m will not cause significant segregation unless the mix design is inappropriate. However, if the stream of concrete flows through rebar or bounces off the side of the hole, segregated material will result, and small voids can develop adjacent to the rebar. To the investigator of structural integrity, segregated concrete will appear in the LST, UST, or GL to have either lower *p*-wave velocity or to be less dense than competent concrete, although minor segregation problems and voids may not be detectable.

A layer of cohesionless soil traverses both shafts in Figure 2b, such that lateral support of the concrete is removed in the recently placed shaft while the second shaft is excavated. The fluid concrete from the first shaft breaks through as the soil caves into the second excavation, causing the setting concrete to slump, dragging and racking the cage and producing voids. If the voids are large enough (occupying about 25 percent of the cross-sectional area of the shaft or greater), they can be detected by LST. They can also be detected by UST or GL, but only if the access tubes are fortuitously placed in the correct position. Steel racking without production of voids in the concrete is difficult to assess remotely. One must generally rely on visual observations of the condition of the steel at the surface during construction or EVI (with chipping of concrete down to the rebar) to ascertain whether racking may have been produced.

In Figure 2c several inches to several feet of water may have accumulated in an otherwise dry borehole before concreting. The water has either not been pumped out or is flowing into the borehole so quickly that pumping is ineffective (in which case the contractor should, but may not, change to an alternate method of construction, possibly the wet method). The water mixes with or leaches the cement out of the concrete and forms potential defects that can be investigated as per Figure 2a plus CD (drilling down to just above the location of the suspected defective zone and coring through that zone). Unless copious amounts of water have mixed with the concrete, however, this defect will be difficult to detect. Similar problems can occur when concreting under a drilling fluid when either the tremie or pump line is inadvertently lifted above the surface of the fluid concrete. LST is not effective unless cement leaching is nearly complete or there is a significant length of degraded concrete over a large part of the cross section (>30 percent).

In Figure 2d the contractor has constructed the shaft out of position, inadvertently on a slight batter, and perhaps too short, yet the reinforcing cage was placed in the proper position (centered on the load). This leads both to inadequate concrete cover on the rebar and eccentric loading of the concrete. In general, drilled-shaft contractors can place shafts so that the center of the excavation is within 3 in. (75 mm) of the planned position and is vertical to within 2 percent. The effect of this tolerance should be analyzed by the designer (for example, by using computer solutions to assess the effects of combined axial and lateral loads resulting from the eccentric load) to determine whether shafts this far out of position (or farther) are satisfactory structurally. It is obvious that if the shaft is small in diameter, these tolerances can result in a load being applied outside the Kern point. Even though this problem is categorized as a construction problem, the designer can mitigate its effect by designing reinforcing cages with at least 6 in. (150 mm) of cover, to allow the cage to be translated 3 in. (75 mm) within the excavation while still leaving 3 in. (75 mm) of actual cover. If necessary, the designer can specify the shaft diameter slightly larger than is necessary from a structural column or geotechnical capacity perspective to accommodate the tolerance. The only aspect of this problem that can be assessed by current integrity testing methods is shaft length, which can be determined by LST, HST, or CD. Possible omission or undersizing of a bell is a related error. Short shafts or undersized bells, if thought to be systematic, can be evaluated by static or dynamic QSLT. It is often possible to locate a bell with LST, but it is difficult to ascertain whether the bell has been cut to the correct diameter.

The defect in Figure 2e occurred after the shaft was successfully installed but while the concrete was still wet, or green. Perhaps mudwaves in the crustal soil were produced when the contractor moved the drilling or concreting equipment. The incidence of this defect is usually indicated through optical survey techniques (lateral displacement of the shaft head) and confirmed by near-surface EVI. Such a defect is almost always avoidable by using short sections of permanent casing to protect the shaft head or by using long-bridge crane attachments in placing shafts.

Defects Arising from Drilling Problems

Common defects produced by drilling are shown in Figure 3. In Figure 3a the contractor is constructing the shaft using the dry method. Cuttings are smeared on the inside face of the borehole as the drilling tool (auger or bucket) is extracted. The problem, common when drilling in clay-shale and mudstone, will virtually destroy side resistance if not corrected. The resulting defect is detectable by EVI, HST, and QSLT. Prevention is achieved by using side cutters on the auger or spiral rougheners on buckets to scrape the loose material off the sides of the borehole before concreting.

Figure 3b shows the general problem of sloughing of soil during concreting in the dry construction method. Sloughing may be an unavoidable natural phenomenon that must be dealt with through the use of casing or drilling fluid, or it may occur through contractor's actions such as developing suction pressures beneath drilling tools, destabilizing the borehole wall, creating stress waves in quasi-stable soil (e.g., clayey or silty sands) by placing concrete by free fall. Intrusion of surface material is a relatively common defect that is preventable with the use of temporary surface casing. Sloughing of the bell may occur where seams or layers of granular soil are present in otherwise stable clays or if the clay being excavated is heavily fissured or slickensided. The practice of making test excavations before finalizing the design will help to identify situations where sloughing may exist. Sloughed cohesive material encapsulated within the concrete is detectable by most integrity testing methods, although it must usually cover at least 25 percent of the cross-sectional area of the shaft to be detected by LST or HST techniques.

A simple drilling error has been made in Figure 3c. The excavation was drilled with a tapered auger, but the contractor did not use a flat-bottomed tool to remove the cuttings from the conical base. As a result, the cuttings are trapped on the

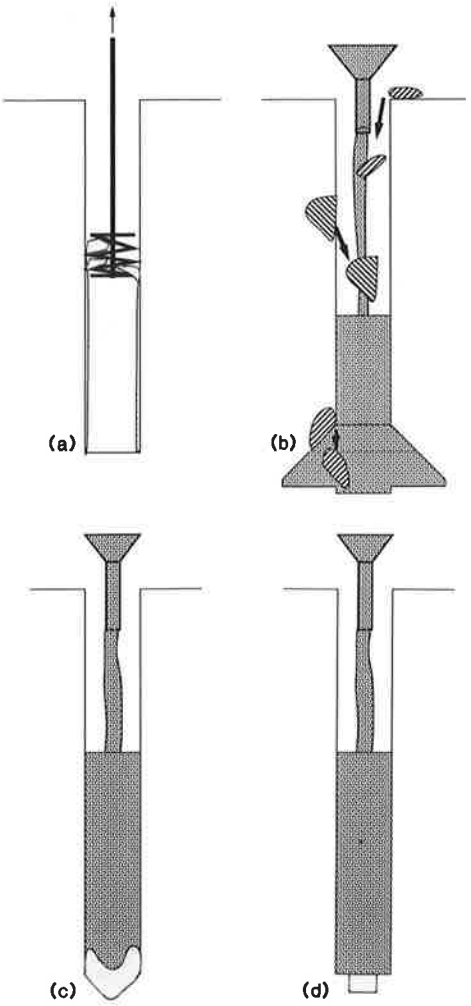

FIGURE 3 Drilling problems and consequences.

bottom as the concrete is placed, which could be a serious defect if the shaft carries a significant amount of its load through base resistance. CD and HST are the most effective means to infer such a defect, although EVI has been used where the shaft is shallow and has not been loaded (or where the load can be removed from the shaft). Other examples of ineffective cleanout can be envisioned; one is shown in Figure 3d. If the contractor does not have drilling equipment powerful enough to excavate a large-diameter borehole in soft rock, he or she may drill a pilot hole with a smaller tool and then "ream" the hole using an overreaming tool that is not capable of excavating down to the base of the pilot hole, which is not cleaned and remains full of cuttings. A similar problem can occur when the borehole is drilled properly but cleaned with a bucket or pan that is smaller in diameter than the borehole. As with the defect in Figure 3c, CD and HST are most effective in detecting this type of defect.

Defects Arising from Casing Management Problems

In the experience of the author, more defects have occurred from the use of temporary casing than from any other cause. A common defect produced by using casing that is excessively rough on the inside or by waiting until excessive concrete slump loss has occurred before extracting the casing is depicted in Figure 4a. Shearing stresses sufficient to lift the column of concrete have developed between the steel and concrete, which causes the concrete column inside the casing to rise and place tension on the concrete just below the original elevation of the bottom of the casing, causing a "neck," with the space previously occupied by the concrete becoming filled with soil or groundwater. Small voids may also form around the rebar if the slump loss is excessive as the concrete level rises. At times, instead of forming a neck, the concrete may completely separate, forming a total discontinuity across the shaft. Upward movement of the concrete or rebar cage is the best indication of a potential defect of this type, which can best be investigated after construction by LST, HST, UST, or GL. Large necks and complete separations are relatively easy to identify with all of these procedures; however, small necks confined to the area outside the rebar cage may not be detectable by any but the GL method.

In Figure 4b the concrete actually set within the casing before the contractor could extract it, and the casing has been left in the hole. Because the casing is normally placed in a slightly oversized borehole, it may not be possible to ensure intimate contact between the casing and soil, and much side

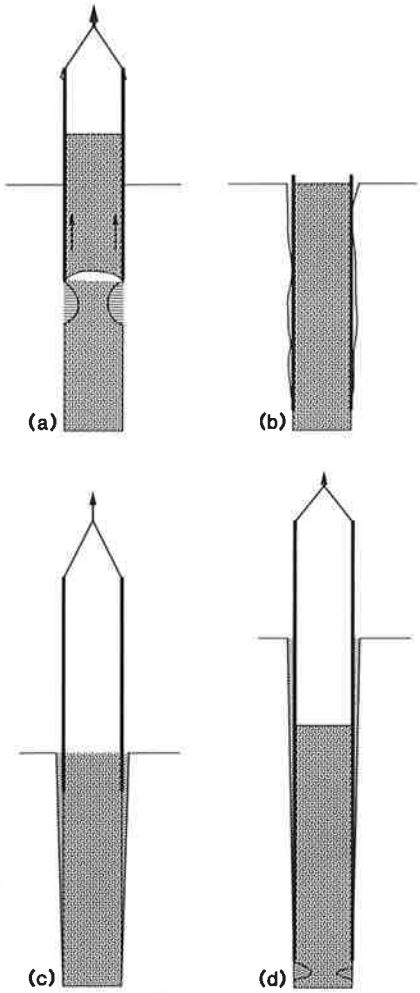

FIGURE 4 Common casing problems.

resistance may be lost within the cased zone (*4*). Even if the casing has been vibrated into position and intimate contact exists between casing and soil, the side resistance may still be less than that used in design because shearing resistance between steel and soil may be less than that assumed in design between concrete and soil. HST and QSLT are currently the only effective means to evaluate the effects of a defect of this nature. A related defect is shown in Figure 4c. The concrete has not bonded to the casing, but either the slump loss is so severe or the initial slump so low that concrete does not flow into the annular space between the casing and the borehole wall to displace groundwater or loosened soil. The consequences of this defect and means of evaluation are identical to those for the defect in Figure 4b. It should be obvious that the defect would be exacerbated by vibrating the concrete, which would fold trapped groundwater into the column of concrete, thereby spreading the defect into the interior of the shaft.

Failure to maintain fluid head within the column of concrete in the casing can also produce defects similar to that shown in Figure 4d. Here, the slurry used to drill the borehole initially has its head at the ground surface, but the concrete head is considerably below the ground surface when the contractor breaks the casing seal and begins removing the casing. Because there can be significant head losses as the concrete begins to flow downward, outward, and into the annular space, the pressure in the slurry can actually exceed that of the fluid concrete at the base of the casing, producing a neck of slurry or promoting mixing of the slurry with the concrete. This type of defect can sometimes be found by LST, HST, UST, or GL, and, if serious mixing with the concrete occurs, by CD (drilling down to the level of the suspected defect, at the elevation of the base of the temporary casing, then coring through the potential defect zone). This defect can also be caused by failure to balance fluid concrete pressure within the casing with external groundwater pressure, which can be a particularly severe problem (but easily solvable by using casing extensions) if the groundwater pressure is artesian. In any event, use of dense concrete and maintenance of concrete head above the groundwater or drilling fluid head should be sufficient to prevent this defect.

Some less common defects associated with casing management are shown in Figure 5. In some geologic settings, telescoping casing is used. In Figure 5a, the outer casing is placed through overburden soil, and the inner casing is placed into decomposed rock. The designer has called for high end bearing stresses and has required the inner casing so the base of the shaft can be dried out, cleaned, and inspected down-hole. Groundwater accumulates in the overlap zone between the two casings. The contractor places concrete to near the top of the inner casing (slightly above the level of the standing groundwater) and slowly extracts the casing, allowing the fluid concrete to flush the standing groundwater up between the two casings. If the inner casing is too short or the contractor overpours the inner casing, the free groundwater will become trapped outside the rebar cage or may become mixed with the fluid concrete. This defect can be difficult to detect, but UST, GL, or CD may reveal the defect if voids are large or if enough water has mixed with the concrete. HST is not a viable option because the shaft needs to be driven with a permanent set for proper evaluation, and it is presumed that

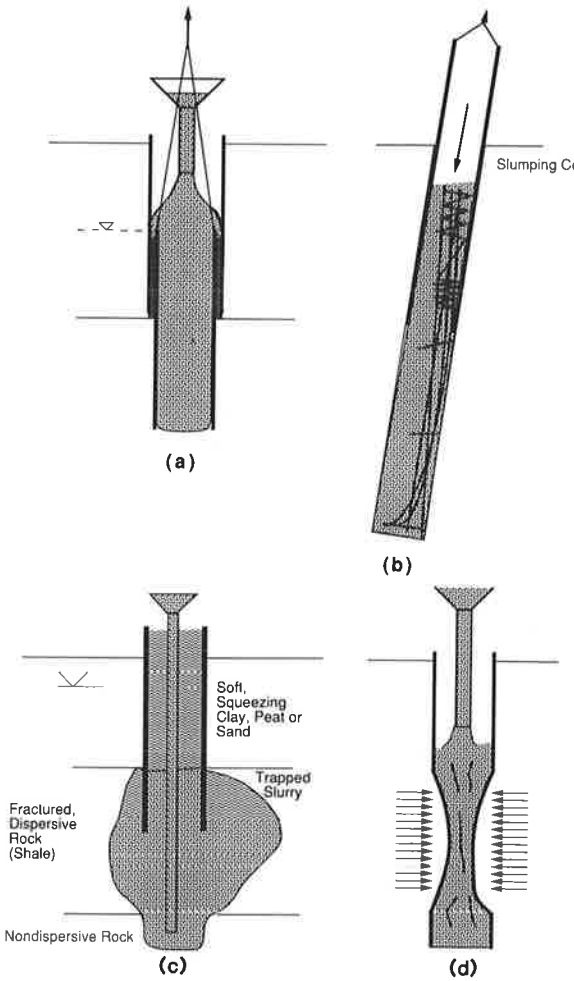

FIGURE 5 Less common casing problems.

the rock at the base is too strong to permit driving the shaft with a permanent set.

In Figure 5b the shaft has been constructed on a batter, but the cage becomes caught on some object inside the casing (joint, caked concrete, etc.), which, along with the downward-moving concrete, causes torsional buckling of the cage. The only viable integrity test for this condition is observation of the movement of the steel during construction. It should be immediately obvious to an experienced construction inspector that cage buckling has occurred. An unusual, but possible, condition is shown in Figure 5c. A contractor has pushed or driven casing through a soft surficial deposit into a fractured shale formation. In order to excavate through the water-bearing shale to an underlying rock formation, the contractor uses either water or slurry to balance the water pressures in the shale. However, many shales and related geologic materials are dispersive, and if appropriate additives are not used in the drilling fluid, the condition shown in the figure may develop. When the concrete is placed (underwater, through a tremie), it cannot flow up behind the casing to the ground surface because the soft surficial soil is impinging tightly against the casing. The trapped slurry is under pressure and may fold back into the concrete within the planned volume of the shaft as the casing is removed further. LST methods can determine

whether an enlarged zone has developed, inferring a defect. UST, GL, and CD methods are effective in detecting whether the fluid has folded back into the concrete in the area of the shaft.

Not to be overlooked is the problem of collapse of casing due to high lateral ground or unbalanced water pressures, particularly when the casing is evacuated (see Figure 5d). Such problems most frequently occur in drilled shafts of 48-in. (1.2-m) diameter or less if casings with wall thicknesses of less than 0.50 in. (12.7 mm) are used. For casings of larger diameter, higher wall thicknesses are frequently necessary. If the casing is long and designed to be left in the hole, it is possible that a collapse near the bottom of the casing will go undetected during the construction process. If the casing is to be withdrawn during concreting, it may not be possible to do so. The resulting structural defect is obviously potentially serious, even if no side resistance is employed in the design. The proper approach to uncovering a defect of this type is to caliper or otherwise determine the diameter of the inside of the casing before placing concrete, although a severe collapse will normally be detectable after concreting by LST and HST, because the resulting neck will result in reflection of energy in the form of tension waves to surface receivers.

Defects Arising from Slurry Management Problems

Underwater construction of drilled shafts has become relatively common during the past 20 years. Often, drilling slurries consisting of bentonite, attapulgite, or polymers are used in lieu of casing to maintain borehole stability during drilling and concreting. Figures 6 and 7 show several defects that can be produced by inattention to construction details. In Figure 6 are shown three situations in which soil (usually sand or silt) in the drilling slurry is not handled properly. In Figure 6a either the base of the shaft excavation has not been cleaned properly (with a cleanout bucket or pan the same diameter as the borehole, a submersible pump, or an air lift), or there is a delay in placing the cage and tremie that has allowed granular material in temporary suspension to settle to the bottom of the slurry column. When the concrete is placed through the tremie (or pump line), the material that has settled from the slurry is pushed to the side, forming a bullet-shaped shaft base, reducing base capacity. In Figure 6b the initial surge of concrete from the tremie has fortuitously caused the concrete to flow under the settled material and float it out. Unfortunately, as the settled material rises it may become loosely attached to the rebar or the side of the borehole and not be fully displaced by the fluid concrete.

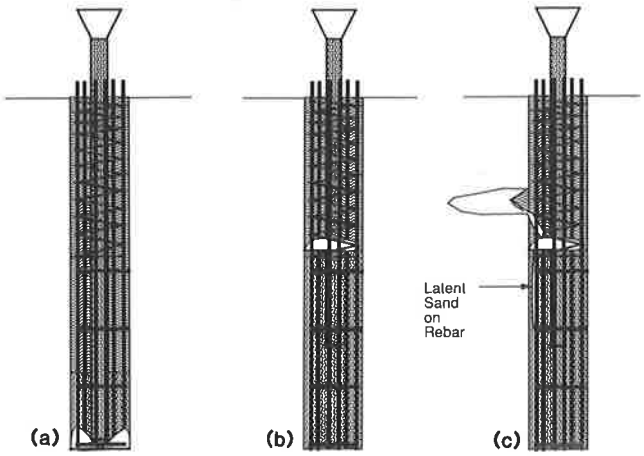

FIGURE 6 Common slurry problems.

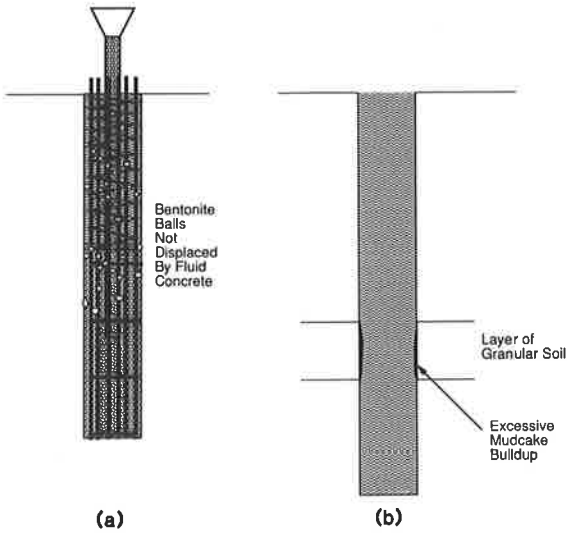

FIGURE 7 Slurry problems associated with improper slurry handling.

The same effect can also occur even if the base is clean at the time of setting the tremie when the slurry is carrying a sand or silt content that is too high to be held in permanent suspension and allows the suspended material to settle on the top of the rising column of concrete. Recent occurrences of this effect have been observed with polymer slurry, which normally does not suspend sand. Either the contractor did not allow sufficient time for the sand in suspension to settle to the base of the shaft, where it could be removed, or the polymer itself had been precipitated by free calcium, which encapsulates sand and silt particles, forming a fluffy, viscous conglomerate often described as "oatmeal." (If such material forms, it can be removed by standard cleanout techniques if it is identified before concreting.)

A related defect is depicted in Figure 6c. In this case the cleanout procedure is correct, and the slurry has been desanded and desilted. However, the drilling operation produced an undercut zone in a granular soil stratum (for example, by sucking the soil into the hole as a result of excavating the hole too quickly or not using pressure relief devices on the drilling tools), allowing sloughing of soil down onto the rising concrete column. When layers of granular soil become undercut, slurry, even with well-developed filter cake, may not be able to ensure hole stability. A similar situation may arise even if the granular stratum is not undercut but is loose and contains no bonding agent, such as clay. (Sloughing can be prevented by weighting the slurry with agents such as barium sulfate.) HST and CD are usually the most effective methods to evaluate a "mushy base" defect (Figure 6a). LST methods normally do not distinguish between the natural materials below the base and loose materials that have settled from the slurry. QSLT can be used if the defect is thought to

be systematic. The defects produced by the practices shown in Figures 6b and 6c can be difficult to detect with any of the methods discussed here, although EVI, with chipping of the concrete to expose the rebar, may be useful where appropriate. In the past, some problems of this type have been uncovered by merely wiggling the longitudinal rebar manually because the coating of granular soil prevents it from bonding to the concrete.

The defects implied in Figures 7a and 7b can occur when a contractor is inexperienced in slurry construction. In Figure 7a the contractor has attempted to mix mineral slurry (bentonite or attapulgite) with water in the borehole. Not all of the solids hydrate, resulting in small balls of unhydrated material that float in the slurry and can become entrapped in the rebar or against the side of the borehole during concreting. This defect is virtually impossible to detect except by EVI. A more subtle problem occurs in Figure 7b. Mineral slurries tend to form a filter cake on the side of the borehole in granular strata (*5*). These cakes tend to become thicker with time, as a result of both filtration (loss of drilling fluid into the stratum) and thixotropy. Leaving mineral slurry in the borehole for more than a few hours without agitation can result in cakes so thick that they cannot be displaced by the upward flow of concrete, resulting in a loss of side resistance. This problem can also occur when casing is used because the cakes can also form from the slurry standing in the annular zone between the casing and the borehole wall. Whereas prevention is straightforward (continual agitation of the slurry or "overreaming" of the borehole before concreting), detection of the defect can be difficult. EVI can be used if the granular material is near the surface, and HST can be effective if the granular layer is deep and the shaft can be driven with a set. LST can possibly provide an indication of the defect if it has significant length and the cake is present around the circumference of the shaft. For example, the measured waveform on a pulse-echo test may be almost perfectly flat in the time interval representing the length of shaft coated thoroughly with a mudcake. Were it not coated, some small wave activity would normally exist as a result of the impedance afforded by the development of shearing resistance between the concrete and the undisturbed soil or rock. Such an interpretation should not be attempted at present, however, without concurrent low-strain wave equation modelling of the phenomenon.

Other miscellaneous defects associated with slurry construction are shown in Figure 8. A slurry-filled (or possibly water-filled) borehole has been excavated into a karstic limestone in Figure 8a. A large, submerged cavity is bridged by debris, such that during concreting the column of fluid concrete rises past the cavity; however, as the column of concrete rises farther, pressure from the column causes it to break though the debris, and the concrete, being heavier than water, is thrust into the cavity. This action allows the concrete level in the shaft to fall, possibly producing small voids around the rebar, and forces the water in the cavity back into the area of the shaft, potentially mixing with the concrete or leaching the cement out of the concrete. Any method that is capable of identifying low-modulus concrete, such as UST, GL, or possibly LST, will be helpful in evaluating the defect. LST can also be used to identify the vertical extent of the affected zone if the bulge is sharp.

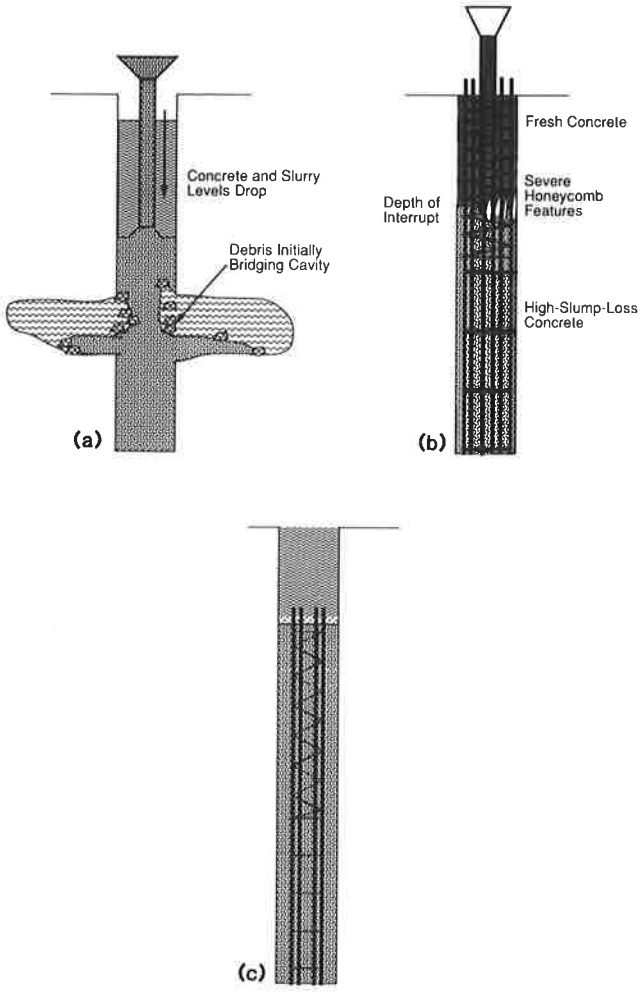

FIGURE 8 Other slurry problems.

A problem associated as much with concrete management as with slurry management is illustrated in Figure 8b. Concrete placement in the wet method of construction should be continuous. When the flow of concrete to the shaft head is interrupted for a significant period of time, it may be necessary for the contractor to remove the tremie or pump line from the column of concrete to avoid having it captured by the setting concrete. When fresh concrete arrives, the contractor may place the tremie or pump line back into the concrete column and try to reestablish flow per the procedure used to initiate flow from the base of the borehole. This process may thrust the upper portion of the old, stiffer concrete (and perhaps sand that has settled out of the slurry during the delay) outward and through the rebar. If slump loss in the old concrete is too great, it may not flow though the rebar properly, producing honeycombing. If the interrupt is near the surface, EVI is the most appropriate integrity test. GL can be useful if the voids are near the access tube. UST is only of use if the voids are large and extend into the interior of the cage.

In Figure 8c the shaft has been drilled and concreted properly, but plans call for cutoff below grade to accommodate future construction operations. This must either result in a cold joint below grade when the shaft is concreted, or the contractor must pour the concrete to grade and chip away the

excess later. If there is to be a cold joint, the contractor must ensure that any debris or contaminated concrete on the surface of the rising column of concrete is removed and sound concrete exposed. (This might be done, for example, by pouring the concrete perhaps 0.5 m above the joint, placing a liner in the borehole well down into the unset concrete, evacuating the slurry from inside the liner, and cleaning the joint, by hand or remotely, before the concrete sets.) A defect will ensue if the joint is not properly constructed. Such a defect, if investigated after placement of concrete above the joint, can often be detected by CD, EVI, or LST.

Defects Resulting from Design Deficiencies

Not all defects are caused by workmanship errors on the part of the contractor. For example, the practice still exists in some organizations to use drilled shafts to replace driven piles on a one-for-one basis. This can lead to shafts that are long and slender yet have high percentages of reinforcing steel (required to resist lateral loading in a cross-section with a low moment of inertia). (See Figure 9a.) Shafts designed to be 18 in. (0.46 m) in diameter or less make it difficult to clean the base and for concrete to flow freely through and around the reinforcing steel cage. Voids in the zone outside the cage are possible even with high-slump concrete. Some agencies, in anticipation of such problems, place access tubes in the shafts for GL or UST tests, which leaves even less room for the flow of concrete and makes the problem even more acute. This sort of design defect is preventable if shafts are designed with diameters no less than about 0.75 m and the reinforcing steel arrangement allows for at least 5 in. (125 mm) of space between bars and 6 in. (150 mm) between the bars and the face of the borehole (by bundling bars, if necessary).

Situations arise in which drilled shafts are placed in alluvium or colluvium containing groundwater flowing horizontally at greater than about 1 ft/sec (0.3 m/sec) (Figure 9b). Even with proper construction the cement can be leached from the concrete by the flowing groundwater. In such a case it may be prudent to design the shaft with a permanent casing or liner through the zone of rapid groundwater flow, discounting side resistance in that zone. GL and UST provide the best chance of detecting this type of defect.

Other design-related defects, not shown in Figure 9, include placing bearing stresses on unreinforced bells that are too large, producing tension cracks in the concrete, misinterpreting the strength and compressibility properties of the intended base bearing stratum, specifying an inappropriate concrete mix design (inadequate flow properties; not resistant to leaching, sulfate attack or other environmental factors at the construction site), and gross errors in establishing the cross-section to take lateral or tension loads leading to significant tension cracking. LST methods are sometimes able to distinguish tension cracks in the concrete. Effects of other design errors may become evident only from the ultimate integrity test, distress in the superstructure.

PERSPECTIVE

Although the subject of this paper is defective drilled shafts, most drilled shafts, when designed properly, are constructed as designed and without incident when competent contractors are employed. Sliwinski and Fleming (*6*) reported a study of LST-type integrity tests on 5,000 drilled shafts in the United Kingdom during 1982. That study is summarized in Table 1.

Only about 1 shaft in 200 developed a detectable defect (covering perhaps one-quarter of the cross section) during drilling and concreting. Of these, the vast majority of defects occurred within 5 m of the surface, which would make their inspection by EVI and CD feasible in many instances. Only about 0.1 percent had detectable deep-seated defects that would require more sophisticated investigation techniques.

The present state of the art, however, does not permit the inference of small defects, unless they are fortuitously encountered by cores or happen to develop around access tubes

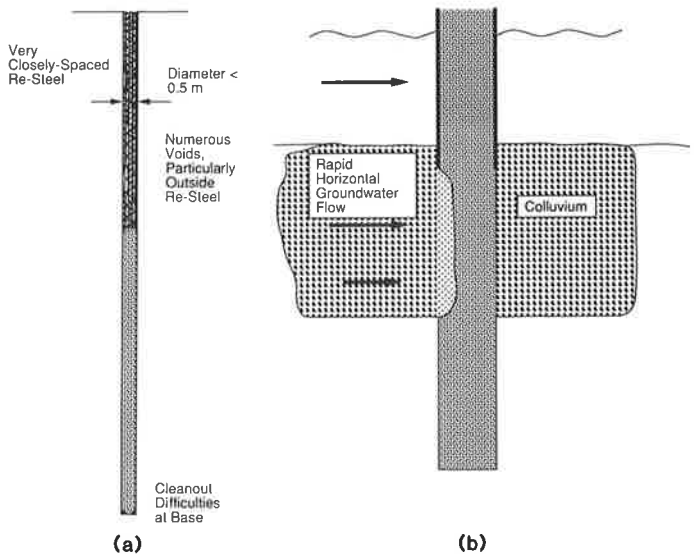

FIGURE 9 Design problems.

TABLE 1 CLASSIFICATION OF DEFECTS IN 5,000 DRILLED SHAFTS CONSTRUCTED IN THE UNITED KINGDOM IN 1982 (*5*)

Type of Defect	No. of Shafts Encountered
Soil contamination in top 2 m	18
Soil contamination or necking for depths of 2 - 5 m	7
Poor quality concrete somewhere along shaft	4
Voids adjacent to shaft with loss of concrete	2
Defects due to trimming top of shafts or to traffic on site	42
Total No. of Defects	73 (1.5%)
Total No. of Defects Excluding Post-Construction Trimming and Damage from Traffic	31 (0.6%)

for GL tests or UST, or are uncovered by meticulous EVI. Despite advances in the state of the art of nondestructive evaluation of drilled shaft integrity, it is important that construction defects be minimized and critical that they be essentially eliminated on drilled shaft foundations that afford no redundancy. This requires expert and diligent inspection that can only be achieved by teaching drilled-shaft inspectors to be wary of situations, such as those discussed in this paper, that produce defects. The Association of Drilled Shaft Contractors and the Deep Foundations Institute (*7*) and Greer and Gardner (*8*) provide excellent references for training and for use in the field by DOT inspectors.

For an organization, such as a state DOT, that has no record of experience in drilled shaft foundation performance, it is recommended that a nondestructive evaluation scheme be selected and applied to a representative number of drilled shafts on each construction project. Frequency of testing should be dictated by the risk of foundation failure that is acceptable for an individual project. For example, every drilled shaft for single-shaft bents in a major interchange connection (no redundancy), every fifth shaft in a normal bent or abutment in a major bridge, or the first drilled shaft constructed on a minor structure might be tested routinely. A policy of testing shafts nonroutinely in which inspectors observe evidence of the potential defects discussed here should also be implemented. As the confidence level in an organization grows, routine tests could be conducted less frequently. One possible routine testing scheme would be to use LST, possibly in a form suitable for detecting near-surface defects, followed by CD when potential defects are indicated. Nonroutine tests could encompass any or all of the methods described here, depending on the nature of the suspected defect.

SUMMARY

A number of relatively common situations that produce defects in drilled shafts have been identified, and general methods that may be appropriate for investigating those defects, illustrated in Figures 2–9, have been suggested. Other defects are possible, as are other integrity testing methods. At present, no definitive method or combination of methods can be recommended for detecting all defects. The subject remains an important research topic.

REFERENCES

1. C. N. Baker, Jr. and F. Khan. Caisson Construction Problems and Corrections in Chicago. *Journal of the Soil Mechanics and Foundations Division,* ASCE, Vol. 97, No. SM2, February 1971, pp. 417–440.
2. L. C. Reese and M. W. O'Neill. *Drilled Shafts: Construction Procedures and Design Methods.* Report FHWA-HI-88-042. FHWA, U.S. Department of Transportation, 1988.
3. L. C. Reese and S. J. Wright. *Drilled Shaft Manual: Vol. I: Construction Procedures and Design for Axial Loading.* Report IP 77-21. FHWA, U. S. Department of Transportation, 1977.
4. M. J. Owens and L. C. Reese. *The Influence of a Steel Casing on the Axial Capacity of a Drilled Shaft.* Research Report 255-1F. Center for Transportation Research, University of Texas at Austin, 1982, 204 pp.
5. L. C. Reese and K. L. Tucker. Bentonitic Slurry in Constructing Drilled Piers. In *Drilled Piers and Caissons II* (C. N. Baker, Jr., ed.), ASCE, 1985, pp. 1–15.
6. Z. J. Sliwinski and W. G. K. Fleming. The Integrity and Performance of Bored Piles. In *Piling and Ground Treatment for Foundations,* Thomas Telford, London, England, 1983, pp. 153–165.
7. *Drilled Shaft Inspector's Manual.* Association of Drilled Shaft Contractors, International Association of Foundation Drilling, and Deep Foundations Institute, 1989.
8. D. M. Greer and W. S. Gardner. *Construction of Drilled Pier Foundations.* Wiley-Interscience, New York, N.Y., 1986.

Development of Nondestructive Small-Strain Methods for Testing Deep Foundations: A Review

ALLEN G. DAVIS AND BERNARD H. HERTLEIN

The first small-strain integrity tests applied to drilled shafts were made in France in 1964. Early tests were limited by the size, slowness, and cost of the available electronics, as well as the variety of geotechnical conditions and construction methods encountered. The various methods and their progress during the past 25 years are reviewed, and their strengths and weaknesses are outlined as an aid to selecting the most appropriate technique for a given set of circumstances. In addition, ideas are proposed for test development and integration in the U.S. market for the near future.

Nearly a quarter of a century has elapsed since the first practical attempts were made using nondestructive test (NDT) methods to assess the quality of piles, drilled shafts, and slurry trench walls after installation.

Discussed here are the origins and development of the techniques commonly used today, as well as how they were influenced by their local engineering environment. Also presented are views of the trends appearing in 1990 in the development of existing and new methods, and improvements in analysis and in the integration of these techniques in contractual matters.

HISTORICAL REVIEW

Progress was made in the 1960s in developing ultrasonic pulse velocity equipment for testing concrete quality. The basic principle is that the velocity of an ultrasonic pulse through concrete is directly proportional to the Young's modulus and density of the concrete (which happen to be interactive variables). Research demonstrated that increasing pulse frequency tended to reduce the effective pulse path length through the concrete.

Nearly all NDT small-strain pile-testing methods in use today apply the principle of the transmission of ultrasonic pulses or acoustic (sonic) waves through pile materials such as concrete, wood, and steel. An exception is nuclear gamma ray transmission, or back scattering, which receives limited application.

Three main techniques form the basis of all the methods developed since 1965: ultrasonic pulse transmission, acoustic wave reflection, and impedance/mobility measurement.

A. G. Davis, Testconsult CEBTP Ltd., 11-12 Trinity Court, Risley, Warrington, England WA3 6QT. B. H. Hertlein, ESSI-Testconsult, Suite 306D, 31 College Place, Asheville, N.C. 28801.

The first two techniques rely on the measurement of wave velocity, whereas the third requires the added measurement of force needed to generate the wave velocity. These methods are described using different names and are categorized respectively by technique: sonic or ultrasonic logging, sonic coring; echo, seismic, sonic or acoustic wave; and vibration, impedance, shock, transient dynamic response, mobility. The three base techniques are referred to here as sonic logging, echo, and impedance.

The development of NDT techniques 25 years ago was influenced in different countries by the nature of the piling market in each country and the limitations of existing electronics technology.

For example, early French workers in this field (*1*,*2*) were influenced by the high proportion of drilled shafts constructed in their country, as opposed to driven precast piles. Paquet (*1*) considered the echo method as a possibility, but suggested that (in 1968) it was not as informative as the impedance test for drilled shafts because of their often irregular profiles.

Briard (*2*) continues this reasoning by describing the application in France of sonic logging and impedance testing only, with limited reference to echo testing.

On the other hand, the prevalence of precast concrete driven piles in Holland meant that the echo tests could be used and developed with greater confidence because of the straight-sided shafts (*3*). Development of this method was emphasized by the Dutch during the 1970s.

The United Kingdom followed the early work in France by applying both sonic logging and impedance testing (*4*–*9*) to drilled shafts, driven cast-in-place piles, and slurry trench walls. This culminated in an important document for the United Kingdom piling industry in which available NDT methods were described (*10*).

Because of this early work in France, Holland, and the United Kingdom, type specifications began to appear that defined procedures for using these tests as quality control tools for new piling construction, as opposed to "pathological" studies of problems noticed during or after construction.

Currently, more than 95 percent of integrity tests on drilled shafts and piles in the United Kingdom and France are performed for quality control. The number of piles tested in this way is still growing, with present annual test rates in the United Kingdom alone at more than 20,000.

Many developments have occurred in electronics during the last 25 years, with more versatile and compact testing equipment as a result and a corresponding increase in the testing

rate. A good example is the evolution of impedance testing equipment; the original method using a pile head vibrator (*7*) needed unrealistic pile head preparation, weighed up to 1,000 lb (450 kg), and was powered by generator or main feed electricity. The arrival of small microprocessors 15 years ago enabled Paquet's theory (*1*) of the application of Fast Fourier Transform to a single blow to become feasible, with more compact equipment as a result (*11*).

Present day impedance testing equipment, such as the MIMP 15 from France, weighs as little as 33 lb (15 kg), is battery powered, fully portable, and can store all data on floppy disk (Figure 1). Instead of 10 to 12 piles per day, testing rates in excess of 100 piles per day can be achieved.

Despite these developments in Europe and the availability of various NDT methods in North America, use of NDT by the piling industry in the United States is still at the exploratory/case study stage. Specifying NDT at the design stage is rare in the United States, and it is pertinent to examine the reasons why.

NORTH AMERICAN CONTEXT

North America is a vast area with a diverse piling market. Many pile and drilled shaft construction methods are used, with sizes ranging from 6-in. diameter micropiles to caissons with diameters greater than 10 ft. Regional preferences for different pile types and construction methods are prevalent, often controlled by local soil conditions, engineering experience, and building codes developed over the years in different regional centers.

FIGURE 1 MIMP 15 integrity testing equipment with transducers shown on pile.

As a result, quality control practice often varies slightly from region to region, but usually is based on close visual inspection during the construction phase and on concrete strengths. No general type specifications are approved by regulatory bodies for quality control with the aid of NDT techniques, although such specifications have been included by engineers in specific contracts.

This pragmatic, deductive approach means that nearly all practicing engineers and regulatory bodies remain to be convinced that NDT methods as currently offered will contribute efficiently to the quality control process, without adding a significant extra cost burden. The fact that these methods are now used regularly in Europe for this purpose is not sufficient in itself.

One major reason for this reticence is the lack of Class A studies to prove the claims made by proponents of the different NDT methods. A Class A study would require construction of deep foundations with carefully controlled defects whose position and size are unknown to the testing teams, followed by assessment of the test results and conclusions by an independent authority.

The only real documented Class A study is reported by Levy (*4*) on behalf of the Greater London Council, England. Drilled shafts with controlled defects were built to test the capability of the sonic logging method.

Other full-scale tests have been performed, but none have reached the stringent control requirements of Class A studies. Examples are the construction of 26 drilled shafts near Newcastle, England (*12*), with preformed faults; the nature and position of the defects and pile lengths were known to participants before testing. Similarly, a series of tests organized by FHWA in San Jose (*13*) allowed knowledge of fault-position and pile length to the testing groups.

One other study with careful control was carried out in Ghent, Belgium (*14*), where shafts contained no defects but shaft length was not given to participants before testing.

Confidence in these methods can only be obtained by (a) a good understanding of the principles and the limitations of the method, (b) an ensuing belief that the test results can be used contractually to help in the acceptance or otherwise of pile foundations, and (c) the elimination of as much subjective test interpretation as possible.

NEW TESTING TRENDS

A clear distinction is emerging between tests that use cross-hole techniques, such as sonic logging, and methods that excite the pile at the head only, such as acoustic wave reflection and impedance testing.

The former is considered to be the most suitable for measurement of the concrete integrity of the total length of large diameter drilled shafts because signal damping problems do not occur as they can in the head-excitation methods.

Present-day equipment allows continuous readings to be obtained of the total pile shaft, regardless of length, and shafts up to 90-m (300-ft) long have been tested. Figure 2 shows results from a sound shaft and a defective shaft with an anomaly at 18 m (59 ft.) below shaft head, approximately 8-in.

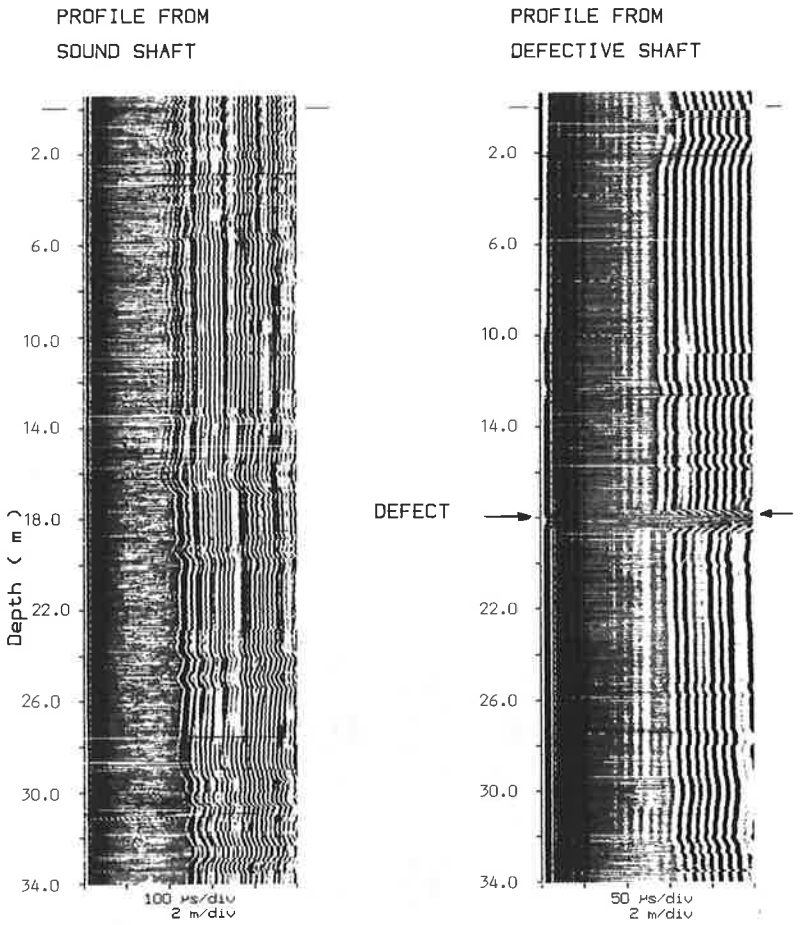

FIGURE 2 Example of sonic logging trace.

(200-mm) thick. This indicates the presence of an inclusion or necking in the pulse path between the two tubes. Bulges outside the normal pile shaft perimeter cannot be detected by this method.

A trend is appearing now for a combination of the two methods when conditions are suitable for acoustic wave reflection and impedance methods. This is made possible by recent developments in data sampling, acquisition, and storage, as well as improved filtering techniques. New equipment can sample both wave reflection and impedance properties of tested shafts.

Measurements of force and velocity response are stored as time base data, with a wide band pass filter and rapid sampling. Resolution of both weak and strong response levels are thus favored.

The time-base response, referred to as a reflectogram, can be amplified exponentially to compensate for damping of the signal toward the shaft base.

The impedance (frequency domain) analysis gives the shaft dynamic stiffness and characteristic mobility, and confirms shaft length. In addition, simulation of the shaft and its surrounding soil can be carried out most efficiently in the frequency domain (*7*). Figure 3 shows a typical reflectogram record with the corresponding real pile data. The reflectogram and the characteristic mobility of the shaft can then be combined to produce a trace referred to as the impedance log (Figure 4).

The output of this analysis is in the form of a vertical section through the shaft, giving a calculated visual representation of the pile shape. The accuracy of this pictorial display is influenced by the signal quality obtained, which in turn is influenced by the quality of the striking surface (hard concrete with no cracking) and operator technique, as well as occasional problems like reinforcement bar "ringing." However, with correct pile head preparation and operator training, the impedance log method can form the basis of a greatly improved shaft-head response method, with the added advantage of a direct visual image of the pile shaft, which is helpful to lay engineers responsible for decisions in pile quality control.

FUTURE DEVELOPMENT

A most important development is understanding the potential of integrity testing as a quality control tool instead of a last resort to assess known problems.

A noticeable effect of integrity testing in Europe has been improvement in construction methods and practices as certain types of problems have been encountered repeatedly. Several large engineering and contracting groups regularly use the methods, not only for in-house quality control, but as research tools to develop more efficient or reliable construction systems.

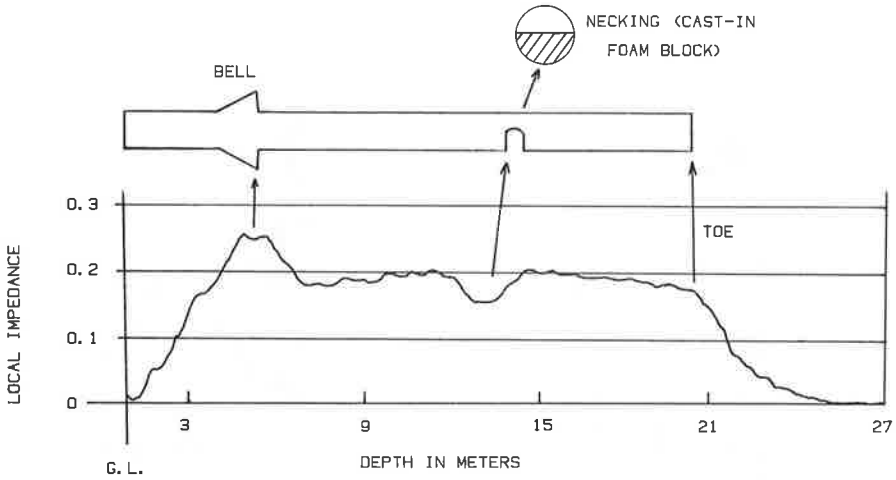

FIGURE 3 Example of reflectogram (for Shaft D, San Jose) and real pile shape.

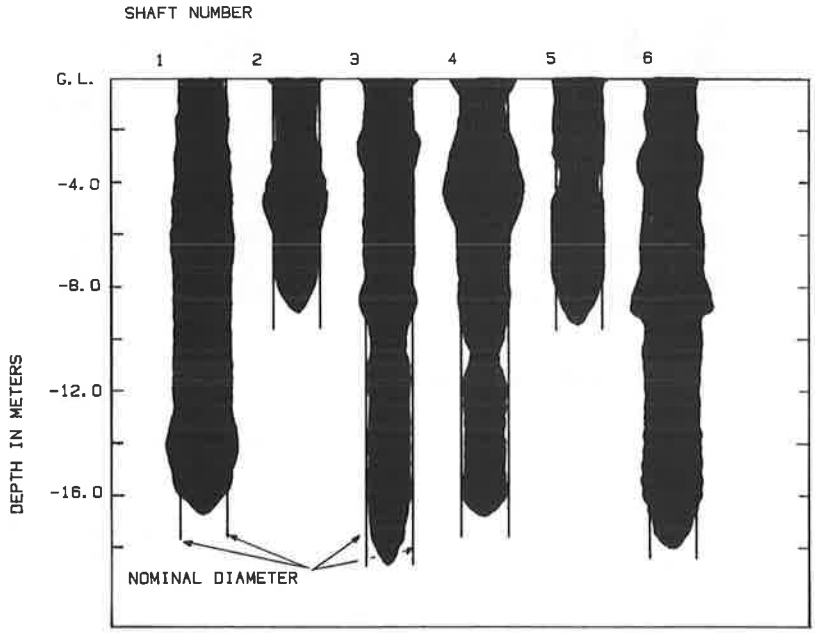

FIGURE 4 Examples of impedance log results.

This is starting to become the case in the United States. However, many engineers and contractors still do not accept the methods as reliable or are awaiting some form of specification from regulatory bodies. They are therefore reluctant to use integrity testing.

For the industry to benefit from the results of integrity testing, it is important that organizations such as FHWA, ASTM, and the Deep Foundations Institute assess and evaluate the methods and endorse those that they find to be effective and reliable or instigate research on those that show promise of fulfilling a quality assurance need.

Impedance Tests

Although the theory of analysis for impedance response curves is well established and confirmed by extensive site experience, there is still room for subjective error, particularly on complex, multiple resonances. Research is continuing in this area, with the ultimate aim of achieving an analysis that will automate the interpretation of data and thus eliminate any subjective error.

The impedance log analysis, previously mentioned, combines the advantages of the impact/echo and impedance methods. Its incorporation into the existing impedance system will greatly simplify automation of the analysis and provide the engineer with a pictorial interpretation of the shaft cross section.

Sonic Logging Tests

The continuous-flight augered (CFA) shaft has gained popularity and acceptance in Europe, particularly since the de-

velopment of systems for using concrete instead of grout. The main advantages of this method are low cost, rapid construction, and minimum environmental disturbance from noise or vibration. The method has become popular for urban redevelopment, where noise and vibration are key concerns. Two drawbacks of the system, however, are the difficulty of placing reinforcing steel, and the irregular cross section that can result from pumping concrete into soft soils.

Concerns with CFA first centered on the difficulty of placing the reinforcing steel, then later the inconclusive nature of low-strain integrity test results caused by the irregular section. Researchers are looking at improved methods of steel placement, including the incorporation of access tubes for sonic logging, which will be able to confirm the integrity of the main body of the shaft, regardless of external shape or oversize sections.

The development of more comprehensively instrumented construction rigs, use of concrete, larger diameters, and a reliable integrity test will help the CFA method of construction gain wider acceptance in the United States, particularly for sensitive inner-city redevelopment work.

Load Testing

The European experience has been that if large numbers of test results for a given soil type in a particular geographic location are correlated with static load test data, it is possible to derive a correlation factor, and by applying this to dynamic stiffness measurements, predict caisson behavior under load from low-strain integrity test results (*9,15*). These correlations are so well established that in many European cities, engineers will reduce the number of load tests required if integrity test results fall within certain predefined limits. In London, for example, sites tend to be small and congested. It is common for the borough surveyor to accept caissons with no load tests if integrity test results fit within the now established range for caissons in London clay.

As more test data become available for American cities, similar correlations may be established, and the need for expensive, time-consuming load tests be significantly reduced.

In addition, most foundation calculations include a safety factor to allow for certain potential defects. As integrity testing becomes more widespread, designers may be able to reduce safety factors, in the knowledge that all shafts meet a certain minimum standard, thus making more efficient use of time and materials. This has been accepted practice in France for some years now.

Specification

All forms of integrity testing require a certain amount of preplanning or preparation, some much more than others. For the tests to gain wide acceptance and bring maximum benefit to the industry, it is important that the type of test is selected and allowed for at the design stage. This may help avoid the current Dutch Auction situation, in which the job is often let to the lowest bidder regardless of the bidder's actual capability or experience with the method. Integrity testing should be part of the quality assurance program to avoid choosing the wrong method because of economic pressures.

For this to be done effectively, engineers must be aware of the abilities and limitations of each method and decide what kind of integrity test data they will need for complete assurance of a quality product. This choice will be dictated by construction method, soil conditions, access, and type of loading on the finished caisson. Only when armed with this knowledge can the engineer select the appropriate method and avoid having to make judgments based on inconclusive results.

Miniaturization

Several recent attempts have been made to reduce testing costs by using small portable data recorders and taking results away for later analysis. Two significant arguments against this approach are as follows: (a) if the data are invalid, the test either is void or must be repeated, causing both expense and delay; and (b) time is often at a premium in construction programs, and the delay between testing and analysis can be expensive.

Because of these problems, it is important that data are visualized on site so that a qualified operator can not only judge the validity of the result, but also instantly recognize and report any potential problems or defects. Future development will take advantage of miniaturization, battery-operated systems, and improvements in transducer design, but the ability to visualize data on site at the time of testing must be retained.

CONCLUSION

A wealth of experience already exists overseas with nondestructive small-strain test techniques covering more than 26 years of development and application to deep foundations.

By drawing on this experience and setting up more evaluation programs to take account of regional requirements, the foundation construction industry in the United States can capitalize on the latest developments in this field to establish an acceptable set of techniques that will further enhance quality assurance methods for the industry.

REFERENCES

1. J. Paquet. Etude Vibratoire des Pieux en Beton; Response Harmonique. *Annales Inst. Tech. Batim.*, Vol. 21, No. 245, May 1968, pp. 789–803.
2. M. Briard. Controle des Pieux par la Methode des Vibrations. *Annales Inst. Tech. Batim.*, Vol. 23, No. 270, June 1970, pp. 105–107.
3. T. Whittaker. Structural Integrity of Piles. *Civil Engineering*, Vol. 44, No. 6, June 1974, pp. 20–23.
4. J. F. Levy. Sonic pulse method of testing cast-in-situ piles. *Ground Engineering*, Vol. 3, No. 3, May 1970, pp. 17–19.
5. R. P. M. Gardner and G. W. Moses. Testing Bored Piles Formed in Laminated Clays. *Civil Engineering and Public Works Review*, Vol. 68, Jan. 1973, pp. 60–63.
6. J. Bobrowski, B. K. Bardhan-Roy, R. H. Magiera, and R. H. Lowe. The Structural Integrity of Large Diameter Bored Piles. *Proc., Conference of the Institute of Civil Engineers*, London, Sept. 1975.
7. A. G. Davis and C. S. Dunn. From Theory to Field Experience with the Non-Destructive Vibration Testing of Piles. *Proc., Institute of Civil Engineers*, Part 2, 57, Dec. 1974, pp. 571–593.

8. A. G. Davis and S. A. Robertson. Economic Pile Testing. *Ground Engineering*, Vol. 8, No. 3, May 1975, pp. 40–43.
9. A. G. Davis and S. A. Robertson. Vibration Testing of Piles. *Structural Engineering*, June 1976, pp. A7–A10.
10. A. J. Weltman. *Integrity Testing of Piles: A Review*. Report PG3. Construction Industry Research and Information Association, England, Sept. 1977, 36 pp.
11. J. S. Higgs and S. A. Robertson. Integrity Testing of Concrete Piles by Shock Method. *Concrete*, Vol. 13, No. 10, Oct. 1979, pp. 31–33.
12. D. M. Lilley, W. M. Kilkenny, and R. F. Ackroyd. *Steady State Vibration Testing of Piles with Known Defects*. 3rd Annual Stress Wave Conference, Ottawa, Bi-Tech Publishers, Vancouver, B.C., 1988, pp. 91–98.
13. C. Baker, F. Mensah, and G. Parikh. *Use of Non-Destructive Testing to Evaluate Defects in Drilled Shafts*. Status of FHWA Research. 14th Annual Deep Foundations Institute Conference, Oct. 1989, pp. 189–216.
14. A. E. Holeyman, C. Legrand, E. Lousberg, and A. D'Haenans. *Comparative Dynamic Pile Testing in Belgium*. 3rd International Stress Wave Conference, Ottawa, Bi-Tech Publishers, Vancouver B.C., 1988.
15. R. T. Stain and A. G. Davis. *Non-Destructive Testing of Bored Concrete Piles—Some Case Histories*. NDT-83: 1st Int. Conf. on Non-Destructive Testing, Heathrow London, Vol. 1, Nov. 1983, pp. 77–87.

Comparison of Pulse Echo and Transient Response Pile Integrity Test Methods

FRANK RAUSCHE, SHEN REN-KUNG, AND GARLAND E. LIKINS, JR.

Pile integrity test methods of driven and cast in situ piles have been developed by several researchers using differing equipment and methods. Some methods require expensive special preparations during pile manufacture or installation. Others can be applied to randomly selected piles or to piles selected on the basis of their installation histories. The latter methods are inexpensive, easily applied, and, therefore, routinely applied worldwide. Often, all piles on a site are tested and problem piles are identified for corrective action. These methods, called low-strain tests, use signals from a hand-held hammer striking the pile top, which generates a compressive stress wave in the pile. Stress wave reflections from nonuniformities or the pile toe are observed at the pile top, processed, and interpreted by the experienced test engineer. The pulse echo method records the pile top velocity as a function of time. The transient response method displays the mobility (i.e., the ratio of frequency spectra of pile top velocity to force). How both low-strain methods can be combined into one method yielding an optimal amount of information is demonstrated. Recommendations for test preparation and data analysis are given. It is concluded that the new method contains more information than either previous method alone and recommended that analyses be made in both the frequency and time domains.

Foundation engineers need an inexpensive and quick method for the integrity testing of foundation piles when installation difficulties are expected or problems arise during construction. Both driven piles and drilled shafts may undergo serious damage during construction. When this is suspected, selected or even all piles on a construction site may require evaluation. However, in general, special advance preparations such as the installation of inspection tubes are not economically feasible.

When a concrete pile, either precast and driven or drilled and cast in situ, is struck with a small hammer, a stress wave is generated, which travels down the shaft to the pile bottom, where it is reflected. When the reflected stress wave returns to the pile top, a measurable pile top motion occurs. If this reflection occurs at the correct time and if no other earlier reflection waves are received at the pile top, the pile shaft is probably free of major defects. Using this concept, the low-strain method of dynamic pile testing was developed. In contrast, the high-strain method measures pile top forces and velocities under a large impact hammer. A comparison of high-strain and low-strain results is given elsewhere (*1*).

When a lightweight hand-held hammer strikes the pile top, a small pile top motion (velocity) is generated. The associated pile strains are of such a low magnitude that they would be measured in the pile only with great difficulty. However, the force applied by the hammer can easily be measured by instrumenting the hammer itself. The velocity record and to a lesser degree the force record contain information about the location and magnitude of pile nonuniformities. Under the assumption of proportional force and velocity records (*2*), and for short-duration impact pulses, the velocity record may be sufficient. One of the distinguishing features of the transient response method (TRM) is that it requires the measurement of both velocity and force, whereas the pulse echo method (PEM) relies only on velocity records. A second difference is the display of the TRM results in the frequency domain. PEM offers powerful record enhancement techniques and presents the resulting curves as a function of time.

Both methods have some advantages and have therefore been combined in a third method, referred to as PIT-FV. All three methods are presented. Using records taken on a drilled shaft with a known cross-sectional change, the features of all three methods are demonstrated.

F. Rausche, Goble Rausche Likins and Associates, Inc., 4535 Emery Industrial Parkway, Cleveland, Ohio 44128. R.-K. Shen, Nanjing Hydraulic Research Institute, 34 Hu Ju Guan Road, Nanjing, China 210024. G. E. Likins, Jr., Pile Dynamics, Inc., 4535 Emery Industrial Parkway, Cleveland, Ohio 44128.

STRESS WAVE PROPAGATION IN A PILE

An impact applied to the pile top generates a momentary compression and a particle motion of the pile top surface. The compression is related to the force, F; the motion causes a particle velocity, v. In concrete, the stress wave travels along the pile with a stress wave speed, c, ranging from 10 to 15 ft/msec (3.3 to 5.0 m/msec). As shown by St. Venant (*3*), the stress wave speed in a long slender rod is given by

$$c^2 = E/\rho \tag{1}$$

where E is the pile's elastic modulus and ρ its mass density. The low-strain methods have also been applied to timber piles. Because of the high ratio of surface area to cross-sectional area, steel piles that are not filled with concrete are difficult to test using low-strain methods. Steel piles are more easily tested with impacts of actual pile-driving hammers (high-strain method).

The traveling wave solution to the one-dimensional wave equation has been discussed in detail by St. Venant and many others (*4*). It forms the basis on which interpretation techniques have been founded for both high-strain and low-strain pile test methods. Figure 1 shows, in the form of a time-depth plot, the path of a stress wave in the pile and the arrival times of reflection waves at the pile top. Cross-sectional changes and soil resistance forces both generate reflection waves. The

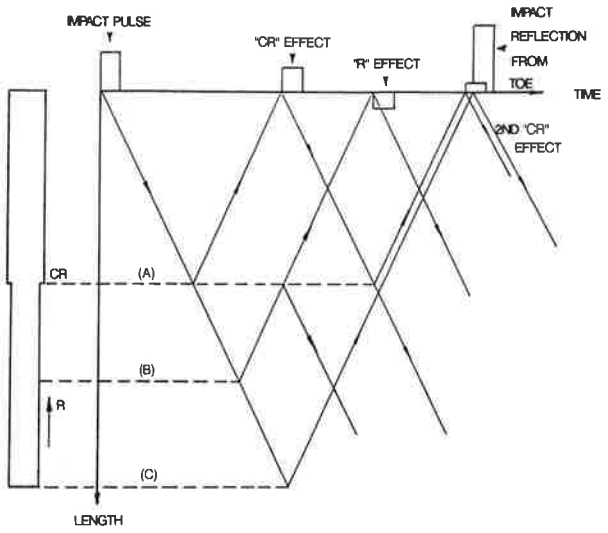

FIGURE 1 Impact pulse and reflections from (A) cross-sectional reduction, CR; (B) shaft resistance, R (modeled velocity proportional); and (C) pile toe.

pile top velocity is affected by and therefore indicates the arrival of both tensile and compressive reflection waves.

PEM

PEM is probably the simplest test method as far as instrumentation and testing effort is concerned. Figure 2 shows the PIT-SC (pile integrity tester—self-contained, so-called because it is battery powered). Important hardware components also include a hand-held hammer with an integral plastic cushion and an accelerometer. The processor shown in Figure 2 provides signal conditioning, digital signal processing, digital signal storage, and, for output, an LCD screen and a built-in graphics printer. Various configurations of this system are possible. For example, the signal conditioning can be connected directly to a standard portable PC with A/D capability. Output can also be produced on a pen plotter.

The first and sometimes most important step for any low-strain test is the preparation of the pile top surface. In fact, depending on the construction method, it may be necessary to remove several inches or feet of the upper concrete if it has been contaminated with soil, bentonite slurry, or other foreign materials during construction. After a clean, healthy, and hard concrete top surface has been created, the accelerometer is attached to the pile top surface with a thin layer of a soft paste like vaseline, petro wax, and so forth.

After this preparation, an impact with the hand-held hammer is applied. The impact generates acceleration in the 10- to 100-*g* range, pile strains around 10^{-5}, velocities near 0.1 ft/sec, and displacements less than 0.001 in. The velocities contain the most useful and usable information. Therefore, accelerations produced by several hammer blows are integrated and displayed on the processor's screen. Figure 3 shows, as an example, records from a specially prepared drilled shaft 20.5 ft (6.2 m) long with 18-in. (460-mm) nominal diameter installed in stiff to very stiff silty clays. Over the bottom 5 ft (1.5 m) of the shaft, the cross-sectional area was purposely

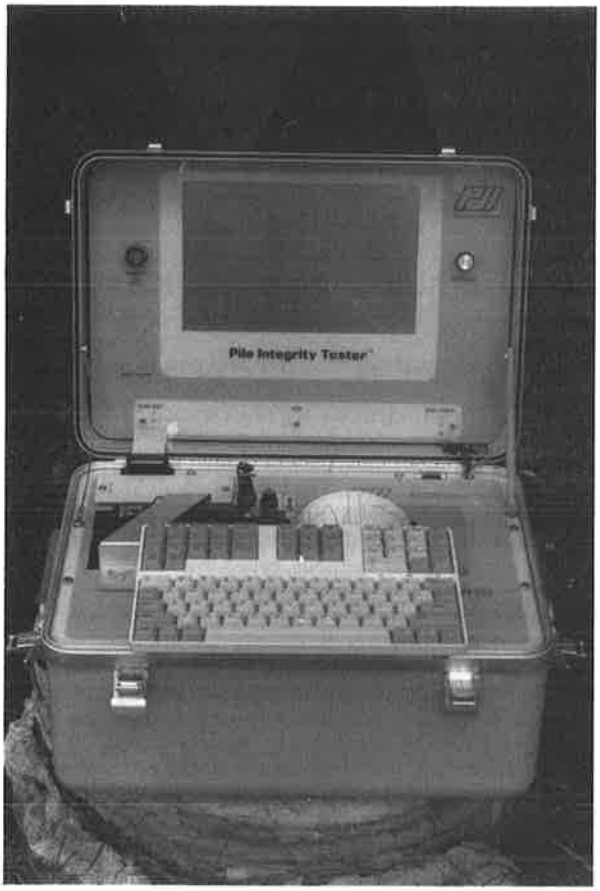

FIGURE 2 PIT-SC. Lid contains LCD screen; battery, keyboard, and printer are beneath.

reduced to 15 in. (380 mm) diameter; this is a 30 percent area reduction. Consistent records are selected, averaged, scaled, and then redisplayed. Averaging reinforces repetitive information from real cross section changes while reducing random noise effect. For the example of Figure 3, the average pile top velocity is shown together with two individual records in Figure 4 (*top*) as a function of both time and length. The length scale is calculated from the time scale by multiplication by an assumed wave speed.

The test engineer inspects the average velocity signal. The first check concerns the "toe signal." If the reflection from

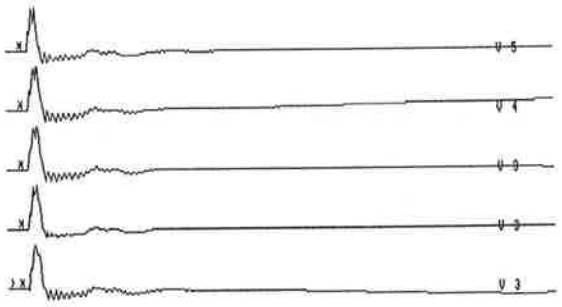

FIGURE 3 Unprocessed velocity records with maximum voltage level and selection marks (*). All selected curves will be averaged, stored, and redisplayed as shown in Figure 4.

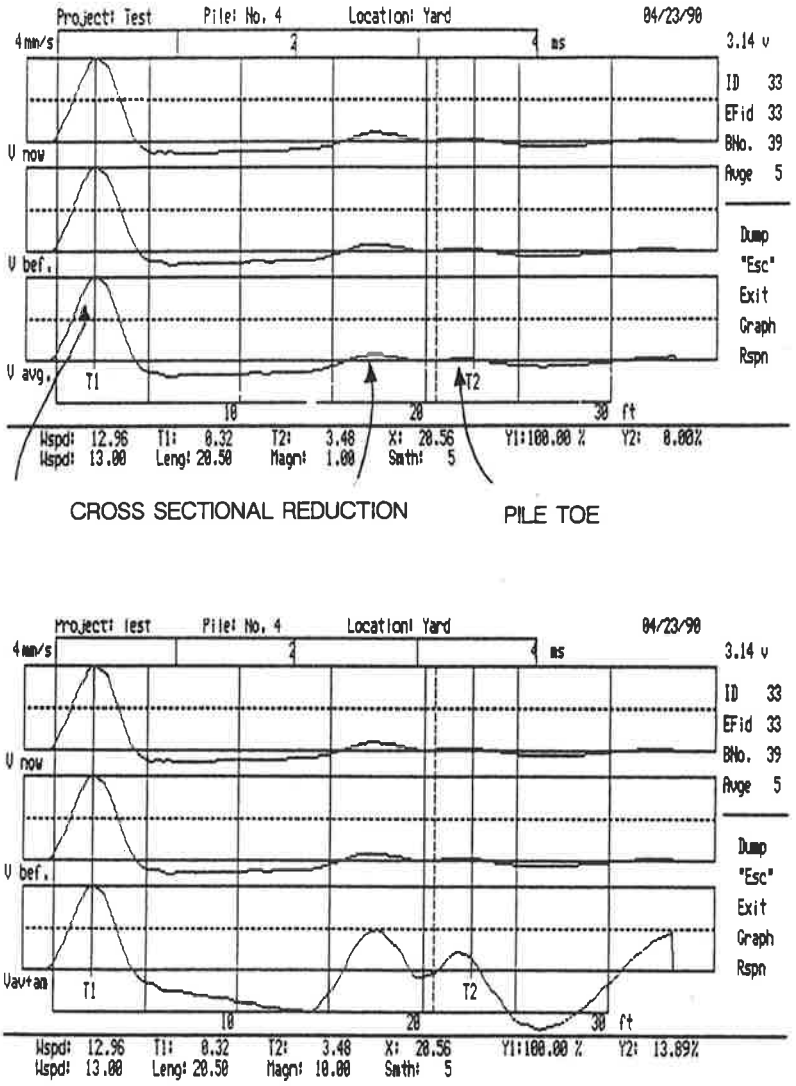

FIGURE 4 PIT-SC display of two individual velocity records and (*top*) the averaged and (*bottom*) the averaged and amplified curves.

the pile toe is not readily apparent [as in the example of Figure 4 (*top*)], then the velocity is multiplied by an amplification function, whose magnitude is unity at impact and increases exponentially with time until it reaches its maximum intensity at time $2L/c$ after impact ($2L/c$ is the time the stress wave requires to travel the pile length, L, and return). In Figure 4 (*bottom*) an amplification of 10 was used. Note how both the cross-sectional reduction and the pile toe now provide clearly identifiable signals. For longer piles or stronger soils, even higher amplification factors are often used; this requires, however, special-purpose signal conditioning with very low noise and high-resolution A/D units operating at fast sampling rates to be successful. If the toe signal is apparent, it is possible to confirm the originally assumed wave speed.

A clearly indicated toe signal and a fairly steady velocity trace between the impact and toe signal are signs of a sound pile. Traces with strong variations may indicate the presence of a pile cross section change or soil resistance changes. For example, relative increases in pile top velocity may be the result of either a cross-sectional decrease or a soft soil layer. The pile impedance (EA/c) is the product of cross-sectional area, A, and elastic modulus, E, divided by the wave speed and is therefore a measure of the pile cross-sectional size and quality. Thus, an impedance reduction can be due to a decrease either in area or in the modulus or concrete strength. Further inspection of Figure 4 (*bottom*) concerns the evidence of impedance reductions along the pile length at about 14 ft (4.2 m) below the top. Correct quantitative interpretations may require signal matching and comparison with records of other piles at the same site (see section on PIT-WAP signal matching).

TRM

TRM requires that both the pile top motion and the impact force be measured. This concept has been borrowed from standard nondestructive testing technology. In fact, the first applications on piles required the measurement of force and velocity under a steady state vibrator that could apply sub-

stantial forces at variable frequencies (5). However, the force frequency spectrum of a hand-held impact hammer is flat over a wide frequency band (see Figure 5). A simple hammer can therefore adequately produce those frequency components to test both well-constructed or defective piles with TRM methods. Although general-purpose equipment (spectrum analyzer) can be used with a velocity and force sensors, the equipment described for PEM is capable of the necessary signal conditioning and analysis provided the simple hammer is instrumented to measure the impact force.

The standard result of TRM is a plot of the ratio of velocity to force (mobility) spectrum. The mobility is the inverse of the impedance and therefore an indication of the pile's velocity response to a particular excitation force.

A mobility peak occurs at a frequency indicative of a positive change of velocity caused by reflection from the pile toe or an intermediate impedance reduction. Furthermore, dividing the velocity by frequency gives the displacement. Dividing force by displacement at a given frequency gives a stiffness value. Thus, in practice, low frequency values are divided by the associated mobility, yielding a dynamic stiffness, E_d. This quantity increases with decreasing pile toe response. A low pile toe response is the result of high soil resistance. However, it may also be the result of high soil or internal pile damping and is therefore only indirectly related to quantitative pile bearing capacity. However, E_d is calculated because it provides a qualitative result for the evaluation of pile quality. Figure 6 shows the mobility spectrum for the present example case and the E_d value for the 32-Hz frequency (selected by the movable cursor, T1).

In both PEM and TRM, the effect from "ringing" due to reinforcement protruding from the pile top can be minimized by using appropriate filtering techniques.

The PIT-FV method is a combination of PEM and TRM. The equipment necessary is the same as for TRM. Force and velocity records are both displayed as a function of time. However, instead of the averaged and amplified velocity, the difference between average velocity and average force (divided by impedance) is calculated and then amplified exponentially (by a factor of 10 for the example case shown in Figure 7). The toe [at 20.5 ft (6.2 m)] and planned cross-sectional reduction [at 14 ft (4.3 m)] are readily apparent in this record. In this curve, any defect near the pile top is more apparent, whereas it may be hidden inside the impact pulse in the normal PEM.

After the display of the average amplified force velocity difference, the mobility is calculated as in TRM (Figure 6). Unfortunately, the mobility spectrum cannot be calculated for the amplified velocity curve. Apparently the shape of the amplification function affects the spectrum, and incorrect conclusions would be drawn. Therefore a weak toe response will result in a mobility spectrum with little information about the basic pile frequency.

PIT-FV provides the engineer with the additional spectra of velocity and force. An example of the force spectrum was shown in Figure 5. Because the mobility is velocity divided by force, the velocity spectrum differs substantially from the mobility spectrum only at higher frequencies where the force spectrum becomes progressively smaller. In the lower frequency range, velocity and mobility spectra are nearly identical because of the flatness of the force spectrum.

Figure 8 shows the PIT-FV velocity spectrum calculated from the velocity time curve. The velocity spectrum lends itself to further analysis if this curve displays peaks at integer multiples of the basic frequency prominently and repetitively. The transform of the velocity spectrum therefore directly indicates the length due to reflections from the pile toe (Figure 9). If other prominent frequency components are contained in the velocity spectrum, because of impedance changes along the shaft, for example, then several peaks may result. Obviously the mobility or velocity spectrum is not as easily in-

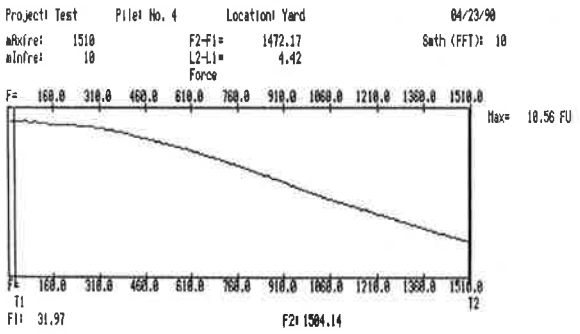

FIGURE 5 Frequency spectrum of a force record obtained on an instrumented hammer.

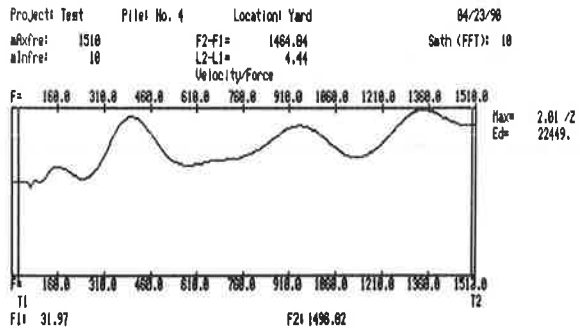

FIGURE 6 Mobility for 20.5-ft nonuniform pile. F2-F1 and L2-L1 values are not meaningful. T1-cursor had been set to low frequency for E_d evaluation, which is 22,449 kips/ft in this example at 32-Hz frequency.

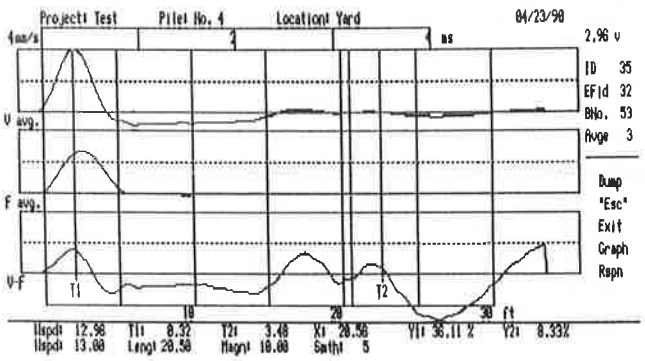

FIGURE 7 Screen display of average velocity, average force, and average velocity minus force, amplified exponentially. Positive V-F at impact indicates slight pile top impedance reduction.

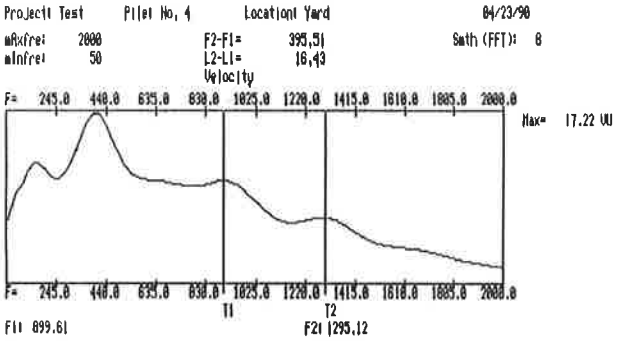

FIGURE 8 Velocity spectrum. This spectrum, divided by the force spectrum of Figure 5, yields the mobility spectrum of Figure 7. Cursors were set to a frequency interval indicating a length of 16.4 ft.

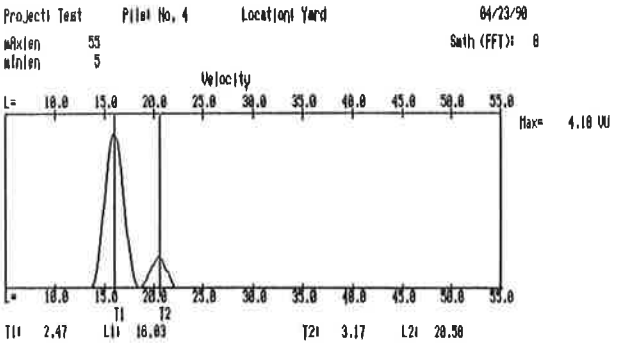

FIGURE 9 Reflectors from Fourier transform of velocity spectrum. T1 and T2 cursors were set to the nonuniformity indicator at 16 ft (built at 15 ft) and the length indicator, which is exact.

terpreted. Again, the amplified velocity cannot be analyzed in this manner. PIT-FV offers this important additional result as an aid in interpretation. In the example presented here, the cross-sectional reduction is easily observed in the high marker, and the pile toe with a smaller reflection.

CALCULATED RESPONSE

The low-strain pile integrity test methods yield some form of pile top motion curve. Interpretation of these curves is left to the engineer. Similar curves developed analytically are an invaluable aid in interpretation. The special-purpose computer program PIT-WAP (Pile Integrity Testing Wave Analysis Program), written using CAPWAPC (CAse Pile Wave Analysis Program—Continuous version) (*6*) as a starting code, requires that the description of pile and soil be input and generates pile top velocity versus time or the mobility spectrum as an output. A voluminous catalog of these calculated responses was compiled as a guide for record interpretation. Only one of many demonstration cases is discussed in the following.

Figure 10 shows the calculated curves for a pile with sufficient uniform shaft resistance to reduce the pile toe reflection to a small pulse. The pile was 20 ft (6.1 m) in length. With a wave speed of 13 ft/msec, the wave travel time ($2L/c$) was approximately 3.1 msec. The corresponding frequency is 325 Hz. This frequency is apparent in the uniform case (Figure 10). Piles with an impedance reduction (Figure 11) and with an impedance increase (Figure 12) over the lower quarter of the pile were also analyzed. A pile impedance versus depth profile separates time from frequency plots. The beginning of the cross-sectional change, in Figures 11 and 12, produces a pile top reflection at 2.3 msec or 430 Hz. Unfortunately, no really clear response frequency is apparent in the corresponding spectra. The output sheet also includes E_d values at five different frequencies.

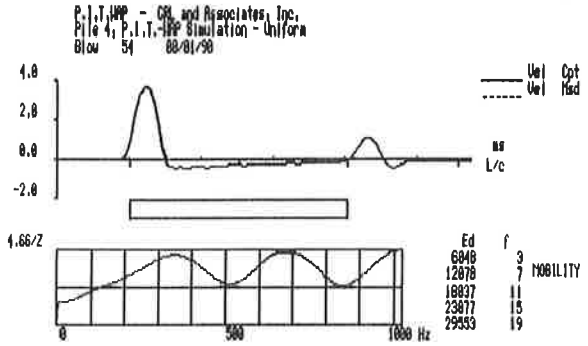

FIGURE 10 Results from PIT-WAP simulation for uniform 20-ft pile.

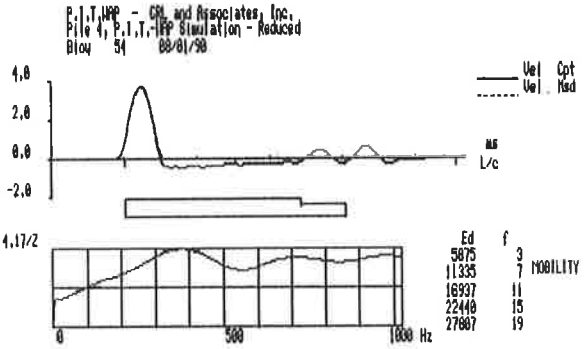

FIGURE 11 Results from PIT-WAP simulation for pile with reduced impedance from 15 to 20 ft.

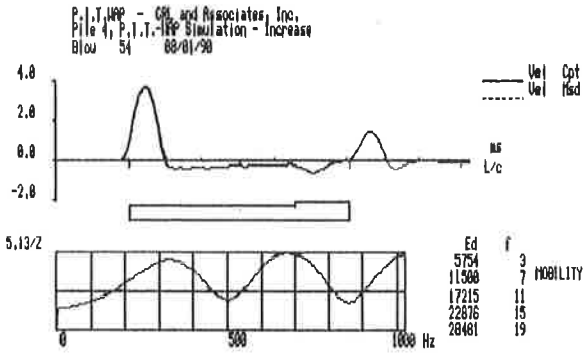

FIGURE 12 Results from PIT-WAP simulation for pile with increased cross section between 15- and 20-ft depth.

PIT-WAP SIGNAL MATCHING

The PIT-WAP program can also be used in the interpretation of measured PIT-FV velocity or velocity and force records. Suppose that the measured force record is imposed as a pile top boundary condition for an analytical model of pile and soil. One result of this analysis would be the calculated pile top velocity. Comparison of the measured with the computed velocity allows the engineer to gain insight into pile impedance variations. Reanalyzing with a variable impedance pile model should therefore lead to an improved match of measured and calculated pile top velocity. The process of changing impedance and reanalyzing is continued until a good match is achieved. At that point, the most likely pile impedance profile has been determined. The difficulty of this simulation is that the soil resistance effects also influence the pile top velocity. However, comparison of the records of several piles may help identify the normal soil response effect.

Typically, PIT-WAP divides the pile in continuous segments of approximately 10 in. (250 mm) length. The program automatically calculates the pile impedance of all segments after the engineer has decided on a soil resistance model. Note that because of the very low magnitude force inputs, this soil resistance model bears no close relationship to static resistance or damping magnitudes encountered during pile driving. On the other hand, for accurate pile impedance predictions, it is important to realistically model the effect of soil resistance on pile top variables. Generally, it is possible to extract these relative soil resistance parameters from PIT-FV tests on reference piles. The parameters are then used to analyze neighboring piles with impedance variations.

The results from PIT-WAP include both a printed listing and a plot of soil resistance parameters and pile impedance values along the pile length. Furthermore, the "match plot quality" of measured and computed pile top velocities allows the engineer to evaluate the reliability of his conclusions. Figure 13 shows the results obtained from PIT-WAP matching of the records of the example test pile of Figure 4. The plot includes the velocity match, the predicted cross-sectional variation (an unplanned impedance increase from 10 to 15 ft was calculated), the actual measured force and velocity curves, and the resistance distribution assumed for the analysis.

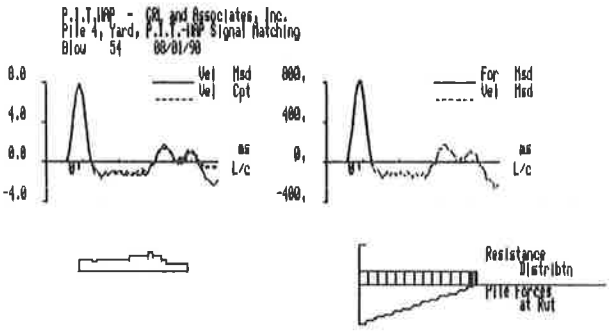

FIGURE 13 Results from PIT-WAP matching. From upper left, clockwise: match of computed and measured velocity, measured velocity, assumed uniform resistance distribution, and predicted pile profile (if higher resistance is used at lower pile, less impedance would result before cross-sectional reduction).

COMPARISON OF METHODS

All three methods require nearly the same testing effort. PIT-FV and TRM involve the calibrated force and velocity measurement and therefore somewhat more care than PEM. Of course, equipment and software of PIT-FV and TRM are also more complicated than PEM. In all methods, pile preparation and the assistance of the pile contractor is usually minimal, allowing the test of many piles to be quickly performed at a low cost. It is possible to test every pile on some sites, and thus low-strain testing can be used as a quality assurance method.

The response recorded by the three methods may differ depending on the sensors and hammer used. It is sometimes even a matter of luck to find the best pile top locations for impact and motion sensing. Contaminated or cracked concrete may adversely affect the measurement results. However, if the measurement engineers have the same experience, apply the same amount of care, select the same pile top location for measurement, and use a hammer with the same properties, the pile top velocity records will probably be very similar. However, the various engineers may prefer to choose different filtering characteristics for their signal-processing equipment and software. The velocity may therefore represent impedance variations over short distances to different degrees.

An important difference occurs when the pile toe response is small. PEM and PIT-FV can exploit the exponential amplification over time, which greatly enhances the record and therefore the power of these methods. TRM cannot resort to this relatively simple numerical enhancement. Observation of a toe signal at least gives assurance of a certain pile length. For piles that are long compared with their diameter, or for piles in soils with high resistance characteristics, exponential amplification may be the only possible method of obtaining a clear presentation of the pile toe signal. Using PEM or PIT-FV, a guideline limit of 30 pile diameters for the pile length is often quoted. In practice, prestressed piles of unlimited length-to-diameter ratios can be tested before installation. Even in soft soils this limiting ratio is often successfully exceeded. In high shaft resistance soils, it may not be possible to detect a pile toe response even at ratios of only 20. However, even if the toe is not readily observed, defects in the upper portion of the shaft (statistically the most likely location of defects) can still be detected, and thus the test is still of value. Several examples of the range of usefulness are given elsewhere. (*7*).

For all three methods the following shortcomings exist. First, the length information obtained from a toe signal (or a governing frequency) is only as accurate as the wave speed value assumed in the processing of the records. Even at sites where concrete quality is well maintained, wave speed variations of 10 percent are not uncommon. A pile length calculated from a toe signal is therefore only well known within ± 5 percent. Second, certain reflections produce secondary and even tertiary wave reflections. For example, if an impedance reduction occurs in the middle of the pile, then what may appear to be the pile toe response may actually be a secondary reflection of the midpile defect. For piles with severe cracks or manufactured mechanical joints, the stress wave will, in general, not be transmitted below the "gap," and

therefore the pile below this "defect" cannot be evaluated. Third, piles with multiple or highly variable cross section changes are difficult to analyze. Piles that are still rigidly attached to other parts of the structure can sometimes be analyzed successfully, but often the analysis is much more difficult.

The additional force measurement of PIT-FV and TRM definitely provides supplemental information of cross-sectional changes occurring near the pile top (i.e., in the distance covered by the impact signal). The extra expense of the force measurement is, therefore, worthwhile whenever questions arise as to the integrity of the upper [say, 5-ft (1.5-m)] pile portion.

The record presentation in the frequency domain may, on occasion, be of benefit. For example, important record components may be hidden in a steady-state signal caused by pile top or reinforcement vibration. They also provide information on dynamic stiffness, although no low-strain method can truly give quantitative information on the ultimate capacity of a pile. In general, however, the interpretation of time records is much simpler than that of frequency records. Time records can also be analyzed simply by the PIT-WAP signal-matching technique.

SUMMARY AND CONCLUSIONS

Three different methods were presented that rely on low-strain measurements taken on a pile struck by a hand-held hammer. These methods are quickly and simply applied at low cost and do not require special preparations during pile construction, making them a good quality assurance tool. PEM has the advantage that very small toe response signals on long piles can be enhanced. TRM provides additional information for integrity evaluation near the pile top. PIT-FV combines the advantages of both methods and provides direct length indication by the second transform of velocity. It also provides the necessary information for signal matching with the PIT-WAP simulation program. TRM and PIT-FV provide relative or quantitative pile stiffness information; however, these values are of limited value for capacity evaluation.

All three methods have similar limitations, which include a generally unknown wave speed and therefore an uncertainty as to the exact location of pile defects or pile toe. Piles with highly variable cross sections are difficult to analyze. Multiple reflections from the same location may mask the wave reflections from lower locations or from the pile toe. It appears that these methods may provide information that can be expressed as follows:

- No significant defect was apparent in the records (the record indicated a pile toe response and no other significant reflection before the pile toe response was apparent).
- No significant defect was apparent in the records; however, the full pile length was not tested because no pile toe reflection was apparent.
- Significant impedance changes were noted. Their magnitude was approximately x percent at a depth of y ft. However, a pile toe response was clearly indicated. The pile may therefore be of limited value.
- Significant impedance changes were noted, and a pile toe signal was not apparent. The pile is highly questionable, and additional tests or replacement of the pile is suggested.

Inconclusive test results are also possible, particularly when very large impedance increases (e.g., a large bulge or outgrowth in shaft diameter in a soft fill) near the pile top prevent a clear stress wave transmission. Some inconclusive results stem from inadequate pile top preparation in obtaining a good testing surface. Of course, such a pile is perfectly capable of performing its service task; however, successful low-strain testing would require additional pile top preparation.

REFERENCES

1. F. Rausche, G. E. Likins, and M. Hussein. Pile Integrity by Low and High Strain Impacts. In *Proc., Third International Conference on Stress Wave Theory on Piles* (B. H. Fellenius, ed.), Ottawa, Ontario, Canada, 1988.
2. F. Rausche and G. G. Goble. Determination of Pile Damage by Top Measurements. Behavior of Deep Foundations, ASTM Symposium, Boston, Mass., 1978.
3. S. Timoshinko and J. N. Goodier. *Theory of Elasticity*. McGraw-Hill Book Company, Inc., New York, 1951.
4. *Proc., Third International Conference on Stress Wave Theory on Piles* (B. H. Fellenius, ed.), Ottawa, Ontario, Canada, 1988.
5. D. M. Lilley, W. M. Kilkenny, and R. F. Akroyd. Steady State Vibration Testing of Piles with Known Defects. In *Proc., Third International Conference on Stress Wave Theory on Piles* (B. H. Fellenius, ed.), Ottawa, Ontario, Canada, May 1988.
6. G. G. Goble, F. Rausche, and G. E. Likins. The Analysis of Pile Driving: A State-of-the-Art. First Seminar on the Application of Stress Wave Theory on Piles, Stockholm, Sweden, 1980.
7. J. A. Berger and D. M. Cotton. Low Strain Integrity Testing of Deep Foundations. *Proc., Deep Foundation Institute Annual Meeting*, Seattle, Wash., 1990.

Use of Nondestructive Testing To Evaluate Defects in Drilled Shafts: Results of FHWA Research

CLYDE N. BAKER, JR., ELLIOTT E. DRUMRIGHT, FRANCIS D. MENSAH, GARY PARIKH, AND CARL D. EALY

Past and current research efforts in the use of nondestructive testing to evaluate the integrity and capacity of drilled shafts containing defects are described. The results of a drilled shaft test program containing both controlled and uncontrolled defects (five shafts at a dense soil site and six shafts at a soft soil site) are presented. The test program was designed to demonstrate in a relative way the ability to find defects, the ability to quantify the location and magnitude of defects, and the correlation of defects with acceptance criteria. Planned defects were created by attaching soil-filled bags to the rebar cages. Uncontrolled defects were created by using improper drilling procedures, such as pulling the tremie pipe out of the concrete, using low slump concrete for portions of the shaft, and using improper slurry control procedures. All shafts contained four preplaced access tubes attached to the rebar cage and were tested using both sonic logging and gamma logging procedures as well as surface reflection techniques (sonic echo test and transient dynamic response test). The approximate costs and relative effectiveness of the different nondestructive techniques in finding and quantifying defects in the shafts are discussed.

Traditional methods for evaluation of defects in drilled shafts include various exploratory methods, some of which are classified as destructive methods. They involve unearthing a portion of the side of the shaft or coring or drilling through the shaft to observe the presence of any defects. Although these methods offer direct observation of the shaft concrete, they tend to be expensive and slow, especially when ongoing construction must be stopped for a period of time. Within the past 20 years, various types of nondestructive testing (NDT) techniques have been developed. They involve either logging of the shaft concrete through preplaced access tubes or using seismic-type methods whereby the shaft is struck on the top with a small hammer. The wave energy travels down the shaft and is reflected from the bottom of the shaft or from defects and is recorded by a geophone or accelerometer on the top. Digital computer advances have allowed refined analysis of the response from both the logging and seismic methods. The results of an FHWA-sponsored project involving the use of NDT techniques to evaluate drilled shafts constructed with planned and unplanned defects are presented.

C. N. Baker, Jr., and E. E. Drumright, STS Consultants, Ltd., 111 Pfingsten Road, Northbrook, Ill. 60062. F. D. Mensah and G. Parikh, PSC Associates, 200 Blossom Lane, Mountain View, Calif. 94041. C. D. Ealy, Turner Fairbank Research Center, Federal Highway Administration, 6300 Georgetown Pike, McLean, Va. 22101.

PROJECT DESCRIPTION

Site Description and Soil Conditions

For this project, two sites with differing soil conditions were selected in the San Jose, California, area. Five of the 11 shafts were constructed on the property of a California Department of Transportation maintenance yard in Cupertino, California. This site, also known as the "dense or dry" site, had a general subsurface profile consisting of sandy clay to a depth of approximately 3 ft below grade, followed by alternating layers of extremely dense, clayey, and sandy gravels to depths of approximately 33 ft below grade. From 33 ft to depths of at least 40 ft, extremely dense, silty, and clean sands were observed. The groundwater table was located deeper than 40 ft beneath the existing ground surface.

The remaining six shafts were constructed beneath an elevated interchange of State Highway 101 and U.S. Highways 280 and 680 in San Jose, California. This site was known as the "soft or wet" site. The general soil profile indicated approximately 3 ft of stiff sandy clay at the surface, followed by predominantly silty and sandy clays of soft to medium consistency to depths of approximately 50 ft below grade. From 50 to approximately 70 ft, additional deposits of stiff silty clay were observed. The clay was noted to transition from a moist to a wet condition approximately 12 to 15 ft beneath the existing ground surface.

Shaft Construction

The shafts at the two sites were constructed as shown in Figures 1 and 2. Shafts 1 through 5 were constructed at the Cupertino (dense) site, using open-hole drilling "in the dry" procedures. The shafts and underreams were excavated using standard auger drilling methods. Full-length reinforcing steel cages were placed in each shaft, to which were attached 2-in. inside-diameter steel and PVC access tubes (two each) for subsequent downhole logging of the caisson concrete.

The elliptical and neck-in type of defects constructed in Shafts 1, 3, and 4 were created by tying sand-filled geotextile bags in prescribed patterns around the reinforced cages before placement in the shafts. The sizes of the defects were selected to obstruct various percentages of the shaft cross section, typically 15 and 45 percent. The soft bottom conditions in

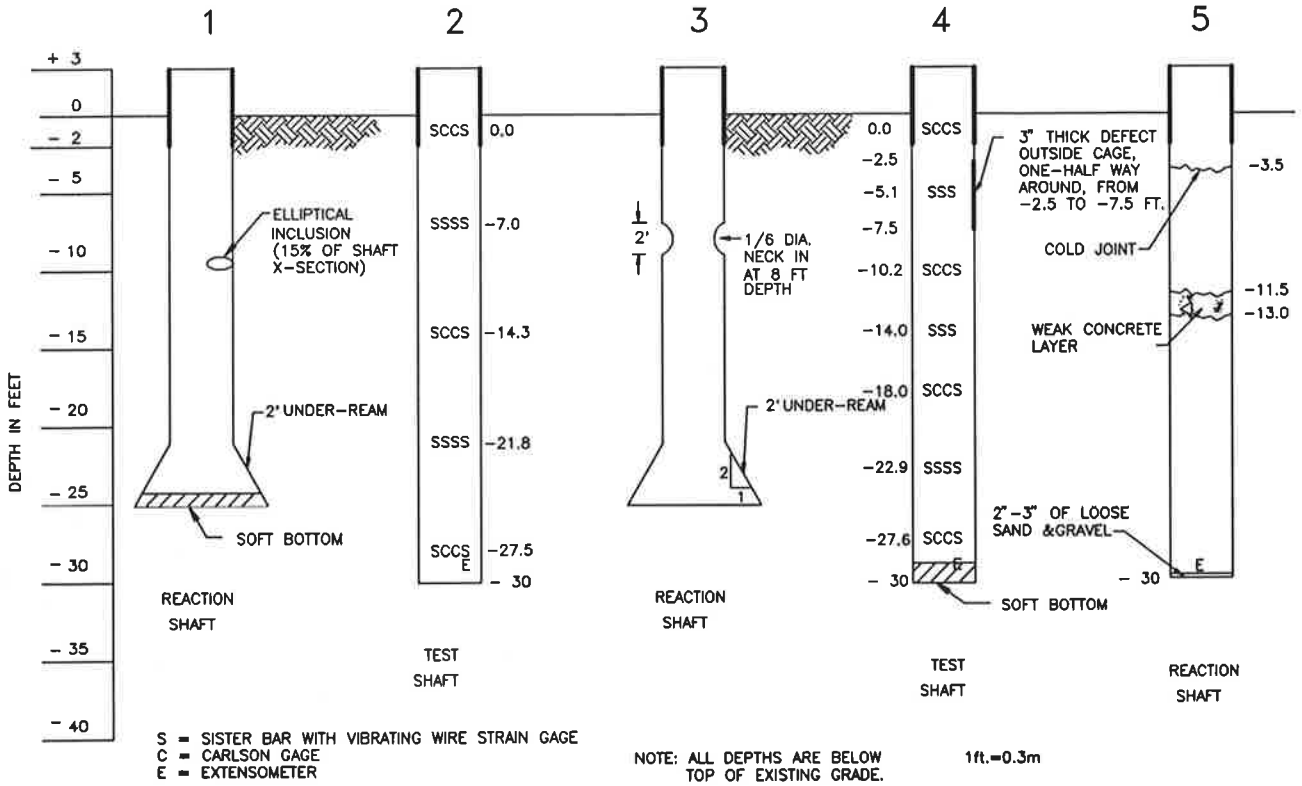

FIGURE 1 Layout of drilled shafts at the Cupertino site.

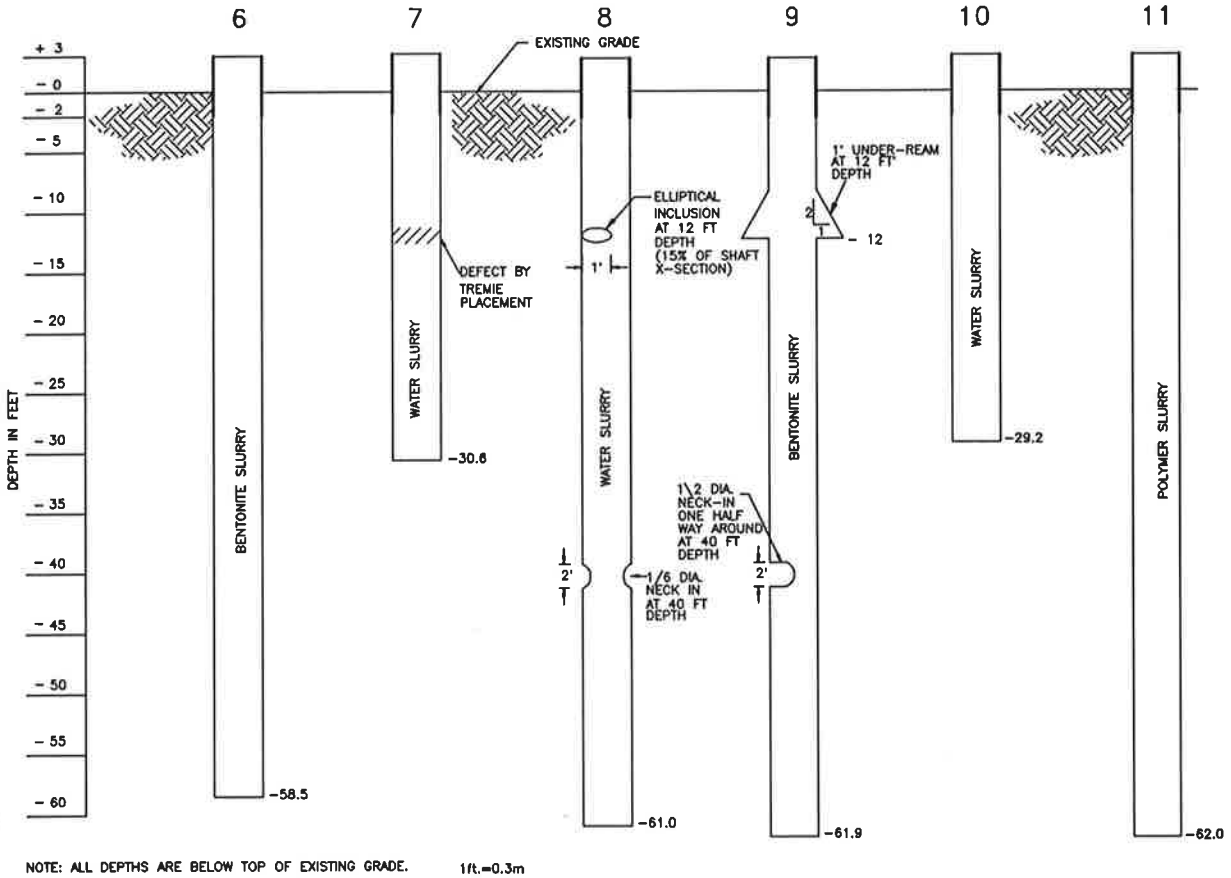

FIGURE 2 Layout of drilled shafts at the San Jose site.

Shafts 1 and 4 were created by placing approximately 1 to 1.5 ft of redwood mulch in the base of the caisson shafts before concreting.

A thin, soft bottom was created in Shaft 5 by disturbing the base of the shaft with the auger without removing the loosened cuttings. Also in Shaft 5, a weak concrete layer was created near the middepth of the shaft by stopping the concrete pour and placing approximately 2 ft of a very weak concrete mix in the shaft. That shaft was then completed up to 3.5 ft below the ground surface and allowed to set overnight. The next day, the shaft was completed to the design grade, thus creating a cold joint. Shaft 2 at the dense site was to be a perfect shaft with no planned defects.

At the San Jose (wet) site, several slurry drilling procedures were used to construct the shafts. Bentonite slurry was used in Shafts 6 and 9; water slurry was used in Shafts 7, 8, and 10; and a polymer slurry was used in the excavation of Shaft 11.

Defects at the wet site consisted of a tremie defect in Shaft 7, which was created during the concrete placement by pulling the pump pipe out of the fresh concrete and allowing the drilling slurry to mix with the concrete intentionally, before replacing the pump pipe in the concrete and completing the shaft. In Shafts 8 and 9, elliptical and neck-in defects were created similar to those at the dense site by tying the sand-filled bags to the reinforcing cages before placement. Also in Shaft 9, a shallow underream was created at a depth of approximately 12 ft below grade during excavation. Shafts 6, 10, and 11 were intended to be perfect shafts with no planned defects. Full-length reinforcing cages were placed in all shafts, with two steel and two PVC access tubes attached to each cage.

At both sites, the shafts were drilled without the use of surface casing, although a cardboard form was used to extend the shafts approximately 3 ft above grade and allow better access for the NDT and large-scale dynamic testing. The concrete at both sites was placed using a concrete pumper truck, with the pipe starting at the bottom of the shafts and progressing upward. The mix design required a minimum compressive strength of 4,000 psi at 7 days. The maximum aggregate size was ⅜ in., with a specified slump of 7 to 9 in. during placement.

As part of the project, electronic instrumentation consisting of sister bar strain gauges and extensometers were attached to the reinforcing cages of Shafts 2 and 4 before concreting. Those instruments were used for subsequent static load tests. In addition, large-scale dynamic tests were completed on all shafts using a 9.75-ton drop hammer and pile analyzer techniques. Those results are discussed by Baker et al. (*1*).

NDT

Methods

On this project, the NDT techniques included gamma-gamma logging, sonic logging, the sonic echo (SE) test, and the transient dynamic response (TDR) test. The gamma-gamma and sonic logging techniques are referred to as direct transmission methods, in that either radiation or sound energy is transmitted and received between parallel coreholes or preplaced access tubes. In the sonic logging method, vibrations are transmitted from one access tube to a receiver in another access tube at the same level while the arrival time and amplitude of oscillation are measured. The shafts are logged continuously, beginning at the bottom and moving to the top. Defects in the shafts are detected through delays or loss of the signal. The transmitter and receiver can be offset in elevation between the tubes to quantify the approximate extent of a defect across the cross section.

In the gamma-gamma logging technique, the radioactive source and counter may be either in separate probes or housed in the same probe. The source is lowered down a preplaced access tube or corehole and raised slowly toward the surface. Lower density zones, such as soil inclusions close to the access tube (within approximately 6 in.), increase the radiation count, because less radiation is absorbed by the defect than in a zone of intact concrete. The advantage of the direct transmission methods is that a continuous record is obtained with depth in the shaft, although defects located more than a few inches beyond the perimeter of the transmission path may not be detected. A primary disadvantage is the requirement for coreholes or preplaced access tubes, which are more expensive than the surface reflection techniques to be discussed subsequently. Typical costs for sonic logging tests are $0.60 to $1.00 per ft, not counting the cost of travel expenses or the access tubes.

The SE and TDR methods are referred to as surface reflection techniques and are described by Stain (*2*). In the SE test, the surface of the concrete shaft is struck near the center with a hand-held hammer, thus sending a compression wave down the shaft to the toe or to a major defect. At a transition of cross section or change of material properties, part of the compression wave is reflected back to the surface and is recorded by an accelerometer or geophone. On the basis of the longitudinal wave velocity of the shaft concrete, the distance to the toe of the shaft or to a discontinuity can be calculated. A typical trace is shown in Figure 3. By plotting pile head velocity versus time, the length of the shaft to the toe or from a significant defect is found from the following equation:

$$L = (V_c \Delta t)/2 \quad (1)$$

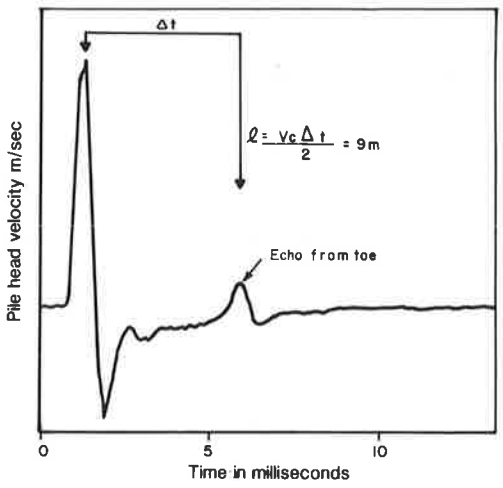

FIGURE 3 Typical response curve from SE test (*2*).

where

L = length of shaft to toe or to a major defect,
V_c = velocity of compression wave in concrete, and
Δt = response time from echo trace.

The TDR test (also known as an impulse or impact response test) is similar to the SE method except that the hammer contains a load cell, which measures the magnitude of the impact force applied to the head of the shaft. Also, the velocity response to the impact recorded by the geophone or accelerometer in the time domain is transformed and reported in the frequency domain. This allows calculation of the length of the shaft to the toe or a major defect and the dynamic stiffness of the upper portion of the shaft, as shown in Figure 4.

In the TDR test, the mechanical admittance or mobility (transforms of velocity/force) is plotted versus frequency. From the characteristic peaks of the trace, the length is calculated as follows:

$$L = V_c/2\Delta f \quad (2)$$

where Δf is peak-to-peak change in frequency and L and V_c are as defined previously.

An indication of concrete quality in the shaft head can be obtained from the mean height (N) of the resonating part of the trace:

$$N = 1/(f_c\, V_c\, A_c) \quad (3)$$

where f_c is the density of concrete and A_c is the cross-sectional area of the shaft.

Finally, the stiffness of the upper portion of the shaft (shaft head stiffness) is computed from the inverse slope of the initial portion of the trace in Figure 4. The stiffness (in units of force/displacement) can be compared with results from static load tests.

The main advantages of the surface reflection techniques are that no preplaced access tubes or coreholes are required and testing is rapid. The principal disadvantages are related to masking of a deeper defect by a reflection from a shallower defect and a practical restriction on the length-to-diameter ratio of the shaft ($L/d < 30{:}1$). Also, some minor preparation of the shaft head is required to obtain a clean response from the hammer impact. Excessive reinforcing steel near the center of the shaft can contribute ringing and electrical noise to the signal.

Assuming access to uncontaminated concrete at the shaft head, typical costs for the surface reflection tests are \$75 to \$125 per shaft, exclusive of travel costs.

For this project, the NDT was performed by four specialty consultants experienced in this type of work. Two of the firms performed TDR testing, three of the four performed SE testing, and two performed sonic logging tests. The gamma logging was performed by one of the coinvestigators of the project.

A first round of testing was performed before the two static load tests at the dense site and before the large-scale dynamic testing. A second round was completed after the large-scale dynamic tests to check for shaft integrity and possible damage, although those results are not discussed here. One consultant was not available for the first round of testing and performed tests approximately 2 months after the large-scale dynamic tests.

Each consultant was provided with information concerning the soil conditions of each site and design drawings similar to Figures 1 and 2 showing the nature of the defects and shaft geometries constructed. A companion phase of this project will be completed at a Texas site in fall 1990. In that phase it is not planned to provide information on the defect location at the outset. Also, the surface reflection tests will be performed before the downhole logging tests.

Results from Surface Reflection Tests

A summary of the defects detected by the TDR and SE tests is given in Table 1. The defects are listed by shaft number, and the consultants are listed as A through D. Although not classified as a defect, an echo or signal return from the base of the shaft is an important record and therefore has been included for each shaft in the table. Of the defects listed, most were planned and were created during construction of the shafts. However, an overbreak was detected by the NDT in Shafts 7 and 11. This was caused by sloughing during excavation of the shaft, resulting in a larger cross section of concrete over a given zone than the nominal shaft size.

Figures 5a, 5b, 6a and 6b display SE test results from Shafts 1 and 8. Data in the "a" and "b" sections were from Consultants C and D, respectively. It is noteworthy that the char-

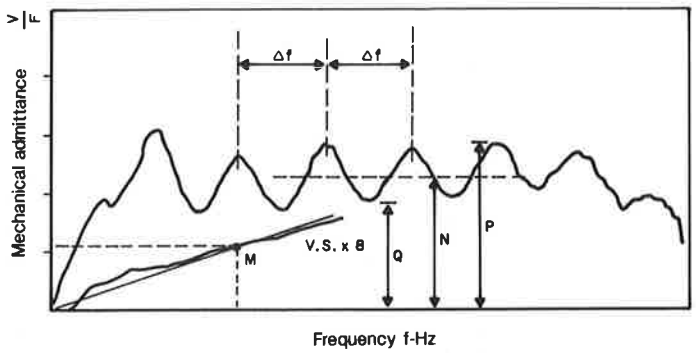

FIGURE 4 Typical response curve from TDR test (*2*).

TABLE 1 SUMMARY OF RESPONSES FROM TDR AND SE TESTS

Shaft No.	Anomaly/ Depth	(2) B (SL)	(1) A (SL)	(1) (GL)
1	Elliptical/13 ft	-	x	x
1	Bell/26 to 27 ft	-	-	-
1	Soft base/27 ft	-	-	-
2	Base/33 ft	-	-	-
3	Neck-in/11 ft	-	-	-
3	Bell/24 to 28 ft	-	-	-
3	Base/28 ft	-	-	-
4	Perimeter/5.5 to 10.5 ft	-	x	x
4	Soft base/32 ft	-	-	?
5	Cold joint/6.5 ft	-	x	?
5	Weak concrete/14.5 to 16 ft	-	?	-
5	Soft base/ 33 ft	-	-	-
5	Base/33 ft	-	-	-
6	Base/61.5 ft	-	x(soft)	x(soft ?)
7	Overbreak/11 to 15 ft	-	-	-
7	Tremie Defect/15 ft	?	x	-
7	Base/33.5 ft	-	x(soft)	x(soft ?)
8	Elliptical/15 ft	x	x	-
8	Neck-in/43 ft	x	x	x
8	Base/64 ft	-	-	-
9	Underream/15 ft	?	x	-
9	Neck in/43 ft	?	x	x
9	Base/65 ft	-	-	-
10	Base/32 ft	-	x(soft)	x(soft ?)
11	Overbreak/30 to 33 ft	-	-	-
11	Base/65 ft	-	-	?

Notes:

(1) Tests run before large-scale dynamic tests

(2) Tests run after large-scale dynamic tests

(SL) = Sonic Log (GL) = Gamma-Gamma Log

X = Detected - = Not Detected ? = Possible Detection

acteristic response was repeatable by two independent consultants. A clear toe response is apparent on all four figures.

In Figures 7a, 7b, 8a, and 8b, TDR test results from Shafts 1 and 8 (after large-scale dynamic testing) are presented. The "a" and "b" sections were generated by Consultants A and B, respectively. Again, the characteristic response was repeatable by both firms. In Figures 7a and 7b (Shaft 1), the response is from the toe, with no response from the shallow inclusion defect. In Figures 8a and 8b, a response from a shallow defect reported at a depth of 9 to 10 ft is superimposed on the response from a larger defect at 40 ft.

In general, a response from the base or toe of the shafts was the most common response recorded and was caused by the sharp change in modulus and, thus, compression wave velocity between the shaft concrete and the underlying foundation soils. Exceptions occurred in Shafts 8 and 9, which were approximately 60 ft long, constructed under slurry, and had significant defects at approximately 40 ft below grade. Responses from the deeper defect masked the echo from the toe, according to two of the consultants. In terms of defect size, the neck-in defects in Shafts 8 and 9 were the largest, obstructing approximately 45 and 50 percent of the shaft cross section, respectively. The smallest defects were elliptical sandbag inclusions placed in Shafts 1 and 8; they obstructed only 15 percent of the shaft cross section. Significant difficulty in detecting those defects was observed by the consultants, even with knowledge of their presence.

Shaft 5 had the most variation in planned defects, with a thin, soft layer at the base of the shaft consisting of 2 to 3 in. of loosened foundation soils. This "defect" was not detected by the consultants. A weak concrete layer at approximately middepth in the shaft was detected by both TDR and SE methods, but not by all consultants. A cold joint approximately 6.5 ft below the top of the shaft was detected by the SE method, and not by the TDR.

Last, changes in cross section of the shaft typically produced responses from the TDR and echo methods. A shallow underream in Shaft 9 was detected by all but one consultant, and the unplanned overbreaks in Shafts 7 and 11 produced reflections at the change in section for those shafts. The modest 2-ft underreams in Shafts 1 and 3 were noted by two of the consultants.

Results from Direct Transmission Tests

The results of the sonic logging and gamma logging tests are presented in Table 2. The format is similar to Table 1. The defects and locations of responses are listed, along with the notation of whether the defect or response location was detected. In general, the defects must be located between or near the access tubes in the case of the sonic logging test or within approximately 6 in. of the tube in the case of the gamma logging method, to be detected. Table 2 indicates that fewer overall defects were detected than from the impact response tests, although clear evidence of detected defects is presented in the logging traces, such as in Shafts 8 and 9. The sonic logging and gamma logging traces for Shaft 8 are shown in Figures 9 and 10. In the sonic log, the loss of signal at the leading edge of the record gives evidence of the defects. In the gamma log, the defect is indicated by the relative change in the gamma count from the background value.

A general opinion of the consultants regarding the use of steel versus PVC access tubes was that a problem with debonding due to shrinkage of the concrete from the PVC tube resulted in a loss of signal in the sonic logging method, usually in the upper zone of the shaft. This type of debonding was not nearly as common or extensive in the case of the steel access tubes. For the gamma-gamma logging method, the higher-density steel attenuated the signal, although defects located near the tubes could still be detected.

Correlation with Acceptance Criteria

Following completion of the Texas test program, all test results will be correlated with a set of preliminary acceptance criteria, which were developed early in the project. It is hoped that the correlation will warrant future publication.

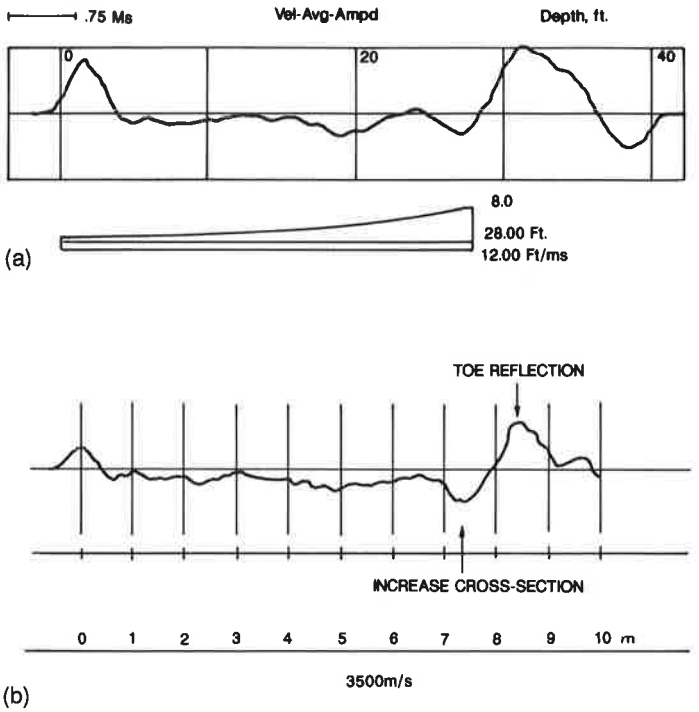

FIGURE 5 Results from SE test of Shaft 1 (*a*, Consultant C; *b*, Consultant D).

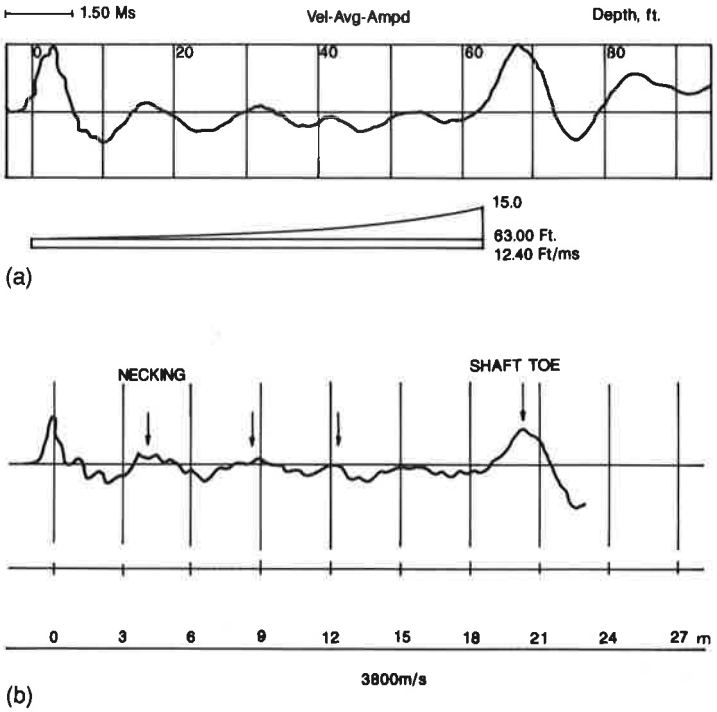

FIGURE 6 Results from SE test of Shaft 8 (*a*, Consultant C; *b*, Consultant D).

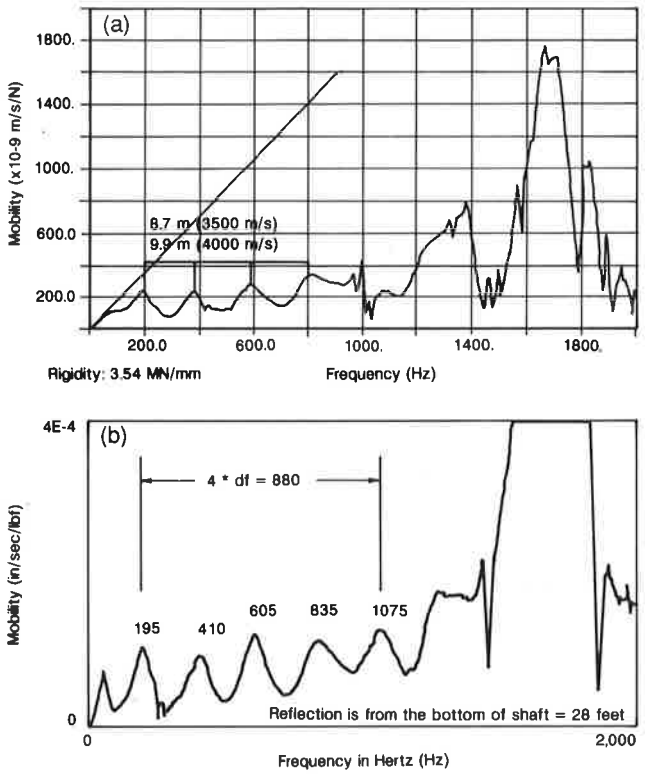

FIGURE 7 Results of TDR test on Shaft 1 (*a*, Consultant A; *b*, Consultant B).

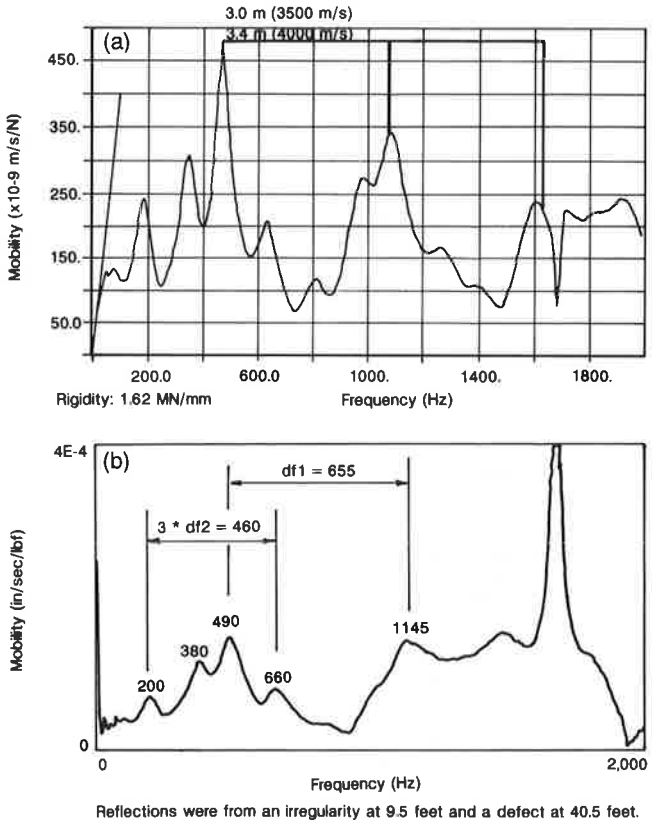

FIGURE 8 Results of TDR test on Shaft 8 (*a*, Consultant A; *b*, Consultant B).

TABLE 2 SUMMARY OF RESPONSES FROM SONIC LOGGING AND GAMMA LOGGING TESTS

Shaft No.	Response/ Depth	(1) A (TDR)	(2) B (TDR)	(2) B (SE)	(1) C (SE)	(1) D (SE)
1	Elliptical/13 ft	-	-	-	-	-
1	Bell/26 to 27 ft	-	-	-	x	-
1	Soft base/27 ft	x	x	x	x	x
2	Base/33 ft	x	x	x	x	x
3	Neck-in/11 ft	-	x	x	x	-
3	Bell/24 to 28 ft	-	-	-	x	x
3	Base/28 ft	x	x	x	x	x
4	Perimeter/					
	5.5 to 10.5 ft	-	x	x	-	-
4	Soft base/32 ft	x	x	x	x	x
5	Cold joint/6.5 ft		-	-	x	x
5	Weak concrete/					
	14.5 to 16 ft	-	x	x	-	x
5	Soft base/33 ft	-	-	-	-	-
5	Base/33 ft	x	x	x	x	x
6	Base/61.5 ft	x	x	x	x	x
7	Overbreak/11 to 15 ft	x	x	x	x	x
7	Tremie Defect/15 ft	x	-	-	-	-
7	Base/33.5 ft	x	x	x	x	x
8	Elliptical/15 ft	?	-	-	x	x
8	Neck-in/43 ft	?	x	x	x	-
8	Base/64 ft	x	-	-	x	x
9	Underream/15 ft	x	x	?	x	x
9	Neck-in/43 ft	x	x	x	-	-
9	Base/65 ft	x	-	-	-	x
10	Base/32 ft	x	x	x	x	x
11	Overbreak/30 to 33 ft	x	-	-	x	x
11	Base/65 ft	x	-	-	x	x

Notes: (Depths are measured from top of shaft)

(1) Test results prior to large-scale dynamic testing

(2) Test results after large-scale dynamic testing

X = Detected - = No detection ? = Possible detection

CONCLUSIONS

On the basis of the results of the study, the following conclusions were drawn:

1. The surface reflection techniques (TDR and SE) could detect the base of the shafts and larger neck-in–type defects. Small or very thin defects, such as the small elliptical inclusion, the cold joint, or changes in concrete properties, were not generally detected. Significant changes in cross section, such as a concrete overbreak or shallow underream, also produced responses from these methods.

2. The direct transmission methods (sonic and gamma-gamma logging) produced clear evidence of defects located near the access tubes, such as the shallow elliptical inclusion defect

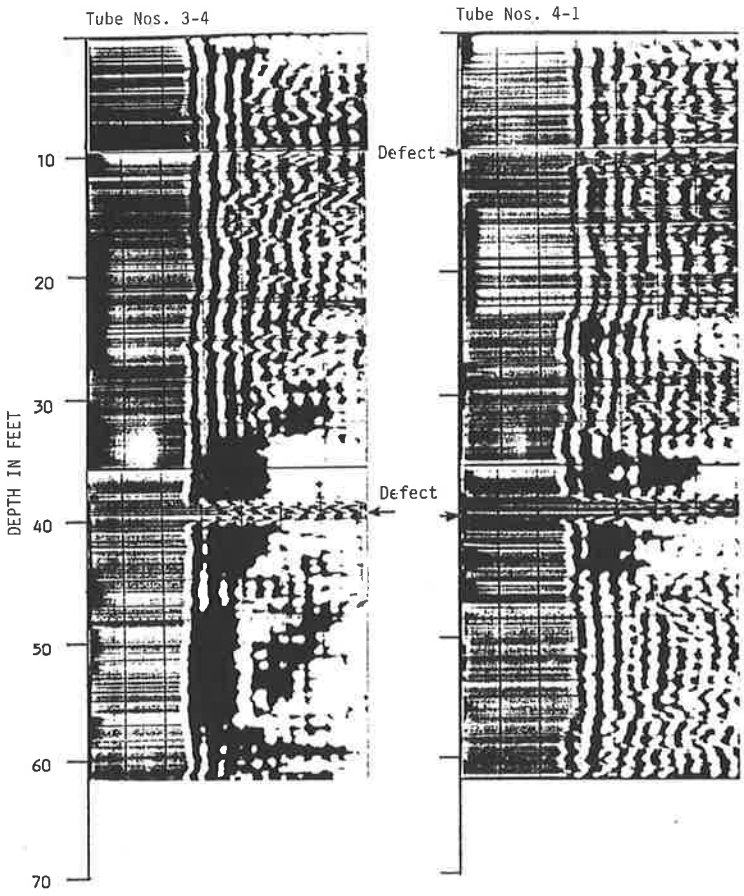

FIGURE 9 Sonic logging record from Shaft 8 (Consultant A).

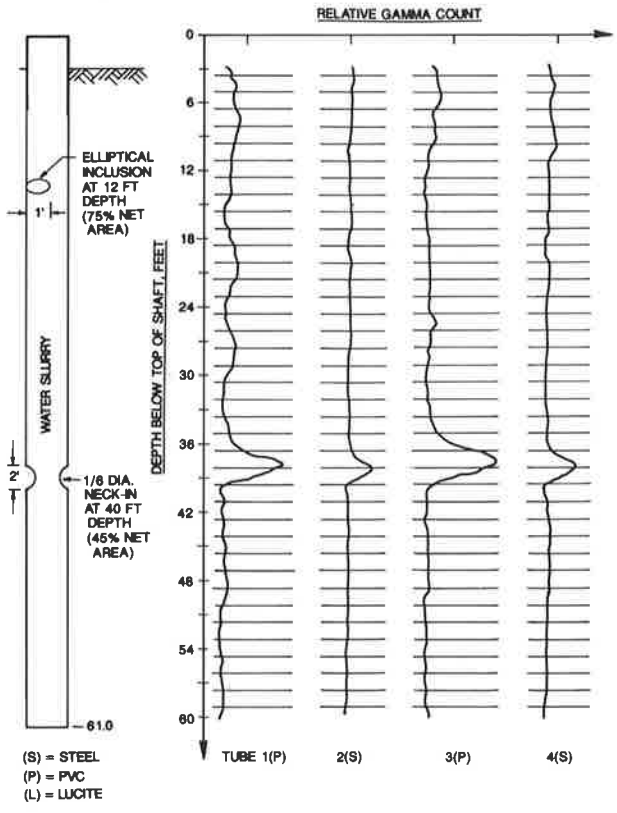

FIGURE 10 Gamma-gamma log from Shaft 8.

and the neck-in defects. For the sonic logging test, use of steel tubes compared with PVC access tubes was shown to reduce the occurrence of debonding between the shaft concrete and tube, thus giving a better signal response.

3. Where different firms used the same testing technique, they reported similar results with regard to depth of a noted defect.

4. NDT techniques, when joined with proper quality control observation during construction, offer a relatively inexpensive method to establish drilled shaft integrity.

ACKNOWLEDGMENTS

This research was supported by FHWA. The project team expresses its appreciation to the Association of Drilled Shaft Contractors, West Coast Chapter, the California Department of Transportation, and particularly the following firms which donated equipment, labor, and materials: Case Pacific Company, Judd Drilling Company, and Malcolm Drilling Company.

REFERENCES

1. C. N. Baker et al. Dynamic Testing To Predict Static Performance of Drilled Shafts. ASCE Geotechnical Engineering Congress, Boulder, Colo. 1991.
2. R. T. Stain. Integrity Testing. *Civil Engineering* (British), April 1982.

Nondestructive Testing of Timber Piles for Structures

M. SHERIF AGGOUR

Though an underwater inspection of the timber piles supporting a bridge at Denton, Maryland, indicated reasonable soundness of the timber, the bridge failed. Laboratory tests indicated a substantial reduction in material strength during the life of the piling. A nondestructive procedure for estimating the strength of in-service piles was therefore needed and was developed under the Maryland Highway Planning and Research program. The procedure is an ultrasonic wave propagation method in which the in-place strength of a timber pile is correlated with the wave velocity normal to the grain and the in-place unit weight of the pile. The relationship was developed and verified by testing yellow pine piles from 11 bridges in Maryland. The technique has been extended to the determination of the condition of piles supporting different types of structures. The nondestructive technique as developed for testing timber piles for bridges is presented. The type of data collected, information needed for data interpretation, equipment description, and factors that affect testing are included, as well as the conditions under which the method can be used and its limitations. The types of decay occurring in timber piles, determined by comparing the behavior of timer piles supporting bridges, asphalt tanks, and buildings, are discussed. It is concluded that the technique can be used in all three cases if the causes and types of deterioration and the limitations of the ultrasonic technique are understood.

Timber piles deteriorate because of the organic composition of wood. The principal causes of deterioration of piles in service are fungi, bacteria, insect attack, fire, mechanical wear, and marine borers. Most wood only decays when placed in conditions that are conducive to the growth and development of fungi. Moisture, oxygen, and mild temperatures are essential to the survival and growth of fungi. Decay occurs most often above the water between high and low tide and at the pile cap in timber piles for bridges.

Bacteria are microscopic organisms that live anaerobically on organic material. It was once believed that timber piles submerged in fresh water or buried underground possess immunity to biological degradation. The belief was based on the assumption that a lack of oxygen deters attack by most microorganisms and the knowledge that anaerobic bacteria, prevalent in such an environment, were generally incapable of causing significant damage to the pile material. However, it has become evident during the past two decades that bacteria play an important role in the degradation of wood. It has also been recognized that bacteria, like fungi, may inactivate or destroy preservatives such as creosotes.

Scheffer et al. (*1*) noted, from studying untreated southern pine piles removed from the Potomac River in Washington, D.C., that after 62 years of service the crushing strength of small specimens prepared from the pile above the mudline had been reduced by 60 percent, and that below the mudline had been reduced by 20 percent. Thus, a substantial reduction in crushing strength of the piles above the mudline and a moderate reduction in strength below the mudline occurred. In a similar study of bridge piles after 85 years in the Milwaukee River, Bendtsen (*2*) reported that the average modulus of rupture of red pine was 32 percent, the modulus of elasticity 27 percent, and the specific gravity 12 percent lower, respectively, than the published values in ASTM. Eslyn and Moore (*3*) showed that bacteria were present in all portions of all pile sections. Boutelje and Bravery (*4*) studied spruce and pine piles from the foundation of a 75-year-old building in Stockholm. The peripheral zone of the piles was soft to a depth of 1 to 2 in., resulting in a marked loss in the compressive strength, bending strength, and modulus of elasticity. Microscopic observations of the decayed material suggested that the degradation could be attributed to bacterial action. Singh and Butcher (*5*) reported on premature decay that was found in treated radiata pine posts in vineyards in the Poverty Bay region of New Zealand. Microscopic investigations indicated that bacteria were the first organisms to attack the post and that fungi infected them secondarily once the treatment had been rendered ineffective by the bacteria.

Despite an underwater inspection that had indicated that the piles were reasonably sound 1 year earlier, a bridge supported by timber piles failed at Denton, Maryland, in 1976. After the failure, laboratory tests on the red pine piles recovered by the state highway department indicated that, whereas there was no loss in cross-sectional area, the material strength of the pile had been significantly reduced.

In general, knowledge of the long-term effects of the environment on wood properties is limited. Bacterial deterioration proceeds slowly compared with fungal decay, and publications on bacterial attacks on wood are scarce.

Several kinds of wood-boring insects attack wood for food and shelter and seriously affect its integrity. The insects include termites, wharfborers, and carpenter ants. Wood consists of organic compounds composed mainly of carbon and hydrogen and thus is combustible. Therefore, fire is a hazard to timber structures in service. Mechanical wear of timber piles may involve abrasion from floating debris and impact by traffic. Several marine organisms, of which teredo and limnoria are the best known, are responsible for losses in cross-sectional area in timber piles in salt water, more so in tropical than in temperate climates. Besides climate, loss in cross-sectional area depends on the species of the borer, the salinity of the water, and the type of wood from which the pile is made.

Civil Engineering Department, University of Maryland, College Park, Md. 20742.

The structural integrity of timber piles and their resistance to bending and crushing may decrease with time in service. The effects of deterioration include loss of density (becomes extremely light in weight), increase in permeability (absorbs liquid and becomes waterlogged much more readily), loss in strength (caused by enzymatic degradation of the wood cellulose and lignin), and loss of cross-sectional area. The extent and effect of the decay or loss in area are difficult to assess visually because the timber pile may be completely decayed internally, whereas its external appearance may be normal.

METHODS OF INSPECTION OF BRIDGE PILES

Because the causes of deterioration are many and varied and the protective measures used to guard against it are no guarantee that deterioration will not occur, timber piles must be inspected periodically to determine whether and to what extent damage has occurred. This information can assist the engineer in determining the safe load-carrying capacity of the structure and in establishing a schedule for the replacement of unsafe piles. There are two basic types of tests: destructive and nondestructive.

Destructive methods, as the name implies, are those that to some degree affect or destroy the structural integrity of the material tested by imposing undue strain on the pile. The effect may be slight, as in probing with an ice pick or knife; moderate, as in taking a small core sample; or totally destructive, as in cutting a pile section and crushing it. The specimens tested represent the entire population of potential samples, a major disadvantage in testing natural materials such as wood. In addition, destructive methods may not give a true representation of the load-carrying capacity of the pile.

Nondestructive testing methods permit inspection of the material without impairing its usefulness. Radiography, resonance, nuclear, and X-ray inspection methods have all proven to be valuable in determining wood properties and the extent of wood deterioration in the laboratory. The equipment required for each of these methods does not as yet lend itself to field testing of piles above and below water. Visual inspection is the most widely used of all nondestructive testing procedures; it is simple, easy to perform, and usually low in cost. The basic disadvantages of this method are that inspection is limited to the surface of the pile and that inspectors may misinterpret what they see. Sounding is also a simple method of testing in-place timber piles above water. The pile is systematically tapped with a hammer, and the sound emitted is interpreted by the inspector who rates the pile. The method is limited to providing an initial indication of deterioration to be followed by destructive methods. Ultrasonic testing is a well-established means of inspection for many kinds of materials, such as metals and concrete, and can be readily used under water. Various nondestructive pulse-measuring instruments have been developed to evaluate the soundness of timber structures in service.

SONIC AND ULTRASONIC TESTING IN WOOD

In the last 30 years several studies have been conducted on the evaluation of the mechanical properties of wood and the detection, by ultrasonic testing, of internal defects in it. Lee (*6*) used the ultrasonic technique to test the structural safety of the damaged roof of an 18th-century mansion. Jensen (*7*) used the sonic test technique for the detection of internal decay in wood poles. He found that the frequencies associated with sound poles were higher than those associated with internally decayed poles. The ultrasonic test technique was used by Muenow (*8*) to inspect 11 sections of wood utility poles from the Commonwealth Edison Company, primarily to determine variations of properties from one pole to another. McDonald et al. (*9*) used ultrasonics in determining the quality of lumber in an attempt to grade it more efficiently during cutting. Pellerin (*10*) measured the transmission time of a stress wave through a piece of wood and showed that stress wave analysis could give a good indication of the quality of the interior of the piling, because the progress of a wave is slowed by increasing numbers and sizes of defects. Agi (*11*) found that the velocity and strength of sound waves passing through wood varied inversely with voids in the wood caused by marine borers, a principle that is used to detect the loss in cross-sectional area of piles due to marine borers. Vanderbilt et al. (*12*) used the sonic test technique for evaluating the strength and stiffness of large timber poles through their service life, and Goodman et al. (*13*) used probability methods in their design. For wood frame structures Lanius et al. (*14*) used a stress-wave propagation technique to examine the strength of joists in a structure. Pellerin et al. (*15*) used stress-wave measurements in estimating the ultimate compressive stress of decayed and termite-attacked wood specimens, as did Hoyle and Rutherford (*16*) in the inspection of timber bridges and decks.

A research project supported by the Maryland State Highway Administration and FHWA was conducted at the University of Maryland. A large number of new piles and piles from 11 bridges in Maryland were tested to develop a reliable nondestructive method to determine the strength of timber piles above and below water using ultrasonic wave propagation. In ultrasonic tests, pile sections are subjected to rapidly alternating stress waves at low amplitudes. Undamaged wood is an excellent transmitter of these waves; damaged and decayed wood delays transmission. This provided an opportunity to compare nondestructive testing results from field measurements in piles before they were removed from service with laboratory nondestructive tests on the same piles. The data were correlated with strength determination values from compression tests. In addition, small specimens were cut from the piles and the mechanical properties determined for such variables as unit weight, moisture content, effect of treatment, and direction of grain. Statistical relationships between the wave velocity, compressive strength of the piles, and unit weight were developed that enable an engineer to determine the strength of a pile in place. Full details of the research project are given elsewhere (*17–20*).

PRINCIPLE OF ULTRASONIC TESTING AND EQUIPMENT

Principle of Ultrasonic Testing

Ultrasonic waves are stress waves at frequencies above 20 kHz and are termed elastic waves because it is the elastic

property of the medium that is responsible for the sustained vibrations required for ultrasonic wave propagation. Wood is characterized by three mutually perpendicular axes of symmetry: longitudinal (L), normal (N), and tangential (T) to the wood grain, as shown in Figure 1. There are major differences in the strength and elastic properties in the directions longitudinal and normal to the grain, whereas the differences between the tangential and normal directions are relatively small. The quality of wood can be determined from ultrasonic pulse velocity measurements using equipment that generates pulses and accurately measures the time of the transmission through the specimen. By measuring the distance through which the pulse is propagated, the velocity can be computed.

Three arrangements are possible when using ultrasonic equipment to measure the transit time of the wave: a direct transmission arrangement in which the transducers are facing each other across the section of the material tested, a semidirect transmission in which the two transducers are also across the section but at different levels, and an indirect transmission with both transducers on the same surface. Tests conducted in the direction normal to the grain on species of new pine piles indicated a 10 percent higher velocity compared with the tangential velocity. Wave velocity in the longitudinal direction was shown to be two to three times that of the velocity normal to the grain. In testing old piles (yellow pine), it was found that the relationship between the velocity in the directions normal and longitudinal to the grain was no longer two to three, but a function of the unit weight of the wood.

For this study, wave propagation in the normal direction was used because it is more sensitive to detecting defects that are perpendicular to the pulse. Because the objective was to determine the in-service strength of a pile and because the strength is not uniform across the cross section of a pile, measurements in the normal direction are more representative of the section tested. In addition, the transducers are highly directional, and the pulses propagated are mainly in the direction normal to the face of the transducers so that the direct arrangement results in a maximum transfer of energy. The effective path length, being the distance between the faces of the transducers, is well defined. For these reasons, the direct transmission mode was selected.

Ultrasonic Equipment

The equipment is a commercial testing apparatus consisting of a portable ultrasonic digital readout meter and two ceramic transducers, each mounted in a stainless steel case and having a frequency of 54 kHz. Electrical pulses generated by one of the transducers are passed through the test specimen and picked up by the receiving transducer, which transforms these mechanical pulses back into electrical pulses. The time-measuring circuit in the readout meter then displays the transit time between the transducers.

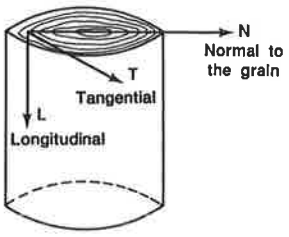

FIGURE 1 Timber pile axes of symmetry.

Factors Affecting the Testing

The surface of the pile (above and below water) must be cleaned of foreign material to obtain a smooth surface where tests are to be conducted. The equipment must be calibrated each time it is used. Air-free contact is necessary between the transducer and the surface of the pile to transmit the ultrasonic energy, because any air contact will attenuate the incident energy. A high-vacuum, silicon-based grease can be used as a couplant for testing above water. Because water is an excellent couplant, there is no need for additional couplant when testing under water.

INTERPRETATION OF DATA TO DETERMINE PILE CONDITION

Data obtained from the ultrasonic tests are used to characterize the in-service condition of the timber piles. The equations were obtained by correlating (*a*) the velocity of the ultrasonic wave in the pile sections, (*b*) strength values from compression tests conducted on the same sections, and (*c*) unit weight. Relationships were developed that can be used to establish the in-place strength of bridge timber piling if both the wave velocity and unit weight are known.

To determine the reduction in strength of the piles tested while in service, it was necessary to compare their existing properties with those of new piles. Therefore, tests were conducted on full-size sections from both new piles and old piles removed from service. The new piles were both treated and untreated southern yellow pine. Sections were cut from in-service treated yellow pine piles from 11 bridges that had either been replaced or were being repaired. Several of the piles were tested ultrasonically in place, removed, sectioned, and tested in compression after their unit weights were calculated.

Pile Condition Rating

Properties of New Piles

New full-size piles of yellow pine, both untreated and creosote treated, were tested in the laboratory to determine their properties. The average compressive strength parallel to the grain and wave velocity normal to the grain of these new piles are presented in Table 1. These data can be used as a basis on which to determine the in-service condition of piles.

Properties of In-Service Piles

The compressive strength of the pile is a function of both the wave velocity and its in-place unit weight. Because it is dif-

TABLE 1 AVERAGE VALUES OF COMPRESSIVE STRENGTH, WAVE VELOCITY, AND UNIT WEIGHT FOR SECTIONS CUT FROM NEW PILES

	Compressive Strength σ_{cr} (psi)	Wave Velocity V_N (ft/sec)	Unit Weight γ pcf
Untreated Yellow Pine (N=20)	6227	6340	34.9
Treated Yellow Pine (N=34)	5005	6010	43.2

N = number of sections

ficult to determine the unit weight by nondestructive means, it is more convenient to determine the condition of the pile on the basis of the wave velocity only, which can be obtained easily. The criteria in Table 2 are estimates that were developed to classify the condition of dry treated yellow southern pine piles on the basis of wave velocity. For example, a velocity of less than 3,000 ft/sec indicates that the pile is in poor condition, generally indicating that the center of the pile is rotten. When no reading is obtained, the pile probably has a large internal decayed area. Caution should be exercised in using this information alone, without consideration of the unit weight.

Strength Determination for Testing Above Water

Dry, New Treated Sections

For new treated sections of yellow pine (and a velocity of approximately 4,500 ft/sec or higher), the compressive strength of a timber pile can be predicted by using a multivariable model that regresses the compressive strength on the wave velocity normal to the grain of the pile and its unit weight. The empirical relationship developed on the basis of the results of the experimental tests is

$$\sigma_{cr} = 0.535V_N + 41.35\gamma \quad (1)$$

TABLE 2 APPROXIMATE CRITERIA FOR PILE CONDITION (DRY)

Wave Velocity, V_N ft/sec	Pile Condition
5500 and higher	excellent (new)
4500 - 5500	very good (new)
4000 - 4500	good
3500 - 4000	average
3000 - 3500	questionable
less than 3000	poor

where

σ_{cr} = average compressive strength (psi),
V_N = wave velocity normal to the grain (ft/sec), and
γ = in-place unit weight (pcf).

The first coefficient in this equation indicates the sensitivity of the model to wave velocity across the section of the pile, and the second coefficient indicates the sensitivity of the model to the unit weight of the material.

Moist, Old Treated Sections

For a moisture content close to the fiber saturation point and old treated sections having a wave velocity between 3,000 and 4,500 ft/sec, the following model can be used, where γ is the moist unit weight:

$$\sigma_{cr} = 0.537V_N + 6.34\gamma \quad (2)$$

Dry, Old Treated Sections

For dry and old treated sections having a wave velocity between 3,000 and 4,500 ft/sec, the following model can be used, where γ is the dry unit weight:

$$\sigma_{cr} = 0.292V_N + 46\gamma \quad (3)$$

Dry, Very Decayed Treated Sections

For dry and very decayed sections have a wave velocity less than 3,000 ft/sec, the following model can be used:

$$\sigma_{cr} = 0.127V_N + 40\gamma \quad (4)$$

Strength Determination for Testing Below Water

It is known that as the moisture content increases, the velocity decreases and the total unit weight increases. The wave velocity for several sections from different piles having different degrees of decay was determined when the sections were dry. The sections were then allowed to absorb water by storing them in a tank full of water. The absorbed water caused swelling and resulted in weakening of the fibers. The wave velocity was then determined under water over a period of several months until the time reading became constant. These wave velocities are shown in Figure 2, which can be used to determine the velocity through the wood in air-dry condition if the velocity under water is known, or vice versa.

The data points on the figure are concentrated in two regions. In one, the underwater velocity is more than 4,000 ft/sec and the corresponding velocity in air-dry condition is about 10 to 20 percent more than the underwater velocity. This range represents piles in good condition, and the difference in velocity is due to the moisture content. In the other region, the velocity under water is less than 2,000 ft/sec, and the corresponding velocity in air-dry condition is almost twice the

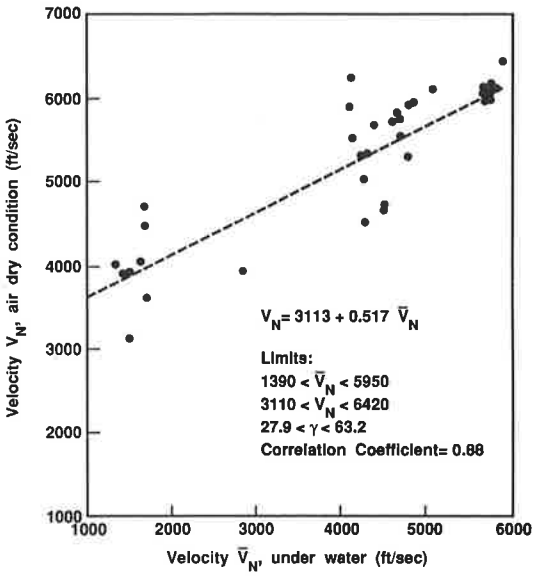

FIGURE 2 Relationship between wave velocity in air-dry condition to wave velocity under water.

underwater velocity. This range represents piles in poor condition.

In field applications the velocity under water is determined, and the velocity in air-dry condition can then be estimated using Figure 2. The velocity in air-dry condition being known, Equations 1, 3, and 4 can then be used.

Two sets of sections were prepared using the same treated piles from different bridges for the purpose of performing compression tests parallel to grain; one set at air-dry condition and the other at wet condition. It was found that the crushing strength of the sections at air-dry condition was about 1.48 times that of the few sections tested at wet condition.

Determination of In-Place Unit Weight

To predict the compressive strength of a pile section using the equations developed, it is necessary to measure the velocity across the section in the direction normal to the grain and the average unit weight of the section in place. The velocity can be easily determined; however, the unit weight is more difficult to determine. The engineer has several options. At present, the most accurate way to determine the unit weight of a full cross-sectional slice of a pile is by weighing the section, measuring its volume, and calculating its unit weight at the specified moisture content. For in-service piles a convenient method is to use small cores bored from the pile. It is also possible to compare the pulse velocity from a suspected area of deterioration with that from an area known to be sound, thereby eliminating the need to determine the unit weight of the timber. When it is not possible to determine the average unit weight of a pile, an approximate value for the unit weight can be estimated from knowledge of the wave velocity. Naturally, the use of such approximate relationships reduces the accuracy of the strength computed. The following are approximate unit weight equations using the ultrasonic method.

Moist Treated Piles

An approximate linear relationship between the wave velocity and the unit weight for moist wood is

$$V_N = 7{,}845 - 67\gamma \tag{5}$$

where V_N is the wave velocity normal to the grain (ft/sec) and γ is the in-place unit weight of the material (pcf). The equation can be used to predict an approximate unit weight of a moist pile from the wave velocity. However, this equation is limited to velocities ranging between approximately 3,500 and 5,500 ft/sec, as shown in Figure 3. For velocities below 3,500 ft/sec or above 5,500 ft/sec, it is recommended that a constant value of unit weight equal to 65 pcf and 35 pcf, respectively, be used.

Dry Treated Piles

The unit weight of dry sections versus the wave velocity normal to the grain was plotted as shown in Figure 4. To predict an approximate value of the unit weight of a dry treated pile, for a wave velocity of 4,000 ft/sec and higher, use the approximate linear relationship

$$V_N = 250\gamma - 4{,}750 \tag{6}$$

For a velocity less than 4,000 ft/sec, use the approximate relationship

$$V_N = 156\gamma - 1{,}460 \tag{7}$$

Stiffness Determination

To evaluate the load-carrying capacity of a pile, the prediction of the in-place strength is most important. Stiffness is also important because the deformation and vibrational characteristics of the pile, and hence the structure, are a function of the modulus of the pile. Both the modulus and the dete-

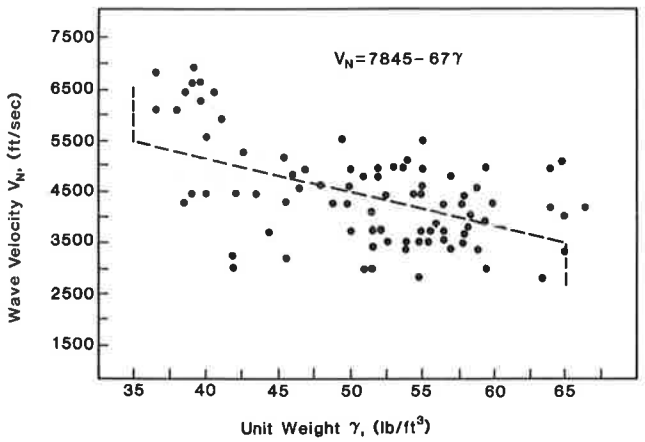

FIGURE 3 Average relationship between wave velocity and unit weight of moist treated pile sections.

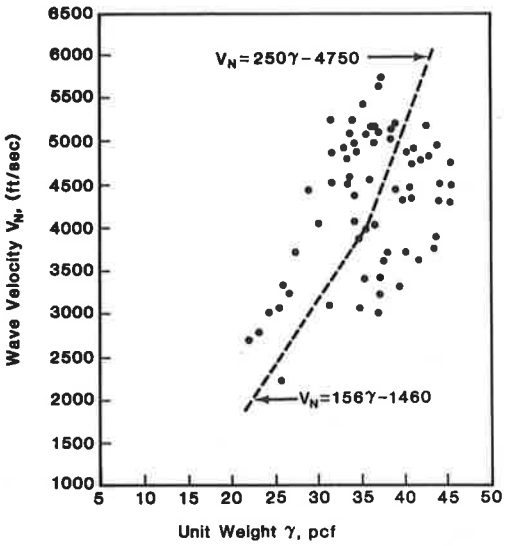

FIGURE 4 Average relationship between wave velocity and unit weight of dry treated file sections.

riorated length of the pile, relative to its total length, were shown to have a significant effect on the behavior of the pile. To determine its modulus the following relationship was developed from experimental data for dry in-service treated piles:

$$E_L = 0.465V_N^{1.232} \quad (8)$$

where E_L is the dynamic modulus parallel to the grain in ksi and V_N is the wave velocity normal to the grain in ft/sec.

CONSIDERATIONS IN ASSESSING PILE CONDITION

Several factors affect an accurate assessment of timber piling using the ultrasonic method presented, including the number of tests needed at an elevation, the effect of a crack on transit time measurements, and the spacing requirements versus desired accuracy.

Number of Tests Needed at an Elevation

Because the pulses propagated from the transducers are mainly in the direction normal to the face of the transducers, depending on the number of measurements at each section, some blind areas (i.e., areas that are not tested for possible decay) will be encountered. Figure 5 shows the relationship between the untested area of a pile section and the number of measurements made for piles with diameters of 10 and 12 in. and transducers having a diameter of 2 in. After two measurements in two perpendicular directions, four wedges, each 14 percent of the total pile area, remain untested. After three measurements in different directions, six untested wedges, each approximately equal to 6.5 percent of the total area, remain. Therefore, at least two readings taken normal to each

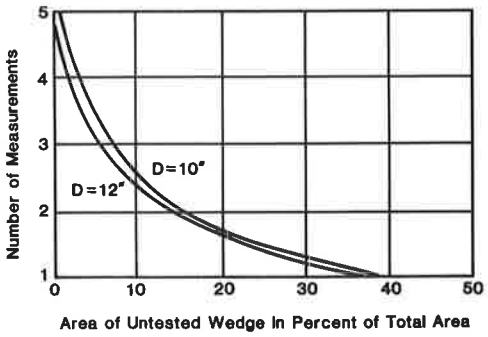

FIGURE 5 Effect of number of measurements on area of untested wedge.

other at the same elevation should be made if reliable data are to be collected.

Effect of a Crack on Transit Time Readings

Repeatability of transit time readings taken at a specific location and in the same direction through a pile has been demonstrated. A variance of less than 4 percent was shown in 50 tests. Variances up to ±45 percent were experienced for some transit time readings taken at the same elevation of a pile for readings normal to each other. The considerable difference between the two readings can be explained as follows: the longer of the two readings passed through a "pocket" of decay not encountered by the other reading; the longer of the two readings traveled around the periphery of a natural flaw, such as a crack filled with air (as when shakes are present); or a combination of these causes.

Inspection of decayed piles shows that decay almost always starts at the center of a pile and radiates outward as it advances. The decay can almost always be detected because all transmitted waves travel through the center of the pile. In some piles, however, the decay was not located in the center; such decay will probably be detected through the use of multiple readings.

To study the effect of naturally occurring cracks in wood on the wave velocity, transit time readings were taken across two smooth wood sections separated by predetermined distances that simulated cracks of various widths. The transit time increased as the width of the gap increased. A gap of 0.1 in. reduced the velocity by an average of 28 percent. Therefore, a narrow crack can affect the velocity considerably.

From tests performed on dry timber piles with and without decay, it was found that wood without decay has a unit weight greater than about 35 pcf, whereas wood with decay has a unit weight less than 35 pcf. Thus, in pile sections free of knots (because knots change the homogeneity of a section), different time readings taken at the same elevation in different directions in a pile indicating variances in transit times are suspect.

Consider a pile section of yellow pine 10 in. in diameter that was tested ultrasonically. The first reading was 180 μsec, giving a V_N of 4,630 ft/sec. From Equation 6, $\gamma = 38$ pcf, and from Equation 1, $\sigma_{cr} = 4{,}048$ psi. The data indicate that decay is not present in this pile. If a second reading is 270 μsec, 50

percent higher than the first reading, then V_N = 3,086 ft/sec. From Equation 7, γ = 29 pcf, and from Equation 3, σ_{cr} = 2,235 psi. The second reading indicates that decay is present, but it conflicts with the first reading. The second reading was probably affected by a crack in the pile. A third reading should be taken and the larger reading discarded. The rejection of a measured value is acceptable because small cracks inside the pile affect the velocity of the wave but not the strength of the pile. However, if two readings of 300 and 400 μsec are obtained, the density is now estimated at 27.2 and 22.7 pcf, respectively. Because each of these numbers is low, decay should be expected. The second reading may indicate either crack in addition to decay or an extra pocket of decay. The computed crushing strength of the pile is 1,440 and 1,173 psi, respectively. Both values indicate a marked reduction in strength over the in-service life of the pile. The difference in the transit time reading in this case is purely academic. When testing below water, the effect of such cracks is negligible, because waves are transmitted across cracks filled with water.

Spacing Requirements for Desired Accuracy

Transit time readings should be taken at regular depth intervals. A 1-ft interval along the pile, up to 4 ft above and below the waterline, and a 3-ft interval elsewhere were found to be adequate. Extra readings should be taken at intermediate points when needed to identify the physical extent of the decay. If the top of the pile is not covered, readings should also be taken there. Methods to define the spacing between test points required for a desired level of accuracy are available elsewhere (*21*).

LIMITATIONS

A detailed description of ultrasonic testing and interpretation is presented in a manual developed for FHWA (*22*). In addition, a videotape demonstrating the use of the ultrasonic method and equipment under various conditions has been prepared and is available from FHWA. The following are the main limitations of the method affecting its use.

- The method is valid in fresh water and in marine environments in the absence of marine borers. If the user knows that there are marine borers or is not sure, caution must be used in interpreting the readings. Small holes caused by marine borers could cause misinterpretation of the data. A large hole is most likely to be missed when measured by direct transmission under water.
- Most of the tests conducted to establish a data bank for new and in-service piles were on southern yellow pine, the main type of timber pile found in Maryland. It is important to know what species of timber is being tested. In many cases the species is not known, and in such a case it is recommended that a section in good condition with no decay be located (borings, sounding, could be used). The wave velocity at any location can then be compared with the readings of the good section and the relative condition of the pile determined. In some cases, the in-place strength of the timber piles is not needed but the relative condition of the piles is. In such cases, changes in the wave velocity may be compared to identify any change in the properties of the wood. There is no need to determine the species of the pile in such a case.
- In the method presented, both the wave velocity and the unit weight of the wood are needed to determine the in-place strength of the timber pile. The velocity at which sound waves travel through the timber pile in a specific direction can be easily determined. The unit weight is difficult to assess because it can only be determined accurately by destructive means. When the unit weight is not determined independently it can be inferred, though not particularly accurately, from the wave velocity. The strength of the pile is then computed on the basis of this information. The wave velocity is the only parameter actually measured to predict the strength. Though acceptable, such a situation reduced accuracy. More accurate results will be obtained when both the wave velocity and the unit weight are determined separately. There is, of course, a trade-off between accuracy and the ease with which the data are collected.
- To determine the loss of strength in a pile, both the original and the in-place strength should be known. However, the original properties of the pile material are usually not known. Average values published by ASTM, for example, can provide a reasonably good basis for comparison. In addition, engineers should keep in mind that each wood species used as piling material has local-property variation within the length of the pile.
- To date a degree of accuracy of ±20 percent in determining the strength of timber piles has been obtained. This degree of accuracy may be sufficient for timber piles, but such criteria may not be sufficient for other wood structures.

CONDITION OF TIMBER PILES IN PLACE

For a successful application of the method in the evaluation of timber piles, an understanding of the causes and types of deterioration of timber piles is essential. Further research into the cause of deterioration is needed, especially in the area of bacterial attack and the environmental conditions conducive to its growth. Figure 6 shows three different types of deterioration that timber piles experience. In the first type the piles are supporting a bridge, in the second a tank, and in the third a building.

Piles Supporting Bridges

From the experimental program, the crushing strength along the length of the piles was determined. The data from the piles tested indicated that along the pile length a reduction in strength between 10 and 40 percent had occurred; however, at the waterline (between high and low tide) a larger reduction took place in two of the bridges (up to 80 percent in one of the piles tested). This means that there existed a severely decayed part at the waterline in some piles, and the degree of decay decreased going either up or down along the pile.

In some cases piling whose external appearance suggested no damage and appeared to be in satisfactory condition indicated no wave transmitted. When these piles were removed it was found that a large decay pocket was present at the

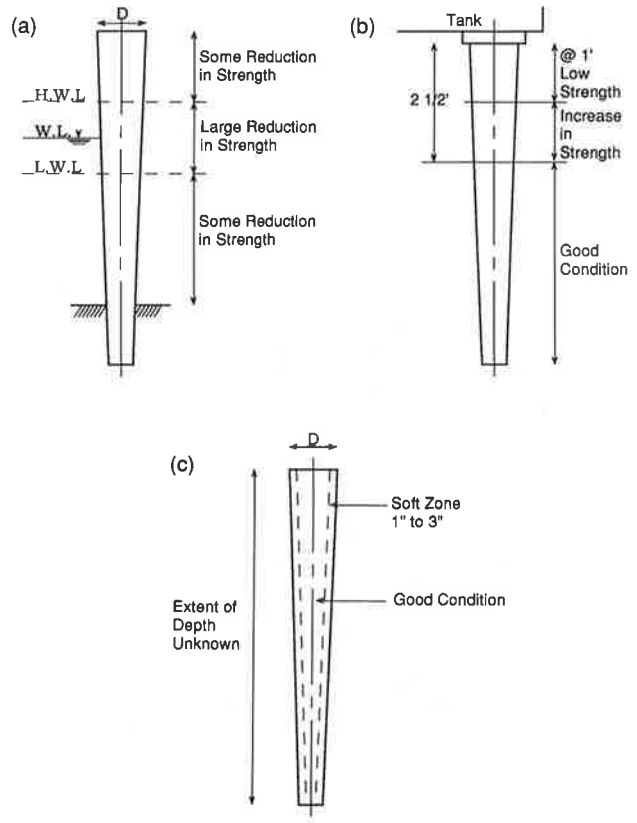

FIGURE 6 Types of deterioration of timber piles: (a) piles supporting bridges, (b) piles supporting tanks, and (c) piles supporting buildings.

center, surrounded by extensive internal decay with a shell of sound wood 2 to 3 in. thick remaining in the pile. In general, it was found that decay had occurred at the pitch of the section, whereas the treated outer ring was in better condition.

The recent failure of a bridge over the Pocomoke River in Maryland in 1988 illustrates the need for further research on the causes of deterioration of timber piles. The highway accident report from the National Transportation Safety Board (*23*) indicated that one of the causes of the failure was the continued effects of fungi, bacteria, aquatic insect larvae infestation (caddisflies), and tidal currents. These worked together to reduce the diameter of the submerged untreated timber piles by more than 2 in. in some of the piles.

Piles Supporting Tanks

Tanks that are used for storing hot asphalt are, in many instances, supported on timber piles. A study of five tanks indicated the following trend: for the top 1 ft, the pile had less than one-fourth the expected strength. For the next 1 to 1.5 ft, the strength improved markedly. Below a depth of 2.5 ft, the ultrasonic testing indicated that the pile was in good condition. Destructive testing was undertaken to verify the ultrasonic testing, and good correlations were obtained between the destructive and nondestructive measurements. The moisture content at the top section of the pile varied from 110 to 200 percent, and in some cases the dry unit weight was as low as 20 pcf. Most of the piles tested were treated Sitka spruce, except for one tank supported by yellow pine piles.

To perform the test, an excavation was undertaken to expose the piles. To minimize the amount of excavation, piles on the outside perimeter and occasionally piles in the second or third row were tested. The high temperature of the hot asphalt in the tank had caused damage to the tops of the piles (*24,25*). The length having a reduced strength, however, will depend on the temperature of the asphalt and the surrounding environmental conditions.

Piles Supporting Buildings

In this area again, limited data are available. From the data presented by Boutelje and Bravery (*4*) on the Stockholm building and from a similar situation in Boston (*26*), it can be stated that the peripheral zone of the piles becomes soft to a depth of 1 to 3 in. The soft zone had a very high moisture content and caused a marked loss in the strength of the pile.

A similar situation was encountered for piles supporting a building. In preparation for tests, excavation exposed the pile tops from 3 to about 10 ft below the cap bottom. Again, a soft zone that could be pealed was encountered under which was a much stronger material where ultrasonic readings were obtained. In the foregoing three cases, bacteria were the suspected cause of the deterioration.

SUMMARY AND CONCLUSIONS

Natural materials such as wood have inherent variances, and when the material is in service it is subjected to different elements that cause deterioration and, therefore, a change in strength. For this reason the prediction of their properties is much more difficult than for man-made materials. The paper discussed the testing method and data interpretation as well as factors that affect the testing, the conditions under which the method can be used, and its limitations.

The use of the technique for the evaluation of timber piles other than for bridges indicated the importance of understanding the conditions that lead to wood deterioration. The results of the field investigation and laboratory testing of bridge timber piles indicated the existence of two types of decay: uniform decay along the length of the piles (with a reduction in strength between 10 and 40 percent) and decay at the waterline or in the splash zone. The length of the decay in the splash zone was about 4 to 6 ft with a larger reduction in strength (up to 80 percent in one of the piles tested). In most cases a decayed or soft area was noted in the center, and the peripheral zone was in good condition. For the piles on the hot asphalt tanks the tops of the piles were soft, and for the buildings the peripheral zone was soft and the inside was in better condition.

An understanding of the causes of decay, the behavior of the ultrasonic technique, and its limitations is important for the successful inspection and evaluation of timber piles. Further research and data are needed to determine the condition of timber piles that have been in service for a long time. This is important for maintenance and replacement to meet current

or anticipated loading demands and to aid in estimating the remaining service life of the structure.

ACKNOWLEDGMENTS

The research reported herein was sponsored by the Maryland State Highway Administration in cooperation with FHWA. The author is grateful to Earle S. Freedman, A. Scott Parrish, Jr., and E. J. White, Jr., of the Maryland Department of Transportation for their support and contributions. The manual and videotape were supported by FHWA. Appreciation goes to Thomas Krylowski for his comments and review.

REFERENCES

1. T. C. Scheffer, C. G. Duncan, and T. Wilkinson. Condition of Pine Piling Submerged 62 Years in River Water. *Wood Preserving*, Vol. 47, No. 1, 1969, pp. 22–24.
2. B. A. Bendtsen. Bending Strength and Stiffness of Bridge Piles After 85 Years in the Milwaukee River. Research Note FPL-0229. Forest Service, U.S. Department of Agriculture, Madison, Wis., 1974.
3. W. E. Eslyn and W. G. Moore. Bacteria and Accompanying Deterioration in River Pilings. *Material and Organismen*, Vol. 19, 1984, pp. 263–282.
4. J. B. Boutelje and A. F. Bravery. Observations on the Bacterial Attack of Piles Supporting a Stockholm Building. *J. Inst. Wood. Sci.*, Vol. 4, 1968, pp. 47–57.
5. A. P. Singh and J. A. Butcher. Wood Degrading Bacteria in Posts. *What's New in Forest Research*, No. 174, 1989.
6. I. D. G. Lee. Ultrasonic Pulse Velocity Testing Considered as a Safety Measure for Timber Structures. *Proc., 2nd Symposium of Nondestructive Testing of Wood*, Spokane, Wash., 1965, pp. 185–203.
7. L. C. Jensen. Sonic Detection of Internal Decay in Wood Poles. *Proc., 2nd Symposium on Nondestructive Testing of Wood*, Spokane, Wash., 1965 pp. 207–221.
8. R. A. Muenow. The Ultrasonic Nondestructive Evaluation of Wood Utility Poles, Wood and Concrete Railway Ties and Trestles, and Other Similar Structures. Technical Paper V-117. James Electronics, Inc., Chicago, Ill., 1966, pp 1–6.
9. K. A. McDonald, R. G. Cox, and E. H. Bulqrin. Locating Lumber Defects by Ultrasonics. Research Paper FPL 120. Forest Service, U.S. Department of Agriculture, Madison, Wis., 1969.
10. R. F. Pellerin. Nondestructive Testing of Wood—A Possible Method for Timber Piling. *Proc., 4th Nondestructive Testing of Wood Symposium*, Vancouver, Wash., 1978, pp 169–174.
11. J. J. Agi. Nondestructive Testing of Marine Piling. *Proc., 4th Nondestructive Testing of Wood Symposium*, Vancouver, Wash., 1978, p. 187.
12. M. D. Vanderbilt, J. R. Goodman, and J. A. Puckett. Testing of Large Timber Poles. Paper A-43. Present at Society for Experimental Stress Analysis Spring Meeting, San Francisco, Calif., 1979.
13. J . R. Goodman, M. D. Vanderbilt, M. E. Criswell, and J. Bodig. *Probability-Based Design of Transmission Line Structures: Vol. I—Strength and Stiffness of Wood Utility Poles*. Report 2040. Electric Power Research Institute, 1981, 453 pp.
14. R. M. Lanius, Jr., R. Tichy, and W. M. Bulleit. Strength of Old Wood Joists. *Journal of the Structural Division*, ASCE, Vol. 107, No. ST12, 1981, pp. 2349–2363.
15. R. F. Pellerin, R. C. DeGroot, and G. R. Esenther. Nondestructive Stress Wave Measurement of Decay and Termite Attack in Experimental Units. *Proc., 5th Nondestructive Testing of Wood Symposium*, Pullman, Wash., 1985, pp. 319–352.
16. R. J. Hoyle, Jr., and P. S. Rutherford. *Stress Wave Inspection of Bridge Timbers and Decking*. Final report. Washington State Transportation Center, July 1987, 156 pp.
17. M. S. Aggour and A. Ragab. *Safety and Soundness of Submerged Timber Bridges Piling*. Interim Report FHWA/MD-82. Maryland Department of Transportation, June 1982, 421 pp.
18. M. S. Aggour, A. M. Ragab, and E. J. White, Jr. Determination of In-Place Timber Piling Strength. In *Transportation Research Record 962*, TRB, National Research Council, Washington, D.C., 1984, pp. 69–77.
19. M. S. Aggour, A. Hachichi, and M. A. Mayer. Nondestructive Evaluation of Timber Bridge Piles. *ASCE Special Publication on Evaluation and Upgrading of Wood Structures*. Structures Congress 86, New Orleans, La., Sept. 1986, pp. 82–95.
20. M. S. Aggour. *Safety and Soundness of Submerged Timber Bridge Piling*. Report FHWA/MD-87-08. Maryland Department of Transportation, Jan. 1987.
21. R. H. McCuen, M. S. Aggour, and B. M. Ayyub. Spacing for Accuracy in Ultrasonic Testing of Bridge Timber Piles. *Journal of Structural Engineering*, ASCE, Vol. 114, No. 12, Dec. 1988, pp. 2652–2668.
22. M. S. Aggour. *Inspection of Bridge Timber Piling, Operations and Analysis Manual*. Report FHWA-IP-89-017. FHWA, U.S. Department of Transportation, 1989.
23. *Highway Accident Report—Collapse of the S.R. 675 Bridge Spans over the Pocomoke River near Pocomoke City, Maryland, August 17, 1988*. PB89-916205, NTSB/HAR-89/04. National Transportation Safety Board, 1989.
24. The Forest Products Laboratory. *Wood Handbook*. USDA Agriculture Handbook 72, U.S. Government Printing Office, 1955.
25. W. L. James. Effects of Temperature and Moisture Content on Internal Friction and Speed of Sound in Douglas Fir. *Forest Products Journal*, Vol. 11, No. 9, 1961, pp. 383–390.
26. G. Kyanka. The Evaluation and Predicted Service of 19th Century Untreated Pilings in an Urban Environment. International Conference on Wood Poles and Piles, Fort Collins, Colo., 1989.

Pile Integrity Testing To Determine Storm-Induced Damage

WILLIAM CAMP AND MOHAMED HUSSEIN

Hurricane Hugo made landfall in 1989 near Charleston, South Carolina, causing extensive damage. A pleasure boat marina was exposed to the full force of the storm. The marina consisted of concrete floating docks held in place by 14-in.-square prestressed concrete piles. The 42-ft-long piles had been driven 2 years before, and installation records were not available at the time of the testing (1990). The water depth was between 2 and 10 ft, and the soil conditions consisted of approximately 10 ft of soft mud overlying the Cooper Marl. During the storm, the surge floated the docks to nearly the pile tops and the extraordinary winds and waves pushed the large pleasure boats against the piles. After the storm, it was observed that some piles could be moved several inches laterally simply by pushing on them while standing on the docks, thereby causing the pile integrity to be questioned. Short on time for the new season, the owner was faced with a serious problem with potentially expensive remedies. Low-strain integrity testing performed on each of the 78 piles provided a timely and cost-effective solution for pile structural integrity assessment. Testing was performed in 2 days at an average cost of less than $100 per pile. Testing indicated that none of the piles were structurally damaged, although some records showed evidence of tensile cracking and an absence of soil resistance. The pile testing program is discussed, and the theoretical background and field testing procedures are discussed.

In September 1989, Hurricane Hugo made landfall near Charleston, South Carolina, causing extensive damage. Many of the structures in the Charleston area were exposed to conditions that met or exceeded their expected design conditions. Most of the damage caused by the storm was obvious. However, for various reasons, the integrity of many seemingly sound structural members was questioned. Such was the case for the dock piles at a pleasure boat marina near the Charleston Harbor. The work performed to assess the poststorm integrity of the piles at this marina is summarized.

PROJECT DETAILS

Marina

The marina contains five concrete floating docks. Each dock consists of linear and perpendicular arrangements of 4-ft-wide concrete-covered foam sections. Pinned or hinged connections are used to connect the individual sections, and driven piles are used to anchor the docks in place. The piles provide lateral support while allowing the docks to rise and fall with the roughly 6-ft tidal cycles.

W. Camp, Westinghouse Environmental and Geotechnical Services, Inc., 840 Lowcountry Boulevard, Mount Pleasant, S.C. 29464. M. Hussein, Goble Rausche Likins and Associates, Inc., 8008 South Orange Avenue, Orlando, Fla. 32809.

Soils and Foundations

A total of seventy-eight 14-in.-square (area = 196 in.^{2}) prestressed concrete piles were used in the construction of the marina docks. The piles had been installed approximately 2 years before the storm. The driving records and the soil boring logs were not available at the time of testing. However, on the basis of conversations with several individuals involved with the original construction and a knowledge of local geology, the profile shown in Figure 1 was assumed to be a reasonable representation of the subsurface conditions. In general, the piles were located in 2 to 12 ft of water and penetrated roughly 10 ft of soft bottom sediments and approximately 10 to 12 ft into a stiff sandy calcareous clay (known locally as the Cooper Marl). Depending on the tides, the pile tops were 8 to 14 ft above the water surface.

During the hurricane, the storm surge caused the docks to rise to nearly the tops of the piles, creating moment arms that probable approached 35 ft. The high wind and wave forces acting on the docks as well as the loads applied by the remaining large pleasure boats must have generated extremely large bending moments in the concrete piles. Although the majority of the piles appeared to be undamaged after the storm, several deflected 2 to 4 in. when pushed laterally. In addition, some piles were left slightly out of plumb after the storm.

TEST DETAILS

All 78 piles were tested over a period of 2 days using the Pile Integrity Tester™ (PIT)—PC version system. The purpose of the tests was to evaluate the pile structural integrity. PIT tests are performed by using an accelerometer and a special power/amplifier-receiver, a small impact device (i.e., a 6-lb hammer), a personal computer with graphics capabilities, and a dedicated software package. The accelerometer is attached to the pile top and a hammer blow is applied. The measured pile top acceleration is recorded and integrated to yield velocity. The curve is displayed on the computer screen over both a time and a pile length scale. The velocity records may be amplified with exponentially increasing intensity over time to compensate for internal pile damping. Usually, a number of these traces are averaged, amplified, and plotted for each pile.

This type of test is often referred to as a low-strain test because the stress wave, generated by only a small hand-held hammer, produces correspondingly small strains. The background and specifics of the method and equipment used and

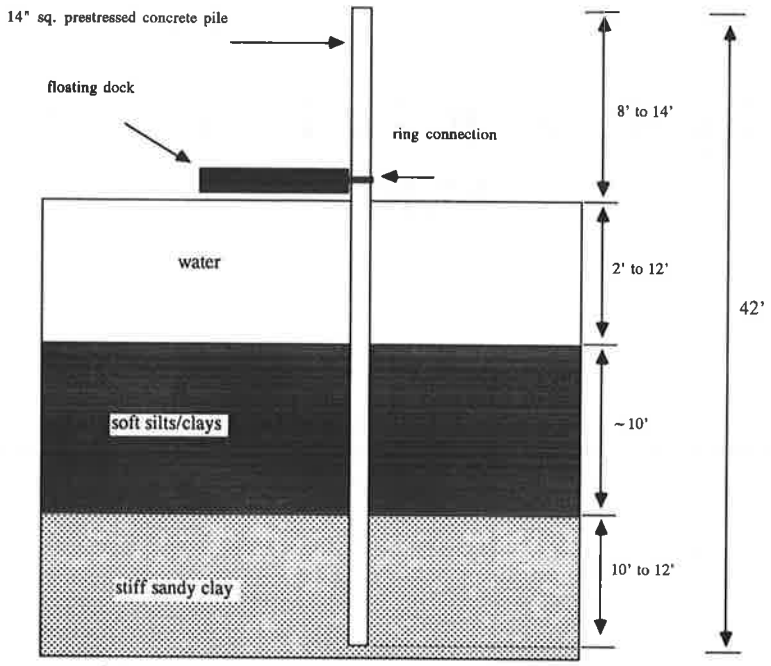

FIGURE 1 Assumed cross section.

an explanation of data interpretation may be found elsewhere (*1*,*2*).

DISCUSSION OF RESULTS

Typically, each test consisted of three or more hammer blows. Data from the blows were averaged, amplified, and plotted in the form of pile top velocity and acceleration as a function of pile length. A material stress wave speed of 14.6 ft/msec was used to convert from a time scale to a length scale. A typical result is shown in Figure 2; averaged and amplified pile top velocity and acceleration records are plotted on a length scale and superimposed pile length graphically depicting the applied data magnification.

Assessments of structural pile integrity were based on the obtained records and their interpretation assuming a stress wave speed of 14.6 ft/msec. Typical data from apparently problem-free piles are shown in Figure 3. In general, the test records indicated that the piles were structurally sound. However, approximately half of the 78 piles had indications of possible minor cracks at roughly the pile midpoint. In making such interpretations, previous test results from two extracted piles lying on the ground were considered. One pile had a major crack 27 ft below the pile top. The record from this pile is shown in Figure 4. The pile was essentially broken but held together by the prestressing cables. The other pile had visible hairline cracks but no other apparent damage. Data from this pile were used as a control record. Pile records from the marina project were compared with this control record to aid interpretation. Such a comparison is shown in Figure 5, which includes the control record and typical records from piles with possible minor cracking.

Low-strain pile top records were also indicative of apparent soil resistance. The majority of the pile records exhibited evidence of soil resistance (a relative decrease in velocity) beginning 7 to 14 ft above the pile toe. However, roughly 25 percent of the piles had very little frictional soil resistance. Figure 6 shows the difference between a pile with no apparent soil resistance and piles with resistance occurring at varying depths.

CONCLUSIONS

The client was informed that from a structural integrity standpoint, all piles were satisfactory. The tensile cracking may have been caused by the storm; however, the location of the cracking generally corresponded to the midpoint of the pile regardless of the depth at which frictional resistance first became apparent. Therefore, it was thought that the cracking had probably occurred during handling or installation of the pile rather than during the storm loading. It was noted that the zone of cracking was frequently above the mudline and in a highly corrosive environment. Consequently, the effect of the cracking on the long term integrity of a pile was unknown. Subsequent integrity testing over the lifetime of the marina could be used to monitor the suspect piles to determine whether significant corrosion was occurring. Because "baseline" records are already available, such an approach should be reliable.

The apparent lack of soil resistance observed on many of the piles is thought to explain the relatively large lateral deflections that occurred, according to the marina personnel, under small loads. The lack of resistance could be a result of a lateral soil failure caused by excessive loading or erosion. Both possibilities could be related to the hurricane. The lack of resistance could also have been caused by design or construction errors. Regardless of the cause, it was recommended that the lateral capacity of the suspect piles be reevaluated

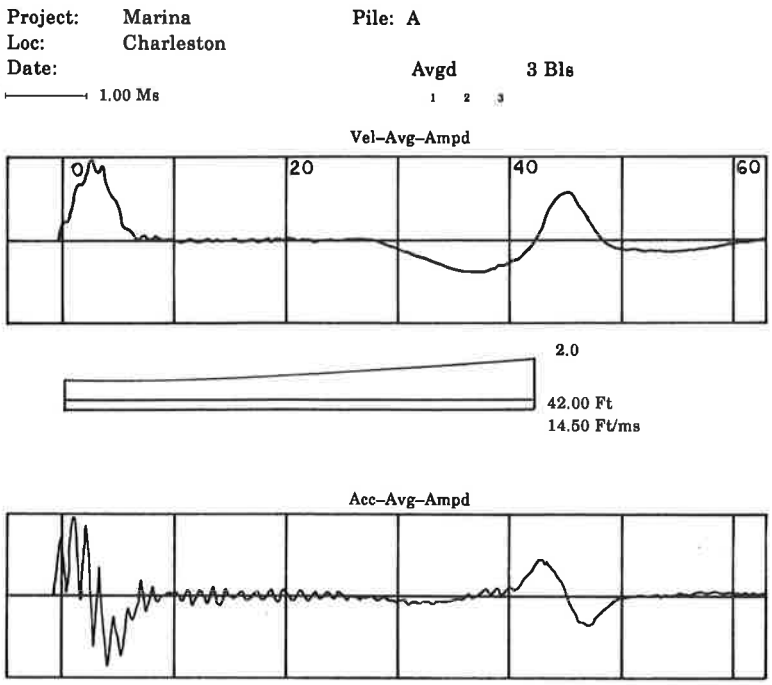

FIGURE 2 Typical PIT results.

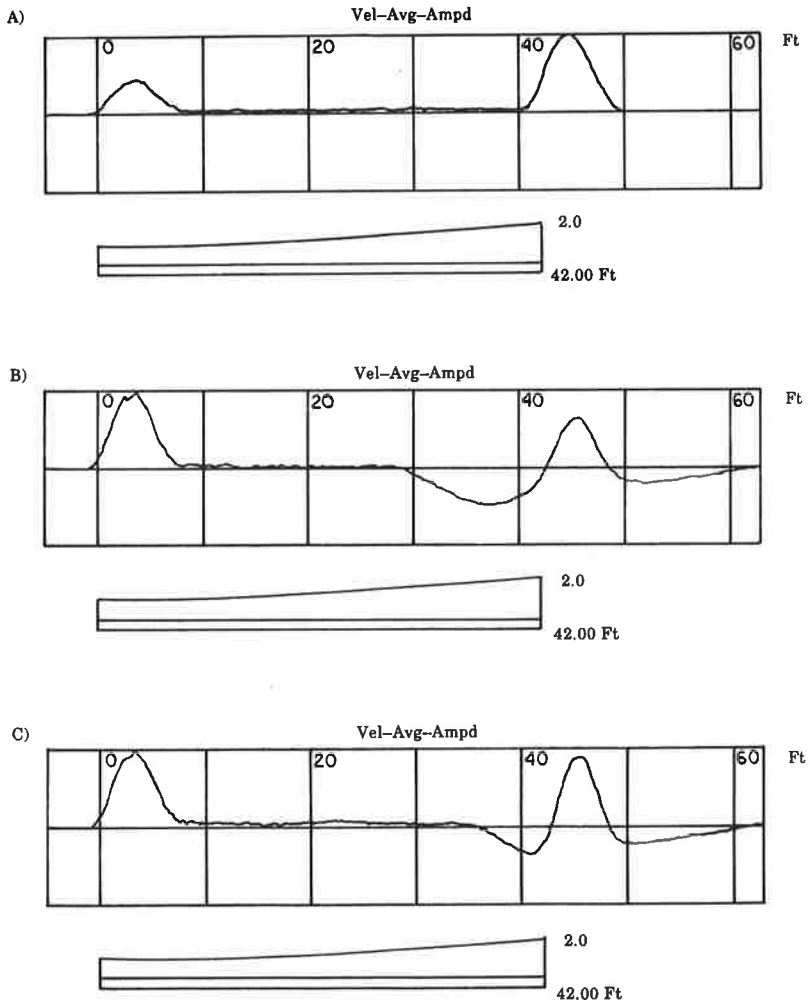

FIGURE 3 Typical results from piles with no integrity problems.

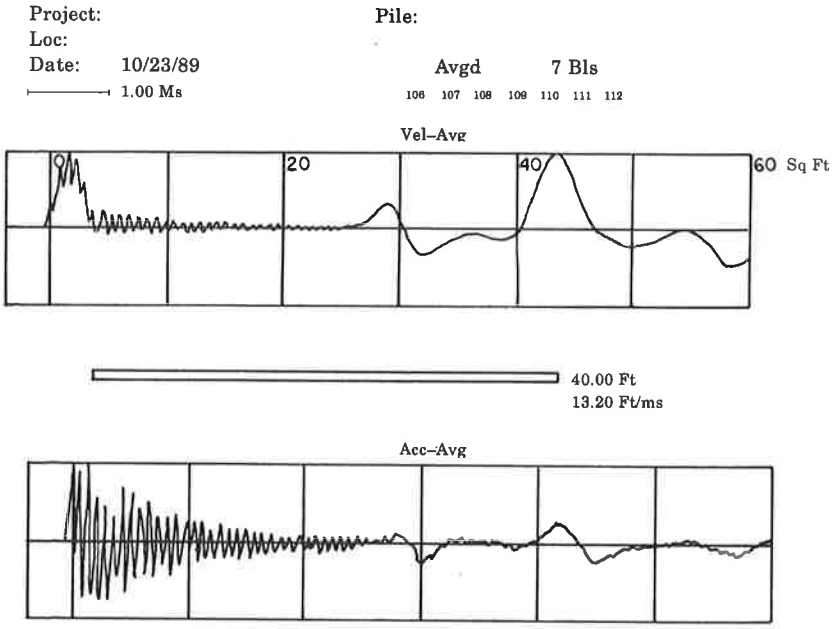

FIGURE 4 Extracted pile with major crack at 27 ft.

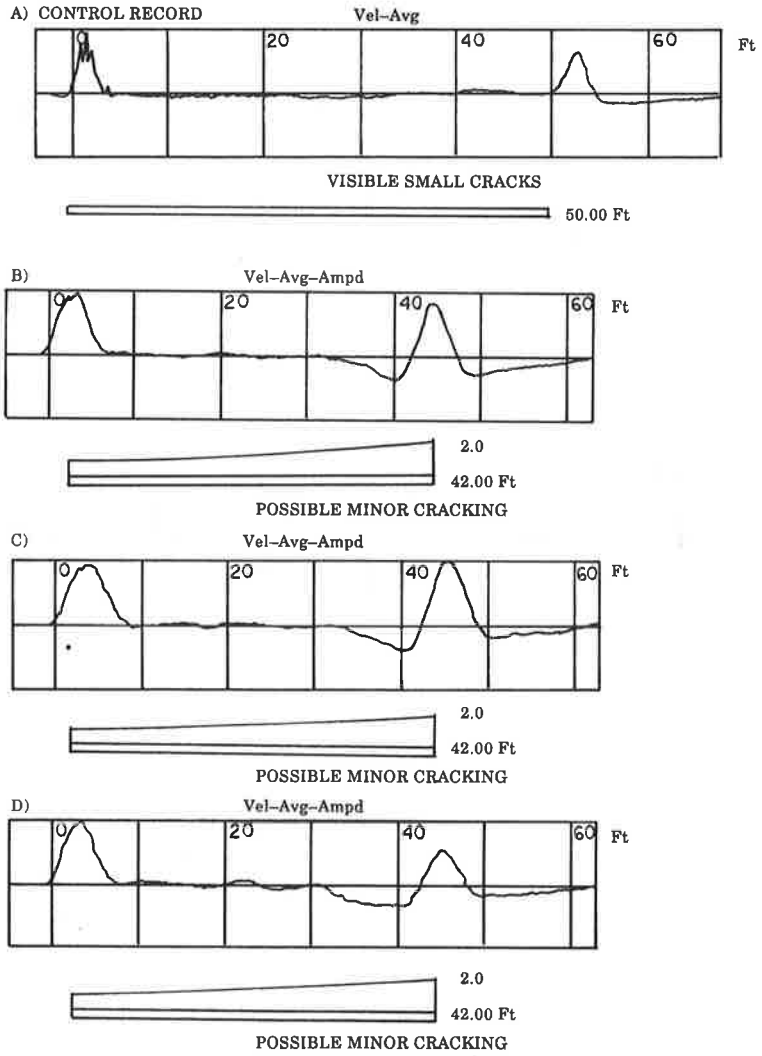

FIGURE 5 Control record and typical records indicating possible minor cracking.

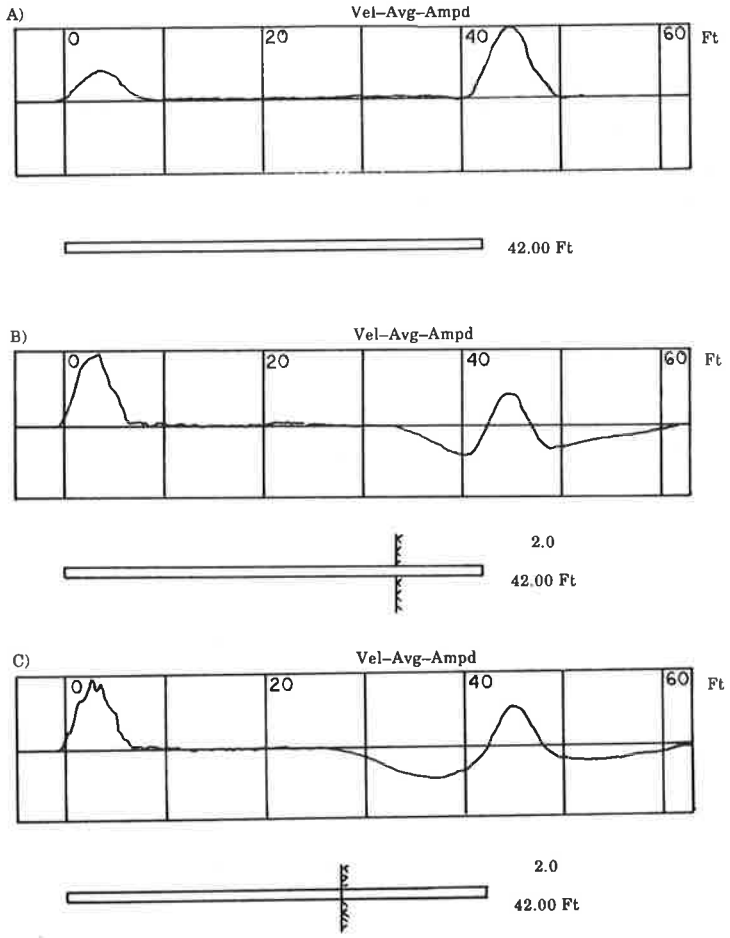

FIGURE 6 Typical records indicating varying amounts of soil resistance: A, no resistance; B, resistance below 34 ft; C, resistance below 28 ft.

through additional exploration and analysis and confirmed via lateral load testing.

For a cost less than $100 per pile, the testing provided the means to rationally evaluate the serviceability of every pile at the marina. The alternatives would have been to do nothing or replace arbitrarily selected piles. In comparison, the low-strain integrity testing provided the most information at the lowest cost.

REFERENCES

1. *Pile Integrity Tester—PC Version Manual*, Goble Rausche Likins and Associates, Inc., Cleveland, Ohio, 1988.
2. F. Rausche, G. E. Likins, and M. Hussein. Pile Integrity by Low and High Strain Impacts. Third International Conference on the Application of Stress Wave Theory to Piles. International Society for Soil Mechanics and Foundation Engineering and the Canadian Geotechnical Society, Ottawa, Ontario, Canada, 1988.

Accuracy and Limitations of Full-Scale Dynamic Shaft Testing

B. HERITIER, J. PAQUET, AND R. T. STAIN

Dynamic methods of load testing driven piles and bored shafts are in common use throughout the United States and Europe. The complex equations and computer programs used to analyze the data from such tests might lead to the assumption that the results are equally precise. In fact, little is known or has been published about the absolute accuracy of such methods. The potential sources of error that may exist in all phases of the operation, from data collection to correlation with static load tests, are described. The differences between the classical CASE method and the SIMBAT technique are discussed.

Method of predicting the capacity of driven piles using dynamic loading have been available for many years and are well documented and extensively used. When these techniques are used on bored cast-in-place shafts, new problems arise, not the least being that of increased scale. More important, the shaft dimensions and properties are more difficult to quantify than those of precast piles, and these factors influence the accuracy of the predictions.

The Centre Experimental de Recherches et d'Etudes du Batiment et des Travaux Publics (CEBTP) has carried out research in dynamic test methods since 1980 and has participated in Class A prediction trials in the United States and Europe. Working tests have been carried out on shafts ranging in diameter from 8 to 48 in. in a wide range of soil conditions. This research led to the development of a methodology specifically adapted to bored shafts known as SIMBAT (Simulation de Battage). It also made the authors aware of the potential errors inherent in all types of dynamic pile test and the difficulty of obtaining genuine static/dynamic correlations.

This paper has the following aims: to create an awareness of the potential cumulative errors that are inherent in dynamic load testing, to highlight the difficulty of obtaining genuine static/dynamic correlations, and to compare the CASE method of predicting static load test results with the SIMBAT technique.

TEST ACCURACY

The result of a dynamic load test is either a single value quoted as being the shaft capacity or a load settlement plot. How accurate are these results? Plus or minus 5 percent? Plus or minus 50 percent? Most engineers would find the former to be an acceptable possible error but the latter unacceptable. A shaft capacity reported as being 100 tons but that could be anything between 50 and 150 tons is of little or no practical use.

The problem is that the real accuracy of dynamic testing is not known. It is all too easy to develop complicated formulas and compute results to the nth decimal place, and when the job is done it looks very accurate. It is an easy and fatal step to think that the accuracy of our arithmetic is equivalent to the accuracy of our knowledge about the problem in hand.

This paper does not attempt to answer these problems but instead considers the various sources of error that can arise. The general arrangement of a dynamic test system is shown in Figure 1, and the separate stages of a test are shown in Figure 2.

The potential sources of error in the various phases of the test are given in Tables 1 through 3. Readers might like to insert their own estimates in the right-hand column. Often, some of these errors will be positive and some negative, and they will partially cancel each other out. They may, however, conspire together and produce a cumulative effect.

In a driven precast pile many of the assumed values are interlocking, and there is less room for global error. For example, the pile impedance is calculated from the same terms as is the conversion of strain to force.

$$Z = \rho CA \tag{1}$$

where

ρ = concrete density,
C = bar wave velocity in pile, and
A = pile cross-section

$$\text{Force} = \text{Strain} \times EA \tag{2}$$

where

$$E = \text{dynamic modulus of concrete} = \rho C^2 \tag{3}$$

For a bored shaft, however, it must be remembered that the strain to force calculation is based on the properties of the instrumented section of shaft, whereas the impedance calculation requires a knowledge of these parameters for the shaft as a whole. It is unlikely, for example, that the shaft cross-sectional area will be uniform over the full length or that the concrete modulus of the shaft will be identical to that of the instrumented section. It is apparent that even if modest values are inserted in the "estimated accuracy" column of Tables 1 through 3, the net effect on global accuracy will be significant.

B. Heritier and J. Paquet, CEBTP, Domaine de St. Paul, B.P. No. 37, 78470 Saint-Remy-les-Chevreuse, Paris, France. R. T. Stain, Testconsult CEBTP Limited, 11 Trinity Court, Risley, Warrington, Cheshire WA3 6QT, United Kingdom.

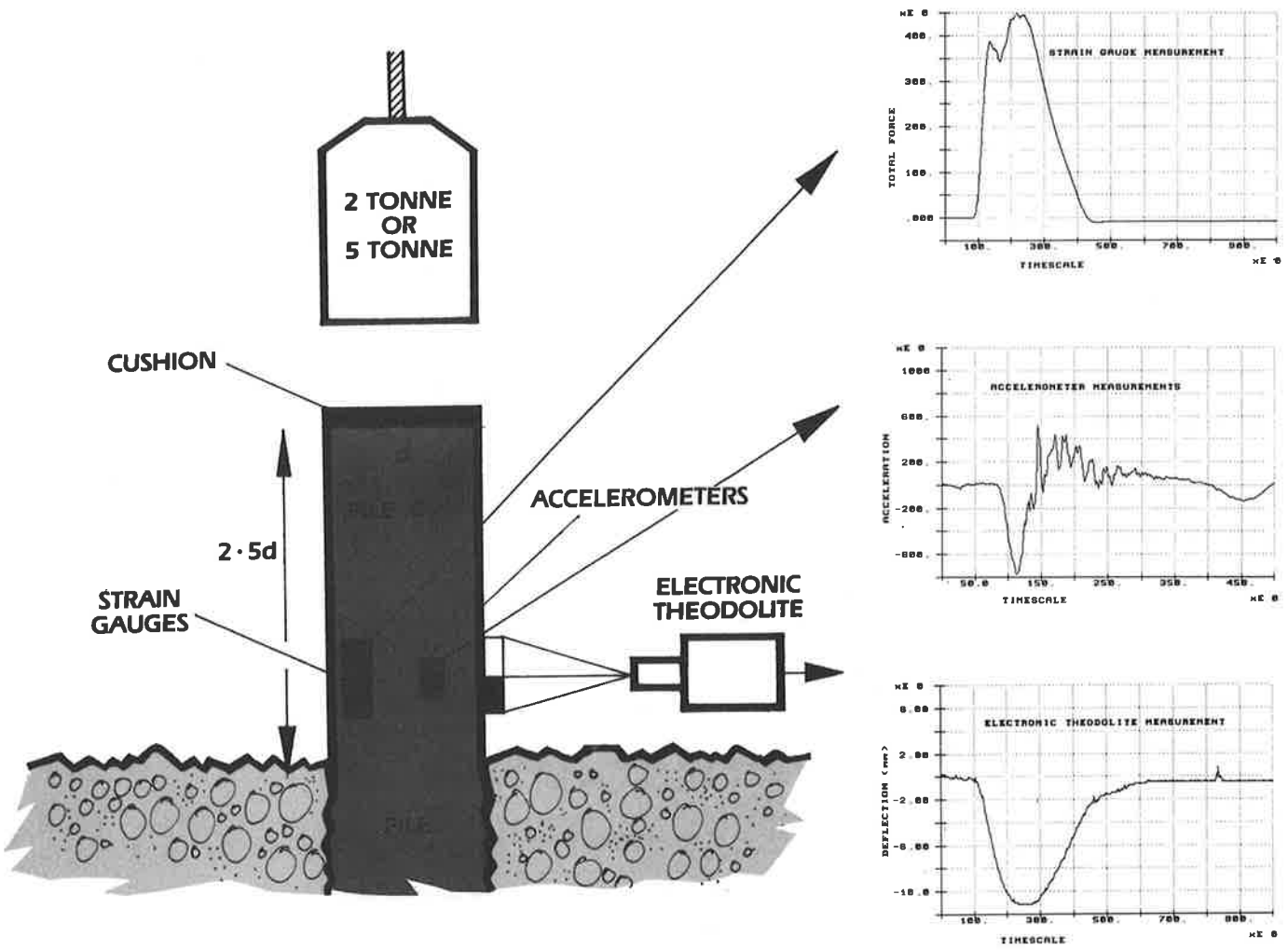

FIGURE 1 General arrangement of system.

A number of measures to improve accuracy are available:

- Low-strain transient dynamic response testing to try to obtain wave velocity and characteristic impedance values for the shaft;
- Ultrasonic testing of a concrete cylinder, representative of the shaft top, to obtain a dynamic modulus value; and
- Use of an electronic theodolite to measure shaft displacement. The shaft top velocity can then be obtained either by integration of acceleration or from the differential of displacement, the two measuring systems being independent.

Finally, construction records of the shaft and a knowledge of the soil conditions are indispensable if useful predictions are to be made.

CORRELATION BETWEEN DYNAMIC AND STATIC LOAD TESTS

The most common form of correlation is a comparison between the predicted "ultimate" capacity from a dynamic test and the "ultimate" capacity as defined by the well-known Davisson criteria from a static result. Whereas this is a convenient method of comparing results, it does not tell the whole story in the way that a full load/settlement plot does. There is also ambiguity in the term "static load test." Is it a constant rate of penetration test or an incremental test with the load maintained for several hours so that creep and possible short-term consolidation can occur? The situation is not clear, and there are at present no universally accepted correlation procedures.

Many researchers, including the authors, believe that for the present the most satisfactory way of comparing results is by means of full load/settlement plots. In this way, any differences such as creep and consolidation can be identified.

Genuine correlations between dynamic and static load tests are difficult to obtain. Once a shaft or pile has been loaded to failure, either dynamically or statically, it is no longer virgin and cannot be expected on retest to behave in the same manner. This is particularly true in cohesive or silty soils. How then can true correlations be obtained?

The simplest and most common method is by carrying out a dynamic test either before or after static loading. This must be considered unreliable, or, at the least, of limited accuracy. It is of course possible to sandwich a static test between two

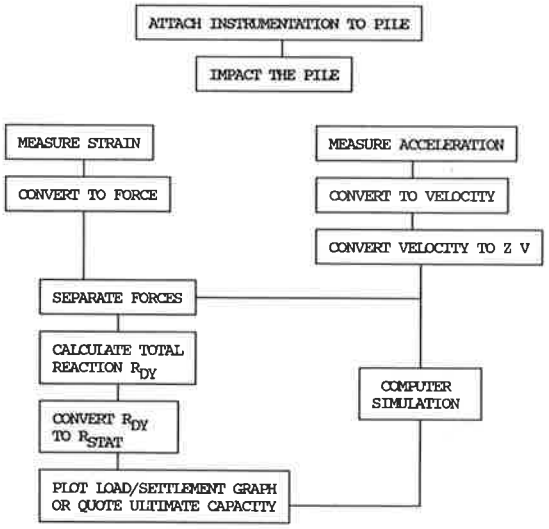

FIGURE 2 Stages of a test.

dynamic tests, one carried out before and one after the static test. This would give a good indication of performance changes brought about by the testing itself—if there were none, the correlation could be considered valid.

An alternative approach, and one which was used on a trial site in Belgium (*1*), was to construct a series of shafts, each with its own twin a few feet away. Dynamic tests were carried out on the first set of shafts, followed by static loading of the twins. One can never know for certain whether the twins were identical, but encouraging results were obtained.

COMPARISON OF THE CASE AND SIMBAT METHODOLOGIES

The SIMBAT technique is a relative newcomer in the field of dynamic load testing. It was developed in France by CEBTP and is the result of some 10 years of research, both in the laboratory and in the field. The system uses many of the

TABLE 1 TOTAL FORCE MEASUREMENT

OPERATION	POTENTIAL SOURCE OF ERROR	ESTIMATED ACCURACY
Attachment of Strain Gauges to Pile Shaft	Poor Bonding/attachment Non-Verticality	± %
Measurement of Strain	Does strain measured at 2 points on pile surface accurately represent average strain over the full shaft section	± %
	Strain gauge accuracy, temperature effects etc.	± %
	Eccentricity of hammer impact on shaft	± %
	Transmission of strain gauge signal through connecting cables to Data Acquisition	± %
	Accuracy and resolution of Data Acquisition System	± %
Conversion of Strain to Force	Force = Strain x Section x Modulus	
	Accuracy of Modulus Assumption (particularly if pile has steel sleeve)	± %
	Accuracy of Section Measurement	± %
	Global Accuracy of Force Measurement	± %

TABLE 2 VELOCITY MEASUREMENT

OPERATION	POTENTIAL SOURCE OF ERROR	ESTIMATED ACCURACY
Attachment of Accelerometers to Pile	Poor attachment Non-Verticality	± %
Measurement of Strain Acceleration	Accelerometer accuracy, temperature effects etc.	± %
	Transmission of signal to Data Acquisition System	± %
	Accuracy and resolution of Data Acquisition System	± %
Conversion of Acceleration to Velocity	Velocity = Integral of Acceleration	
	Progressive errors, integration constant etc.	± %
	Global Accuracy of Velocity Measurement	± %

TABLE 3 PREDICTION OF ULTIMATE CAPACITY FROM FORCE AND VELOCITY

OPERATION	POTENTIAL SOURCE OF ERROR	ESTIMATED ACCURACY
Multiply Velocity by Impedance (Z)	Assumption of $Z = \rho CA$, where ρ = concrete density, C = Bar wave velocity in pile, A = Pile cross-section	± %
Separation of Forces and Calculation of Total Reaction	Choice of position on Force Separation Diagram (See Fig 3)	± %
	Are all the upward forces due to soil effects or, in the case of bored shafts, is there a contribution from shaft enlargements etc.	± %
Conversion of Total Reaction to Static Reaction	Choice of Methodology CASE CAPWAP TNO SIMBAT	± %
Prediction of Ultimate Capacity Velocity	What is Ultimate Capacity? Choice of definitions.	± %
	Have all the soil resistance forces been utilised?	± %
	Global Accuracy of Prediction	± %

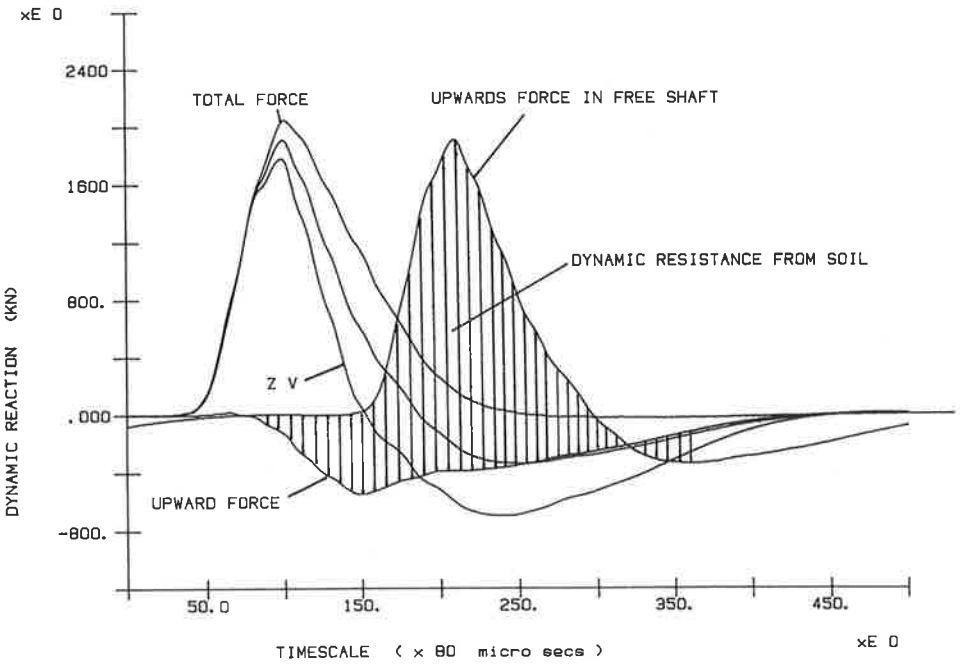

FIGURE 3 Force separation diagram.

original wave equation theories but differs from other systems in a number of areas. These have been described previously by Paquet (*2*). Probably the most important single difference is the conversion of dynamic total resistance to static resistance.

The classical CASE formula states that the dynamic to static conversion is related to the pile top velocity as described by Hannigan (*3*):

$$R_{STAT} = R_{DY} - Jc(ZV_1 + F_1 - R_{DY}) \quad (4)$$

where

R_{STAT} = static resistance,
R_{DY} = dynamic or total resistance,
V_1 = velocity at Time 1,
F_1 = force at Time 1, and
Jc = dimensionless CASE damping factor.

This assumes that all the damping resistances are concentrated at the shaft toe.

In the SIMBAT method it is proposed that the relationship between dynamic and static resistance is a function of the penetration velocity of the shaft with respect to the soil:

$$R_{STAT} = R_{DY} - f(\text{Vpen}) \quad (5)$$

where f(Vpen) is a function of penetration velocity.

The shaft velocity and the penetration velocity are quite different, as can be seen in Figure 4.

The second important difference between methodologies is that SIMBAT uses a series of impacts on the shaft, often 10 or more, the permanent settlement of penetration being measured for each blow. The reactions are then plotted against cumulative penetration. Finally, Equation 5 is applied to the set of results as a whole to obtain a static load settlement plot. This procedure does not require the assumption of a soil damping factor.

The two methods were compared using a series of blows on a driven cast-in-place shaft in France. The shaft was 550 mm in diameter and 16.4 m in length and formed in silty sand. The CASE capacity was calculated for four of the blows using a soil damping factor (J) of both 0.2 and 0.4, these being appropriate values for the soil conditions. The results are given in Table 4 and are plotted in Figure 5. The differences between the two predictions are immediately apparent.

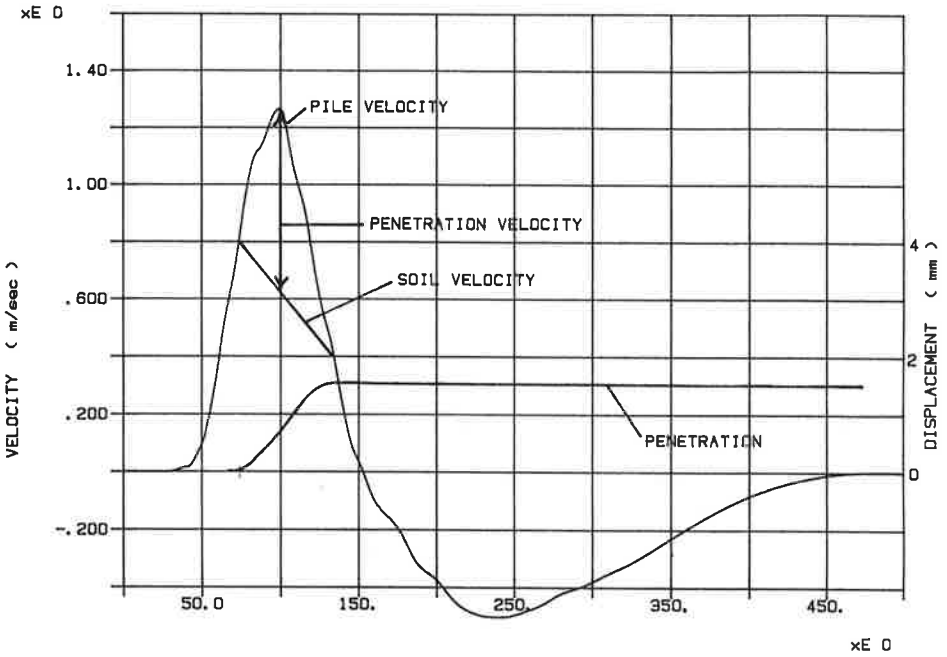

FIGURE 4 Velocities in pile-soil interaction.

TABLE 4 COMPARISON OF CASE AND SIMBAT PREDICTIONS

BLOW No.	DROP HEIGHT (m)	PEN (mm)	DYNAMIC RESISTANCE (KN)	SIMBAT STATIC RESISTANCE (KN)	CASE STATIC RESISTANCE (KN)	
					J = 0.2	J = 0.4
1	0.3	0.85	2300	2650		
2	0.4	0.96	2900	2166		
3	0.5	0.85	2900	2250		
4	0.6	1.48	3460	2328		
5	0.7	1.73	3755	2432		
6	1.0	2.47	4480	2590	3876	3187
7	0.4	0.44	2900	2563		
8	1.0	2.51	4750	2830	4153	3330
9	0.5	0.81	3360	2740		
10	1.2	3.36	5400	2830	4571	3689
11	0.5	1.00	3680	2915		
12	1.5	3.65	6000	3208	5221	4241

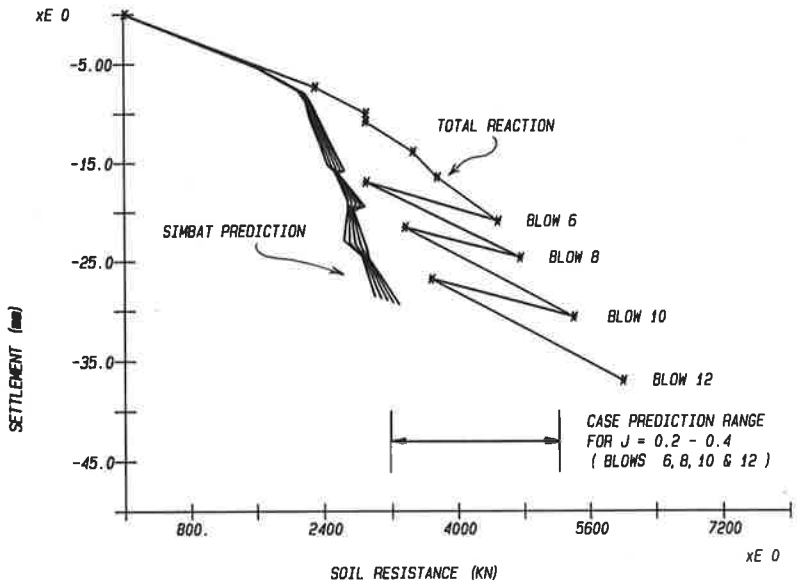

FIGURE 5 SIMBAT and CASE pile capacity predictions.

CONCLUDING REMARKS

It may seem strange that practitioners of dynamic testing should seek to publicize the potential errors and limitations of these methods. The intention is not to discredit such tests, but rather to create an awareness of potential errors and the measures that can be taken to reduce them. Dynamic/static correlations of 1:1 are probably the result of happy coincidence rather than the application of science.

The current Federal Highway Administration program of dynamic testing in California and Texas is providing an enormous data base from which some of the questions raised in this paper may be answered.

REFERENCES

1. P. J. Hannigan. Dynamic Pile Testing and Analysis. 11th Annual Fundamentals of Deep Foundation Design, University of Missouri at Rolla, Rolla, 1986.
2. J. Paquet. Checking Beating Capacity by Dynamic Loading—Choice of a Methodology. Third International Conference on Application of Stress-Wave Theory to Piles, Ottawa, Ontario, Canada, 1988.
3. P. J. Hannigan. Pile Dynamic Testing, Integrity and Bearing Capacity. Conference proceedings. Groupement Belge de la Societe Internationale de Mechanique des Sols et des Travaux de Fondations, Brussels, 1987.

Bearing Capacity of Strip Footing Supported by Two-Layer c-ϕ Soils

G. AZAM AND M. C. WANG

The ultimate bearing capacity of an embedded strip footing supported by two-layer c-ϕ soils has been investigated using an elastoplastic finite-element computer program. In the program the footing material is treated as linear elastic and the foundation soils are idealized as nonlinear elastic perfectly plastic materials that obey the yield criterion of Drucker and Prager. The program also considers initial stresses, interface behavior, and tension failure of soil. The analysis was performed on a VAX 11/785 computer. Three soils—a commercial kaolin, a silty clay, and a clayey sand—were selected for analysis of a representative number of soil layer combinations. The analysis was performed for a constant footing width and varying levels of top-layer thickness. The propagation of plastic yield zones under progressive increments of footing load was investigated, and a generalized procedure for determining bearing capacity from computer-generated pressure-settlement curves was proposed. Meanwhile, on the basis of the analysis results, a semiempirical equation was developed for determining ultimate bearing capacity. A comparison with existing theories indicates that the developed equation can provide more-reasonable results than the existing ones can. Additionally, the developed equation is relatively simple and can be easily applied.

Shallow foundations are sometimes located on a soil layer of finite thickness overlying a thick stratum of another soil. The underlying stratum may be either a bedrock or another soil possessing different strength properties. The bearing stratum of the two-layer deposits can be either softer or stiffer than the underlying stratum. If the footing rests on a relatively thin stiff layer above a soft deposit, it may punch through the top layer into the underlying stratum. In such a case, the settlement and ultimate bearing-capacity behavior of the footing will, to a large extent, be governed by the strength characteristics of the underlying stratum. On the other hand, for a footing resting on a relatively thick soft layer overlying a stiff layer, bearing-capacity failure may be limited to the top layer. In both situations, the settlement and bearing-capacity characteristics of the footing will be greatly influenced by the thickness of the top stratum and the strength properties of the two soil layers.

Bearing-capacity theories for two-layer soil deposits are scarce in published literature, and the theories that have been proposed have limitations that restrict their use to idealized conditions. For example, most of the proposed equations apply either to purely cohesive ($\phi = 0$) two-layer soils or to soil layers made up of a cohesionless ($c = 0$) and a cohesive ($\phi = 0$) soil. Furthermore, the proposed equations for two-layer clay soils usually assume that the top layer is stiffer than the bottom layer, that is, that $c_1 > c_2$.

This paper presents the results of a study involving two-layer c-ϕ soils in which the top layer may be either stiffer or softer than the bottom layer. The results of analyses have been used to formulate a semiempirical bearing-capacity equation, the results of which have been compared with the existing equations.

G. Azam, Directorate of Design and Consultancy, Engineer-in-Chief's Branch, General Headquarters, Rawalpindi, Pakistan. M. C. Wang, Department of Civil Engineering, 212 Sackett Building, Pennsylvania State University, University Park, Pa. 16802.

EXISTING THEORIES

Researchers have proposed relationships for predicting the ultimate bearing capacity of footings on homogeneous two-layer soils. However, as mentioned, all of the proposed equations have limitations. A review of the available bearing-capacity equations and their limitations for two-layer soils is presented in subsequent sections.

Bearing-Capacity Theories for Purely Cohesive Two-Layer Soils

The bearing capacity of strip footings on two-layer clay soils, for a stiff layer overlying a soft stratum and for its converse, has been analyzed by Button (*1*). He assumed a general shear failure along cylindrical slip surfaces that emanate from the edges of the footing. He presented modified bearing-capacity factors (N_c) for ϕ-soils for various values of c_2/c_1, where c_1 and c_2 are the undrained cohesions (or undrained shear strengths) of the top and bottom layers, respectively. However, experimental data of Brown and Meyerhof (*2*) showed that Button's (*1*) assumed failure modes were unrealistic and that the resulting bearing-capacity factors were on the unsafe side. They proposed the following bearing-capacity equation for conditions in which the bearing stratum can be softer or stiffer than the underlying stratum:

$$q_u = c_1 N_m + q \tag{1}$$

where

q_u = ultimate bearing capacity,
q = overburden pressure equal to the unit weight of soil times the depth of foundation, and
N_m = modified bearing-capacity factor that depends on c_2/c_1, the relative thickness of the upper layer (H_1/B), and the footing shape.

Meyerhof and Hanna (*3*) have proposed a bearing-capacity theory for a strip footing supported by a two-layer clay in which the top layer is stronger than the bottom layer. In their failure mechanism, it is assumed that if the top layer is relatively thin, failure takes place when it is punched through and the bottom layer undergoes a general shear failure. However, if the top layer is relatively thick, the failure surface will be fully contained in the top clay layer. Thus, the ultimate bearing capacity of a strip footing can be expressed as

$$q_u = c_2 N_c + \frac{2c_a H_1}{B} + \gamma_1 D_f \leq q_t \tag{2}$$

where

$q_t = c_1 N_c + \gamma_1 D_f$,
N_c = bearing capacity factor = 5.14,
D_f = depth of foundation, and
c_a = soil adhesion, a function of c_2/c_1.

Bearing-Capacity Theories for Sand Overlying Cohesive Soils

Tcheng (*4*) has proposed a bearing-capacity equation for a long rectangular footing resting on a sand layer that is underlain by a purely cohesive soil layer. He reported good agreement between his test results and the proposed equation within the domain $H_1 < 1.5B$. He further reported that the influence of the bottom clay layer on bearing capacity becomes negligible when $H_1 \geq 3.5B$. Tcheng's equation is as follows:

$$q_o = q_o'' \left\{1 - 2(H_1/B)\tan\phi(1 + \sin\phi) \times \exp\left[-\left(\frac{\pi}{4} - \frac{\phi}{2}\right)\tan\phi\right]\right\} \tag{3}$$

where

q_o = bearing capacity of a long rectangular footing resting on the sand layer,
q_o'' = bearing capacity of the same footing resting on the underlying clay layer, and
ϕ = angle of internal friction.

Vesic (*5*) has proposed a more general bearing-capacity equation, which is valid for rectangular footings resting on a top layer with strength parameters (c_1,ϕ_1) that is underlain by a weaker layer with strength parameters (c_2,ϕ_2). It is shown as

$$q_o = [q_o'' + (1/K)c_1\cot\phi_1]\exp[2(1 + B/L) \times K\tan\phi_1(H_1/B)] - (1/K)c_1\cot\phi_1 \tag{4}$$

where

$K = \dfrac{1 - \sin^2\phi_1}{1 + \sin^2\phi_1}$,
L = footing length, and
q_o'' = bearing capacity of a fictitious footing of the same size and shape as the actual footing but resting on the top of bottom layer.

Meyerhof (*6*) and Hanna and Meyerhof (*7*) have studied the ultimate bearing capacity of footings on either a loose or a dense sand layer overlying a clay and have compared the different modes of soil failure with the results of model tests on circular and strip footings. For a strip footing resting on a dense sand that overlies a soft clay, the bearing capacity was found to increase with sand-layer thickness until about $H_1/B \geq 2.5$ (*6*); thereafter, it remained constant at a value equal to the ultimate bearing capacity of an infinitely thick dense sand layer. For a strip footing resting on a dense sand layer that overlies a firm clay, the test results showed a decrease in the ultimate bearing capacity with increasing sand-layer thickness. The bearing capacity decreases from the initial maximum value (for a footing on an infinite clay layer) to the minimum for a footing on a thick sand deposit. For this case, Meyerhof (*6*) has proposed the following equations:

$$q_u = q_t + (q_b - q_t)(1 - H_1/H_f)^2 \tag{5}$$

with a maximum for $H_1/B = 0$

$$q_u = q_b = cN_c + \gamma D \tag{6}$$

and a minimum for $H_1/B \geq H_f/B$

$$q_u = q_t = \frac{1}{2}\gamma B N_\gamma + \gamma D N_q \tag{7}$$

where H_f is the failure depth.

Satyanarayana and Garg (*8*) have proposed a simplified bearing-capacity theory for shallow foundations in c-ϕ soils. According to their theory, the ultimate bearing capacity of a two-layer soil is given by

$$q_u = c_{av}N_c + \gamma_1 D N_q + \frac{1}{2}\gamma_1 B N_\gamma \tag{8}$$

where

$$c_{av} = \frac{H_1c_1 + H_2c_2}{H_1 + H_2},$$

$$\phi_{av} = \tan^{-1}\left(\frac{H_1\tan\phi_1 + H_2\tan\phi_2}{H_1 + H_2}\right),$$

$$H_2 = (2B - H_1)\left(\frac{c_1 + \tan\phi_1}{c_2 + \tan\phi_2}\right), \text{ and}$$

N_c, N_q, N_γ = bearing capacity factors based on ϕ_{av}.

As is seen from the review, only one equation proposed by Satyanarayana and Garg (*8*) is available for predicting the ultimate bearing capacity of two-layer c-ϕ soils. For this equation, the proposers even caution abut applying the equation to all soils.

FINITE-ELEMENT ANALYSIS

A two-dimensional plane strain elasto-plastic finite-element computer program was used for analysis. The program uses incremental stress-strain relations for elastic perfectly plastic materials and either Mohr-Coulomb or Drucker-Prager (*9*) yield criteria to define soil yielding. It was specifically adapted and modified to include (a) capability for incorporating geostatic (initial) stresses to represent the stress state in the soil mass before the application of boundary loads, (b) interface elements to satisfy displacement compatibilities along the vertical boundaries between the foundation and soil, (c) footing material (reinforced concrete) modeled as a linearly elastic material, and (d) soil modeled as nonlinearly elastic in the elastic range. A complete description of the numerical and mathematical formulations of the program, including validation, is available elsewhere (*10*).

The finite-element computer program was used to investigate the behavior of a reinforced concrete strip footing having B = 3.0 ft (91.4 cm) and D_f = 3.0 ft (91.4 cm), shown schematically in Figure 1. The footing was supported by a two-layer soil deposit having four different layer combinations: a soft clay underlain by a stiff clay, a stiff clay underlain by a soft clay, a clayey sand underlain by a stiff clay, and a stiff clay underlain by a clayey sand. The stiff clay was a compacted kaolin, the soft clay was a compacted silty clay, and the clayey sand was a compacted mixture of 90 percent sand and 10 percent kaolin. The strength properties of the three soils used in the analysis are summarized in Table 1; determinations of these strength properties are documented elsewhere (*10*).

In the analysis, the entire soil-footing system was represented by a finite number of eight-node quadrilateral elements interconnected at the nodal points. Because in a continuous footing, a plane of symmetry exists along the vertical-footing axis, only half of the model needed to be analyzed. The nodal points along the vertical side boundaries were restrained in the x-direction; those on the bottom boundary were restrained in x- and y-directions.

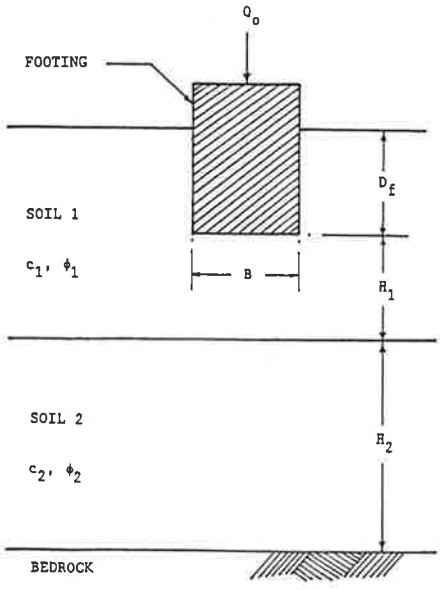

FIGURE 1 Schematic of footing-soil geometry.

To accommodate the nonlinear stress-strain characteristics of the foundation soils in the finite-element analysis, the geostatic stress and footing load were applied in increments. At the initial stage of loading, increments of no more than 10 percent of the total footing load were used; at the final stage, the increments were reduced to 1 percent. For each increment, generally three to five iterations of computations were needed. The computer analysis was performed on a VAX 11/785 computer.

The finite-element analysis provides stresses, strains, and yield condition of each element, pressure-versus-settlement (p-δ) relationship of the footing and contact pressure at footing-soil interface, among others. The p-δ relationships were used to obtain the ultimate bearing capacity for each condition analyzed. As an illustration, a set of typical p-δ curves for soft clay underlain by stiff clay, and its converse, for H_1/B = 1 and 8 are shown in Figure 2. These curves clearly demonstrate the variation in slope (stiffness) and the change in ultimate bearing capacity with changing H_1/B for each layer combination. Such curves are plotted for each condition analyzed, and from these curves the ultimate bearing capacities are determined using the criterion discussed in the following. These ultimate bearing-capacity values form the basis for subsequent presentation and discussion.

ULTIMATE LOAD CRITERION

The p-δ curves obtained from the finite-element analysis do not always show a distinct point for the determination of ultimate bearing capacity. The point on the p-δ curve indicating ultimate bearing capacity depends on the mode of failure, such as general, local, or punching shear failure, which in turn depends on soil type, its relative density, compressibility, footing width, depth of foundation, and so on. Determining ultimate bearing capacity from p-δ curves, therefore, requires some degree of judgment and experience. Researchers have proposed different approaches. For example, Vesic (*11*) has recommended that ultimate load can be taken as the point where the slope of the p-δ curve first reaches zero or steady minimum value. Desai and Christian (*12*) have proposed either using the concept of critical (or tolerable) settlement or choosing the load corresponding to the intersection of the tangents with the initial and ultimate portions of the p-δ curve. However, no single criterion is general enough to apply to all types of soils and all modes of failure.

Consideration of the critical-settlement criterion is justified by the basic philosophy of foundation design, which regards the excessive settlement as a failure of the foundation. There is no single value of critical settlement that satisfies failure conditions in all types of soils and all modes of failure. Observations in saturated clays (*13*) indicate that these settlements may be between 3 and 7 percent of footing width (B) for surface footings, increasing to 15 percent for embedded footings. For footings in sand, somewhat higher values—ranging from 5 to 15 percent for surface footings and as high as 25 percent for embedded footings—have been proposed (*14,11*). Das (*15*) has suggested that for foundations at shallow depth

TABLE 1 MATERIAL PROPERTIES OF FOUNDATION SOILS (1 psi = 6.9 kN/m²)

Material Properties	Silty Clay	Kaolin	Clayey Sand
Initial Modulus in Compression, psi	667	2,880	6,100
Poisson's ratio	0.28	0.39	0.32
Dry Unit weight, pci	0.058	0.052	0.061
Unit cohesion, psi	9.5	23.0	1.33
Internal friction angle, deg.	13.5	8.0	31.0
Initial earth pressure coefficient	0.60	0.64	0.86
Tensile strength, psi	2.00	7.00	0.54
Initial modulus in tension, psi	1,505	7,000	11,300
Soil constant (R_f)	0.80	0.77	0.86

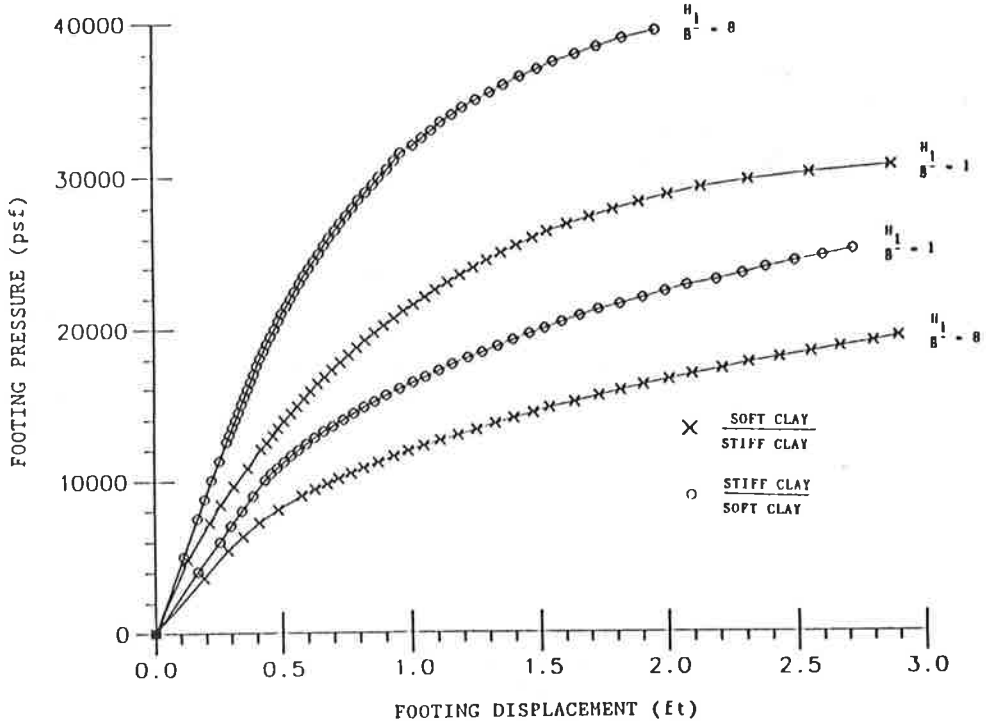

FIGURE 2 Comparison of p-δ curves for soft clay underlain by stiff clay and its converse for $H_1/B = 1$ and 8 ($B = 3.0$ ft, $D_f = 3.0$ ft).

and for those likely to fail by general shear, the ultimate load may occur at foundation settlement of 4 to 10 percent of footing width (B); however, for local or punching shear failure, the ultimate load may occur at settlements of 15 to 24 percent of B. Thus, in the selection of a particular value of critical settlement, one should take into account not only the depth of foundation but also the soil type and its likely failure mode. On the basis of these considerations and the fact that the soils of this study are not uniform but layered and contain a highly compressible clay and a sandy soil, a critical settlement equal to 20 percent of B was chosen as one of the criteria for determining the ultimate bearing capacity.

In addition, because the ultimate load takes place in the state of failure, it is reasonable to take into account the rate of yielding in the determination of the ultimate bearing capacity. Such an approach, in which the yielding rate of soil elements is considered in conjunction with other techniques, has been adopted here. The number of yielded elements is plotted against the applied pressure, and the yielding rate is observed from the slope of this curve. The point at which the curve exhibits a distinct change in the average slope, signifying accelerated plastic yielding, is an indication of the ultimate bearing capacity. The overall technique for determining the ultimate bearing capacity from p-δ curves adopted in this study is summarized in the following:

1. If the p-δ curve shows a distinct yield point, then that point is taken to signify the ultimate bearing capacity. Such a curve would satisfy Vesic's criterion (*11*).
2. If the curve exhibits no distinct yield point, as in Figure 3, but instead appears to suggest continued penetration, then the following steps are executed:

–The point given by the intersection of tangents to the initial and ultimate portions of the p-δ curve is noted (Figure 3). This gives one possible value of ultimate bearing capacity.

–The point that indicates an increase in the rate of element yielding on the pressure–versus–number of yielded elements curve, such as Point A in Figure 4, is noted. This gives a second value of ultimate bearing capacity.

–Whichever point is the lesser value is chosen as the ultimate bearing capacity.

3. If the chosen value is greater than that dictated by settlement considerations (i.e., pressure at a settlement of 20 percent of B), then the latter value is taken as the ultimate bearing capacity.

SPREAD OF PLASTIC YIELD ZONES

Study of the plastic flow behavior gives insight into the progressive yielding of soil under a load and can indicate the dominant failure mode. Selected figures depicting the spread of plastic yield zones in two-layer soils are presented here. Figures 5–8 illustrate plastic yielding for a weak clay layer underlain by a stiff clay and its converse for two levels of the ratio of top-layer thickness to footing width, that is, H_1/B = 1 and 4.

Figure 5 shows that when the top layer is thin (H_1/B = 1), the yield zones at the collapse stage extend into the bottom layer and propagate to the surface. The spread of yield zones to the ground surface indicates that at the collapse stage the soil yielding is analogous to a plastic flow under squeezing action. A yield-zone pattern of this type indicates a possible general shear failure involving both soil layers. When the top clay layer becomes thick (H_1/B = 4), as in Figure 6, the yielding is confined to the top layer. The yield zones appear to stop spreading into the stiff clay layer below, indicating that the elements in the lower layer have not yet reached their yield state. This behavior suggests that at H_1/B = 4, the ultimate bearing capacity will be dictated predominantly by the strength properties of the top layer, though some influence of the lower layer may still be present. The yield pattern of Figure 6 further indicates that the failure mode is a possible local shear failure confined to the top layer.

Figures 7 and 8 show a stiff clay underlain by a weak clay for H_1/B = 1 and 4, respectively. These figures reveal that the yield zones extend deep into the weaker layer below even when the top layer is sufficiently deep (e.g., H_1/B = 4). This yield pattern is typical of a punching shear failure of the top layer followed by a general shear failure of the bottom layer. Thus, the bearing capacity of such a layer combination will be largely controlled by the strength properties of both layers.

DISCUSSION OF RESULTS

The objective of this analysis was to establish the relationship between the ultimate bearing capacity (q_o) and top-layer thickness for various soil layer combinations. Accordingly, four soil-footing systems (H_1/B = 1, 2, 3, and 8) were analyzed for the four two-layer combinations. Figure 9 shows the variation of ultimate bearing capacity (q_o) with H_1/B for two clay layer soils—soft clay over stiff clay and stiff clay over soft clay. It is noted from this figure that when the top layer is a soft clay, the bearing capacity decreases with an increase in the top-layer thickness and ultimately attains a steady value equal to its own bearing capacity at approximately H_1/B = 6. The yield patterns given in Figures 5 and 6 can be used to

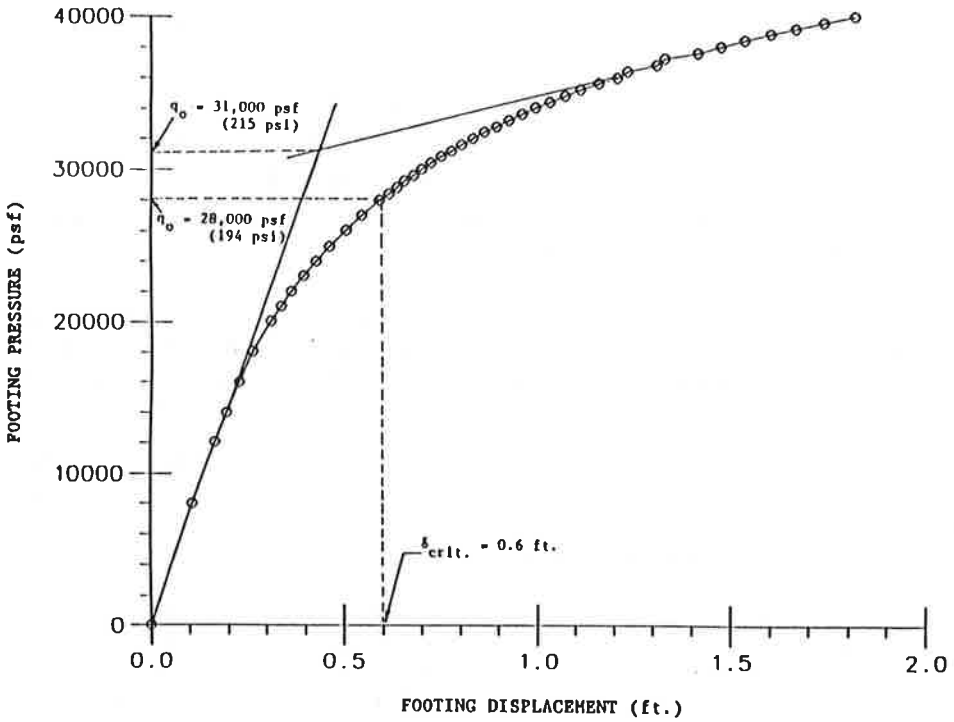

FIGURE 3 p-δ **curve for uniform kaolin, illustrating the application of ultimate-bearing-capacity criterion (B = 3.0 ft, D_f = 3.0 ft).**

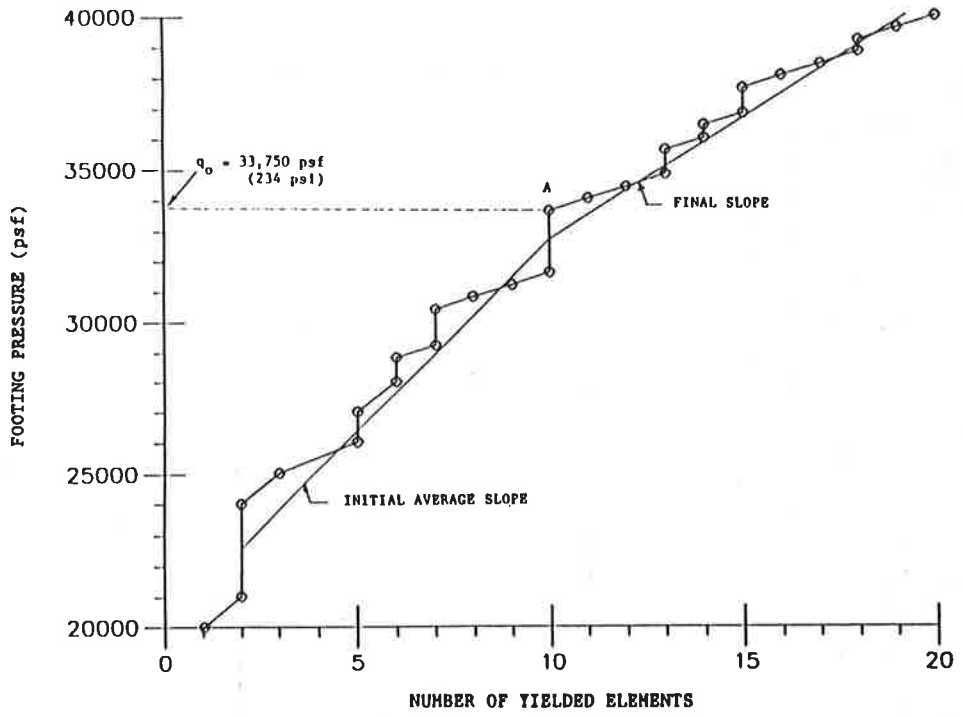

FIGURE 4 Pressure-element yield rate curve for uniform kaolin, illustrating the application of ultimate-bearing-capacity criterion.

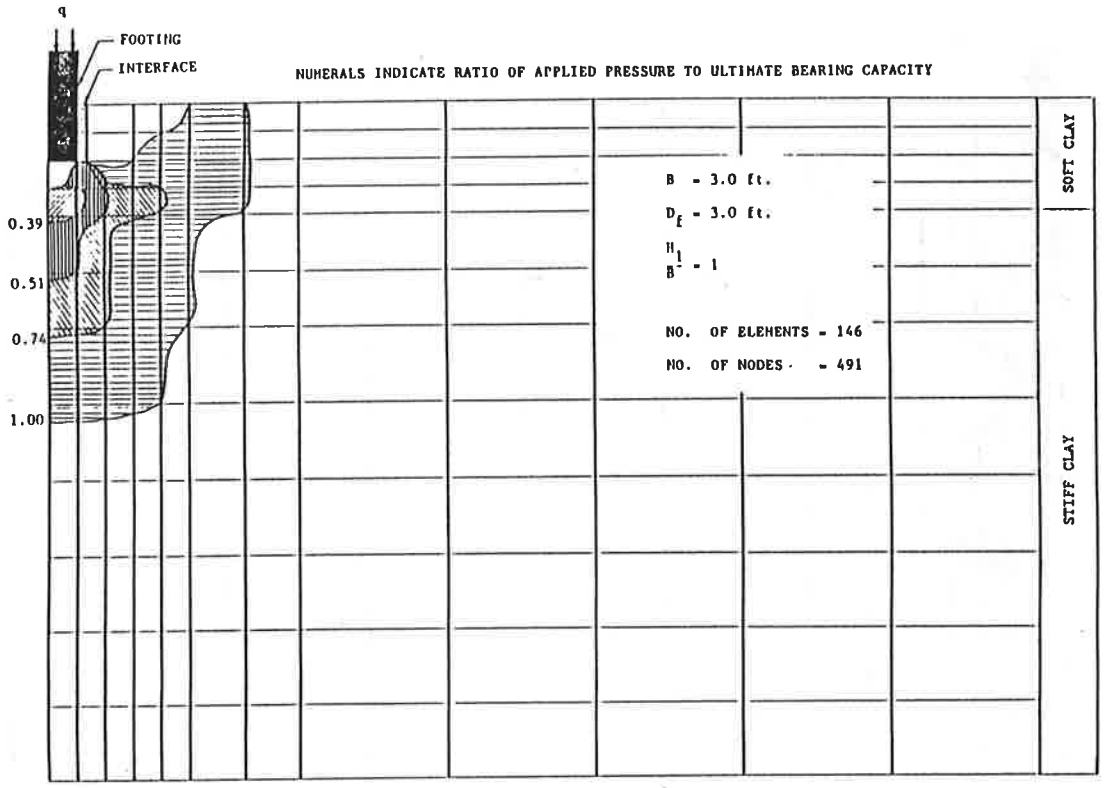

FIGURE 5 Spread of plastic yield zones at various pressure levels in two-layer soil with soft over stiff clays and $H_1/B = 1$.

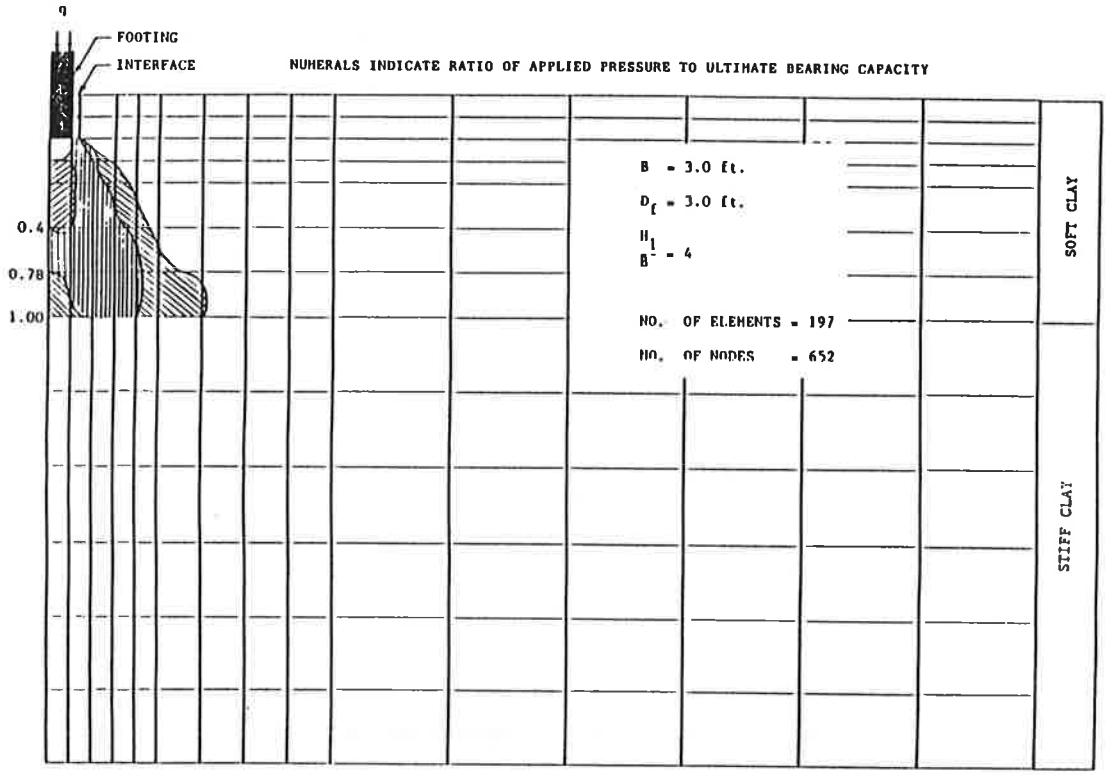

FIGURE 6 Spread of plastic yield zones at various pressure levels in two-layer soil with soft over stiff clays and $H_1/B = 4$.

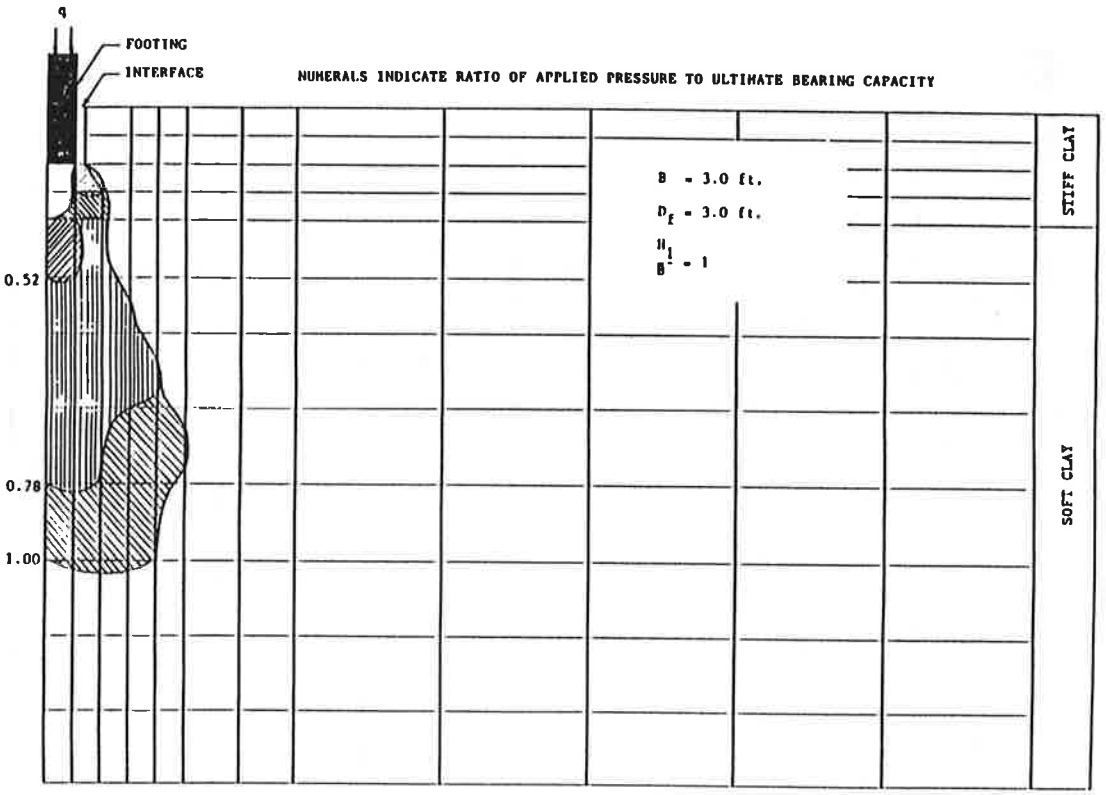

FIGURE 7 Spread of plastic yield zones at various pressure levels in two-layer soil with stiff over soft clays and $H_1/B = 1$.

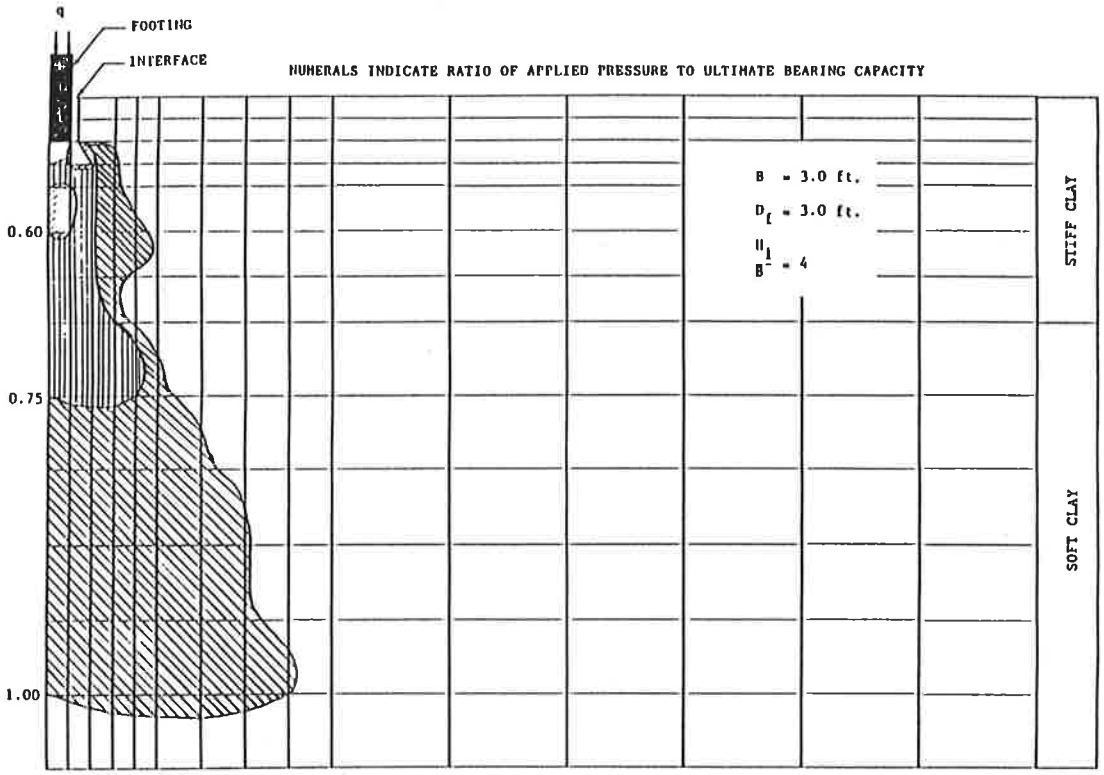

FIGURE 8 Spread of plastic yield zones at various pressure levels in two-layer soil with stiff over soft clays and $H_1/B = 4$.

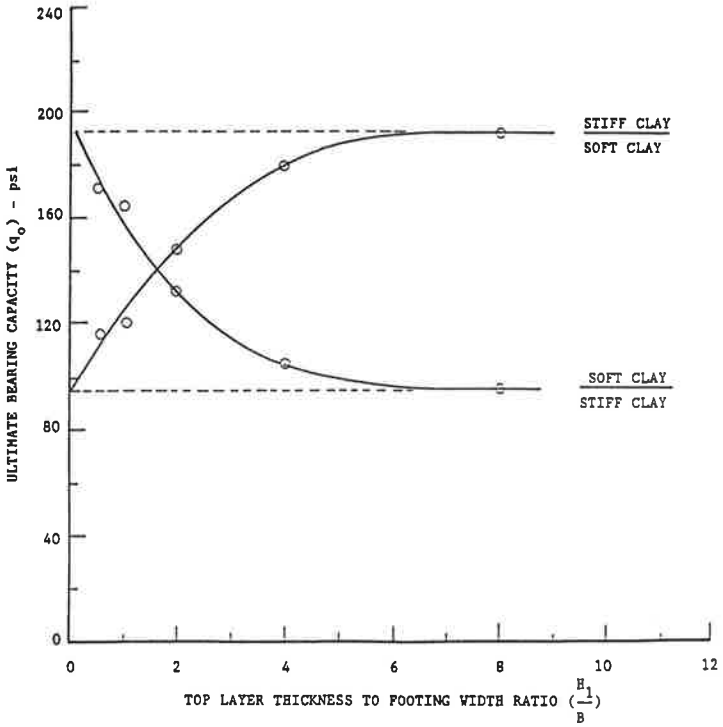

FIGURE 9 Variation of ultimate bearing capacity with top-layer thickness for soft clay over stiff clay and its converse ($B = 3.0$ ft, $D_f = 3.0$ ft, $H_2 = 30.0$ ft).

explain the observed behavior. The greater bearing capacity at a smaller H_1/B ratio is possibly because at small H_1/B ratios, the failure zone extends into the lower stiff clay layer and the higher strength of the lower layer contributes toward a greater ultimate bearing capacity. However, when the top soft clay becomes thicker, the major portion of the failure zone is within the top layer. As a result, the lower strength of the top layer reduces the ultimate bearing capacity.

The trend of bearing-capacity variation for a stiff clay underlain by a soft clay layer (Figure 9) is almost the exact opposite of the preceding case. The ultimate bearing capacity increases with top-layer thickness and ultimately attains a steady value equal to the bearing capacity of the top layer at approximately $H_1/B = 6$. The explanation for this behavior, as before, is that at small H_1/B ratios the failure zone extends into the bottom layer, whose lower strength reduces the ultimate bearing capacity; at higher H_1/B ratios the failure zone remains confined within the top clay layer, resulting in a greater ultimate bearing capacity.

The variations of ultimate bearing capacity with top-layer thickness for a sand underlain by a stiff clay and its converse are illustrated in Figure 10. The bearing capacity of the former case decreases with increasing sand-layer thickness from a maximum at $H_1/B = 0$ (i.e., the footing rests on the clay layer) to a minimum value equal to that for a footing resting on an infinitely thick sand deposit. The ultimate bearing capacity in this case attains a steady value at about $H_1/B = 3$. This H_1/B value is in good agreement with the value of approximately 2.5 obtained by Meyerhof (*9*) from model tests on loose sand overlying stiff clay and the value of 3.5 suggested by Tcheng (*4*).

PROPOSED EQUATION

The bearing-capacity equation is formulated by curve fitting. The data base for formulation is the bearing-capacity–versus–top-layer-thickness relationship discussed earlier and presented in Figures 9 and 10. The variations of bearing capacity seen in these figures dictate that a semiempirical approach is most appropriate for formulating a single equation for all four curves. Of the various relationships attempted, the empirical parabolic interaction relationship appears to best fit the data base. On the basis of this relationship, the following bearing-capacity equation is proposed:

$$q_o = q_t + (q_b - q_t)[1 - m(H_1/B)]^2 \quad (9)$$

where

q_o = ultimate bearing capacity of strip footing over two-layer soil;
q_t = ultimate bearing capacity of the footing supported by an infinitely thick top-layer soil, computed by the traditional bearing-capacity equation using factors recommended by Vesic (*5*);
q_b = ultimate bearing capacity of the footing supported by an infinitely thick bottom-layer soil, computed by the same method as q_t;
m = layer factor, which is 0.17–0.23 for two layers of clay (use of the lower value is recommended if one clay layer is highly compressible, otherwise use the average value) and 0.30 for a sand-clay layer combination; and

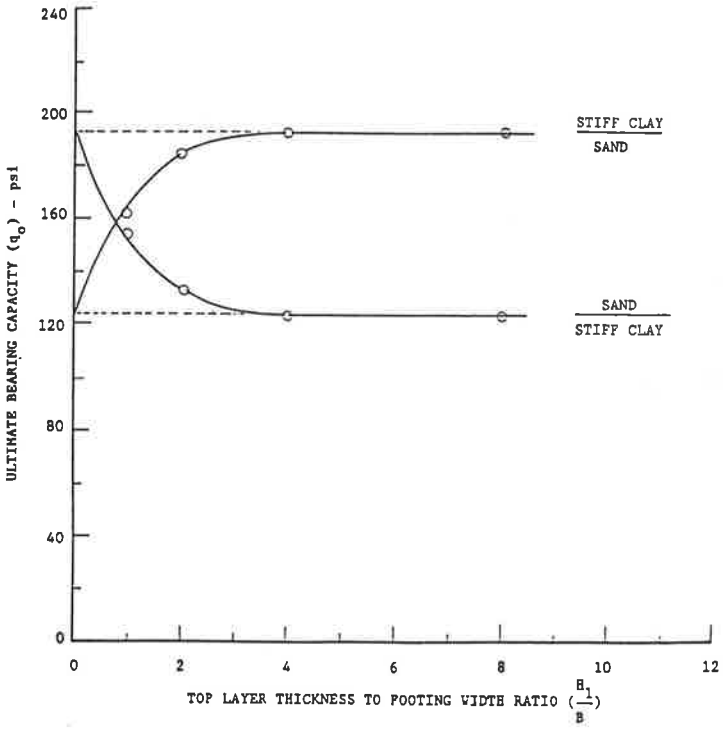

FIGURE 10 Variation of ultimate bearing capacity with top-layer thickness for clayey sand over stiff clay and its converse (B = 3.0 ft, D_f = 3.0 ft, H_2 = 30.0 ft).

H_1/B = top-layer-thickness–to–footing-width ratio, which is no more than 6 for clay-clay layers and no more than 3.5 for sand-clay layers.

The results computed from Equation 9 are compared with the available theories in Figures 11 and 12. The comparison reveals that the bearing-capacity variations predicted from equations of Vesic (*5*) and Satyanarayana and Garg (*8*) attain steady values at approximately $H_1/B = 1$ and 2, respectively, signifying that the bottom layer ceases to have any influence beyond these top-layer thicknesses. On the other hand, the bearing capacity determined from Equation 9 approaches a steady value at a gradual rate, indicating a pronounced influence of the bottom-layer soil up to approximately $H_1/B = 6$. Such a gradual variation of bearing capacity with the top-layer thickness appears to be more reasonable.

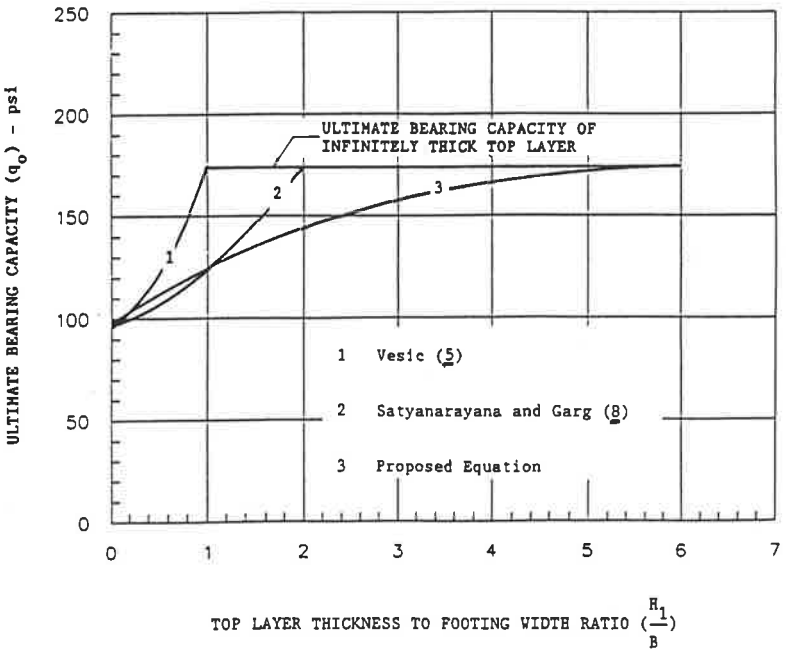

FIGURE 11 Comparison of proposed equation with available theories for stiff clay underlain by soft clay.

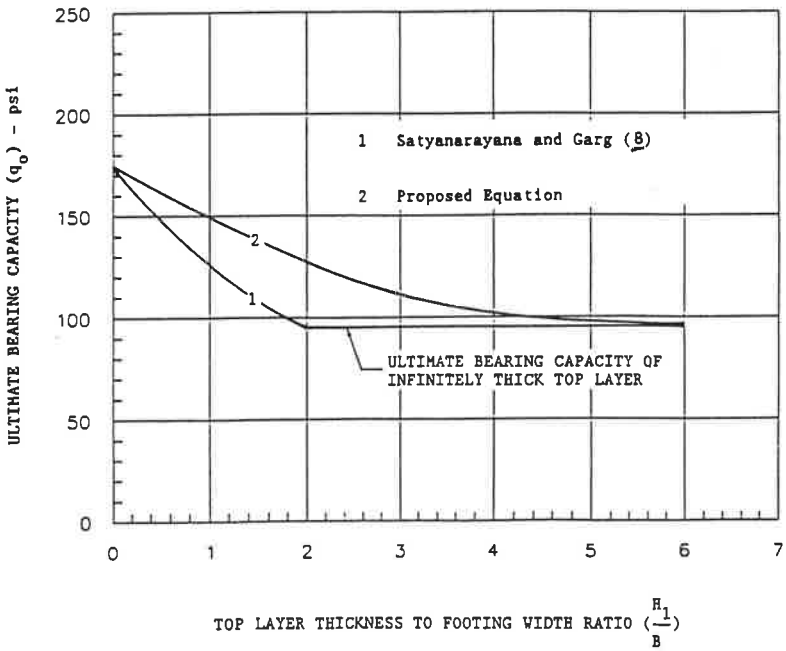

FIGURE 12 Comparison of proposed equation with available theories for soft clay underlain by stiff clay.

SUMMARY AND CONCLUSIONS

The ultimate bearing capacity of a shallow continuous footing supported by two-layer c-ϕ soils has been investigated using an elasto-plastic finite-element computer program. Three soils—a soft clay (silty clay), a stiff clay (kaolin), and a clayey sand (90 percent sand + 10 percent kaolin)—were used to form representative soil layer combinations. The effect of top-layer thickness (H_1) on bearing capacity was investigated for each layer combination. Footing width (B) and depth of foundation (D_f) were kept constant at 3.0 ft (91.4 cm). The results of the analysis led to the formulation of a semiempirical bearing-capacity equation that is simple in its application.

The results of the analysis indicate that when the top layer is a thin weak clay underlain by a stiff clay, the failure mode is predominantly a general shear failure involving both clay layers. But when the top layer is a thin stiff clay underlain by a weak clay, the plastic yield pattern suggests a predominantly punching shear failure of the top clay layer.

For a thin sand layer underlain by a stiff clay, the yield patterns suggest a local shear failure limited to the sand layer. For a thin layer of stiff clay underlain by sand, the failure mode is predominantly a punching shear failure of the top clay layer.

The thickness of top soil layer has a marked influence on the ultimate bearing capacity. The bearing capacity decreases steadily with increasing top-layer thickness when the top layer is weaker than the bottom layer, and vice versa. The bearing capacity attains a steady value at a specific top-layer thickness, depending on the strength properties of the two soils.

The developed bearing-capacity equation is compared with available solutions. Results of the comparisons indicate that the developed equation can provide a more reasonable bearing-capacity value than existing ones.

ACKNOWLEDGMENT

The study was partially sponsored by the National Science Foundation. This support is gratefully acknowledged.

REFERENCES

1. S. J. Button. The Bearing Capacity of Footings on a Two-Layer Cohesive Subsoil. *Proc., 3rd International Conference on Soil Mechanics and Foundation Engineering*, Zurich, Switzerland, Vol. 1, 1953, pp. 332–335.
2. J. D. Brown and G. G. Meyerhof. Experimental Studies of Bearing Capacity in Layered Clays. *Proc., 7th International Conference on Soil Mechanics and Foundation Engineering*, Mexico City, Mexico, Vol. 2, 1969, pp. 45–51.
3. G. G. Meyerhof and A. M. Hanna. Ultimate Bearing Capacity of Foundations on Layered Soils Under Inclined Load. *Canadian Geotechnical Journal*, Vol. 15, 1978, pp. 565–572.
4. Y. Tcheng, Foundations superficielles en milieu stratifie. *Proc. 4th International Conference on Soil Mechanics and Foundation Engineering*, London, England, Vol. 1, 1957, pp. 449–552.
5. A. Vesic. Bearing Capacity of Shallow Footings. In *Foundation Engineering Handbook* (Winterkorn and Fang, eds.), Van Nostrand Reinhold, New York, N.Y., 1975.
6. G. G. Meyerhof. Ultimate Bearing Capacity of Footings on Sand Layer Overlying Clay. *Canadian Geotechnical Journal*, Vol. 11, 1974, pp. 223–229.
7. A. M. Hanna and G. G. Meyerhof. Design Charts for Ultimate Bearing Capacity of Foundations on Sand Overlying Soft Clay. *Canadian Geotechnical Journal*, Vol. 17, 1980, pp. 300–303.
8. B. Satyanarayana and R. K. Garg. Bearing Capacity of Footings on Layered c-ϕ soils. *Journal of the Geotechnical Engineering Division*, ASCE, Vol. 106, No. GT7, 1980, pp. 819–824.
9. D. Drucker and W. Prager. Soil Mechanics and Plastic Analysis in Limit Design. *Quarterly of Applied Mathematics*, Vol. 10, No. 2, 1952, pp. 157–165.
10. G. Azam. *Stability of Shallow Continuous Footings Supported by Two-Layer Soil Deposits with an Underground Void*. Ph.D. thesis. Pennsylvania State University, University Park, Aug. 1990.
11. A. Vesic. Bearing Capacity of Deep Foundations in Sand. In *Highway Research Record 39*, HRB, National Research Council, Washington, D.C., 1963, pp. 112–143.
12. C. S. Desai and J. T. Christian. *Numerical Methods in Geotechnical Engineering*. McGraw-Hill, New York, N.Y., 1977.
13. A. W. Skempton. The Bearing Capacity of Clays. *Proc., Building Research Congress*, London, England, 1951, pp. 180–189.
14. E. E. De Beer. Bearing Capacity and Settlement of Shallow Foundations of Sand. *Proc., Symposium on Bearing Capacity and Settlement of Foundation*, Duke University, Durham, N.C., 1965, pp. 15–34.
15. B. M. Das. *Principles of Foundation Engineering*. Brooks/Cole Engineering Division, Monterey, Calif., 1984, pp. 101–104.

Subgrade Modulus of Laterally Loaded Piles in Clays

DANIEL O. WONG

Pile-soil interaction of laterally loaded piles may be characterized by either linear subgrade modulus methods or the nonlinear load transfer relationships, termed *p-y* curves. The selection of a subgrade modulus to analyze lateral behavior of piles relies heavily on individual judgment because the subgrade modulus itself is a function of pile deflection. Analyses of laterally loaded piles by means of *p-y* curves often require extensive numerical procedures on a digital computer. A concept of equivalent subgrade modulus, which incorporates the nonlinear nature of the *p-y* model, is derived from a parametric study of the effects of pile-soil stiffness under three well-known clay criteria: soft clay and stiff clay above and below the water table. Design curves of equivalent subgrade modulus versus a dimensionless lateral load factor are developed. A design procedure to predict maximum deflection and maximum moment of laterally loaded piles in clays is proposed and used to predict published field test data.

Deep foundations are frequently designed to resist lateral loading. Typical examples include pile-supported bridges, buildings, and offshore structures. Of primary interest to geotechnical and structural engineers is the prediction of deflection and bending moment of deep foundations under lateral loads. The most convenient method of analysis for laterally loaded piles involves the theory of subgrade reaction (*1*), in which load-deflection relationships for the supporting soil are assumed to be linear functions. However, soil response to lateral loading is highly nonlinear, especially at high stress levels. Lateral soil response is also greatly affected by soil depth and in situ stress conditions. To overcome the aforementioned difficulties, soil response can be modeled by nonlinear unit load transfer functions, termed "*p-y*" relationships, which are mathematical representations of the soil reaction versus the lateral pile deflection per unit length along the pile. There are several *p-y* criteria for clays based on various soil properties and conditions: soft clay (*2*), stiff clay above the water table (*3*), and stiff clay below the water table (*4*,*5*). Analysis of laterally loaded piles can be performed with these *p-y* criteria by employing finite difference or finite element analyses on a digital computer (*6*,*7*). However, computer analysis is a more extensive numerical procedure compared with the linear subgrade modulus method, such that the latter method may be preferred by design engineers in preliminary computations and for relatively simple design cases. There have been attempts in the past to develop a simplified method to analyze laterally loaded piles (*8*).

The objective of this paper is to provide engineers with a representative subgrade modulus in which nonlinear pile-soil interaction is implicitly taken into account and a step-by-step design procedure to analyze laterally loaded piles in clays. A family of design curves of equivalent subgrade modulus k_{eq} in terms of dimensionless lateral load factor for soft clay and stiff clay above and below the water table is developed by means of a parametric study of a hypothetical problem. The parametric study is basically an analytical procedure to integrate the simplicity of the linear method with the complex rationality of the load transfer criteria. It involved determining the deflection of a hypothetical pile in clays using a numerical model on a computer. A subgrade modulus under a lateral load was then backcalculated from the obtained deflection using a linear equation. Relationships of subgrade moduli and corresponding lateral loads were developed. Among the parameters investigated in this study are lateral load, pile stiffness, and soil properties.

McBride-Ratcliff and Associates, Inc., 7220 Langtry, Houston, Texas 77040.

AVAILABLE ANALYTICAL METHODS

The theory of subgrade reaction assumes that the unit soil reaction p with respect to a laterally loaded pile increases linearly with the lateral deflection y, as expressed in the following equation:

$$p = ky \tag{1}$$

where k is the subgrade modulus. Once a subgrade modulus is known, the behavior of a laterally loaded pile may be evaluated by linear methods such as the Broms equations (*1*) and nondimensional solutions (*9*,*10*). A brief description of the Broms equations and the nondimensional solutions is included in the following paragraphs.

Broms Equations

Broms used a dimensionless βL to define short or long piles, where L is the length of the pile and β is defined as

$$\beta = (kB/4EI)^{0.25} \tag{2}$$

where B is the diameter of the pile and EI is its stiffness.

Broms recommended that the lateral deflection y_o of a free-head long pile in clays ($\beta L > 2.5$) at the ground surface may be determined as

$$y_o = 2P\beta\,(e\beta + 1)/kB \tag{3}$$

or

$$y_o = 2P\beta/kB \qquad \text{for } e = o \tag{3a}$$

in which P is the applied lateral load and e is the distance of the lateral load above the ground surface and can also be calculated from an applied moment at the ground surface M as

$$e = M/P \tag{4}$$

For a restrained-head long pile in clays ($\beta L > 1.5$) where the slope at the pile head is zero, deflection can be calculated from

$$y_o = P\beta/kB \tag{5}$$

Nondimensional Solutions

Nondimensional solutions for laterally loaded piles require an iterative procedure to achieve convergence of the relative stiffness factor T, which is defined as

$$T = (EI/k_n)^{0.2} \tag{6}$$

where k_n is a constant relating to the subgrade modulus of soil to depth Z as

$$k_n = kB/Z \tag{6a}$$

The lateral deflection y and bending moment m of the pile can be obtained from the following equations:

$$y = \frac{A_y PT^3}{EI} + \frac{B_y MT^2}{EI} \tag{7}$$

$$m = A_m PT = B_m M \tag{8}$$

in which A_y, B_y are deflection coefficients due to applied lateral load P and applied moment M, respectively, and A_m, B_m are moment coefficients due to applied lateral load P and applied moment M, respectively.

Depending on the value of the maximum depth coefficient Z_{max}, deflection and moment coefficients can be obtained at any depth along the pile. Coefficient charts are available in the paper by Matlock and Reese (*9*). Z_{max} is defined as

$$Z_{max} = \frac{L}{T} \tag{9}$$

In the absence of applied moment at the pile head, the maximum deflection and moment coefficients can be found in Table 1. Using the maximum coefficients in Table 1, the maximum deflection and maximum moment of piles under lateral loads can be calculated from Equations 7 and 8, respectively.

The accuracy of the Broms equations lies heavily on the selection of the subgrade modulus k, which is recommended by Broms to be taken as the average value within a depth equal to $0.8\beta L$. Because it has been suggested that the load-deflection relationship is highly nonlinear, the value of this average k is obviously dependent on the magnitude of the lateral load. Therefore, the Broms equations are convenient and simple to use at low stress levels where linearity is not a severe modeling limitation. The nondimensional solutions may handle nonlinearity problems but require a somewhat time-consuming iteration procedure and also the availability of respective p-y data. Nonlinear modeling of a laterally loaded pile problem can be performed, as previously mentioned, by the load transfer method.

PARAMETRIC STUDY

It is the intent of this study to integrate the linear Broms procedures and the nonlinear load transfer methods empirically on a parametric basis to develop a simple procedure as convenient as the Broms solutions and with the power and broad range of applications of the load transfer solutions. The purpose of the parametric study is to develop an equivalent subgrade modulus under a specific pile-soil condition. The procedures to develop the equivalent subgrade modulus are presented in this section.

By employing a numerical computer solution for laterally loaded piles, COM 624 (*7*), a parametric study was performed on a hypothetical problem to determine the lateral deflections under various prescribed conditions. Soil models selected for investigation in the study were soft clay (*2*), stiff clay above the water table (*3*), and stiff clay below the water table (*5*).

The soil parameters investigated in this study are represented by a selected range of subgrade modulus k and summarized as follows (1 pci = 271.7 kN/m³):

- Soft clay: 30, 100, and 300k (pci);
- Stiff clay above or below the water table: 300, 1,000, and 3,000k (pci).

The pile parameters considered in this study are as follows (1 in. = 2.54 cm; 1 psi = 6.89 kN/m²):

Pile Material	*Pile Diameter B* (in.)	*Young's Modulus E* (psi)	*Moment of Inertia I* (in.⁴)
Concrete	36	3×10^6	82447.9
Steel	12	30×10^6	1017.9

TABLE 1 MAXIMUM DEFLECTION AND MOMENT COEFFICIENTS DUE TO LATERAL LOAD ONLY

Z_{max}	A_y		A_m	
	Free-Head	Restrained-Head (Slope = 0.0)	Free-Head	Restrained-Head (Slope = 0.0)
10	2.435	0.820	0.772	0.93
4	2.445	0.829	0.767	0.93
3	2.723	0.968	0.704	0.97
2.2	4.011	1.268	0.557	1.06

The soil and pile parameters selected in this study are believed to cover the spectrum of regular design conditions.

On the basis of the control parameters shown above and a selected pile length of 40 ft (12.2 m), values of βL are determined and summarized in Table 2. The Broms assumption of an infinitely long pile is satisfied by all these βL values for both free-head and restrained-head cases of the hypothetical pile.

Relationships between undrained cohesion of clay C_u with subgrade modulus k and strain at one-half of the maximum principal stress difference ε_{50} were used based on Reese and Sullivan's recommendation (*7*) and are shown in Table 3.

Average values of cohesion in Table 3 were plotted against k and ε_{50} and presented in Figure 1. The relationships in Figure 1 were used to develop the *p-y* relationships and relevant input data for the parametric study in this paper.

Once deflection y_o was determined using COM624 for a prescribed condition under a particular lateral load P, the equivalent subgrade modulus k_{eq} was found by substituting Equation 2 into Equations 3a and 5 and rewriting Equations 3a and 5 as follows:

$$k_{eq} = \left(\frac{P^4}{y_o^4}\frac{4}{B^3EI}\right)^{0.33} \quad \text{for free-head pile} \tag{10}$$

$$k_{eq} = \left(\frac{P^4}{y_o^4}\frac{1}{4B^3EI}\right)^{0.33} \quad \text{for restrained-head pile} \tag{11}$$

It should be noted that one value of k_{eq} would be found corresponding to a lateral load magnitude. Different values of k_{eq} would be determined from a range of lateral loads under the same soil conditions. Eventually relationships of equivalent subgrade modulus and lateral load may be developed for the three clay criteria employed in this study.

Soft Clay

Matlock proposed a method to generate *p-y* curves for laterally loaded piles in soft clays based on the analyses of field and laboratory data (*2*). Two failure modes are defined for the ultimate lateral resistance of soils: wedge failure above a critical depth Z_{cr} and plastic failure below Z_{cr}, which is defined as

$$Z_{cr} = \frac{6B}{\frac{\gamma B}{c_u} + J} \tag{12}$$

TABLE 3 RELATIONSHIPS OF C_u, k, AND ε_{50} (*7*)

Cohesion, Cu (psf)	k (pci)	ε_{50}
250 - 500	30	0.02
500 - 1000	100	0.01
1000 - 2000	300	0.007
2000 - 4000	1000	0.005
4000 - 8000	3000	0.004

Note: 1 psf = 47.9 N/m^2; 1 pci = 271.7 kN/m^3

where γ is the effective unit weight and J is an empirical constant (0.5 for offshore soft clays in the Gulf of Mexico and 0.25 for stiffer clays). The ultimate lateral resistance per unit length of pile p_u is written as

$$p_u = Npc_uB \tag{13}$$

where Np is the ultimate lateral soil resistance coefficient.

For depth $Z < Z_{cr}$, c_u is taken as the average value between the ground surface and depth Z. Np can be calculated as

$$Np = 3 + \frac{\gamma Z}{c_u} + \frac{JZ}{B} \tag{14}$$

For depth $Z > Z_{cr}$, c_u is taken as the value at depth Z and Np is 9.0.

The characteristic *p-y* curve for Matlock's soft-clay criterion is defined as

$$p = 0.5p_u(y_o/y_c)^{0.33} \tag{15}$$

where

p = lateral soil resistance per unit length,
y_o = pile deflection, and
y_c = reference pile deflection = $2.5\varepsilon_{50}B$,

and ε_{50} can be obtained from Figure 2.

By employing the soft-clay criterion, a parametric study was performed using computer program COM624 as described in the previous section. The *p-y* curves were internally generated in the program and deflections were computed for various values of lateral load P. Figures 2 and 3 show the relationships of equivalent subgrade modulus k_{eq} and dimensionless lateral load factor $P\beta/kBu$ for free-head and restrained-head conditions,

TABLE 2 CONTROL PARAMETERS

Pile Material	Pile Diameter B (in)	Initial Subgrade Modulus k (pci)	β (Eq.2)	βL
Steel	12	30	0.0074	3.6
		100	0.0100	4.8
		300	0.0131	6.3
		1000	0.0177	8.5
		3000	0.0233	11.2
Concrete	36	30	0.0058	2.8
		100	0.0078	3.7
		300	0.0102	4.9
		1000	0.0138	6.6
		3000	0.0182	8.7

Note: 1 in = 2.54 cm; 1 pci = 271.7 kN/m^3

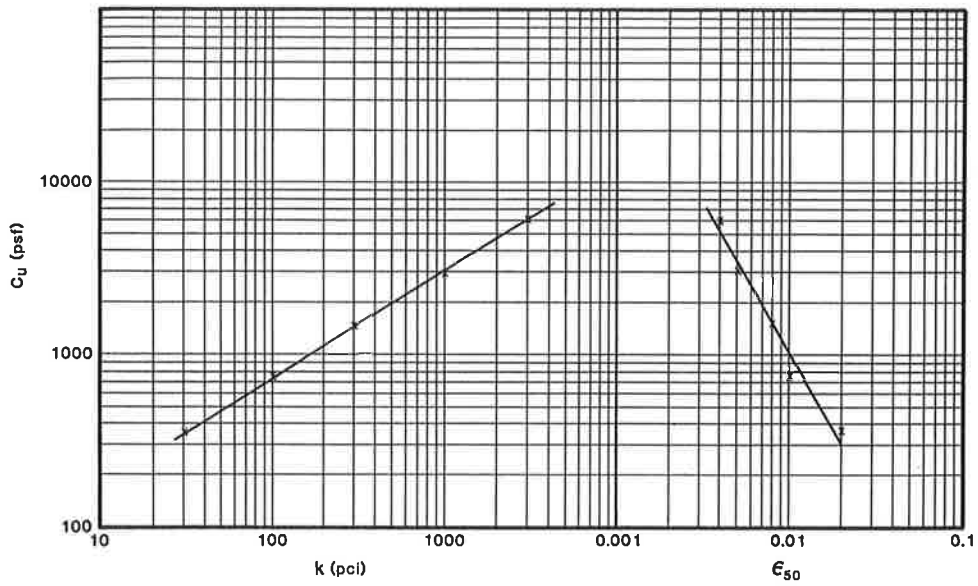

FIGURE 1 Relationships of C_u versus k and ε_{50} (1 psf = 47.9 N/m²; 1 pci = 271.7 kN/m³).

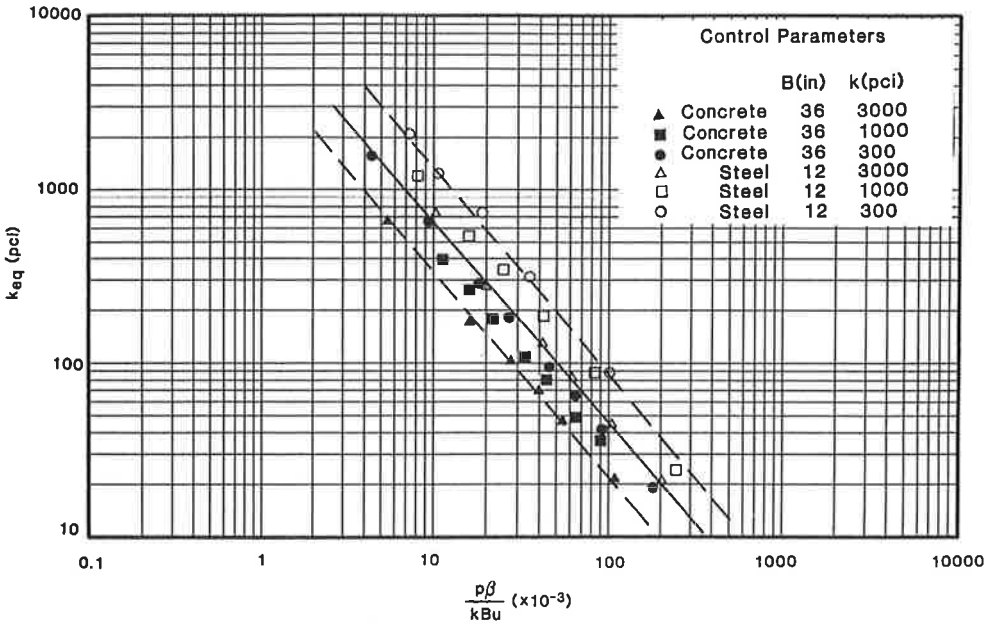

FIGURE 2 Equivalent subgrade modulus versus dimensionless lateral load factor for soft clay: free-head condltions (1 in. = 2.54 cm; 1 pci = 271.7 kN/m³).

respectively. The parameter u is defined as a unit pile length and is used to make the lateral load factor dimensionless.

Different slopes for k_{eq}-dimensionless lateral load factor curves are observed for free-head and restrained-head cases. The observation implies that in the absence of applied moment, lateral deflection at ground surface for free-head piles, as calculated in Equation 3a, would not be exactly twice (i.e., twice flexible) that for restrained-head piles (Equation 5), as suggested by the Broms equations.

Stiff Clay Above the Water Table

The criterion was developed on the basis of the experimental data from a series of lateral load tests on instrumented drilled piers documented by Reese and Welch (*3*). Matlock's expression to estimate the ultimate soil resistance p_u was adopted in this criterion, as shown in Equations 13 and 14. The characteristic shape of the p-y curve for stiff clay above the water table is expressed as follows:

$$p = 0.5p_u(y_o/y_c)^{0.25} \tag{16}$$

Equations 15 and 16 are expressed similarly, with the only difference being the exponent values.

COM624 was used with internally generated p-y curves to estimate lateral deflection under a specified range of lateral loads. The equivalent subgrade modulus k_{eq} was obtained from Equations 10 and 11. Figures 4 and 5 show k_{eq} versus

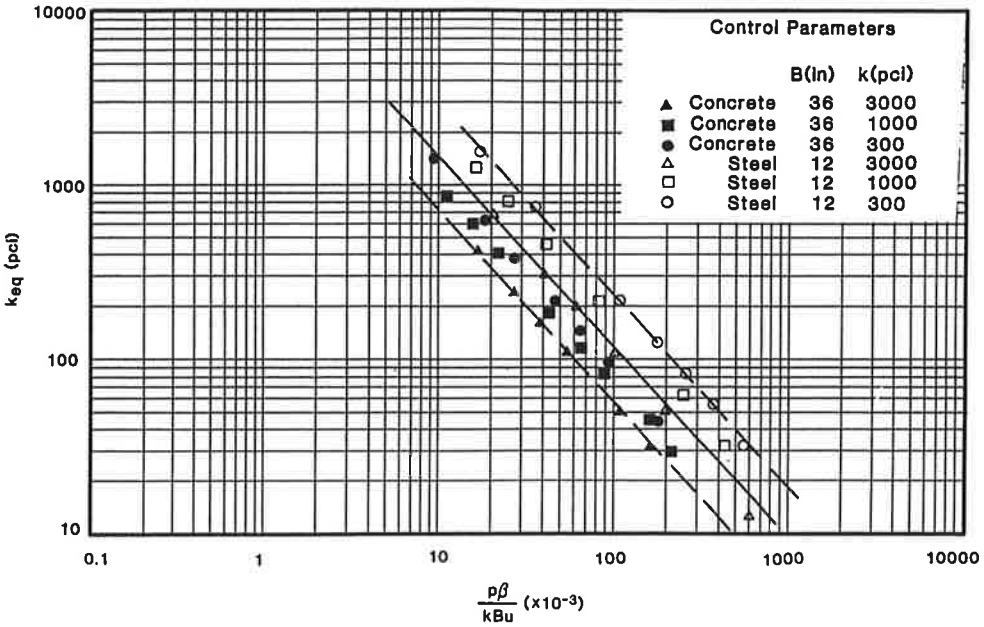

FIGURE 3 Equivalent subgrade modulus versus dimensionless lateral load factor for soft clay: restrained-head conditions (1 in. = 2.54 cm; 1 pci = 271.7 kN/m³).

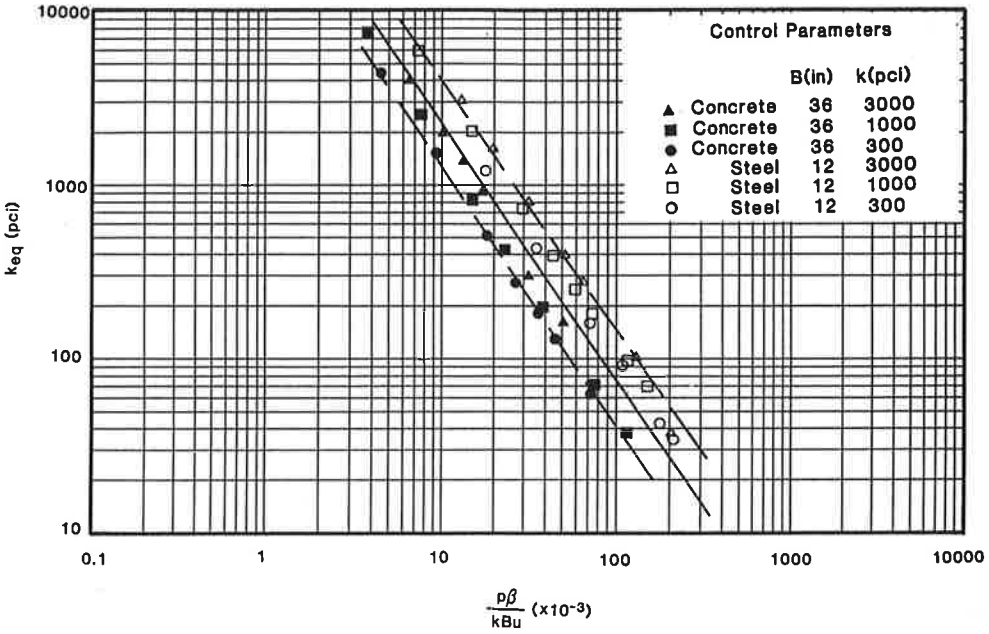

FIGURE 4 Equivalent subgrade modulus versus dimensionless lateral load factor for stiff clay above water: free-head conditions (1 in. = 2.54 cm; 1 pci = 271.7 kN/m³).

the dimensionless lateral load factor for free-head and restrained-head conditions, respectively.

Stiff Clay Below the Water Table

The submerged stiff-clay criterion for the *p-y* relationship based on full-scale pile test data was developed by Reese et al. (*4*). A statistical evaluation by Gazioglu and O'Neill (*11*) was performed on all the available *p-y* criteria for clays to assess the levels of uncertainty. O'Neill and Gazioglu (*12*) concluded that Reese's criterion for stiff clay below the water table yields the greatest uncertainty on the grounds that the criterion was derived from the field data collected in an expansive clay environment. Dunnavant and O'Neill (*5*) performed an independent series of full-scale lateral pile tests in submerged stiff clays and proposed an improved *p-y* criterion. The characteristic *p-y* curve for the improved criterion is defined as

$$p = 1.02p_u \tanh [0.537(y_o/y_{50})^{0.7}] \qquad y \leq 8y_{50}$$

$$p = 1.02p_u \qquad y > 8y_{50} \tag{17}$$

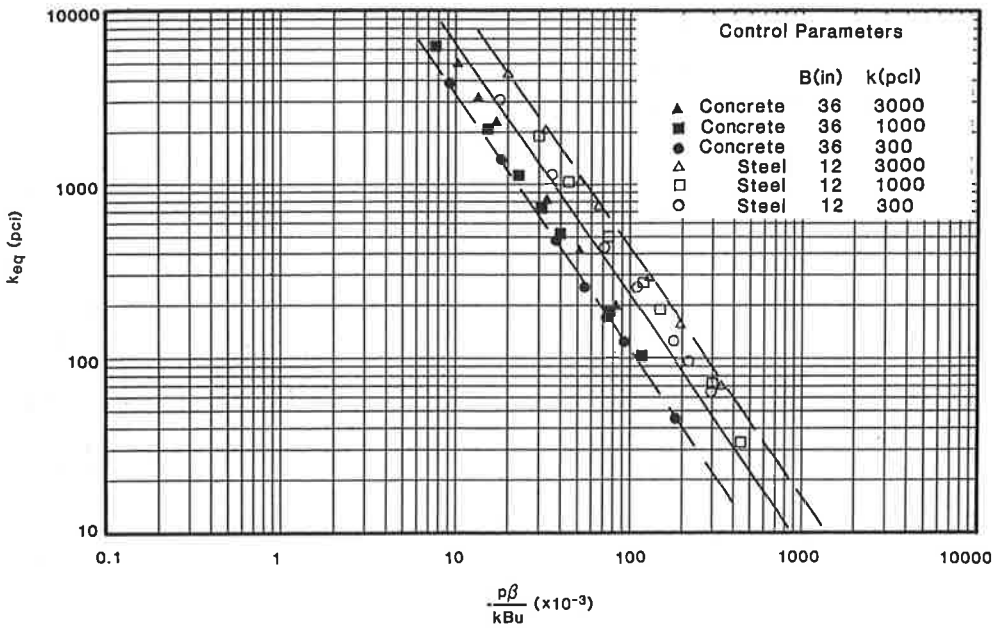

FIGURE 5 Equivalent subgrade modulus versus dimensionless lateral load factor for stiff clay above water: restrained-head conditions (1 in. = 2.54 cm; 1 pci = 271.7 kN/m³).

The ultimate lateral resistance p_u is calculated by employing Matlock's expression, but with a different lateral resistance coefficient Np, as shown in Equations 18 and 19.

$$p_u = Npc_uB \tag{18}$$

$$Np = 2 + \frac{\gamma Z}{c_u 2} + \frac{JZ}{B} \leq 9 \tag{19}$$

where J is 0.4. The term y_{50} is suggested to be a nonlinear function of the pile diameter and is expressed as

$$y_{50} = 0.0063\varepsilon_{50}BK_R^{-0.875} \tag{20}$$

$$K_R = (EI/E_SL^4) \tag{21}$$

where E_S is the soil modulus, which may be represented by a secant modulus at a deviator stress level one-half the deviator stress at failure in undrained triaxial compression tests. A correlation between the average UU triaxial compression shear strength and the soil modulus is tabulated in the paper by Gazioglu et al. (*11*). The mean values are plotted in Figure 6. The pile length L in Equation 21 is limited numerically to $3B(EI/E_SB^4)^{0.286}$, below which the pile has a negligible effect on pile-head behavior.

Table 4 summarizes the parameters used to generate the required p-y curves for the submerged stiff clay criterion in this study.

Figures 7 through 9 give the p-y curves generated using the submerged stiff clay criterion of Dunnavant et al. (*5*). The curves were used as input data in the computer program COM624 to conduct the described parametric study. Relationships of k_{eq} versus the dimensionless lateral load factor for stiff clay below the water table under free-head and restrained-head conditions are presented in Figures 10 and 11, respectively. It is shown that k_{eq} seems to be constant below a threshold lateral load factor; that is, the load-deflection relationship is a linear function. Furthermore, when Figures 2 and 3 are compared with Figures 7 and 9, the curves for the submerged stiff clay criterion above the threshold lateral load factor tend to overlap those corresponding to the soft clay criterion, which is shown in the next section.

DESIGN PROCEDURE

A compilation of curves for k_{eq} versus the dimensionless lateral load factor is presented in Figures 12 and 13 for free-head and restrained-head piles, respectively, for the three p-y criteria employed in this study. The simplified design procedure to estimate the maximum deflection and moment for laterally loaded piles in clays involves the use of these relationships. The required known parameters for the proposed procedure are pile diameter B, pile bending stiffness EI, and undrained cohesion of soils c_u. Using Broms's criterion for coefficient of subgrade reaction (*1*), the value of c_u can be taken as the average within a depth equal to 0.8 βL. Once the undrained cohesion has been determined, the following step-by-step design procedure is recommended:

1. Find the subgrade modulus k from Figure 1,
2. Obtain the coefficient β using Equation 2,
3. Calculate the dimensionless lateral load factor $P\beta/kBu$,
4. Determine the equivalent subgrade modulus k_{eq} from either Figure 12 or Figure 13 depending on given boundary conditions and clay criteria,
5. Calculate the maximum deflection from Equation 3 or Equation 5 by using β from Step 2 and substituting k_{eq} into k, and
6. Calculate the maximum moment from Equation 8.

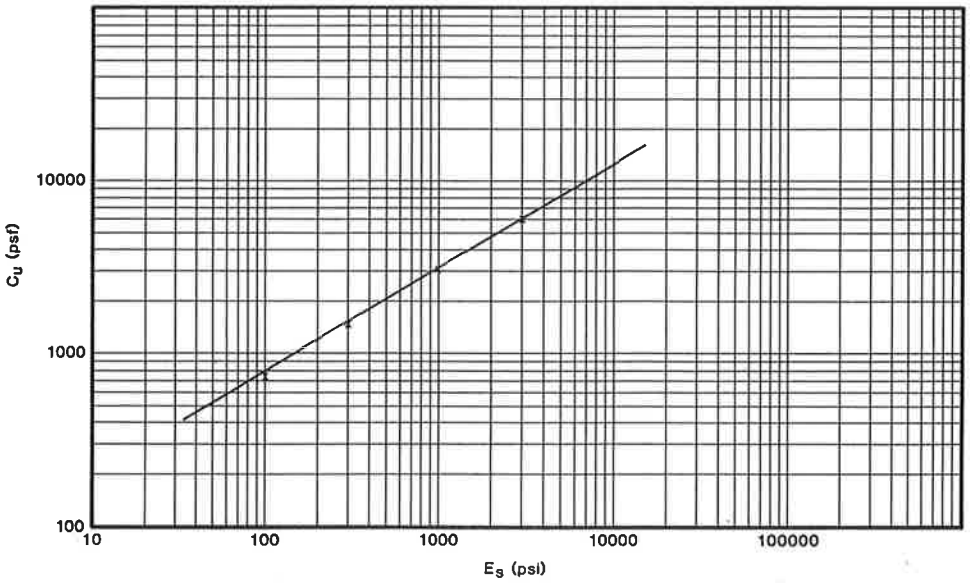

FIGURE 6 Relationship between C_u and E_s (1 psf = 47.9 N/m²; 1 psi = 6.89 kN/m²).

TABLE 4 PARAMETERS REQUIRED TO GENERATE *p-y* CURVES FOR SUBMERGED STIFF CLAYS

Pile Dia. B (in) (Control Parameter)	Soil Stiffness k (pci)	Cohesion c^u (psf) (Figure 2)	ϵ_{50}	Soil Modulus E_S (psi) Figure 7	K_R ($X10_{-8}$) (Eq 17)	y_{50} (Eq 16)
12	300	1500	0.007	300	1.9	0.126
36					15.5	0.061
12	1000	3000	0.005	1000	0.6	0.259
36					4.7	0.124
12	3000	6000	0.004	3000	0.2	0.541
36					1.5	0.260

Note: 1 in = 2.54 cm; 1 pci = 271.7 kN/m³; 1 psi = 6.89 kN/m²; 1 psf = 47.9 N/m²

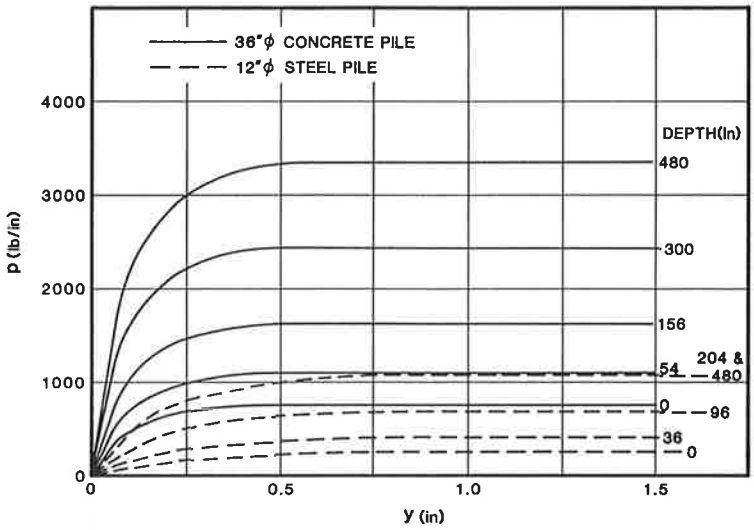

FIGURE 7 *p-y* Curves generated for submerged stiff clay: k = 300 pci (1 in. = 2.54 cm; 1 pci = 271.7 kN/m³; 1 lb/in. = 175.2 N/m).

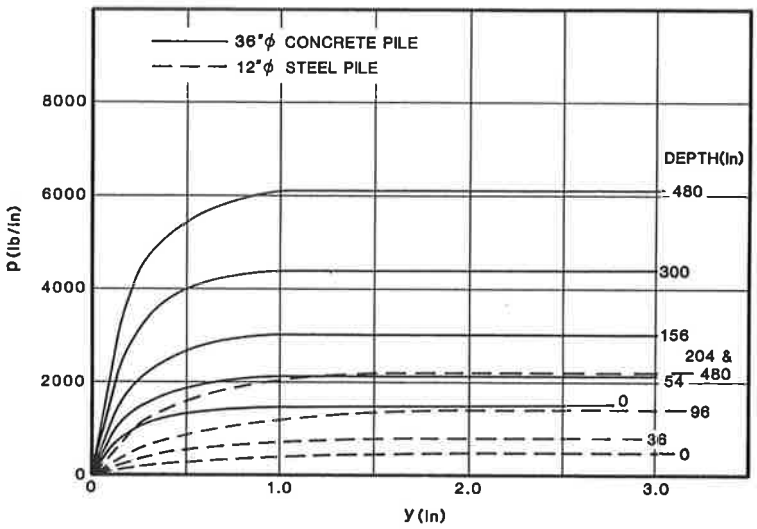

FIGURE 8 *p-y* **Curves generated for submerged stiff clay: k = 1,000 pci (1 in. = 2.54 cm; 1 pci = 271.7 kN/m³; 1 lb/in. = 175.2 N/m).**

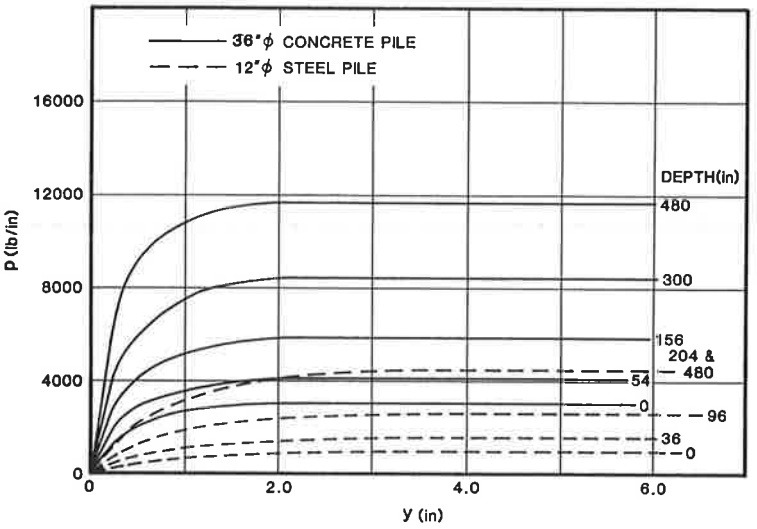

FIGURE 9 *p-y* **Curves generated for submerged stiff clay: k = 3,000 pci (1 in. = 2.54 cm; 1 pci = 271.7 kN/m³; 1 lb/in. = 175.2 N/m).**

The maximum deflection can also be estimated from Equation 7 using the nondimensional method. However, it is shown later that the prediction is not as good as that by Broms's equation.

In order to examine its effectiveness, the design procedure is used to predict the published field test data. Table 5 summarizes the parameters derived by the proposed procedure for load-deflection prediction. As an example to demonstrate the proposed step-by-step design procedure, the published data for stiff clay above the water table (*3*) (Table 5) were used. English units as from the published data were used for this example. For C_u of 2,200 psf, k was found to be about 600 pci from Figure 1 according to Step 1. The coefficient β in Step 2 was calculated to be 0.0139 from Equation 2. The dimensionless lateral load factor shown in Step 3 was found to be 0.0618 assuming a lateral load of 80 kips and using B of 30 in. From Figure 12 according to Step 4, k_{eq} was taken as 160 pci. The maximum deflection for an 80-kip load was calculated to be 0.463 in. according to Step 5 (Equation 3) as shown in Table 6. Maximum moment can also be found using E and I from Table 5 and Equations 6 and 8.

Table 6 presents the predicted and published maximum deflections and moments for the criterion of stiff clay above the water table. These data show a relatively poor prediction of maximum deflections at large lateral loads by the nondimensional solutions (Equations 6 and 7) by substituting k_{eq} for k_n in Equation 6. It is speculated that the error is possibly due to a deeper depth influence under larger lateral load, which may imply a smaller actual k_{eq}, as indicated in Equation 6a.

Table 7 presents the predicted values corresponding to the published data available for the soft clay and submerged stiff clay criteria. Only Broms's equation (Equation 3) was used to predict the maximum deflection.

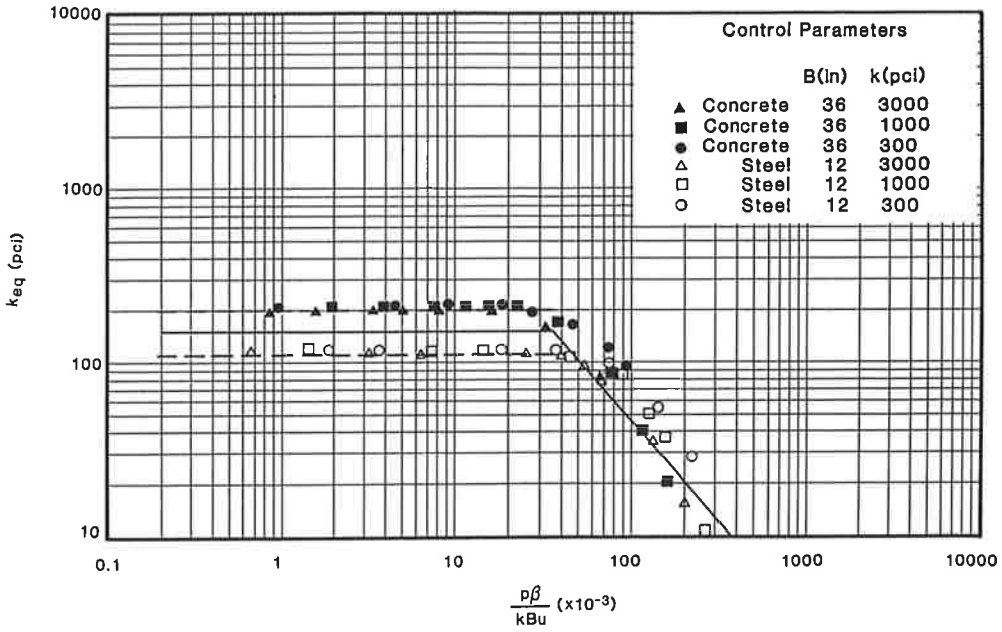

FIGURE 10 Equivalent subgrade modulus versus dimensionless lateral load factor for stiff clay below water: free-head conditions (1 in. = 2.54 cm; 1 pci = 271.7 kN/m³).

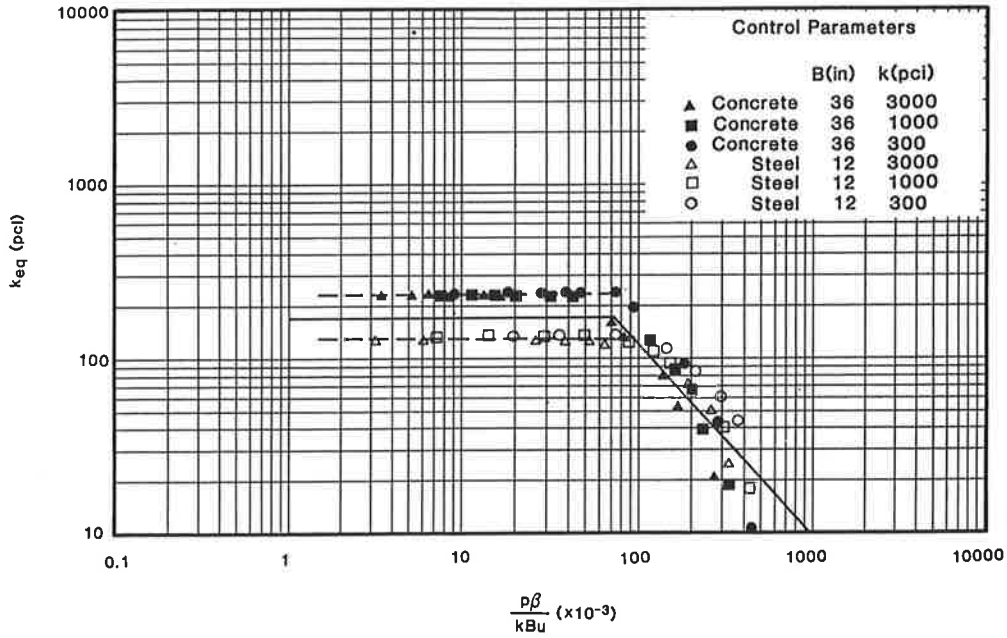

FIGURE 11 Equivalent subgrade modulus versus dimensionless lateral load factor for stiff clay below water: restrained-head conditions (1 in. = 2.54 cm; 1 pci = 271.7 kN/m³).

The overall comparison between predicted and published values in Tables 6 and 7 is favorable.

CONCLUSIONS

The concept of equivalent subgrade modulus for laterally loaded piles in clays was developed to represent nonlinear pile-soil behavior within a simplified analytical procedure involving linear modeling. The modulus is shown to be a simple function of the dimensionless lateral load factor and can be easily determined provided pile properties and undrained cohesion of soils are known. Maximum deflection and maximum moment of laterally loaded piles in clays can be readily predicted using the design curves for equivalent subgrade modulus versus dimensionless lateral load factor for free-head and restrained-head conditions. An efficient and easy-to-follow design procedure is also proposed. The procedure was tested by predicting published field test data and judged to yield reasonable and useful results.

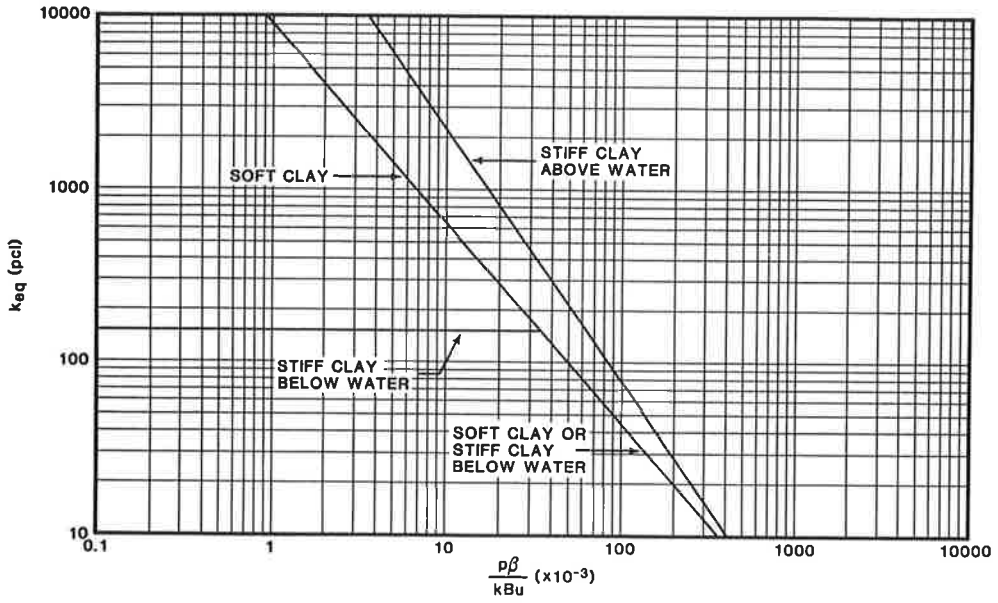

FIGURE 12 Design curves of equivalent subgrade modulus versus dimensionless lateral load factor: free-head conditions (1 pci = 271.7 kN/m³).

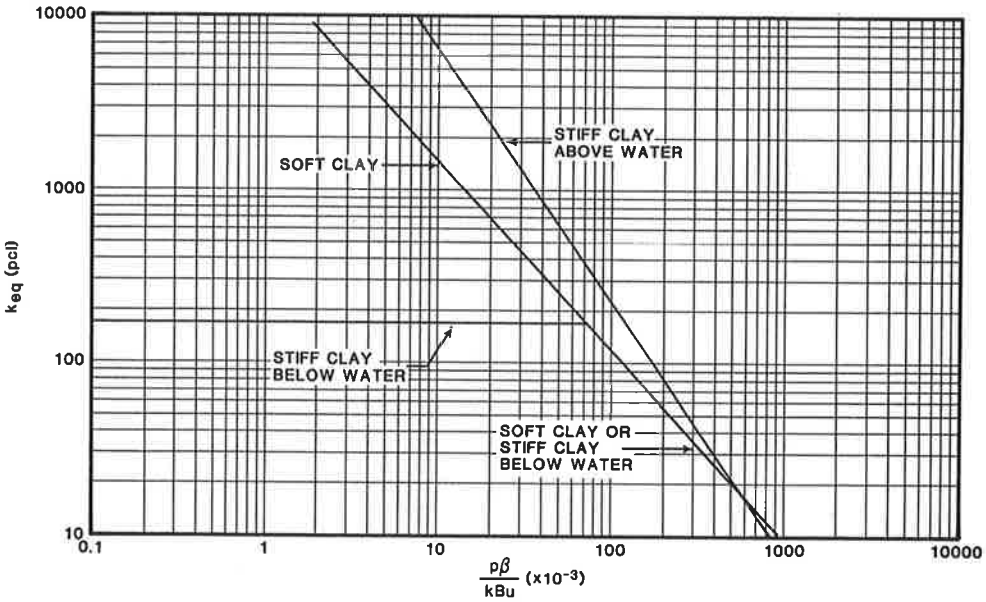

FIGURE 13 Design curves of equivalent subgrade modulus versus dimensionless lateral load factor: restrained-head conditions (1 pci = 271.7 kN/m³).

TABLE 5 PARAMETERS USED TO PREDICT PUBLISHED FIELD DATA

Criteria	Published Data		Calculated Data			
	B (in)	Cu (psf)	E[4] (psi)	I (in^4)	k[5](pci)	β[6]
Soft Clay[1]	12.75	300	3×10^7	155	25	0.0114
Stiff Clay Above Water[2]	30	2200	3×10^6	39761	600	0.0139
Stiff Clay Below Water[3]	48	1671	3×10^7	26302	350	0.0086

Note: 1 in = 2.54 cm; 1 psf = 47.9 N/m^2
1 psi = 6.89 kN/m^2; 1 pci = 271.7 kN/M^3

1. Matlock (2)
2. Reese & Welch (3)
3. Pile 2, Dunnavant & O'Neill (5)
4. Assume 3×10^7 psi for steel and 3×10^6 psi for concrete
5. From Figure 1
6. From Eq. 2

TABLE 6 PREDICTED AND PUBLISHED MAXIMUM DEFLECTIONS AND MOMENTS FOR STIFF CLAY ABOVE THE WATER TABLE (*3*)

Lateral Load (kip)	Maximum Deflection (in)				Maximum Moment (in-lb)x 10^6		
	Measured	Computed[1]	Predicted (Eq. 3)	Predicted (Eq. 7)	Measured	Computed[1]	Predicted (Eq. 8)
	(Published Data)				(Published Data)		
20	0.020	0.027	0.015	0.026	0.583	0.539	0.618
40	0.090	0.114	0.088	0.096	1.33	1.62	1.51
60	0.254	0.282	0.222	0.193	2.39	2.81	2.50
80	0.586	0.540	0.463	0.335	3.88	4.04	3.64
100	1.160	0.875	0.840	0.540	5.55	5.53	4.94

Note: 1 in = 2.54 cm; 1 in-1b = 113 mm-N; 1 kip = 4.45 kN

[1]Published data which were computed using the p-y relationship.

TABLE 7 COMPARISON OF PREDICTED AND PUBLISHED DATA FOR SOFT CLAY (*2*) AND SUBMERGED STIFF CLAY (*5*)

Lateral Load (kip)	Maximum Deflection (in)		Maximum Moment (in-lb)x10^6	
	Measured (Dunnavant et al., 1989)	Predicted (Eq. 3)	Measured (Matlock, 1970)	Predicted
4	-	-	0.168	0.134
8	-	-	0.395	0.317
16	-	-	0.992	0.741
50	0.13	0.12	-	-
75	0.25	0.21	-	-
150	0.70	0.76	-	-
195	1.50	1.54	-	-
240	1.96	2.34	-	-

ACKNOWLEDGMENTS

The author is grateful to McBride-Ratcliff and Associates, Inc. for providing the computer facilities for this study. The author also thanks Michael O'Neill from the University of Houston and Charles Williams from McBride-Ratcliff and Associates, Inc. for their many helpful suggestions.

REFERENCES

1. B. B. Broms. Lateral Resistance of Piles in Cohesive Soils. *Journal of the Soil Mechanics and Foundations Division*, ASCE, Vol. 90, No. SM2, 1964, pp. 27–63.
2. H. Matlock. Correlations for Design of Laterally Loaded Piles in Soft Clay. *Proc., Second Annual Offshore Technology Conference*, Vol. 1, Houston, Texas, 1970, pp. 577–594.
3. L. C. Reese and R. C. Welch. Lateral Loading of Deep Foundations in Stiff Clay. *Journal of the Geotechnical Engineering Division*, ASCE, Vol. 101, No. GT7, 1975, pp. 633–649.
4. L. C. Reese, W. R. Cox, and F. D. Koop. Field Testing and Analysis of Laterally Loaded Piles in Stiff Clay. *Proc., Seventh Annual Offshore Technology Conference*, Vol. 2, Houston, Texas, 1975, pp. 671–690.
5. T. W. Dunnavant and M. W. O'Neill. Experimental p-y Model for Submerged, Stiff Clay. *Journal of the Geotechnical Engineering Division*, ASCE, Vol. 115, No. 1, 1989, pp. 95–114.
6. H. Matlock and T. A. Haliburton. A Program for Finite-Element Solution of Beam-Columns on Nonlinear Support. University of Texas, Austin, 1964.

7. L. C. Reese and W. R. Sullivan. *Documentation of Computer Program COM624*. Geotechnical Engineering Software GS80-1. Geotechnical Engineering Center, University of Texas at Austin, 1975, pp. 633–649.
8. L. T. Evans, Jr., and J. M. Duncan. *Simplified Analysis of Laterally Loaded Piles*. Report UCB/ET/82-04. University of California, Berkeley, July 1982, p. 245.
9. H. Matlock and L. C. Reese. Generalized Solutions for Laterally Loaded Piles. *Journal of the Soil Mechanics and Foundations Division*, ASCE, Vol. 86, No. SM5, 1960, pp. 63–91.
10. L. C. Reese and H. Matlock. Non-Dimensional Solutions for Laterally Loaded Piles with Soils Modulus Assumed Proportional to Depth. In *Proc., Eighth Texas Conference on Soil Mechanics and Foundation Engineering*, Special Publication 29, Bureau of Engineering Research, University of Texas, Austin, 1956.
11. S. M. Gazioglu and M. W. O'Neill. Evaluation of p-y Relationships in Cohesive Soils. In *Analysis of Design and Pile Foundations* (J. R. Meyer, ed.), ASCE, San Francisco, Calif., 1984, pp. 192–213.
12. M. W. O'Neill and S. M. Gazioglu. *An Evaluation of p-y Relationships in Clays*. Report PRAC 82-41-2. American Petroleum Institute, Dallas, Texas, 1984.

Lateral Response of Rigid Piers in Sand, Clay, and Layered Profiles

ROY H. BORDEN AND MOHAMMED A. GABR

A simple model incorporating the contribution of base resistance to the lateral response of rigid piers is reviewed. The general applicability of the model and the importance of including base resistance are investigated through a parametric study and a comparison between predicted and measured responses of 16 load tests reported in the literature. The test piers were constructed in sand, clay, and layered soil profiles. In general, it is shown that the model incorporated in the software LTBASE tends to underestimate the measured field capacity at pier rotations of 1 and 2 degrees by about 10 percent on the average, with a standard deviation of 18 percent.

Laterally loaded piers are used to support a variety of structures, including light poles, highway overhead signs, transmission line towers, and bridges, for which the pier is extended up to the superstructure deck. Such foundation types often have length/diameter (L/D) ratios less than five. In most cases, the lateral loads transferred to the piers from the superstructure result in high overturning moment accompanied by modest shear.

In general, the load-deflection analysis of laterally loaded rigid piers is conducted without consideration of the influence of soil resistance at the pier base. Although this assumption is valid for piles and piers with relatively large L/D ratios, base conditions do influence the lateral response of short rigid piers. Ignoring the contribution of the base resistance to the overall response is conservative but may not be economical.

The subgrade reaction approach has been used by many researchers for the analysis of laterally loaded piles and piers (*1–6*). Using this approach, the soil-pier interaction mechanism is postulated by an assemblage of a finite number of nonlinear springs, as shown in Figure 1. The subgrade reaction concept provides a rational approach that permits an approximate description of the nonlinear behavior of the pier-soil system. Alternative models for the analysis of laterally loaded rigid piers also have been presented (*7–9*).

A simple model incorporating the contribution of base resistance to the lateral load-deflection response of rigid piers is used to evaluate the significance of including the base resistance and identify factors that affect the magnitude of its contribution. This model was developed as a supplement to the current subgrade reaction method of analysis that is familiar to and often used by many engineers in practice. Predictions made using the developed model are compared with measured field behavior of 16 pier load tests reported in the literature. Subsurface soil conditions encountered at the test sites included sand, clay, and layered soil profiles. Such a variety provides a strong basis to evaluate the model performance. Predictions using other existing models are also presented.

R. H. Borden, Center for Transportation Engineering Studies, Department of Civil Engineering, North Carolina State University, Raleigh, N.C. 27695–7908. M. A. Gabr, Woodward-Clyde Consultants, 904 Wind River Lane, Gaithersburg, Md. 20878.

BASE RESISTANCE MODEL

For short rigid piers with small L/D ratios, it is expected that both normal stress and horizontal shear stress would be mobilized at the interface between the pier base and soil. Because existing solutions utilizing the finite difference technique were derived mainly for long piles, the effect of the base resistance on the imposed boundary condition at the tip was not included. Considering this effect, a difficulty arises from the fact that the determination of such a boundary condition is dependent on both the soil reaction and the pier response; to use a more common term, it is dependent on the soil-structure interaction. The interaction behavior is described by the dependence of the magnitude of the base resistance on the amount of deformation at the base, and the determination of such deformation is contingent on the magnitude of base resistance.

The evaluation of the "soil-structure interaction boundary condition" was obtained using the principle of subgrade reaction (*10*). Referring to Figure 2, and assuming rigid body motion, the base normal, shear, and moment resistances are derived as follows.

$$V_b = v_A K_v (D^2/6) \quad (1)$$

$$M_b = v_A K_v (\Pi D^3/64) \quad (2)$$

$$H_b = V_b \text{ Tan } (\delta) + Ca(\Pi D^2/8) \quad (3)$$

where

K_v = vertical modulus of subgrade reaction,
v_A = vertical and horizontal displacement of Edge A due to rotation (θ),
V_b = normal soil reaction mobilized at the base,
M_b = mobilized resisting moment at the base,
H_b = horizontal shear resistance at the base,
δ = angle of friction between base and soil,
Ca = undrained shear strength x adhesion factor, and
D = pier diameter.

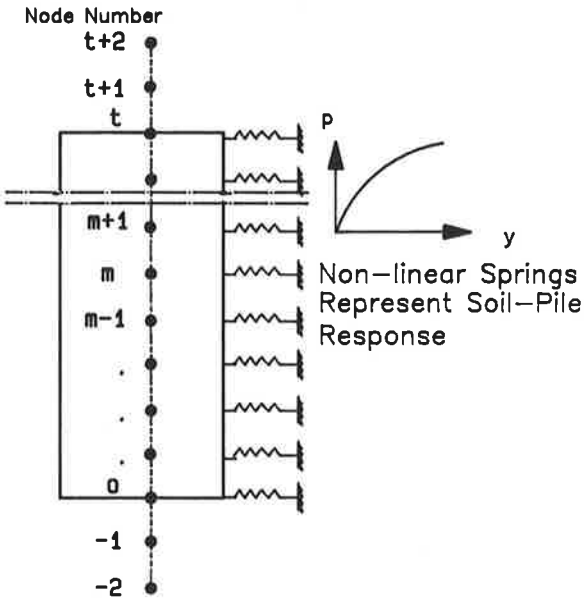

FIGURE 1 Finite difference discretization and soil representation.

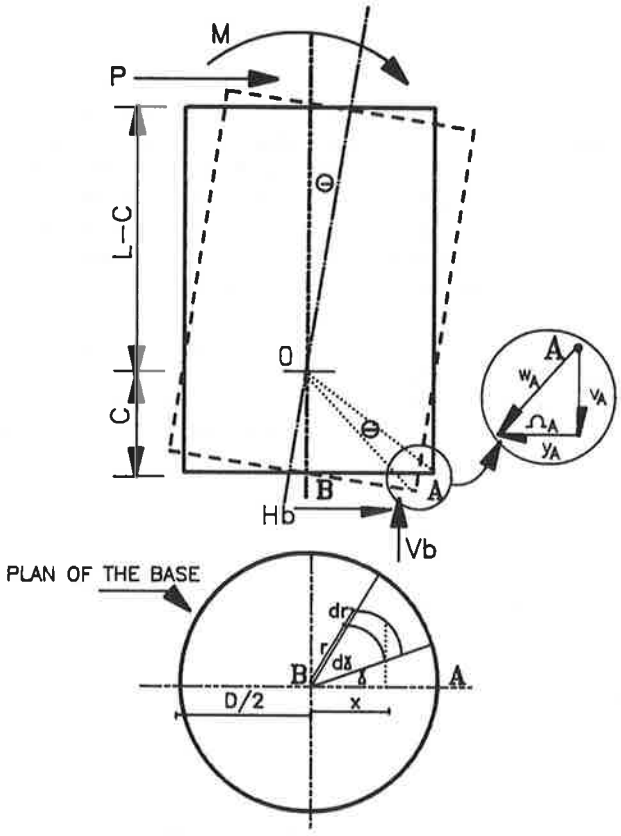

FIGURE 2 Pier deformation as a function of pier rotation.

This base resistance model was implemented in the computer program LTBASE (*11*). Simplified load-displacement curves used to define the base shear and normal springs are shown in Figure 3. Although experimental results suggest nonlinear springs for the base shear and normal resistance, a simpler representation is justifiable because in most cases the

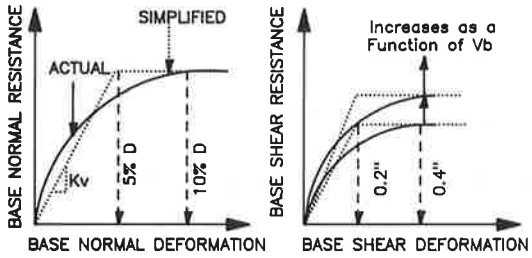

FIGURE 3 Base shear and normal springs.

contribution of the base resistance is expected to be significantly smaller than that of the lateral resistance.

A linear relationship is assumed to exist between base normal resistance and normal deformation up to the failure of the soil under the base. Similarly, the shear force–lateral displacement relationship is assumed to have a linear relationship between the horizontal shear force, developed between the base and the soil, and the lateral displacement of the base, up to the mobilization of the full shear force. However, as the overturning moment increases, an increasing normal force on the base is created. Accordingly, the resultant base shear-deflection relationship varies as a function of the normal force at the base, as shown in Figure 3. Experiments suggest that the ultimate shear resistance would develop at a shear displacement of 0.2 to 0.4 in., whereas a downward movement of about 5 to 10 percent of the pier diameter is necessary for mobilizing the full vertical base resistance (*12–19*). The lower limits of these bounds were used (in this case 0.2 in. and 5 percent *D*) to approximate the shape of the nonlinear curves as shown in Figure 3. The shear spring stiffness is defined as a function of the base normal force as well as the shear displacement.

The solution of the problem also requires that the soil adjacent to the pier be replaced by a set of springs that define the soil resistance (p) (force per unit length along the pile) as a function of pile deflection (y). Several methods of formulating p-y curves have been proposed (*3,7,20–24*). The soil response or p-y curves are generated internally in LTBASE according to the procedures described by Reese and Allen (*3*) and Murchison and O'Neill (*20*) for sands. In the case of clay, the unified method, presented by Sullivan (*22*), is used to formulate the p-y curves.

PARAMETRIC STUDY

The significance of including the base resistance component was evaluated by conducting a parametric study. The lateral load-deflection response of piers having diameters of 24, 36, 48, and 60 in. was evaluated using the computer program LTBASE with and without the inclusion of base resistance.

L/D ratios of 2, 3, and 4 were used in the analysis to investigate the percent increase in the pier lateral capacity as a function of the L/D ratio, as well as the pier diameter. The applied loads were taken as applied horizontal load (P) at the top of a 30-ft column supported by the pier being analyzed. This load is then translated to an applied ground line force (P) and moment (M).

SOIL IDEALIZATION

The soil was chosen to consist of a uniform sand deposit with ϕ equal to 30 degrees. The *p-y* curves were generated internally using LTBASE according to the procedure described by the Reese and Allen (*3*). The coefficient of lateral subgrade reaction (K_h) was taken equal to 100 lb/in.^{3}, and the base vertical subgrade reaction coefficient (K_v) was obtained by dividing the base ultimate normal resistance by 5 percent of the pier diameter (5 percent D represents the deformation assumed necessary to develop the ultimate resistance). The ultimate normal base resistance as a function of depth was obtained using the formulation given by Kulhawy (*25*). The variation of K_v as a function of L/D is given in Figure 4 for the different diameters investigated. For constant values of L/D, as the pier diameter increases the pier length also increases and the value of K_v decreases. This results because the ultimate normal base resistance increases at a decreasing rate with depth, whereas the deformation required to develop the ultimate resistance (5 percent D) increases linearly with increasing diameter. Thus, a lower K_v for larger diameters is computed.

EFFECT OF L/D RATIO

Figure 5 presents the relationship between pier capacity and L/D for pier diameters of 24, 36, 48, and 60 in. in the uniform cohesionless soil profile. To investigate the effect of L/D on the magnitude of base resistance contribution, the ultimate capacity of the piers was defined as the moment resistance corresponding to a 2-degree rotation of the pier. For an L/D ratio of 2, for example, the 2-degree rotation corresponds to a lateral pier-top deflection of 1.1, 1.67, 2.2, and 2.75 in. for pier diameters of 24, 36, 48, and 60 in., respectively. As expected, the ultimate resistance is observed to increase as the L/D ratio increases. Figure 6 shows the ratio of base resistance to the total moment resistance as a function of L/D ratio for a pier diameter of 36 in. For an L/D ratio of 2, the model indicated that the capacity can be underestimated by as much as 40 percent if the base resistance is not included. For a given L/D ratio, this percentage is approximately the same for different diameters because as the diameter increases the base and the side resistance increase concurrently. As L/D increases, a smaller base deformation is obtained, and

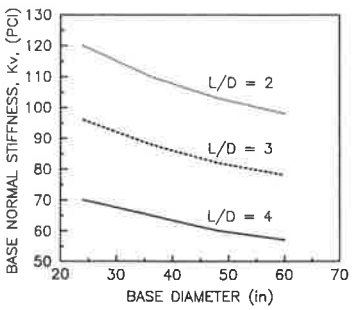

FIGURE 4 Base normal stiffness as a function of L/D ratio, ϕ = 30 degrees.

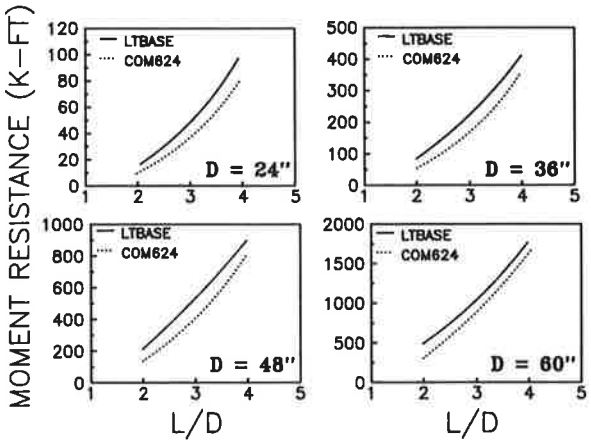

FIGURE 5 Moment capacity at 2-degree rotation as a function of L/D ratio.

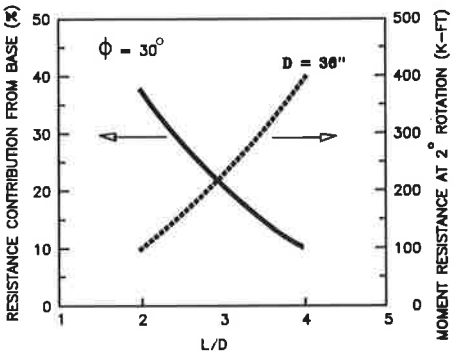

FIGURE 6 Percent resistance contribution from the base as a function of L/D ratio.

the contribution of the base resistance is shown to be of less significance. For piers having L/D greater than 4, less than 15 percent of the overall resistance is from the base contribution. However, if the full available base resistance is mobilized (for example, in calculating the ultimate resistance for determining the factor of safety against failure), the base contribution to the overall capacity is significantly higher.

EFFECT OF ϕ ON BASE RESISTANCE INFLUENCE

The influence of the angle of internal friction (ϕ) on the base resistance component of lateral resistance was also investigated. Analyses were performed using values for ϕ of 30, 35, and 40 degrees for the 36-in.-diameter pier. Figure 7 shows that the percent increase in capacity is practically independent of the value of ϕ. As ϕ is increased from 30 to 40 degrees, a slight decrease in the resistance contribution from the base (about 2 percent) is observed. This response is because the relative stiffness of the soil at the sides of the pier to that of the soil at the base remains essentially constant. For the same L/D ratio and given that ϕ is assumed to be the same at the base and at the sides of the pier, as ϕ increases approximately the same percentage increase in side resistance occurs as in base resistance.

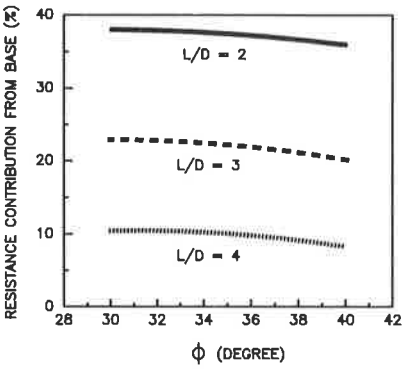

FIGURE 7 Percent resistance contribution from the base as a function of ϕ.

BASE RESISTANCE AS A FUNCTION OF DEFLECTION

Although the preceding analyses presented the contribution of base resistance to the overall capacity as a function of pier rotation, it is also of interest to present the same findings as a function of pier-top deflection. Viewing the contribution of the base component in such context becomes important for cases in which the piers are used to support structures that can tolerate only small lateral displacements. Figure 8 illustrates the ratio of the predicted resistance, including base resistance to the predicted resistance without such a contribution, as a function of pier-top lateral deflection. As would be expected, the significance of including the base resistance increases as the L/D ratio decreases. In this particular illustration, for an L/D ratio of 2, and at about 2 in. lateral deflection, the prediction accounting for base resistance generated a capacity that is about 70 percent higher than that ignoring the base contribution. However, at a smaller deflection level, for example 0.25 in., and for L/D ratio of 4 the inclusion of the base resistance accounts for only a 5 percent increase in resistance.

BASE RESISTANCE IN CLAY

To illustrate the influence of soil type on the significance of the base resistance component, an analysis was performed assuming a uniform soil deposit of normally consolidated clay. The undrained shear strength (*Cu*) was chosen equal to 10 psi, and the adhesion factor was equal to 0.5, as given by Tomlinson (*26*). The percent increase in resisting moment as a function of L/D ratio is presented in Figure 9. The increase in moment capacity due to base resistance ranged from 50 percent for an L/D of 2 to about 15 percent for an L/D equal to 4 at the 2-degree pier-top rotation. This behavior is similar to that observed in sand and indicates that the influence of the base resistance, for the same soil properties at the sides and the base, is a function of the L/D ratio and the magnitude of the base deformation.

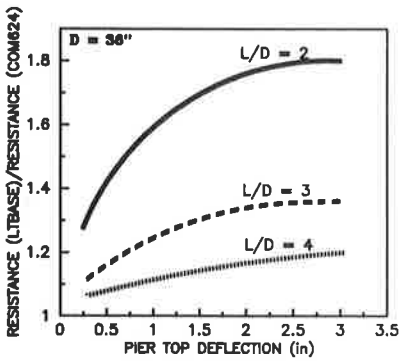

FIGURE 8 Base significance as a function of pier-top deflection.

MODEL PREDICTIONS OF FIELD BEHAVIOR

Predictions of the lateral load-deflection response of 16 load tests performed by others and reported by Davidson (*7*) were carried out using LTBASE. An extensive documentation of the load test procedures, soil properties, idealized profile of each site, and the cosponsoring organization can be found elsewhere (*7*). A brief description of the generalized soil profiles is given in Figure 10. Test locations, pier dimensions, and the values of the calculated base soil stiffness are given in Table 1.

The soil properties utilized as input data were those reported by the test performers. The *p-y* curve procedure developed by Reese et al. (*27*) was used whenever a sand profile was encountered, and the Unified procedure recommended by Sullivan (*22*) was used for clay. The Unified procedure for clay requires the prior choice of two parameters, *A* and *F*. These parameters basically convert the Unified method to either the soft clay procedure of Matlock (*23*) or the stiff clay procedure of Reese and Welch (*28*). The values recommended by Sullivan (*22*) for *A* and *F* are 2.40 and 1.00 for *Cu* equal to 2 psi and 0.35 and 0.50 for *Cu* equal to 17 psi. In this study, *A* and *F* values were estimated by linear interpolation between maximum and minimum values as a function of *Cu*. The base load-deformation relationships were developed following the procedure described previously.

The measured versus predicted capacities using LTBASE are plotted for 1 and 2 degrees of pier rotation in Figure 11. For tests in which the relationship between the degree of rotation and the applied moment was not given, the pier

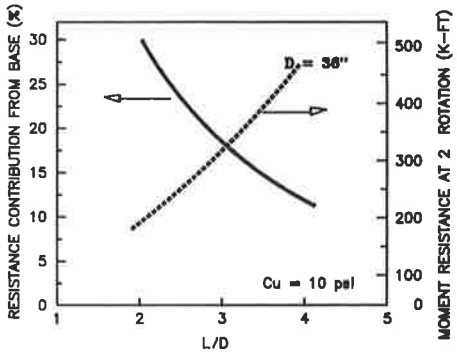

FIGURE 9 Percent resistance contribution from the base as a function of L/D ratio in clay.

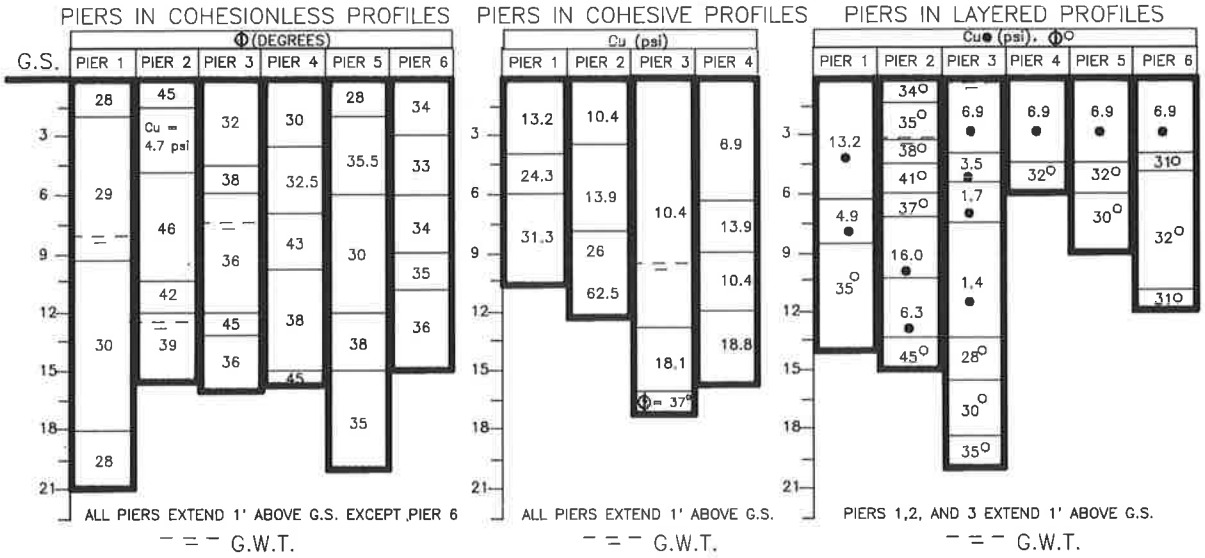

FIGURE 10 Soil properties and pier dimensions.

TABLE 1 PIER PROPERTIES AND BASE SOIL STIFFNESS

Test No.	Site Location	Pier Dimensions (diameter × length) (ft)	Pier Stiffness 10^{-12} (lb/in.^{2})	K_v (lb/in.^{3})
Load Tests in Cohesionless Profiles				
1	Greensburg, Pa.	4.5 × 16.0	2.24	70
2	Hrightstown, N.J.	5.0 × 16.8	2.29	100
3	St. Charles, Mich.	5.5 × 17.2	2.80	65
4	Phoenix, Ariz.	4.8 × 17.0	1.72	100
5	Garden Grove, Calif.	5.0 × 21.3	2.60	80
6	Hager City, Wis.	11.0 × 15.0	58.90	50
Load Tests in Cohesive Profiles				
1	Richmond, Va.	4.5 × 12.9	1.40	105
2	Oklahoma City, Okla.	5.0 × 13.5	2.25	190
3	Portland, Oreg.	4.5 × 18.5	1.39	65
4	Omaha, Nebr.	4.5 × 16.0	1.50	65
Load Tests in Layered Profiles				
1	Springdale	4.5 × 15.0	1.50	100
2	Kinston, N.C.	4.5 × 15.9	1.37	65
3	Salt Lake, Utah	5.0 × 21.0	2.60	80
4	Hager City, Wis.	6.0 × 6.0	5.20	35
5	Hager City, Wis.	6.0 × 9.0	5.20	45
6	Hager City, Wis.	6.5 × 12.0	7.18	55

rotation was computed based on the assumption that the point of rotation lies at two-thirds of the pier length, down from the top. Rotations of 1 and 2 degrees correspond to pier-top lateral deflections of 2.8 and 5.6 in., respectively, for a pier length of 20 ft. Predictions made assuming no base resistance as well as results from the Electric Power Research Institute computer program PADLL are also presented in Figures 12 and 13, respectively. PADLL predictions were reported by Davidson (*7*). The data are shown in conjunction with a 45-degree line (indicating perfect agreement between measured and predicted responses). Also shown are lines representing predicted values equal to 1.20 and 0.80 times the measured response.

DISCUSSION OF RESULTS

In general, the predicted responses using LTBASE agree reasonably well with the field measured responses. In cohesionless profiles, the predicted capacities were within 20 percent of the measured capacities, as shown in Figure 11. In cohesive profiles, the capacities of piers 2 and 3 were underestimated at 2 degrees rotation. Capacities of piers 2 and 3 constructed in layered profiles were significantly underestimated at 1 and 2 degrees rotation. Note that for piers 2 and 3 in cohesive profiles and piers 2 and 3 in layered profiles, both PADLL and LTBASE models significantly underestimated the measured response, as shown in Figures 11 and 13. This might

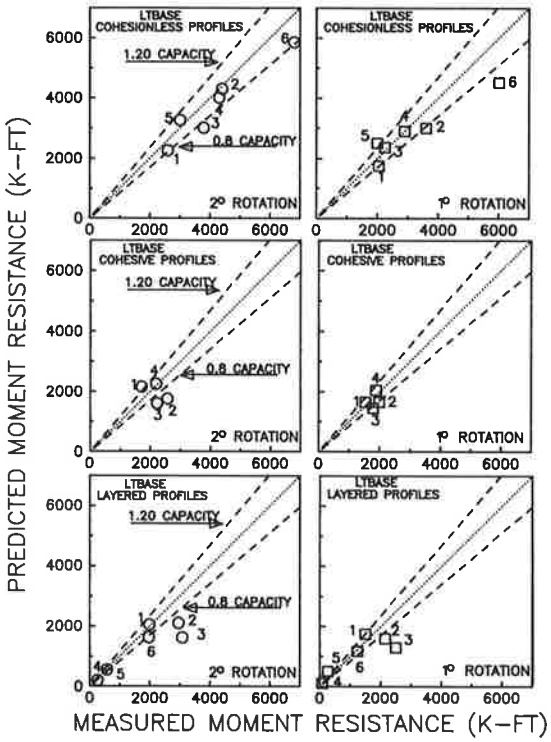

FIGURE 11 Applied versus predicted moment resistance with base resistance (LTBASE).

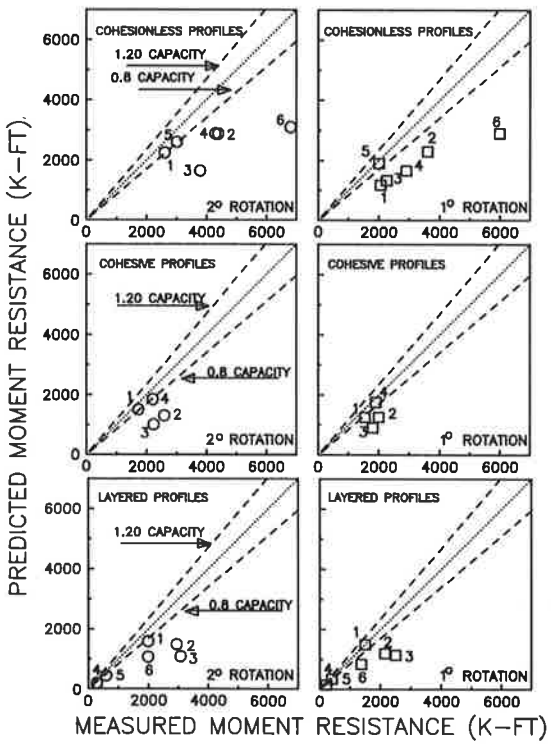

FIGURE 12 Applied versus predicted moment resistance with no base resistance (LTBASE).

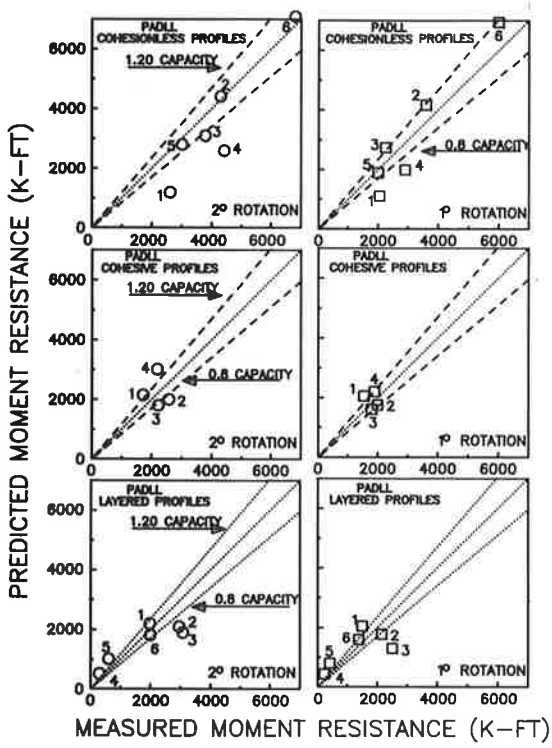

FIGURE 13 Applied versus predicted moment resistance (PADLL).

suggest the use of conservative soil strength properties in both analyses.

In all tests, analyses that ignored base resistance emphasize the importance of its inclusion. The percent increase in the predicted capacity as a result of including the base was as high as 88 percent for Pier 6 in cohesionless profile (L/D = 1.4) and Pier 4 in a layered profile (L/D = 1). For piers in cohesive profiles, the percent increase in predicted capacity caused by the inclusion of base resistance was as high as 43 percent for Pier 1 (L/D = 2.8).

As an overall evaluation of the test data analyzed, with the inclusion of base resistance the measured capacities of approximately 19 percent of the test piers at 1-degree rotation and 31 percent of the piers at 2-degree rotation were underestimated by more than 20 percent, whereas the predicted capacities of 12.5 percent of the piers were more than 20 percent greater than the measured capacities at 2-degree rotation. At 1-degree rotation, none of the measured capacities were overestimated.

In comparison, ignoring the base resistance contribution resulted in the measured capacities of 69 percent of the piers at 1-degree rotation and 56 percent of the piers at 2-degrees rotation being underestimated by more than 20 percent. Predictions obtained using PADLL underestimated the measured capacity by more than 20 percent for 25 percent of the piers at 1-degree rotation and 37.5 percent of the piers at 2-degree rotation. Using the same model, predicted capacities were more than 20 percent greater than the field measured capacities for about 19 percent of the piers at 1-degree rotation and 31 percent of the piers at 2-degree rotation. Table 2 summarizes the percentage of the tests piers for which the mea-

TABLE 2 PREDICTIONS GREATER OR LESS THAN 20 PERCENT OF MEASURED CAPACITY

	Pier Rotation (degrees)					
	One			Two		
Predictions (%)	LTBASE	No base resistance	PADLL	LTBASE	No base resistance	PADLL
Greater than 1.20 of Measured Capacity						
Cohesionless profiles (6 tests)	0.0	0.0	0.0	0.0	0.0	0.0
Cohesive profiles (4 tests)	0.0	0.0	0.0	25.0	0.0	50.0
Layered profiles (6 tests)	0.0	0.0	33.3	16.7	0.0	50.0
Less than 0.80 of Measured Capacity						
Cohesionless profiles (6 tests)	16.7	83.5	33.3	16.7	66.6	50.0
Cohesive profiles (4 tests)	0.0	50.0	0.0	50.0	50.0	50.0
Layered profiles (6 tests)	33.3	66.0	33.3	33.3	50.0	16.7

sured responses were either overestimated or underestimated by more than 20 percent.

Using LTBASE, at 2-degree rotation, the ratio of the predicted to measured moment capacity (*Mp/Mm*) ranged from 0.52 for Pier 5 in a layered profile to 1.25 for Pier 1 in a cohesive profile, with a mean value of 0.91 and a standard deviation of 0.18 for the 16 piers. For predictions made ignoring the base resistance contribution, *Mp/Mm* ranged from 0.42 for Pier 6 in a layered profile to 0.95 for Pier 1 in a cohesive profile, with a mean value of 0.64 and a standard deviation of 0.18 for the 16 piers. For the PADLL model, *Mp/Mm* ranged from 0.52 for Pier 5 in a layered profile to 1.46 for Pier 1 in a cohesionless profile, with a mean value of 1.01 and a standard deviation of 0.29 for the 16 piers.

CONCLUSIONS

The significance of including base resistance in the prediction of the lateral load-deflection response of rigid piers and factors affecting the magnitude of its contribution were presented in this paper. This study was made using a simple model that was developed as a supplement to the current subgrade reaction method of analysis, which is familiar to and often used by many engineers in practice. This model was implemented in the computer program LTBASE. Predictions made by LTBASE for 16 load tests performed external to this study were compared with measured field responses. Based on the results of a parametric study and analysis of the 16 load test predictions, the following conclusions can be advanced.

1. The significance of base resistance increases as the L/D ratio decreases. The percent increase in resisting moment due to the inclusion of base resistance in sand having a ϕ of 30 degrees could be as high as 65 percent for L/D of 2. For clay having an undrained shear strength of 10 psi, the percent increase in capacity was about 50 percent for an L/D of 2.
2. For L/D ratios greater than 4, assuming the pier behavior is still rigid, the mobilization of the base resistance requires relatively large base deformations, which in most practical cases will result in relatively large pier-top lateral deformation. For a pier-top deflection corresponding to a 2-degree pier rotation, the percent increase in the capacity was less than 15 percent for an L/D ratio equal to 4.
3. The magnitude of the mobilized base resistance expressed as a percentage of the overall lateral capacity is independent of the relative density of a cohesionless soil, providing that the soil properties at the sides and base of the pier are the same.
4. An overall evaluation of LTBASE predicted and field measured responses indicated that this model, incorporating the influence of base shear and moment resistance, is capable of predicting field behavior for a range of L/D ratios.
5. In general, it was shown that the model incorporated in LTBASE tends to underestimate the measured field behavior on the average by about 10 percent, with a standard deviation of 18 percent. The measured capacities of approximately 19 percent of the test piers at 1-degree rotation and 31 percent of the piers at 2-degrees rotation were underestimated by more than 20 percent, whereas the predicted capacities of 12.5 percent of the piers were more than 20 percent greater than the measured capacities at 2-degrees rotation. At 1-degree rotation, none of the measured capacities were overestimated.
6. The significance of the base contribution diminishes as the L/D ratio increases. Analysis of the load tests evaluated indicated that the percent increase in predicted capacity due to the inclusion of base resistance is as high as 88 percent for an L/D ratio of 1.4 and about 16 percent for an L/D ratio of 5.

ACKNOWLEDGMENTS

This research was sponsored by the North Carolina Department of Transportation (NCDOT) in cooperation with FHWA. A technical advisory committee chaired by W.G. Marley that included D. Bingham, J. Ledbetter, R. Martin, P. Strong, and J. Wilder of NCDOT, and J. Wadsworth of FHWA aided in the coordination of the research and is gratefully acknowledged.

REFERENCES

1. J.-L. Briaud, T. Smith, and B. Meyer. Laterally Loaded Piles and the Pressuremeter: Comparison of Existing Methods. In *Laterally Loaded Deep Foundations: Analysis and Performance*, STP 835, ASTM, Philadelphia, Pa., 1984, pp. 97–111.
2. S. M. Gleser. Behavior of Laterally Loaded Vertical Piles. In *Laterally Deep Foundations: Analysis and Performance*, STP 835, ASTM, Philadelphia, Pa., 1984, pp. 72–96.

3. L. C. Reese and J. D. Allen. *Drilled Shaft Manual, Volume II—Structural Analysis and Design for Lateral Loading*. FHWA, U.S. Department of Transportation, 1984.
4. F. Baguelin, R. Frank, and Y. H. Said. Theoretical Study of Lateral Reaction Mechanism of Piles. *Geotechnique*, Vol. 27, No. 3, 1977, pp. 405–434.
5. H. Matlock and L. C. Reese. Generalized Solution for Laterally Loaded Piles. *Transaction*, Vol. 127, Part I, ASCE, New York, N.Y., pp. 1,220–1,246.
6. K. Terzaghi. Evaluation of Coefficient of Subgrade Reaction. *Geotechnique*, Vol. 5, 1955, pp. 297–326.
7. H. L. Davidson. *Loaded Drilled Pier Research*. Final Report. Electrical Power Research Institute, Palo Alto, Calif., Vol. I and II, EL-2197.
8. C. V. Vallabhan and F. Alikhanlou. Short Rigid Piers in Clay. *Journal of Geotechnical Engineering*, Vol. 1,028 No. GT10, Oct. 1982, pp. 1,255–1,272.
9. K. Bhushan, S. Haley, and P. Fong. Lateral Load Tests on Drilled Piers in Stiff Clays. *Journal of Geotechnical Engineering*, Vol. 105, No. GT5, pp. 696–984.
10. M. A. Gabr and R. H. Borden. Influence of the Base Resistance on the Lateral Load Deflection Behavior of Rigid Piers in Sand. *Proc., Soil-Structure Interaction Conference*, Paris, May, pp. 219–226.
11. M. A. Gabr and R. H. Borden. LTBASE: A Computer Program for Analysis of Laterally Loaded Piers Including Base and Slope Effects. In *Transportation Research Record 1169*, TRB, National Research Council, Washington, D.C., 1989, pp. 83–93.
12. J. M. Polo and J. L. M. Clemente. Pile Group Settlement Using Independent Shaft and Point Loads. *Journal of Geotechnical Engineering*, Vol. 114, No. GT4, pp. 469–487.
13. T. B. Aschenbrenner and R. E. Olson. Prediction of Settlement of Single Piles in Clay. In *Analysis and Design of Pile Foundations*, Proc., ASCE National Convention, San Francisco, 1984, pp. 41–58.
14. H. Ko, R. H. Atkinson, G. G. Goble, and C. D. Ealy. Centrifugal Modeling of Pile Foundations. In *Analysis and Design of Pile Foundations*, Proc., ASCE National Convention, San Francisco, 1984, pp. 21–40.
15. F. H. Kulhawy, C. H. Trautmann, J. F. Beech, T. D. O'Rourke, W. McGuire, W. A. Wood, and C. Capano. *Transimition Line Structure Foundations for Uplift-Compression Loading*. Report El-2870. Electrical Power Research Institute, Palo Alto, Calif., 1983.
16. H. G. Poulos and E. H. Davis. *Pile Foundation Analysis and Design*, John Wiley and Sons, 1980.
17. J. Focht and C. Drash. Behavior of Drilled Piers in Layered Soils on Texas Barrier Islands. *Drilled Piers and Cassions II*, ASCE, New York, N.Y., May 1985, pp. 76–98.
18. L. C. Reese, F. T. Touma, and M. W. O'Neill. Behavior of Drilled Piers Under Axial Loading. *Journal of Soil Mechanics and Foundations Division*, Vol. 102, No. GT5, 1976, pp. 493–510.
19. M. W. O'Neill and L. C. Reese. *Behavior of Axially Loaded Drilled Shafts in Beaumont Clay*. Research Report No. 89–8. Center for Highway Research, University of Texas, Austin, 1970.
20. J. M. Murchison and M. W. O'Neill. Evaluation of P-Y Relationships in Cohesionless Soils. In *Analysis and Design of Pile Foundations*, Proc., ASCE National Convention, San Francisco, 1984, pp. 174–191.
21. R. F. Scott. *Analysis of Centrifuge Pile Tests; Simulation of Pile Driving*, American Petroleum Institute; OSPAR Project 13, California Institute of Technology, 1980.
22. W. R. Sullivan. Development and Evaluation of a Unified Method for the Analysis of Laterally Loaded Piles in Clay. Thesis. University of Texas, Austin, 1977.
23. H. Matlock. Correlation for Design of Laterally Loaded Piles in Soft Clay. *Proc., 2nd Annual Offshore Technology Conference*, OTC 1204, Houston, Texas, 1970, pp. 577–594.
24. F. Parker, Jr. and L. C. Reese. *Experimental and Analytical Studies of Behavior of Single Piles in Sand Under Lateral and Axial Loading*. Research Report 117–2. Center for Highway Research, University of Texas, Austin, 1970.
25. F. H. Kulhawy. Limiting Tip and Side Resistance: Fact or Fallacy. In *Analysis and Design of Pile Foundations*, Proc., ASCE National Convention, San Francisco, 1984, pp. 80–98.
26. M. J. Tomlinson. *Pile Design and Construction*, 3rd ed. Pitman, London, 1975.
27. L. C. Reese, W. R. Cox, and F. D. Koop. Analysis of Laterally Loaded Piles in Sand. *Proc., Sixth Annual Offshore Technology Conference*, Vol. 2, Paper 2080, Houston, Texas, 1974, pp. 473–485.
28. L. C. Reese and R. C. Welch. Lateral Loading of Deep Foundations in Stiff Clay. In *ASCE Proc.*, Vol. 101, No. GT7, Feb. 1975, pp. 633–649.

Pile-Supported Bridge Foundations Designed for Impact Loading

DAN A. BROWN AND HENRY T. BOLLMAN

Bridge piers designed for impact loading from barges or other vessels represent a large investment of highway dollars in southeastern states, particularly Florida. Recent experimental research on the behavior of groups of piles subjected to large lateral loads has provided insight into the influence of group effects (pile-soil-pile interaction) for such loading conditions. Procedures currently used in design do not reproduce the observed behavior; thus, improved design techniques are needed. Outlined is a design procedure recommended by the authors that is based on the results of recent well-instrumented, large-scale experiments. Recommendations for modification of *p-y* curves as a function of row position in a rectangular group arrangement are presented. The procedure is relatively simple and should be easily incorporated into design but should be considered an interim approach because of the limited experimental data that is available on the subject. An example use of the method is provided.

Southeastern coastal states, particularly Florida, have a large number of bridges that span navigable waterways. Current practice is to design exposed bridge supports for impact of barges or other vessels using an equivalent static lateral load applied at the waterline. In general, the foundations for these bridge piers are designed to consist of large groups of piles, and the design for this impact loading often controls the number and types of piles selected. A great deal of uncertainty exists regarding the magnitude of the applied load; however, this paper deals only with foundation design once the equivalent static lateral load is established.

Groups of piles with typical spacings of around three diameters on center will have a capacity to resist lateral load that is less than the sum of an equal number of isolated piles due to group effects (pile-soil-pile interaction). Recent experimental research on large-scale groups that were instrumented (*1–4*) indicates that the distribution of load to the piles and the individual pile response is dominated by row position within the group more than any other aspect. Analytical research using three-dimensional nonlinear finite element analyses (*5*) has indicated similar behavior and suggests the procedure outlined in this paper. Currently used design techniques that rely on either elastic pile-soil-pile interaction or treat the group as a single entity (*6*) do not account for this type of behavior and thus do not realistically model the problem.

Presented here is a procedure for design of groups of piles subjected to large lateral loading that incorporates existing techniques for analysis of individual piles subjected to lateral load along with existing techniques for structural analysis of a bridge bent. The method uses empirical factors for modification of *p-y* curves for the piles based on row position. These factors are derived from back analysis of the relatively few available large-scale experiments and analytical research and apply only to loads of large magnitude [i.e., loads large enough to produce deflections of ½ to 1 in. (12.7 to 25.4 mm) or more]. A method for conveniently incorporating the predicted pile response into a routine structural analysis is also described.

D. A. Brown, Department of Civil Engineering, Auburn University, Ala. 36849. H. T. Bollman, Florida Department of Transportation, Room 334, Mail Station 33, 605 Suwannee Street, Tallahassee, Fla. 32399–0450.

GENERAL PROBLEM

In general, ship impact will occur on a structure similar to that shown in Figure 1. A particular bridge bent is supported by two or more columns that in turn are supported by a rectangular group of piles. The load from impact of a vessel will occur at or near the waterline, as shown in Figure 1. Clearly, a great deal of uncertainty exists regarding the kinetic energy of the impacting vessel, energy transferred to the bridge on impact, and so forth. These considerations are beyond the scope of this paper; however, the policy of the Florida Department of Transportation (DOT) is to estimate an equivalent static load using the simplified procedure outlined in a study sponsored by the Louisiana Department of Transportation and Developments (DOTD) (*7*). This strategy will at least provide a rational and consistent basis for design.

For the foundations shown in Figure 1, the major portion of the load will be resisted by the impacted pier, but some of it will be transferred through the structure to adjacent foundations. The problem is thus one in which structural analysis and foundation design are interrelated. Important parameters relative to pile selection will be shear force and moment at the top of the pile and lateral deflection under the design load condition. In general, pile-supported foundations subjected to vessel impact are not governed by rotation of the pile cap and the resulting axial loads in the piles. Batter piles tend to be efficient only for large groups in relatively deep water because of the variable direction of loading, the tendency for batter piles to produce load concentrations within the group, and the increased costs associated with installing batter piles over water. Piles are typically spaced at around three diameters on center.

RESPONSE OF PILE GROUPS

Experimental research by the first author and others has indicated that a group of piles spaced at approximately three

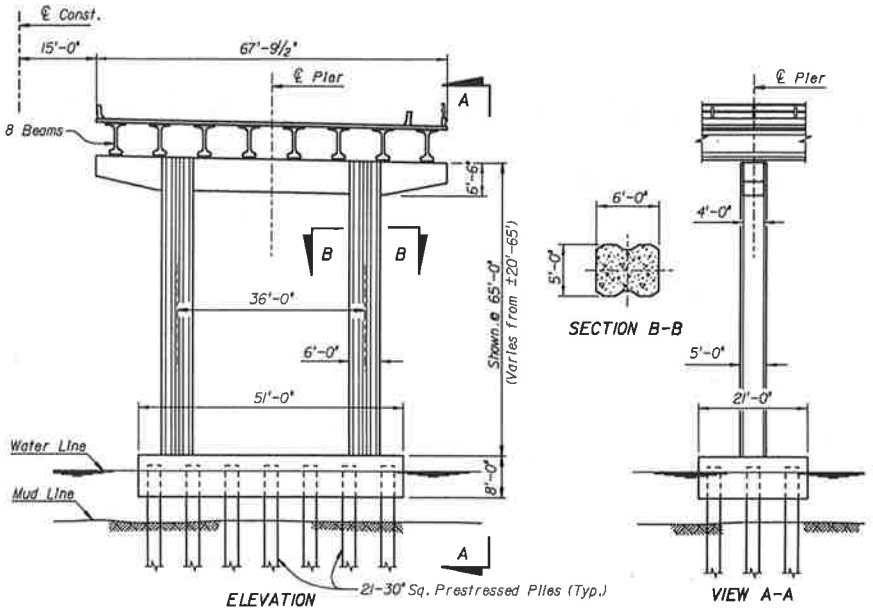

FIGURE 1 Impact load on a pile-supported bridge bent.

diameters on center can be expected to undergo significantly greater deflection at a given load than would an equal number of isolated piles. This reduced efficiency is due principally to the effect of "shadowing," in which the piles in trailing rows can mobilize only a reduced soil resistance because of the influence of the piles in the leading row. The piles in the leading row undergo a slightly reduced soil resistance due to stress overlap and superposition of strain in the soil ahead of the piles. Bending moments tend to be maximum in the piles of the front row because of the bias in load distribution at a given deflection.

One of the widely accepted approaches to the design of piles for lateral loading is the use of a Winkler model for the soil utilizing nonlinear *p-y* curves to represent the soil response. A rational approach to design of groups uses this approach, with modifications of the *p-y* curves used for an isolated single pile to account for group effects. The *p-y* curves for a single pile might be generated using correlations with soil properties, in situ pressuremeter tests, or other means.

Shown in Figure 2 is the concept of a *p*-multiplier (P_m). A reasonable method of accounting for the effect of pile-soil-pile interaction within a group is to modify the *p-y* curves for an individual pile in a group based on row position using a *p*-multiplier that has been empirically derived from experimental data (*1*).

Back analyses have been performed on the relatively few large-scale experiments for which there are rectangular groups loaded to large deflections and for which there are bending moment data with depth for at least several piles in the group. Presented in Table 1 are the backfigured P_m values for three load tests. P_m values were determined for the experiments using the following procedure.

1. Using either the actual *p-y* curves from a single pile experiment at the site or analytical *p-y* curves fitted to the single pile experimental results, perform an analysis of a single laterally loaded pile using COM624 (*7*) to confirm that the predictive model is appropriate for the specific research site.

2. Perform a number of analyses using COM624 with *p-y* curves that have been modified using different P_m values; all of the *p-y* curves are adjusted using the same (constant) value of P_m.

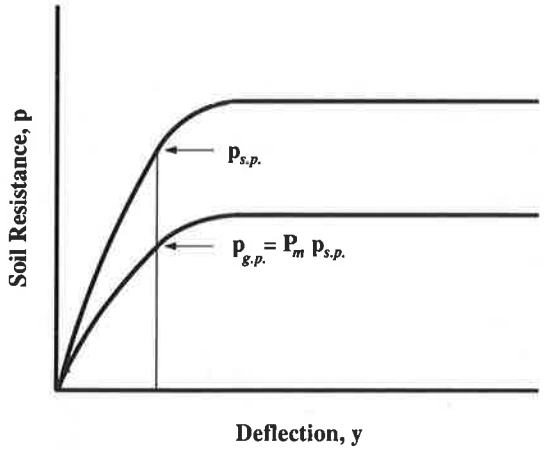

FIGURE 2 Concept of *p*-multiplier (P_m).

TABLE 1 P_m VALUES FROM SELECTED LARGE-SCALE EXPERIMENTS

Reference	Deflection (in.)	Front Row	2nd Row	3rd Row
Brown et al, 1988; Sand,	1.0 to 1.5	0.8	0.4	0.3
Brown et al, 1987; Stiff Clay,	1.2	0.7	0.6	0.5
Stiff Clay,	2.0	0.7	0.5	0.4
Meimon et al, 1986; Soft Silty Clay	0.6	0.9	0.5	-

3. For piles representative of each row in a group, select the value of P_m that provides the best agreement in terms of pilehead load versus deflection in the ½ to 1 in. deflection range (12.7 to 25.4 mm) and in terms of depth to and magnitude of the maximum moment in the pile. P_m is thus not directly backcalculated but selected based on agreement between analytical and experimental results.

Note that because these back analyses have been performed using *p-y* curves fitted to actual data from a single pile load test on the same site, it may reasonably be concluded that the observed effects are due to group action and not simply errors in the site-specific *p-y* curve formulation. Although P_m need not be constant with depth, the P_m values shown in Table 1 were derived as constants; given the limited experimental data, there appears to be little justification in attempting greater precision by varying P_m.

The P_m values shown were found to provide good agreement with both measured bending moments in the piles as well as pilehead load-deflection relationships. The group effects were larger with increasing deflection (load level), which may account for the relatively larger values of P_m derived for the test piles described by Meimon et al. (*3*); these piles were loaded to static deflections of only about 0.6 in. (15 mm), which were not as large as those of the other test cases.

PROPOSED DESIGN PROCEDURE

The proposed design procedure uses the *p*-multiplier concept described previously, along with a relatively simple way of incorporating this approach into a conventional structural analysis. The procedure is briefly described here.

1. Develop equivalent static loads for barge impact following the Louisiana DOTD guidelines (*7*).
2. Develop *p-y* curves for an isolated individual pile using the best available means; this might be done using available published correlations with strength and other soil properties, using in situ data from a pressuremeter or other device, or using a site-specific load test.
3. Perform analyses using a code such as COM624 (*7*) to develop load-deflection and load-moment data for piles using the *p-y* curves developed in Step 2, modified using the P_m values appropriate for a given row position. In general, and until further research provides more complete design guidance, it is suggested that the soil resistance values for the isolated pile be multiplied by $P_m = 0.8$ for the front row, $P_m = 0.4$ for the second row, and $P_m = 0.3$ for the third and all subsequent rows. These values are considered to be reasonable for pile spacing of about 3 diameters on center and for deflections at the groundline of about 10 to 15 percent of the pile diameter; they may be somewhat conservative for larger spacing or smaller deflections. For most cases in which the piles in the group are embedded into a thick concrete cap, it will be appropriate to assume a top boundary condition in which the piles are fixed against rotation and subjected to a specified shear or deflection. Once a shear load versus deflection relationship is established for piles in each row, it is possible to estimate deflections of the group for a given lateral load. One may generally assume the cap to be rigid, so that the piles all undergo the same deflection.
4. After an initial estimate of deflection and pilehead shear is obtained for the piles of each row, an equivalent length of fixity (L_{eq}) is estimated for the piles in each row using the relationship

$$L_{eq} = [12EI/(P/Y_t)]^{1/3}$$

where

P = Lateral load at top of pile,
Y_t = Deflection at top of pile,
E = Young's modulus of pile material, and
I = Pile bending moment of inertia.

This equivalent length will allow the piles in the group to be modeled in the structural analysis as cantilevered beams, fixed at the base, in order to give an appropriate load-deflection response from the piles for the structural analysis. Note, however, that the equivalent length used is only appropriate for a limited range of deflection because the true load-deflection response of each pile is nonlinear. It would also be possible to model the foundation by replacing the piles with springs of different equivalent stiffness; the equivalent length approach is primarily used for convenience.

5. Perform the structural analysis of the frame with the piles in the group modeled as cantilevered beams. Note that the cantilevered beam model is only to match the lateral load-deflection response at the pilecap, and the computed bending moments at the point of fixity are irrelevant. Likewise, if significant axial loads are associated with the ship impact, the axial load-deformation response of the piles using this model may not be appropriate. A two-dimensional analysis is typically performed, with each cantilevered beam representing an actual row of piles. As a result of the structural analysis, the shear at the top of each pile and pile group deflection (Δ) is computed.
6. Because some of the load is typically transferred through the frame to other parts of the structure, Δ is usually slightly less than the deflection estimated in Step 3. If these deflections are not within a few percent, return to Step 4 for a revised estimated L_{eq} based on a deflection equal to Δ, and iterate to convergence.
7. Once the lateral load and deflection at the top of each pile is established, check the structural adequacy of the piles using the bending moments computed in Step 3 for that load. Because the piles in the front row attract the most shear load, the front row piles usually govern the structural design of the piles.

Because the procedure is specifically for two-dimensional analysis of rectangular groups, impact loads that are skewed are resolved into two orthogonal load components that are analyzed separately. The row positions of each pile will be different for the two orthogonal load cases, and the L_{eq} values used for each row will likely differ. Stresses and displacements are summed using superposition. Although this approach to a skewed loading condition is a simplification of the actual three-dimensional problem, the effects of shadowing in a skewed loading are likely to be less severe, and thus, the approach is a rational simplification. No experimental data exist for such a condition to provide guidance for design, so there does not seem to be sufficient justification for a more complicated procedure.

EXAMPLE

To illustrate the proposed procedure, a simple example is provided. A 4 × 5 pile group of prestressed concrete piles is to be analyzed, as shown in Figure 3. An equivalent static lateral load of 1,600 kips (7,120 kN) is used to represent the impact load. The computer code COM624 is used to analyze the piles in each row using the criteria for sand proposed by Reese et al. (*8*), modified by f_m values of 0.8, 0.4, 0.3, and 0.3 for each row, front to back, respectively. COM624 generates the *p-y* curves internally, and the addition of the P_m modification to the code is relatively simple. The load-deflection and moment-deflection curves resulting from these analyses are shown in Figure 4. Note also that the average

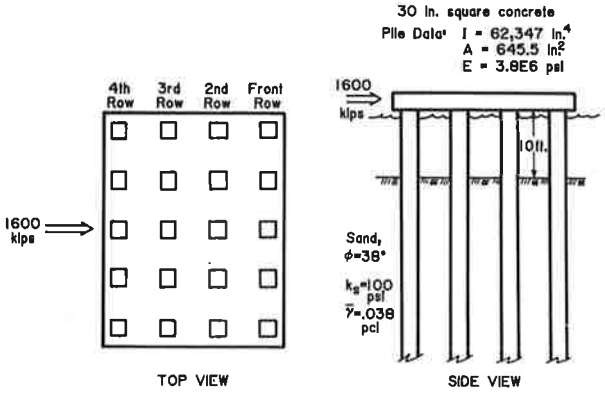

FIGURE 3 Design example (1 in. = 25.4 mm, 1 kip = 4.45 kN, 1 psi = 0.145 kPa).

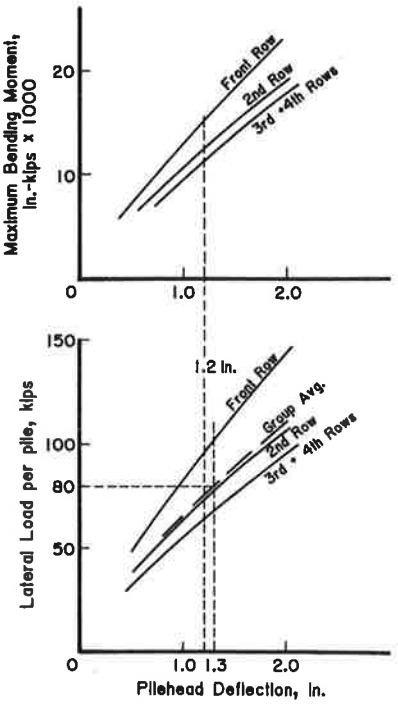

FIGURE 4 Plots of load versus deflection and moment versus deflection for design example (1 in. = 25.4 mm, 1 kip = 4.45 kN).

TABLE 2 COMPUTED L_{eq} VALUES AT 1.3 in. (33.0 mm) DEFLECTION

Position	Shear (kips)	L_{eq} (feet)
Front Row	103.	27.5
Second Row	79.	30.0
Third Row	69.	31.4
Fourth Row	69.	31.4

TABLE 3 COMPUTED L_{eq} VALUES AT 1.2 in. (30.5 mm) DEFLECTION

Position	Shear (kips)	L_{eq} (feet)
Front Row	98.	27.2
Second Row	74.	29.7
Third Row	64.	31.1
Fourth Row	64.	31.1

pile load-deflection curve is plotted by averaging the load at a given deflection from the piles in all rows. Using this average pile curve, at an average load of 80 kips (350 kN) per pile, a deflection of 1.3 in. (33.0 mm) is computed.

For the piles in each row at 1.3 in. (33.0 mm) of deflection, the lateral shear load at the pilehead can be determined from Figure 4, and the equivalent length for the piles in each row computed as presented in Table 2. A structural code such as STRUDL is used to analyze the pier-superstructure-pile interaction with the piles modeled as cantilevered beams fixed at the bottom of length L_{eq}, and a pilecap deflection of 1.2 in. (30.5 mm) is computed. Another iteration is performed using the equivalent lengths computed at a 1.2-in. (30.5-mm) deflection (shown in Table 3), and convergence is achieved. Note that the resulting shear force on the group is now 1,500 kips (6,675 kN); 100 kips (445 kN) has been transmitted to other parts of the structure. Maximum bending moments in the piles are determined from the moment-deflection diagram in Figure 4. Note that the results of a COM624 analysis for the entire length of pile can be produced using the final pilehead shears or deflections, but normally the pile reinforcement is not varied to adjust for changes in computed bending moments.

For conceptual design and initial sizing of the group, engineers at Florida DOT have developed design charts for some typical soil conditions by plotting curves of equivalent length of fixity below the mudline versus lateral load for selected piles. Limiting values of lateral load are indicated for selected piles. In this manner, a group can be sized relatively quickly for further analysis using the procedure identified here.

Note also that for concrete piles or shafts, the stiffness in bending (*EI*) will vary with the level of bending stress. If *EI* is to be a constant, a value of *EI* that is representative of the pile or shaft behavior at the computed bending stresses should be chosen.

CONCLUSION

Data from large-scale experiments on groups of piles subjected to lateral loading have been analyzed for insight into

design of pile groups for ship impact loading. A rational design procedure is proposed that includes the most important aspect of pile-soil-pile interaction—"shadowing," in which piles in trailing rows are subject to reduced soil resistance. The design procedure proposed incorporates existing techniques for design of piles for lateral loading as well as existing techniques for structural analysis of bridges. The procedure is limited to analysis of rectangular pile group arrangements subjected to relatively large loads and deflections. Experiments indicate that group effects are less significant at lesser load levels. The procedure is based on a center-to-center pile spacing of about three pile diameters; experimental data are insufficient to extrapolate to other arrangements or spacings. The limited amount of experimental data available to guide designers in this area emphasizes the need for additional research.

REFERENCES

1. D. A. Brown, C. Morrison, and L. C. Reese. Lateral Load Behavior of Pile Group in Sand. *Journal of Geotechnical Engineering*, Vol. 114, No. GT11, 1988, pp. 1,261–1,276.
2. D. A. Brown, L. C. Reese, and M. W. O'Neill. Behavior of a Large Scale Pile Group Subjected to Cyclic Lateral Loading. *Journal of Geotechnical Engineering*, Vol. 113, No. GT11, 1987, pp. 1,326–1,343.
3. Y. Meimon, F. Baguelin, and J. F. Jezequel. Pile Group Behaviour Under Long Time Lateral Monotonic and Cyclic Loading. *Proc., Third International Conference on Numerical Methods in Offshore Piling*, Institute Francais Du Petrole, Nantes, pp. 285–302.
4. D. M. Holloway, Y. Moriwaki, R. J. Finno, and R. K. Freen. Lateral Load Response of a Pile Group in Sand. *Proc., Second International Conference on Numerical Methods in Offshore Piling*, ICE, London, pp. 441–456.
5. D. A. Brown and C. F. Shie. Numerical Experiments into Group Effects on the Response of Piles to Lateral Loading. *Computers and Geotechnics*, 1990.
6. L. C. Reese. *Handbook on Design of Piles and Drilled Shafts Under Lateral Load.* Report FHWA-IP-84-11. FHWA, U.S. Department of Transportation, 1984.
7. Modjeski and Masters. *Criteria for the Design of Bridge Piers with Respect to Vessel Collision in Louisiana Waterways.* Louisiana Department of Transportation and Developments; FHWA, U.S. Department of Transportation, 1984.
8. L. C. Reese, W. R. Cox, and F. D. Koop. Analysis of Laterally Loaded Piles in Sand. Paper OTC 2080. *Proc., Fifth Annual Offshore Technology Conference*, Houston, Texas, 1974.

Low-Frequency Vibropile Driving and Prediction of Dynamic Tip Resistance of Piles

M. A. SATTER

Experimental tests have been conducted on mainly open-ended pile models driven into fine-grained sand (soil) by low-frequency vibratory excitations. The minimum input force amplitude that causes a pile to penetrate the soil and the optimum amplitude that ensures the quickest penetration of the pile to the ultimate depth have been determined. Postoptimum force levels have been found to induce a high impactive reaction at the pile tip (i.e., dynamic tip resistance), and this phenomenon has been investigated. A mathematical theory to predict the dynamic tip resistance is proposed. Piles with various tip configurations have been tested.

It is economically important to optimize pile-driving parameters, especially the input power level and the rate of penetration, to achieve the ultimate depth of the pile. It was shown in an earlier study (*1*) that it is possible to use pile records to predict optimum driving parameters. The study was conducted using a model pile with a closed tip driven into loose, fine-grained sand (soil). The vibratory excitation frequency was kept in the range 5 to 60 Hz, substantially below the fundamental longitudinal frequency of the pile. At this range of excitation the elastic deformation of the pile was negligible, thus the pile was considered as a rigid body in the relevant mathematical formulations. A minimum input vector force was found that caused the pile to begin to penetrate the soil very slowly. Likewise, there was an optimum level of input force that ensured the quickest penetration of the pile to the ultimate depth. Furthermore, it was observed that if the input force exceeded the optimum level corresponding to the applied surcharge (Figure 1), no further penetration of the pile was effected. Instead, the pile underwent steady-state vibration, including impactive reaction (dynamic reaction) from the soil.

It was clearly established that the soil reaction was that of a nonlinear cubic spring. A nonlinear equation of motion of the pile was developed, which enabled the accurate prediction of the pile's tip resistance from the pile's dynamical records. The existence of dynamic reaction between the pile and soil has been reported by other researchers (*2*,*3*).

In vibropile driving, vibrocompaction causes the mechanical properties of soil around the pile to change (*4*,*5*). The driving parameters and the shape of the pile tip determine the degree of compaction and hence the stiffness of the soil, which in turn influences the dynamic tip resistance of the pile. For the same soil under identical driving inputs, vibrocompaction is expected to be different for differently shaped pile tips. In other words, the degree of compaction of soil will not be the same for closed and open piles, so their dynamic tip resistances can be expected to be different. This paper investigates the depth of penetration and the corresponding level of the optimum force and then studies the dynamic resistance of mainly open piles under the postoptimum condition. Open pile tips with circular and elliptical geometries have been used. The results are compared with those of a closed-tip pile.

Yuasa Battery Ltd., 60/1 Purana Paltan, 2nd Floor, Dhaka, Bangladesh. Current affiliation: Department of Mechanical Engineering, Shiraz University, Shiraz, Iran.

EXPERIMENTS AND RESULTS

Laboratory tests have been conducted on model piles with open tips, but a closed-tip pile was included in the tests for comparison purposes. The soil consists of brown subangular sand from Shiraz, Iran. The granular size of sand corresponds to the 16/40 U.S. standard sieve size. The model pile data are as follows:

- Material: mild steel,
- Length: 0.8 m,
- Outside diameter: 0.019 m, and
- Inside diameter: 0.017 m.

The fundamental longitudinal frequency of the pile is 950 Hz, and the equivalent dynamic mass including that of the pile is 0.7 kg. Among the piles tested, the length and the dynamic mass were the same but the embedded tips were either circular or elliptical. For the piles with elliptical tip openings, the embedded end was tapered to various lengths. The dimensions of the tapers appear in Table 1 and Figure 2.

In the experimental setup (Figure 1), the pile under consideration was connected to a shaker that was fastened with a steel rope and counterbalanced by a suitable weight. The rope was supported by two pulleys affixed to a frame. Frictional force between the rope and the pulleys was kept to a minimum, as was the eccentricity between the shaker and the pile. The excitation frequency was kept at 40 Hz, which was found to be convenient for the pile-soil combination. As is the practice in vibratory pile driving, the combined weight of the shaker, pile, and attachments is balanced by a counterweight, and then a small bias weight, called a static surcharge,

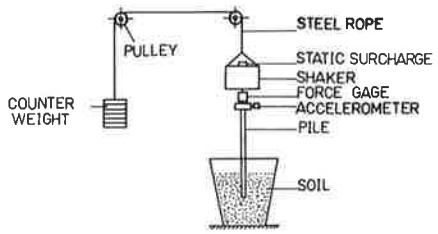

FIGURE 1 Schematic diagram of experimental setup.

is added (Figure 1). The static surcharge is necessary for a pile to penetrate the soil. Static surcharges from 0 to 26.7 N were used for the pile models tested.

Depth of Penetration

The records of soil penetration of various piles against input forces are shown in Figures 3–7. The depth of penetration depends on both the input force level and the applied static surcharge. Generally, the pile achieves deeper penetration for a heavier static surcharge, but this necessitates a higher input force level. The embedded tip configuration of a pile has a marked effect on the depth of penetration. For an applied surcharge of 8.9 N, the maximum depths of penetration achieved by the open and closed piles are about 320 and 35 mm, respectively (Figures 3 and 4). Piles with tips lying between the fully open and fully closed configurations will achieve intermediate depths of penetration (Figures 5–7). The three piles (A, B, and C) in Table 1 have almost equal tip openings but different taper lengths. The maximum depths of penetration of the piles with taper lengths of 100, 50, and 35 mm are 90, 165, and 192 mm, respectively, for the applied surcharge of 8.9 N. Thus, the pile with a shorter taper penetrated deeper into the soil than the piles with longer tapers.

Minimum and Optimum Force Levels

Experiments were also conducted to determine the minimum and optimum levels of input force necessary for vibropile driving. The minimum force level is defined here as the force that causes the pile, under a certain static surcharge, to begin penetrating very slowly into the soil. The optimum force level, however, is defined as the input force under which the pile achieves the ultimate penetration within the shortest possible time. If the input force level is increased beyond the optimum

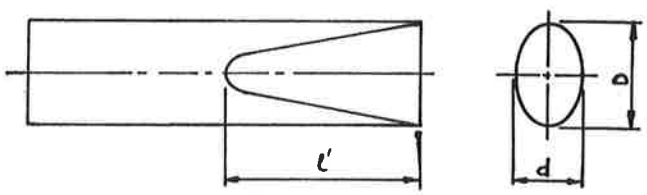

FIGURE 2 Geometry of tapers for Table 1.

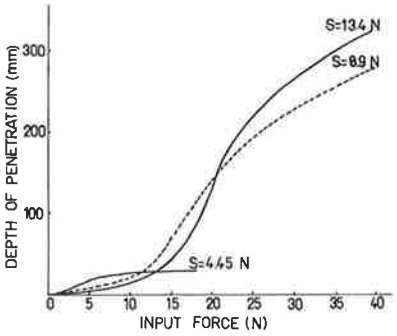

FIGURE 3 Depth of penetration against input force level (open pile).

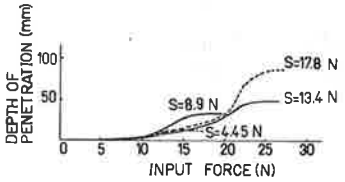

FIGURE 4 Depth of penetration against input force level (closed pile).

TABLE 1 DIMENSIONS OF TAPER (mm)

Type of Pile		length (ℓ') of taper									
		0	10	20	30	40	50	60	80	100	120
Pile A	D	25.11	--	23.99	-	22.81	-	21.89	20.93	19.52	19.52
	d	7.63	--	9.92	-	11.91	-	13.22	14.31	16.52	19.52
Pile B	D	25.31	24.31	23.19	21.91	20.63	19.61	19.50	-	-	-
	d	7.21	9.10	10.81	12.49	14.29	16.31	19.50	-	-	-
Pile C	D	25.21	24.29	22.62	20.78	19.50	-	-	-	-	-
	d	7.31	8.68	10.69	14.58	19.50	-	-	-	-	-

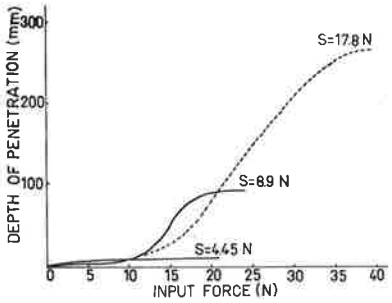

FIGURE 5 Depth of penetration against input force level (Pile A, Table 1).

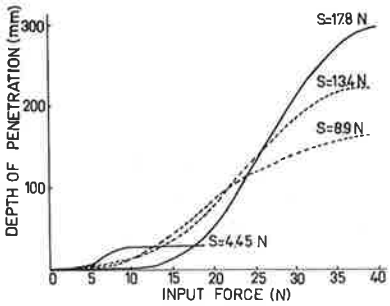

FIGURE 6 Depth of penetration against input force level (Pile B, Table 1).

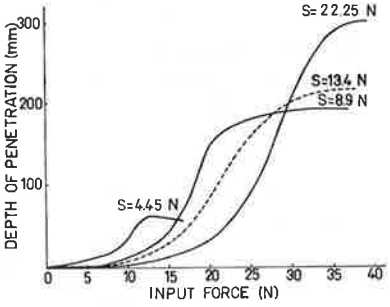

FIGURE 7 Depth of penetration against input force level (Pile C, Table 1).

level, no appreciable increase in the depth of penetration takes place. The minimum and optimum force levels for various tip configurations of the piles are shown in Figure 8.

For all the piles tested, the minimum input force level is the same, and its value should be equal to the applied static surcharge—or slightly greater than it, if some friction is present. Thus, the relationship between the minimum force level and the applied static surcharge is linear, irrespective of the tip configuration. But the optimum force level depends greatly on the shape of the pile tip. A linear relationship between the optimum force level and the applied static surcharge can be observed for a closed pile; the constant of proportionality is given by $\alpha = F_o/S = 2.45$. With a slightly open pile, the optimum force level increases rapidly; the greatest increase occurs for a fully open pile, which also achieves the deepest

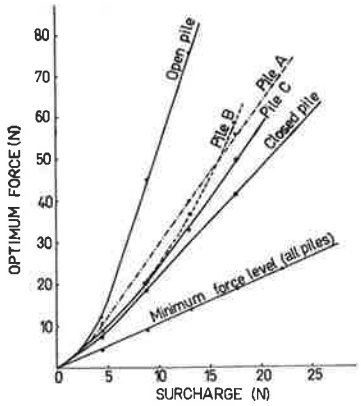

FIGURE 8 Minimum and optimum force levels against static surcharge.

penetration. For a low surcharge domain, the relationship between optimum input force and applied surcharge appears to be nonlinear. This is probably due to the predominance of a small friction force that is present. The effect of the tip opening on the optimum force level and the respective depths of penetration are clearly seen in Figure 8. For example, for an applied surcharge of 8.9 N, the optimum force levels for closed, semiopen (Pile A), and open piles are 18, 28, and 46 N, and the depths of penetration are 4, 6.5, and 17 mm, respectively.

Dynamic Tip Resistance

As stated earlier, a pile under a certain static surcharge penetrates the soil to an ultimate depth under the influence of the optimum force. If the applied force is then increased beyond the optimum level and the surcharge is not increased, the pile does not penetrate the soil further. Instead, the pile undergoes steady-state vibration, and the dynamic tip resistance at this condition is investigated here.

The theoretical basis for the measurement of tip resistance is explained as follows: because the pile undergoes a rigid body motion, the tip resistance may be expressed simply by

$$TR = F(t) - m\ddot{x}$$

where

TR = tip resistance,
$F(t)$ = input force,
m = effective mass of the pile and its attachments, and
$\ddot{x}$ = instantaneous acceleration of the pile.

This equation neglects skin friction of the pile. The loss of accuracy for this assumption is found to be insignificant. A small clearance is probably created around the pile during the steady-state vibratory condition, so the effect of skin friction becomes negligible. There is no tip resistance ($TR = 0$) while the pile vibrates outside the soil; therefore $F(t) = m\ddot{x}$. In the experimental setup, a force gage and an accelerometer may be used to measure the input force [$F(t)$] and the pile inertia ($m\ddot{x}$). The signals of the transducers may be adjusted and

combined to produce a null resultant for the unembedded pile. Phase distortion was kept to a minimum. The signals of tip resistance for various piles are similar, and only a representative set of signals is plotted on an enlarged scale in Figure 9. The results are summarized in Table 2. The results for a closed pile have been included for comparison.

In Figure 9, the phase difference between the input force (Curve A′) and the inertia (Curve B′) of the pile while it is vibrating outside the soil is 180 degrees, and their algebraic sum (A′ plus B′) is zero. However, while the embedded pile undergoes steady-state vibration, the inertia signal (Curve B) changes its phase by almost 180 degrees because of soil reaction, and it reinforces the input force signal (Curve A). The resulting signal (Curve A + B) shows a series of peaks spaced by the period of excitation.

For any type of pile (open or closed), a higher static surcharge warrants a greater input force level, which in turn induces greater tip resistance. The optimum input force level of an open pile is normally higher than that of a closed pile.

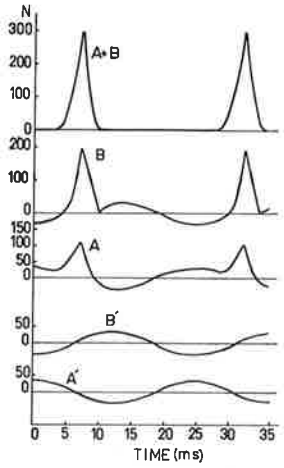

FIGURE 9 Dynamic tip resistance of an open pile, S = 6.7 N, F = 40 Hz.

This is because an open pile penetrates deeper than a closed pile under identical conditions. The tip resistance of an open pile, however, does not increase in the same proportion with respect to the applied force as the tip resistance of a closed pile does. For example (Table 2), the tip resistance of an open pile is only 197 N for the applied force of 49 N, whereas the tip resistance of a closed pile is 107 N for the applied force of 13.7 N; the static surcharge in both cases is 6.7 N. In this instance, the ratio (open/closed) of the applied force levels is 3.58, whereas the ratio of the tip resistances is 1.84. This indicates that for a fixed set of driving parameters, the closed pile will experience greater tip resistance than an open pile will. Also from Table 2, it is clear that, depending on the tip opening area, a semiopen pile will experience tip resistance greater than that of an open pile but less than that of a closed pile.

THEORY

When the experimental results of the dynamic tip resistance of an open pile are compared with those of a closed pile, it becomes apparent that there are similarities in the nature and duration of the reaction between the pile and soil. A pile-soil model is shown in Figure 10 in which the soil is represented

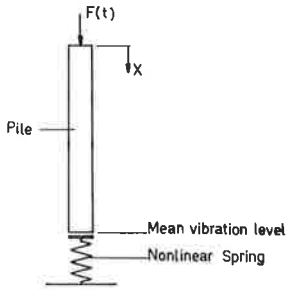

FIGURE 10 Theoretical model of pile vibration.

TABLE 2 COMPARISON OF THEORETICAL AND EXPERIMENTAL RESULTS

Type of Pile	Static Surcharge S(N)	Frequency (Hz)	Applied Force F_o(N)	ACC (Expt.) (g)	Expt. TR max(N)	TR max(N) (Eq. 5′)	Discrepancy
Closed Pile	6.7	40	13.7	10	107	111.3	+4%
	17.8		39.3	25	276	285	+3%
Open Pile	6.7	40	49	14.0	197	196	-0.5%
Pile A	8.9	40	24	9.4	116	120	+3%
	17.8		49	25.0	328	300	-8%
Pile B	8.9	40	22	11.9	140	140	0%
	13.4		24	12.5	153	148.5	-3%
Pile C	8.9	40	26	7.5	105	105	0%

by a nonlinear cubic spring. The pile-soil reaction takes place only during the downward motion from the mean vibrational level of the pile. The tip resistance of a pile can then be written as

$$TR = R[H(t - t_1) - H(t - t_2)]x^3 \quad (1)$$

where

R = dynamic soil parameter to be determined,
x = pile displacement,
$H(t - t_1)$ = unit step function, and the expression in brackets represents a filter function.

Neglecting the skin friction, the steady-state vibrational motion of the pile may be expressed by

$$m\ddot{x} + R[H(t - t_1) - H(t - t_2)]x^3 = S + F_o \sin \omega t \quad (2)$$

where

S = static surcharge,
F_o = input force amplitude, and
ω = excitation frequency.

Equation 2 is nonlinear (*6*,*7*), and its approximate solution is assumed to be $x(t) = a \sin \omega t$, where a is the amplitude of vibration to be determined. Adding $\omega^2 x$ to both sides of Equation 2 and substituting $x(t) = a \sin \omega t$ into the right-hand side obtains

$$\ddot{x} + \omega^2 x = \frac{S}{m} + \left\{\frac{F_o}{m} + \omega^2 a - \frac{3Ra^3}{4m}[H(t - t_1) - H(t - t_2)]\right\} \times \sin \omega t + \frac{Ra^3}{4m}[H(t - t_1) - H(t - t_2)] \sin 3\omega t \quad (3)$$

To avoid the secular term (*7*) in Equation 3, impose the condition

$$\frac{F_o}{m} + \omega^2 a - \frac{3Ra^3}{4m}[H(t - t_1) - H(t - t_2)] = 0 \quad (4)$$

Equation 4 is significant because it relates the two important unknown quantities a and R. Normally, a can be measured and hence R can be expressed in terms of other measurable quantities. Thus, for $t_1 \leq t \leq t_2$,

$$R = (4F_o + 4m\omega^2 a)/3a^3$$

and

$$Ra^3 = (4F_o + 4m\omega^2 a)/3 = TR \quad (5)$$

After deleting the secular term, Equation 2 may be reduced to

$$\ddot{x} + \omega^2 x = \frac{S}{m} + \frac{Ra^3}{4m}[H(t - t_1) - H(t - t_2)] \sin 3\omega t \quad (6)$$

From Satter and Ghahramani (*1*), the solution of Equation 6 is given by

$$x(t) = \frac{S}{m\omega^2} + \left(a - \frac{S}{m\omega^2}\right) \sin \omega t - \frac{Ra^3}{32m\omega^2}(\sin \omega t + \sin 3\omega t) \quad (7)$$

The acceleration

$$\ddot{x}(t) = \frac{S}{m} - \omega^2 \left[\left(a - \frac{S}{m\omega^2}\right) \sin \omega t - \frac{Ra^3}{32m\omega^2}(\sin \omega t + 9 \sin 3\omega t)\right] \quad (8)$$

In Equation 8, the constant acceleration term is added to account for the static surcharge.

As mentioned earlier, the inertia signal changes its phase by 180 degrees during pile-soil reaction; hence, in computing the tip resistance from Equation 5, the following restrictions must be observed:

$$TR = F(t) - m\ddot{x} \qquad \text{for } t_1 \leq t \leq t_2 \quad (9)$$

and

$$TR = 0 = F(t) + m\ddot{x} \qquad \text{for } t < t_1 \text{ or } t > t_2 \quad (10)$$

In the case $TR = 0$, amplitude (a) must be calculated from $a = F_o/m\omega^2$. The dynamic tip resistance may be calculated easily from Equation 5.

DISCUSSION OF THEORETICAL AND EXPERIMENTAL TIP RESISTANCE

Both theoretical and experimental values of tip resistance for various piles are summarized in Table 2. The theoretical results have been calculated from Equation 5, but the values of pile acceleration required for the calculations are those obtained experimentally. It is clear that the theoretical and experimental values of the tip resistances for various piles have good agreement. With the exception of one reading (Pile A), the theoretical results are within 4 percent of the experimental values. For the open pile, the theoretical tip resistance value is within 0.5 percent of the experimental value. It is noted from Equation 5 that the tip resistances do not depend directly on the applied static surcharge but on the applied force level. Surcharge, however, influences the tip resistance indirectly because it controls the level of applied optimum force to the pile.

CONCLUSIONS

This study has provided several useful observations about low-frequency vibropile driving. As expected, for a fixed set of static surcharges, an open pile will achieve the greatest depth of penetration and a closed pile will achieve the least; a semiopen pile will achieve intermediate depth. The minimum force level

that the shaker must supply for the pile to begin penetration does not depend on the tip configuration (open or closed). The optimum force level at which the pile achieves the ultimate depth of penetration corresponding to a certain applied static surcharge is generally greater for the open pile than that for the semiopen or closed pile. The geometry of the pile tip has a marked effect on dynamic tip resistance. Under the same driving conditions, an open pile experiences the least tip resistance, a closed pile experiences the greatest, and a semiopen pile experiences levels in between. The pile-soil reaction occurs during the downward motion of the pile from the mean vibration level, and its duration is about one-quarter of the period of excitation. The dynamic tip resistance is proportional to the cube of the pile's steady-state displacement, and it does not depend directly on the applied static surcharge. The knowledge of the input force amplitude and pile inertia level are the measured quantities necessary to commute the pile tip resistance from the theory provided in the paper. The theoretical and experimental results have good agreement.

ACKNOWLEDGMENTS

The author expresses his thanks to A. Ghahramani and N. Mostaghel of Shiraz University for useful discussions, to the reviewers for useful suggestions for improving the paper, and to Shiraz University for provision of facilities. Thanks are also due to Mrs. Shaterpouri for typing the manuscript.

REFERENCES

1. M. A. Satter and A. Ghahramani. Prediction of Tip Resistance from Pile Dynamics. *Iranian Journal of Science and Technology* (in preparation).
2. F. Rausche, F. Moses, and G. G. Goble. Soil Resistance Predictions from Pile Dynamics. *Journal of the Soil Mechanics and Foundations Division*, ASCE, Vol. 98, No. SM9, 1972, pp. 917–937.
3. R. H. Scanlan and J. J. Tomko. Dynamic Prediction of Pile Static Bearing Capacity. *Journal of the Soil Mechanics and Foundations Division*, ASCE, Vol. 95, No. SM2, 1969, pp. 583–604.
4. Y. Koizumi et al. Field Tests on Piles in Sand. *Soils and Foundations*, Vol. 11, No. 2, 1971, pp. 29–49.
5. D. D. Barkan. *Dynamics of Bases and Foundations* (translated from Russian by L. Drashevska). McGraw-Hill, New York, N.Y., 1962.
6. I. I. Bykhovsky. *Fundamentals of Vibration Engineering*, (translated from Russian by V. Zhitomirsky). Mir Publishers, Moscow, Russia, 1972.
7. Y. Panovko. *Elements of the Applied Theory of Elastic Vibration* (translated from Russian by M. Konyaeva). Mir Publishers, Moscow, Russia, 1971.